



The University of
Nottingham

**THE MECHANICAL BEHAVIOUR OF
CEMENTED GRANULAR MATERIALS AT
HIGH PRESSURES**

by

AMANULLAH MARRI, M. Eng.

Thesis submitted to The University of Nottingham for
the degree of Doctor of Philosophy

September 2010

TABLE OF CONTENTS

LIST OF FIGURES	VIII
LIST OF TABLES	XX
NOMENCLATURE	XXI
ACRONYMS	XXIII
ACKNOWLEDGEMENTS	XXV
ABSTRACT	XXVI
CHAPTER 1 INTRODUCTION	1
1.1 Background.....	1
1.2 Research objectives.....	4
1.3 Scope	5
1.4 Thesis structure	7
CHAPTER 2 LITERATURE REVIEW	9
2.1 Introduction.....	9
2.2 Carbonate soils.....	10
2.3 Artificial cementation.....	12
2.4 Methods of specimen preparation	12
2.4.1 Uncemented specimen preparation.....	14
2.4.2 Cemented specimen preparation	15
2.5 Factors affecting the strength of cemented soils	17

2.6	Micromechanics of cemented sand	18
2.7	Isotropic compression behaviour.....	22
2.7.1	Density and cement content effect on compression	22
2.7.2	Particles crushing and cement bond breakage during isotropic compression.....	25
2.8	Triaxial compression behaviour	27
2.8.1	Drained behaviour	27
2.8.2	Undrained behaviour	29
2.8.3	Comparison of drained and undrained behaviour	33
2.9	Failure characteristics	35
2.9.1	Types and modes of failure.....	36
2.9.2	Failure criterions	37
2.9.3	Strain localization and shear band characterization	40
2.10	Stress-dilatancy theory.....	43
2.10.1	Dilatancy angle.....	45
2.10.2	Stress-dilatancy relation	47
2.11	Yielding characteristics of cemented sand	50
2.11.1	Identification of yield point	51
2.11.2	Yield stress in isotropic compression.....	53
2.11.3	Yield stress in shearing.....	54
2.12	Pre-failure deformation characteristics	55

2.13	Critical state behaviour.....	59
2.13.1	Critical state concept in cemented materials	62
2.13.2	Problems in identifying the critical state for cemented sand	63
2.14	Summary.....	64
CHAPTER 3 METHODOLOGY		70
3.1	Introduction.....	70
3.2	Materials	70
3.2.1	Portaway sand.....	70
3.2.2	Particle shape and mineralogy.....	72
3.2.3	Cement.....	70
3.3	Sample preparation procedures	74
3.3.1	Preparation of uncemented specimens	77
3.3.2	Preparation of cemented specimens.....	83
3.4	Testing setup	85
3.4.1	Bishop-Wesley triaxial system	85
3.4.2	High-pressure triaxial system	88
3.4.3	Cell base connections	90
3.4.4	Cell usage	91
3.4.5	Digital controller	95
3.5	Salient features of high-pressure triaxial testing system.....	95

3.6	Scanning electron microscope	97
3.7	Testing procedure	100
3.7.1	Saturation.....	100
3.7.2	Consolidation	102
3.7.3	Drained shearing.....	103
3.7.4	Undrained shearing.....	103
3.8	Strength control	104
3.9	Homogeneity of the cemented specimens	106
3.10	Effect of cement content on specific volume.....	108
3.11	Calculations of derived parameters	109
3.11.1	Constant dry unit weight	109
3.11.2	Void ratio.....	109
3.11.3	GDS software calculated parameters	111
3.12	Problems involved with triaxial testing of cemented soils.....	112
3.12.1	Stratification of the samples.....	113
3.12.2	Membrane puncture.....	115
3.13	Repeatability of test results.....	119
3.14	Summary.....	120
CHAPTER 4 ISOTROPIC COMPRESSION TESTS		122
4.1	Introduction.....	122

4.2	Effect of initial void ratio	123
4.3	Effect of cement content	125
4.4	Deformation of cemented sand during compression	130
4.4.1	Effect of cement content on particle crushing	130
4.4.2	Effect of dry density on particle crushing	135
4.5	Summary	141
CHAPTER 5 TRIAXIAL COMPRESSION TESTS		144
5.1	Introduction.....	144
5.2	Drained behaviour.....	147
5.2.1	Effect of confining pressure	147
5.2.2	Effect of cement content	148
5.2.3	Drained shear strength	154
5.3	Undrained behaviour	154
5.3.1	Effect of confining pressure	165
5.3.2	Effect of cement content	167
5.3.3	Undrained shear strength.....	169
5.4	Comparison of drained and undrained behaviour.....	170
5.5	Failure characteristics	173
5.5.1	Failure criteria	174
5.5.2	Modes of failure.....	179

5.5.3	Strain localization and shear band characterization	183
5.6	Summary	185
CHAPTER 6 STRESS-DILATANCY RESPONSE OF CEMENTED SAND.....		189
6.1	Introduction.....	189
6.2	Effect of initial relative density	192
6.3	Effect of cement content	193
6.4	Effect of confining pressure	197
6.5	Dilation angle	199
6.6	Stress-dilatancy relation.....	203
6.7	Idealization of dilatancy phenomenon	207
6.8	Summary	211
CHAPTER 7 GENERAL CEMENTED SAND BEHAVIOUR AT HIGH PRESSURES		213
7.1	Introduction.....	213
7.2	Yielding characteristics of cemented sand.....	213
7.2.1	Location of yield point	214
7.2.2	Yield stress during isotropic compression	217
7.2.3	Yield stress during triaxial shearing	219
7.3	Deformation characteristics.....	222
7.3.1	Determination of elastic parameters.....	224
7.3.2	Deformation during drained shearing	230

7.3.3	Deformation during undrained shearing	233
7.3.4	Measurement of stiffness and stiffness degradation	234
7.4	Critical state behaviour	240
7.4.1	Problems in identifying critical state for cemented sand	242
7.4.2	Critical state surface	248
7.5	Summary	253
CHAPTER 8 CONCLUSIONS AND RECOMMENDATIONS		256
8.1	Introduction.....	256
8.2	Summary of experimental results.....	257
8.2.1	Difficulties in high-pressure triaxial testing	257
8.2.2	Isotropic compression.....	258
8.2.3	Failure characteristics	260
8.2.4	Stress-dilatancy	262
8.2.5	Yielding characteristics	263
8.2.6	Strength and deformation	263
8.2.7	Critical state behaviour	264
8.3	Potential applications.....	265
8.4	Recommendations	266
REFERENCES		269

LIST OF FIGURES

Figure 2.1 Example of natural marine cementation: (a) Ooid sand with carbonate cores; (b) Ooid sand cemented by coarse crystalline of fibrous aragonite (after Molenaar and Venmans 1993).	11
Figure 2.2 Typical drained test results of cemented carbonate soils obtained from the N-W shelf of Australia (after Airey 1993).	11
Figure 2.3 Comparison of drained tests conducted on WS and MT specimens: (a) axial strain vs. deviatoric stress; (b) axial strain vs. volumetric strain (after Wanatowski and Chu 2008).	13
Figure 2.4 SEM micrograph of RT* sample cemented with (a) calcite; (b) Portland cement (after Ismail <i>et al.</i> 2002).	20
Figure 2.5 Relationship between unconfined compressive strength (q_{ucs}) and cement content for Portland cement (after Ismail <i>et al.</i> 2002).	21
Figure 2.6 Isotropic compression responses (after Airey 1993).	23
Figure 2.7 Isotropic compression lines for sand, fibre reinforced sand, cemented sand, and cemented fibre reinforced sand (after Dos Santos <i>et al.</i> 2009).	24
Figure 2.8 Isotropic compression data for sand and fibre-reinforced sand (after Consoli <i>et al.</i> 2005).	24
Figure 2.9 Isotropic compression curves of Cambria sand at different initial void ratios (after Bopp and Lade 2005).	25
Figure 2.10 High-pressure isotropic compression test on dense Cambria sand (after Yamamuro and Lade 1996).	26

Figure 2.11 Idealized behaviour of cemented soil: (a) stress-strain curves; (b) effective stress paths (after Coop and Atkinson 1993).	29
Figure 2.12 Illustration of undrained strength and stress paths (after Yoshimine <i>et al.</i> 1999).	32
Figure 2.13 Typical behaviour of loose and dense sand under undrained conditions: (a) stress-strain curves; (b) effective stress paths (after Tsai <i>et al.</i> 2010).....	33
Figure 2.14 Undrained stress paths at a depth of: (a) at 1 m; (b) at 5 m (after Futai <i>et al.</i> 2004).	34
Figure 2.15 Effective stress paths for drained and undrained tests of Tehran alluvium with cement contents of: (a) 0%; (b) 1.5%; (c) 3%; (d) 4.5% (after Asghari <i>et al.</i> 2003).	35
Figure 2.16 Mohr diagram showing possible modes of failure and fracturing (after Nygard <i>et al.</i> 2006).....	37
Figure 2.17 Failure criterion in normal stress-shear stress space (after Houlsby 1986).	39
Figure 2.18 Illustration of progressive failure of sands in drained triaxial tests: (a) initial condition; (b) occurrence of dilative strain areas; (c) continuous linking of dilative strain areas; (d) fully developed shear band; (e) further occurrence of dilative strain areas; (f) continuous link of dilative strain areas; (g) “diagonally crossing shear bands;” and (h) q versus ε_a (after Suzuki and Yamada 2006).	42
Figure 2.19 Void-ratio variations of Portland cement sand samples in response to shearing at 100 kPa confining pressure (after Wang and Leung 2008).....	45
Figure 2.20 Stress-dilatancy behaviour of artificially cemented sands: (a) effect of cement content; (b) effect of initial mean effective stress (after Yu <i>et al.</i> 2007).....	49

Figure 2.21 Determination of the primary yield point in isotropic compression (after Rotta <i>et al.</i> 2003).	51
Figure 2.22 Location of yield point in stress-strain curve (after Wang and Leung 2008).	52
Figure 2.23 Typical location of yield point in stress-time curve for granular quartz sand (after Karner <i>et al.</i> 2003).	52
Figure 2.24 yielding stresses in isotropic compression (a) Representative e -log p' curves; (b) relationship between the crushability ΔS and mean effective stress p' (after Kwag <i>et al.</i> 1999).	53
Figure 2.25 Variation of primary yield stress with cement content (after Rotta <i>et al.</i> 2003).	54
Figure 2.26 Illustration for the determination of deformation modulus with external load cell and internal local deformation transducers (LDT) during triaxial compression [redrawn from Goto <i>et al.</i> (1991) and Tatsuoka <i>et al.</i> (1994)].	57
Figure 2.27 Initiation of dilation: (a) dilation rate-axial strain; (b) stress-strain curve with maximum rate of dilation regions (after Asghari <i>et al.</i> 2003).	58
Figure 2.28 The onset of dilation correlated with deformation modulus (after Stein 2004).	58
Figure 2.29 Critical state of soil (after Wood 1990).	61
Figure 2.30 Different definitions of critical state for drained test with dilating sand. 62	
Figure 3.1 Grain size distribution curve.	71
Figure 3.2 Shape of the Portaway sand particles (Wang 2005).	72
Figure 3.3 Energy dispersive spectrum (EDS) of uncemented sand (Wang 2005).	73
Figure 3.4 Energy dispersive spectrum (EDS) of cemented sand.	73

Figure 3.5 Rubber membranes: (a) Latex; (b) Neoprene.....	76
Figure 3.6 The sequential steps for the preparation of uncemented samples for conventional triaxial testing from: (a) to (p).	80
Figure 3.7 The sequential steps of the preparation of uncemented samples for high-pressure testing from: (a) to (j).....	83
Figure 3.8 Specimen placed on the cell base.....	85
Figure 3.9 Bishop-Wesley triaxial setup and working mechanism (after Wang 2005).	87
Figure 3.10 The modified experimental set up for conventional pressure triaxial testing system.	87
Figure 3.11 High-pressure triaxial testing system: (a) schematic diagram; (b) photograph of the cell in the loading frame.....	90
Figure 3.12 High-pressure triaxial cell: (a) Schematic cross-section and Cell photograph; (b) cell base schematic diagram and Cell base photograph.	91
Figure 3.13 High-pressure triaxial cell.	94
Figure 3.14 High-pressure triaxial cell: (a) Placement of clamp rings; (b) Placement of retaining ring.....	94
Figure 3.15 Digital controller of high-pressure triaxial testing system.	95
Figure 3.16 Scanning Electron Microscope: (a) outside views; (b) inside views.	99
Figure 3.17 Typical failure mode of cemented specimen in unconfined compression test.	105
Figure 3.18 Effect of cement content on unconfined compressive strength of Portaway sand.....	105

Figure 3.19 Microstructure of dense cemented sand with cement content of: (a) 5%; (b) 10%; and (c) 15%.	107
Figure 3.20 Effect of Portland cement and gypsum content on the specific volume of cemented sand.....	108
Figure 3.21 Stratification of cemented materials prepared by the method of undercompaction compressed at high confining pressures: (a) before isotropic compression; (b) after isotropic compression.....	114
Figure 3.22 Homogeneity check of cemented materials prepared by density controlled vibratory tamping method compressed at high confining pressures (a) before isotropic compression; (b) after isotropic compression.	114
Figure 3.23 membrane puncture along the edge of the specimen.....	116
Figure 3.24 Membrane damage and puncture: (a) due to sharp edges of particles; (b) along shear plane.....	116
Figure 3.25 Membrane puncture: (a) Loose and porous cemented specimen resulting; (b) the membrane punctures due to penetration.....	117
Figure 3.26 Avoiding membrane puncture: (a) the top and bottom edges of the specimen; (b) Membrane strip provided to avoid penetration and puncture at sharp edges.....	117
Figure 3.27 Avoiding membrane puncture: (a) Pores on the surface of the sample (b) Pores are filled with clay sand mixture to avoid membrane punctures.	118
Figure 3.28 Successfully completed experiments after remedial measures against punctures: (a) sample with diagonal shear band; (b) sample with conjugate shear band.	118

Figure 3.29 Repeat tests on Portaway sand during isotropic loading and unloading.	119
Figure 3.30 Repeat tests on cemented Portaway sand during consolidated drained compression.....	119
Figure 4.1 Isotropic compression curves of uncemented Portaway sand at different initial void ratios.	124
Figure 4.2 Isotropic compression curves of cemented Portaway sand at different initial void ratios.	125
Figure 4.3 Variation of void ratio at the end of consolidation with effective confining pressure at different cement contents.....	128
Figure 4.4 Effect of cement content on isotropic compression curves of dense Portaway sand at constant dry unit weight.....	129
Figure 4.5 $e-\ln(p')$ curves of Portaway sand with different cement contents prepared at constant initial void ratio.....	129
Figure 4.6 Normal compression lines for uncemented and cemented Portaway sand.	130
Figure 4.7 High-pressure isotropic compression test on dense Portaway sand.	132
Figure 4.8 High-pressure isotropic compression test on cemented Portaway sand with: (a) 5% cement content; (b) 10% cement content.	133
Figure 4.9 Effect of cement content on isotropic compression at high-pressure.....	134
Figure 4.10 SEM photographs of specimens after isotropic compression at high pressures: (a) specimen showing crushing of particles and had dip on the compression curve (b) specimen showing no significant crushing of particles and had no dip on the compression curve.	135

Figure 4.11 Effect of initial dry density on isotropic compression at high-pressures:
(a) relatively loose sand with $D_r = 48\%$; (b) relatively dense sand with $D_r = 89\%$138

Figure 4.12 SEM photographs of uncemented sand after isotropic compression at $\sigma'_3 = 50$ MPa: (a) relatively loose sand with $D_r = 48\%$; (b) relatively dense sand with $D_r = 89\%$138

Figure 4.13 Effect of initial dry density on isotropic compression at high-pressures:
(a) relatively loose cemented sand with $D_r = 40\%$; (b) relatively dense cemented sand with $D_r = 81\%$139

Figure 4.14 SEM photographs of cemented sand specimens after isotropic compression at high-pressures with initial relative densities of: (a) $D_r = 40\%$; (b) $D_r = 62\%$; (c) $D_r = 81\%$141

Figure 5.1 Effect of confining pressure on the stress-strain behaviour of sand with different cement contents: (a) 0%; (b) 5%; (c) 10%; and (d) 15%.152

Figure 5.2 Effect of cement content on the stress-strain behaviour of sand with different confining pressures of: (a) 1 MPa; (b) 4 MPa; (c) 8 MPa; and (d) 12 MPa. 153

Figure 5.3 Failure envelopes of specimens with different cement contents during drained compression.157

Figure 5.4 Effect of confining pressure for a wide range of cement contents at failure state on: (a) stress ratio (q/p'); (b) frictional angle.158

Figure 5.5 Effect of cement content on: (a) failure envelopes; (b) cohesion; and (c) frictional angle.159

Figure 5.6 Typical undrained response of uncemented sand: (a) loose sand; and (b) dense sand.163

Figure 5.7 Typical undrained response of cemented sand at: (a) 10 MPa; and (b) 20 MPa.	164
Figure 5.8 Undrained test responses under the effect of confining pressure at cement content of: (a) 0%; (b) 5%; (c) 10% and (d) 15%.	167
Figure 5.9 Effect of cement content on the undrained behaviour of Portaway sand: (a) stress-strain curves; (b) effective stress paths; (c) excess pore water pressures.	169
Figure 5.10 Effect of confining pressure for a wide range of cement contents at undrained frictional angle.....	170
Figure 5.11 Drained and undrained stress paths and failure envelopes for cemented Portaway sand with the cement content of: (a) 0%; (b) 5%; (c) 10%; and (d) 15%. .	172
Figure 5.12 Comparison of the effective frictional angles for undrained and drained compression tests with cement contents of: (a) 0%; (b) 5%; (c) 10%; and (d) 15%..	173
Figure 5.13 Comparisons of failure criteria based on the effect of cement content and confining pressures during drained compression tests at effective confining pressures of: (a) 0.5 MPa; (b) 1MPa; and (c) 8 MPa.....	177
Figure 5.14 Comparisons of failure criteria based on the effect of: (a) confining pressure; and (b) cement content during undrained compression tests.....	178
Figure 5.15 Effect of confining pressure on brittleness index.	182
Figure 5.16 Mode of failure of cemented Portaway sand: (a) brittle; (b) Transitional; (c) Ductile.	182
Figure 5.17 Illustration of shear band pattern after shearing, sketched from the tested samples.	183

Figure 5.18 shear band characterization of sand at the cement contents of: (a) 5%; (b) 10%; and (d) 15%.....	184
Figure 6.1 The effect of initial relative density on the dilatancy of uncemented sand.	193
Figure 6.2 The effect of initial relative density on the dilatancy of cemented sand.	193
Figure 6.3 Volumetric responses of cemented sand at high pressures with cement contents 0 to 15 % at effective confining pressures of: (a) 1 MPa; (b) 4 MPa; (c) 8 MPa; and (d) 12 MPa.	195
Figure 6.4 Location of the point of maximum dilation in the (a) stress-strain; (b) volumetric response; and (c) stress-dilatancy relationship.....	196
Figure 6.5 Typical SEM micrograph demonstrating the cement bond breakage during consolidated drained triaxial compression.....	197
Figure 6.6 Suppression of the dilatancy by the gradual increase in confining pressure for the specimens with cement contents of: (a) 0%; (b) 5%; (c) 10%; and (d) 5%. ...	199
Figure 6.7 Effect of confining pressure on peak dilatancy angle derived from the rate of dilatancy.....	201
Figure 6.8 Angles of shearing resistance and dilatancy in triaxial compression for different cement contents.....	202
Figure 6.9 Effect of confining pressure on peak dilatancy angle derived from peak frictional and critical state/ultimate state angle.	202
Figure 6.10 Effect of cement content on maximum dilatancy angle.	203
Figure 6.11 Inter-particle bonding due to cement content.....	205
Figure 6.12 Incorporation of cohesion component due to cement content.....	205

Figure 6.13 The stress-dilatancy relationships of Portaway sand: (a) effect of confining pressure; (b) effect of cement content.....	206
Figure 6.14 Typical results demonstrating how the onset of dilation is affected by: (a) confining pressure; (b) cement content; and (c) initial relative density.	209
Figure 6.15 Illustration of dilatancy from multi-linear idealized deformation curve.	210
Figure 6.16 Development and coalescence of micro-structural damage during triaxial compression of cemented sand.....	210
Figure 7.1 The primary yield point during isotropic compression of Portaway sand.	216
Figure 7.2 Location of the primary yield point in the stress-strain curve.	216
Figure 7.3 Effect of cement content on the primary yield point of cement treated Portaway sand during isotropic compression.	218
Figure 7.4 Effect of cement content on the primary yield point of cement treated Portaway sand during isotropic compression.	218
Figure 7.5 Effect of cement content and confining pressure on the location of primary yield point at the effective confining pressures of: (a) 1MPa; (b) 4MPa; (c) 8MPa; and (d) 12MPa.	220
Figure 7.6 Effect of cement content on primary yield stress at different confining pressures.....	221
Figure 7.7 Effect of confining pressure on the primary yield stress at different cement contents.	221
Figure 7.8 Effect of cement contents on the yield locus of Portaway sand at high pressures.....	222

Figure 7.9 Variation of Poisson's ratio with: (a) different cement contents; (b) effective confining pressures.....	226
Figure 7.10 Variation of elastic moduli with different cement contents and confining pressures.....	229
Figure 7.11 Microstructure of the uncemented Portaway sand after CD test at 20 MPa.	231
Figure 7.12 SEM photograph of bulging section of cemented sand after isotropically consolidated drained shearing at $c = 15\%$ and $\sigma'_3 = 20$ MPa.	232
Figure 7.13 SEM photograph of shear plane section of cemented sand after isotropically consolidated drained shearing at $c = 15\%$ and $\sigma'_3 = 1$ MPa.	232
Figure 7.14 SEM photograph of bulging section of cemented sand after isotropically consolidated undrained shearing at $c = 15\%$ and $\sigma'_3 = 20$ MPa.....	234
Figure 7.15 SEM photograph of shear plane section of cemented sand after isotropically consolidated undrained shearing at $c = 15\%$ and $\sigma'_3 = 20$ MPa.	234
Figure 7.16 Onset of pre-failure deformation correlated with deviatoric stress and volumetric strain curves with the cement content of: (a) 0%; and (b) 5%.....	239
Figure 7.17 Effect of: (a) cement content; and (b) confining pressure on stiffness degradation during drained compression.	239
Figure 7.18 Effect of: (a) cement content; (b) confining pressure on stiffness degradation during undrained compression.	239
Figure 7.19 Comparison of the effect of: (a) cement content; and (b) confining pressure on stiffness degradation during undrained and drained compression.	240
Figure 7.20 Effect of confining pressure on ultimate state/critical state void ratio during triaxial compression.	243

Figure 7.21 State paths and limiting stress envelopes at conventional pressure.	246
Figure 7.22 Effect of cement contents on state paths and limiting stress envelopes at high pressures with cement contents of: (a) 0%; (b) 5%; (c) 10%; and (d) 15%.....	247
Figure 7.23 The stress paths for uncemented and cemented sand with cement content of: (a) 0%; (b) 5%; (c) 10%; and (d) 15%.	249
Figure 7.24 Critical state lines in $q-p'$ space.	251
Figure 7.25 Critical state zone in $q-p'$ space.	251
Figure 7.26 Critical state lines for cemented and uncemented soils in $v:\ln(p')$ space the curvatures were ignored.	252

LIST OF TABLES

Table 3.1 Index properties of Portaway sand.....	71
Table 3.2 Technical specifications of GDS high-pressure triaxial apparatus.	89
Table 3.3 Average values of unconfined compression test parameters.	104
Table 4.1 Summary of typical isotropic compression tests.	122
Table 5.1 Summary of isotropically consolidated drained compression tests	146
Table 5.2 Summary of isotropically consolidated undrained compression tests (failure parameters).	162
Table 6.1 Summary of isotropically consolidated drained compression tests (dilatancy parameters).	191
Table 7.1 Summary of isotropic compression tests (yield parameters).	215
Table 7.2 Summary of isotropically consolidated drained compression tests (elastic parameters).	215
Table 7.3 Summary of isotropically consolidated drained compression tests (critical/ultimate state parameters).	241

NOMENCLATURE

$D_{ro} = (e_{max} - e_{min}) / (e_{max} - e)$	= Relative density
e	= Void ratio
e_0	= Initial void ratio
e_c	= Void ratio at the end of consolidation
e_{cr}	= Critical state void ratio
e_{max}	= Maximum void ratio
e_{min}	= Minimum void ratio
E	= Young's modulus
$I_B = q_f / q_u - 1$	= Brittleness index
$p' = (\sigma'_1 + 2\sigma'_3) / 3$	= Cambridge mean effective stress
$q = \sigma_1 - \sigma_3$	= Deviatoric stress
p'_f	= Cambridge mean effective stress at failure
q_f	= Deviatoric stress at failure
q_y	= Deviatoric stress at primary yield point
q_u	= Unconfined compressive strength

ν	= Poisson's ratio
ε_a	= Axial strain
ε_r	= Radial strain
ε_v	= Volumetric strain
$\varepsilon_q = \varepsilon_s = \frac{2}{3}(\varepsilon_a + \varepsilon_r)$	= Deviator/shear strain
σ_1	= Major principal stress
σ_3	= Minor principal stress
ϕ	= Frictional angle
ψ	= Dilatancy angle
λ	= Gradient of normal compression line
γ	= Bulk unit weight
γ_d	= Dry unit weight
Δu	= Excess pore water pressure

ACRONYMS

CD	= Isotropically consolidated Drained compression test
CU	= Isotropically consolidated undrained compression test
CD-xCyM	= CD tests with 'x' (%) Cement and 'y' (MPa) of confining pressure e.g., CD-5C10M stands for consolidated drained test with C = 5% and $\sigma'_3 = 10$ MPa
CSL	= Critical state line
CSSM	= Critical state soil mechanics model
CU-xCyM	= CU tests with 'x' (%) Cement and 'y' (MPa) of confining pressure
DPVC	= Digital pressure volume controller
EDS	= Energy dispersive spectrum
FSL	= Failure state line
IC	= Isotropic compression/consolidation
GDS	= Global Digital Systems Ltd.
(LDT)	= Internal local deformation transducers
LVDT	= Linear variable differential transformer
xClyM	= 'x' (%) loose cemented and 'y' (MPa) of confining pressure
MT	= Moist tamping method

NCL	= Normal compression line
QSS	= Quasi steady state
WS	= Water sedimentation method
SEM	= Scanning electron microscope
USL	= Ultimate state line
USC	= Unconfined compressive strength
USS	= Ultimate steady state
VIS	= Virtual infinite stiffness

ACKNOWLEDGEMENTS

I would like to express my deepest gratitude and appreciation to my Supervisors, Professor Hai- Sui. Yu and Dr. D. Wanatowski, for their valuable guidance, support, and assistance during the course of my present research work. Without their encouragement and guidance throughout the length of this investigation, its completion would not have been possible. Thanks are also due to Dr. David J Reddish for his guidance and support.

I would like to thank Ian Richardson for his assistance on matters relating to laboratory experimentation. Thanks are also due to all my colleagues; in particular, I am grateful to Zaheer Ahmad Almani, Riaz Hussain Mari, Zulfiqar Ali Laghari, and Syed Salahuddin for giving me such a wonderful time at Nottingham.

I would like to acknowledge the financial support of NED University and Higher Education Commission of Pakistan (HEC). The author is deeply indebted to all these sources.

Last but not least, my warmest love goes to my parents, and rest of the family for their loving care and unconditional backing during all these years. It is to them and in their honour that I wish to dedicate this thesis. Special thanks to my brother Wahid Bukhsh for his attachment and supporting the family in my absence. All my dedications go to my beloved father late Haji Jumma Khan who steered me right, may Allah keep his soul in peace.

ABSTRACT

The mechanical behaviour of cemented granular materials has been an important topic in geotechnical engineering since decades. Historically, most research on cemented granular materials has been performed at relatively low confining pressures. Problems relating to cemented granular materials at high-pressure are still not fully understood. However, understanding of the behaviour of cemented granular materials at high-pressure is highly important in deep foundations, particularly for offshore piling, deep mine shafts, high earth dams, and oil-bearing strata. To address the problem, artificially cemented sand specimens with varying degrees of cement contents and initial relative densities were prepared in the laboratory to simulate the natural cementation characteristics. A high-pressure triaxial compression apparatus was utilized to investigate the effect of initial relative density, cement content, and confining pressure on the mechanical behaviour of artificially cemented sand. High-pressure tests including isotropic compression, drained and undrained triaxial shearing and microscopic studies of the materials were carried out on the artificially cemented sand specimens in the Nottingham Centre for Geomechanics laboratory at the University of Nottingham. Complexities with artificial specimen preparation and with high-pressure testing were identified and tackled. The experimental results indicate that there is significant effect of cement contents and confining pressures on the mechanical behaviour of cemented materials. Particularly, these effects were notified on isotropic compression, peak strength, strength parameters, shear banding, particle crushing, yielding, and stress-dilatancy relationships. For example, reduction in compressibility, reduction in particle crushing and shift in normal compression line

by the increase in cement content of the material during isotropic compression were significant. Progressive suppression in the dilation of cemented sand by the gradual increase in confining pressure, increase in the peak strength, developing of curved failure envelope, increase in the yield strength and formation of conjugate shear banding during progressive failure during triaxial compression were worth noticeable. This concludes that the significance of high-pressure and cement content cannot be ignored in the design considerations. However, more research needs to be carried out at further high pressures in order to see the convergence of failure envelopes and the initiation of bond breakage and particle crushing to give a reasonable design framework for foundations.

INTRODUCTION

1.1 Background

It is widely recognized that the offshore foundation soils in many parts of the world generally consist of sediments. These sediments in most of the cases are cemented due to calcinations because of various geological processes, which create bonds between soil grains (Coop and Atkinson 1993, Huang and Airey 1993, Ismail *et al.* 2000). The study of cemented granular materials is of considerable interest to engineering community owing to difficulties that have arisen with the foundations of offshore structures located on these sediments. All offshore oil and gas exploration structures inevitably rest on the ocean floor if it is not a floating platform. In many parts of the world, the essential soil ingredients at these offshore places are calcareous sediments both in cemented and uncemented form. The common properties of these calcareous sediments are high in-situ void ratio, presence of soft/crushable particles and collapsible cement content. These typical characteristics of calcareous soils have been creating construction problems in offshore structures for many years. For example, the free falling of piles after the first 7.5 m penetration through variably cemented material was observed during the construction of platform in Arabian Gulf in 1968 (McClelland 1988). The most serious problem occurred on Australia's North West Shelf where 1.8 m diameter piles fell as much as 60 meters under their own weight and all the piles showed less driving resistance than anticipated. Soil deposits in Australian North West Shelf; have posed many technical challenges

to the engineering community because of their high void ratios and highly variable cement content. The degree of cement content and porosity can vary significantly over distances of less than 10 cm (Apthorpe *et al.* 1988). This makes the natural sediments unsuitable for fundamental study of the parameters affecting the monotonic or cyclic response of these soils. These uncertainties and the problems associated with calcareous soils have led to a great deal of research interest for geotechnical engineers.

There is then the concern about the appropriateness of artificial cements. A review of soils with bonding has shown that the patterns of behaviour observed in all cemented soils are similar even though the cement content may result from different causes. Therefore, artificial soils may be expected to show many of the characteristics of naturally cemented materials.

In March 1988, the initial findings of the research activities on cemented materials carried out by different researchers were presented in the International Conference on Calcareous Sediments held in Perth, Australia. In that conference, McClelland (1988) highlighted the importance of the degree of cementation and its quantification for the proper design of foundations to be laid on calcareous sediments. Since 1988, several studies have been conducted into the behaviour of cemented carbonate sediments (e.g. Airey 1993, Coop and Atkinson 1993, Huang *et al.* 1994, Ismail *et al.* 2000, Sharma 2001). These studies highlighted the importance of cementation of sands due to calcination because of various geological processes that create bonds between soil grains. One of the features of naturally cemented materials is that they have variable densities and degree of cement contents and this is particularly the

case for some calcarenites i.e. cemented carbonate sand (Airey 1993). These variable densities and difficulties of sampling without disturbing the cement bonding make it difficult to study the fundamental behaviour of naturally cemented materials. To avoid these difficulties, artificially cemented soils have been used in many studies (e.g. Clough *et al.* 1981, Boey and Carter 1988, Leroueil and Vaughan 1990, Airey 1993, Coop and Atkinson 1993, Haeri *et al.* 2006). However, these studies have investigated only a narrow range of confining pressures. For instance, Boey and Carter (1988) had applied the mean effective stress of 20-500 kPa, Airey (1993) of 600-670 kPa, and Huang and Airey (1997) of 0.1-5.0 MPa. However, a wide range of interesting scientific and engineering questions are still remain to be addressed, with problems relating to these materials whose complex behaviour is still not fully understood. Furthermore, the mechanical response of these materials at high pressures that can be significant in offshore piling, the construction of deep galleries, deep mine shafts, high earth dams and the mechanics of oil-bearing strata is not fully explored and investigated.

Recent developments in the massive offshore structures, particularly for oil exploration have highlighted the importance of *high pressure*, which is transmitted to foundations as a result of these structures. Depth in the case of many oil reservoirs, reach over 1000 m subjecting to high overburden pressures of several hundred tons (Rosa *et al.* 2008). The terminology of "high pressure" originally developed by Vesic and Clough (1968) is adopted to define the pressure ranges. Describing specific pressure levels, low pressure refers to pressures in the range from zero to 1 MPa, elevated pressures range from 1 to 10 MPa, high pressures range from 10 to 100 MPa, very

high pressures range from 100 to 1000 MPa, and ultra-high pressures are those greater than 1000 MPa. In this thesis, the term "high pressure" will be used as a generic term to describe research at elevated pressures and above.

Experimental investigations of cemented sands at high pressures can give a reasonable assessment of the behaviour of these materials, which is highly important for deep foundations, particularly for offshore piling, deep mine shafts, high earth dams, and oil-bearing strata. All offshore oil and gas exploration structures inevitably rest on these ocean floors (McClelland 1988).

Bearing in mind, the limited understanding of the complicated behaviour of calcareous soils, it is vital to investigate the mechanical behaviour of both cemented and uncemented sands for a wide range of cement contents at high pressures. In understanding the behaviour of cemented granular materials at high pressures, special attention is required to the challenging problems with the focus on compressibility, dilatancy, critical state behaviour, and yielding of cemented sand.

1.2 Research objectives

The objectives of the present research were to study the mechanics of cemented granular materials at high pressures. This research encompasses for a wider range of cement contents and high confining pressures to give a reasonable qualitative assessment of the effect of cement content and confining pressure on the mechanical behaviour of cemented sand. The compressibility, yield strength, stress-dilatancy relationship, critical state behaviour and exploring the underlying mechanisms of the unique behaviour of artificially cemented sands are the point of interest. In addition,

a direct comparison with the response of the uncemented soil to verify the likelihood of expressing the influence of cement content with reference to the measured behaviour of the same uncemented soil is focussed.

As a result, the motivations behind this study were as follows:

- 1) To evaluate and extend the capabilities of the triaxial systems at the University of Nottingham to include the testing of cemented sand along with uncemented granular materials to high pressures.
- 2) To gain better understanding and broaden the chain of previous studies on Portaway sand by incorporating the effect of cement content and high pressures.
- 3) To investigate experimentally the effect of high confining pressures on cemented materials with varying degree of cement contents and densities to add somewhat to the existing knowledge.
- 4) To bridge up the gap in the literature by the incorporating the cemented materials' behaviour at high pressures because previously comprehensive experimental data at high pressures is only available for uncemented granular materials.

1.3 Scope

This study presents a review of laboratory testing of calcareous soils. Special attention has been paid to the challenging problems of in situ density capturing and laboratory sample preparation. Recently developed techniques for preparing reconstituted samples with relatively high voids ratios were described. The study encompassed discussion of procedures used to prepare artificially cemented soil specimens, the mechanical behaviour of cemented calcareous sands, as well as some re-

cent findings on the underlying mechanics of calcareous sediments, and the behaviour of both uncemented and cemented calcareous soils under undrained static loading. Some recent developments in laboratory apparatus and testing techniques are also described.

Despite with significant progress in the high-pressure triaxial testing and incorporation of investigating the mechanical behaviour of cemented materials, there were certain limitations of this study, such as:

- 1) The triaxial cell of high-pressure triaxial system is made of non-transparent steel; therefore, the specimens cannot be seen inside the cell. Therefore, the real-time analysis of the specimens during different stages of shearing could not be undertaken.
- 2) There were no LVDT's installed for local strain measurements; therefore, the stress-strain measurements were made through internal load cell and displacement transducers. Moreover, the load cell capacity limit was 100 kN, therefore, the tests were run within this loading range.
- 3) The isotropic compression tests were run up to the confining pressure of 50 MPa. However, the drained and undrained shearing tests limited up to 20 MPa of effective confining pressure, to avoid exceeding the maximum load cell limit.
- 4) Due to the time constraints, the scope of the work was limited to one type of base material (i.e., Portaway sand) and therefore, the effects of different type of base materials were not investigated.

1.4 Thesis structure

The thesis is organised as follows:

Chapter 1 gives the background, objectives, scope, limitations, and motivations of the dissertation.

Chapter 2 provides an overview of challenges in the foundations laid on the calcarenite sand, sampling problems for subsequent investigations, alternative artificial cementation, methods of specimen preparation, high-pressure triaxial testing, and review of the existing related work on the mechanical behaviour of cemented materials.

Chapter 3 discusses the methodology. It describes the materials and index properties, sample preparation, test setup, testing procedures, and problems involved in sample preparation and high-pressure triaxial testing's.

It also describes the microstructure of uncemented and cemented sands, as well as the consistency and homogeneity of the sand-cement mix.

Chapter 4 discusses the isotropic compression characteristics of cemented and uncemented sands. Effect of initial relative density, cement content, and confining pressures were investigated over the cement bond breakage, particle crushing during compression and the microstructure of the material after compression.

Chapter 5 explores the drained and undrained behaviour of cemented sand. Effect of cement contents and confining pressures on the stress-strain behaviour, failure

characteristics, and the microstructure of the material after shearing were investigated.

Chapter 6 is focussed on stress-dilatancy relation of cemented materials. Inclusion of cohesion component into stress-dilatancy, volumetric dilation, and progressive suppression of dilation by the gradual increase in confining pressure were studied.

Chapter 7 is about general cemented sand behaviour. Yielding, pre-failure deformation, and critical state mechanism of the material were addressed. Stiffness degradation and problems in identifying critical state parameters for cemented sand at high pressures were mainly focussed.

Chapter 8 draws the conclusions of the research work, potential applications, and future recommendations.

LITERATURE REVIEW

2.1 Introduction

Design of offshore foundations, deep mines etc in cemented calcareous sediments requires full understanding of the strength and deformation properties of cemented soils. A full understanding of the response of cemented sands is hampered by the difficulties in obtaining high quality samples of natural materials. The natural materials cover a range of densities and high spatial variability in the degree of cementation. In addition, obtaining natural undisturbed samples from offshore sites is very expensive. To avoid these difficulties (of variation in densities, cement content, and sampling without disturbing the cementation) artificially cemented soils have been used in many studies; (e.g. Clough *et al.* 1981, Boey and Carter 1988, Leroueil and Vaughan 1990, Airey 1993, Coop and Atkinson 1993, Haeri *et al.* 2006). Since undisturbed samples of cohesionless soils are typically too difficult or costly to obtain, reconstituted samples need to be prepared using a method that most closely replicates the in-situ stress, density, and fabric or the arrangement of particles within the soil (Mitchell and Soga 2005).

This literature review focuses on to a framework of questions in order to understand and analyse the mechanical behaviour of cemented granular materials over a wider range of confining pressure, initial relative density, and degree of cementation. It also includes the critical review of the specimen preparation techniques, testing pro-

cedures, and difficulties/problems with high-pressure triaxial testing. The mechanical behaviour of cemented sand is focussed on the compressibility, yielding, stress-dilatancy, and critical state behaviour.

2.2 Carbonate soils

Carbonate soils are defined as those in which carbonate minerals, most commonly calcium carbonate, predominate. Carbonate soils consist of the remains of either marine plants or animals. They cover about one half of the continental shelves, more than one-half of the deep-sea abyssal plain, and part of the continental slope and rise. On the global scale, they cover more than 55% of the sea floor.

Carbonate sands found in the coastal zone and shallow water consist of porous or hollow particles with rough texture of mainly remains of corals, shells of molluscs and algae (Grine and Glendenning 2007). In sands, the cementing agents are often found to be silicates, amorphous silica, iron oxide, and calcium carbonate (Clough *et al.* 1981). Natural calcarenite (carbonate) specimens (as shown in Figure 2.1) are found to have wide variations of dry density and degree of cementation (Airey 1993). These variations complicate interpretation of the test data of actual test specimens as shown in Figure 2.2. Previous studies carried out on cemented carbonate soils such as Airey (1993), Coop and Atkinson (1993) and Haeri *et al.* (2006), also pointed out the complexity of cemented nature. Complex behaviour of cemented granular materials can lead to a significant error in the determination of bearing capacity of the foundation strata. The variable densities and difficulty of sampling without disturbing the cementation make it difficult to study the fundamental behaviour of

naturally cemented materials. Test data obtained from naturally cemented carbonate sediments are frequently highly scattered. Therefore, a general framework for the behaviour of cemented carbonated sands is very difficult to develop from the natural cemented materials. In addition, identical samples of natural cemented sand cannot be replicated for parametric studies.

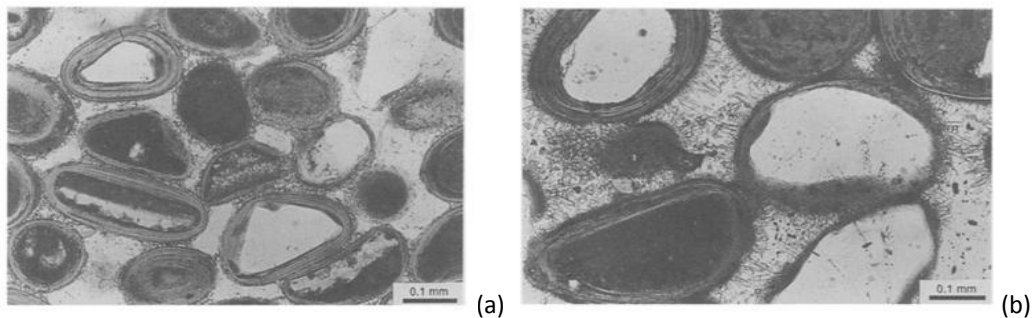


Figure 2.1 Example of natural marine cementation: (a) Ooid sand with carbonate cores; (b) Ooid sand cemented by coarse crystalline of fibrous aragonite (after Molenaar and Venmans 1993).

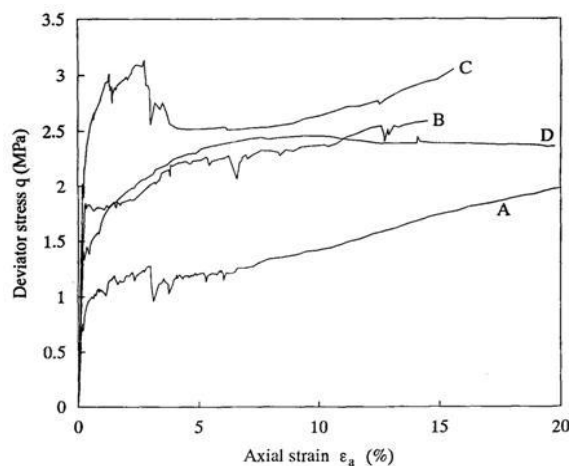


Figure 2.2 Typical drained test results of cemented carbonate soils obtained from the N-W shelf of Australia (after Airey 1993).

To examine the basic behaviour of calcarenites it is convenient to test artificially cemented carbonate sands (Coop and Atkinson 1993). In order to study the mechanics of cemented soils, it is argued that artificially cemented soil should be used in a systematic experimental study (Rosa *et al.* 2008, Lee *et al.* 2009).

2.3 Artificial cementation

Along with naturally cemented soils, several studies have been carried out on artificially bonded soils. The artificially cemented soils were created in the laboratory to simulate natural soils. By artificial cementation, the problems of variability in cement nature and cement contents were avoided that are usually associated with cementation after deposition (Clough *et al.* 1981, Coop and Lee 1993, Consoli *et al.* 2000). The studies, which were carried out using artificially cemented sands (e.g. Abdulla and Kiousis 1997, Huang and Airey 1998, Ismael 2000, Ismael 2001, Schnaid *et al.* 2001, Consoli *et al.* 2002, Castellanza and Nova 2004, Dano *et al.* 2004, Arroyo *et al.* 2005, Haeri *et al.* 2006, Consoli *et al.* 2007, Consoli *et al.* 2009, dos Santos *et al.* 2010), have provided some useful insight into the influence of cement content on the mechanical behaviour of sands. However, specimen preparation techniques must be optimized carefully in order to give reasonably close resemblance to the naturally cemented materials. Traditionally, cementing of the soils have been modelled by mixing Portland cement or gypsum powder with the uncemented soil in appropriate proportions to obtain a given strength through proper specimen preparation procedures (Ismail *et al.* 2000).

2.4 Methods of specimen preparation

It is a well-established fact that without good quality specimens no reliable experimental results could be achieved. One of the most important aspects of testing in the laboratory is using samples that are simulating their in-situ conditions. It has also been recognized by many researchers (e.g. Oda 1972, Ladd 1974, Ladd 1977, Mulilis

et al. 1977, Yamamuro and Wood 2004, Miura and Toki 1982, Kuo and Frost 1996, Frost and Park 2003, Wanatowski and Chu, 2008), that different preparation methods result in different fabrics of granular soils and, consequently, in different stress-strain characteristics of reconstituted specimens as shown in Figure 2.3. Owing to this, a number of experimental studies discussing the various effects of sample preparation methods on the stress-strain behaviour of granular soils have been reported in the past. Among the first attempts to study the effects of the specimen preparation methods on the behaviour of reconstituted sand were those of Ladd (1974, 1977), who observed that the method of specimen preparation could have a significant effect on the cyclic shear strength of sand. Similar observations were also made by Mulilis *et al.* (1977).

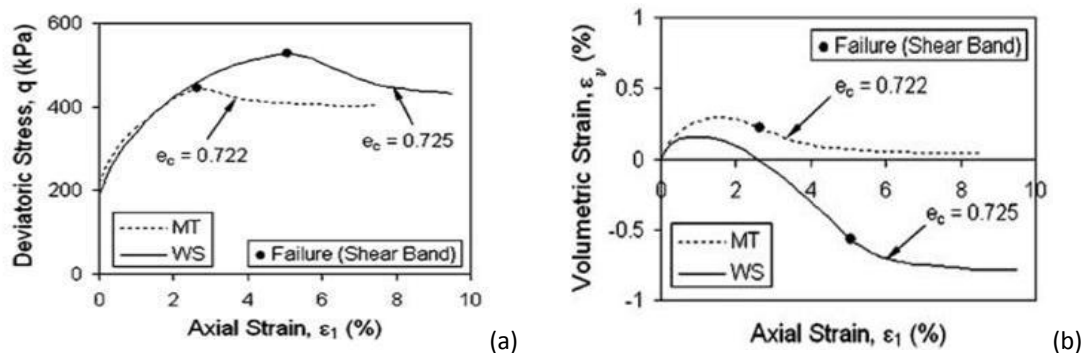


Figure 2.3 Comparison of drained tests conducted on WS and MT specimens: (a) axial strain vs. deviatoric stress; (b) axial strain vs. volumetric strain (after Wanatowski and Chu 2008).

As were reported by Huang and Airey (1998), Jiang *et al.* (2007) and several others, that the density and degree of cementation of naturally cemented carbonate sands are variable. Moreover, the materials are experienced under varying degree of confining pressures (Coop and Atkinson 1993). Therefore, these factors i.e., variation in

initial relative density, degree of cement content and magnitude of confining pressure must be considered during the specimen preparation.

2.4.1 Uncemented specimen preparation

The specimen preparation procedures for uncemented sand, which were most commonly described in the literature on triaxial testing, are air pluviation (AP), water pluviation (WP) and moist tamping methods (MT). Mulilis *et al.* (1977) observed that the MT specimens were more non-uniform than the others were. Therefore, in order to improve the uniformity of the MT specimens Ladd (1978), proposed an undercompaction procedure. In this method, the specimen is prepared using a number of layers, and each layer is compacted to a selected percentage of the required density of the specimen. Mulilis *et al.* (1978) also verified that the MT specimens prepared by the undercompaction method were more uniform than comparable specimens prepared by the constant compactive effort method proposed by Castro (1969). Vaid and Negussey (1988), on the other hand, promoted pluviation methods. They reported that pluviated specimens were more uniform than moist-tamped specimens were. A detailed study of density variations in sand specimens conducted by Gilbert and Marcuson (1988) has shown, however, that some non-uniform density redistributions within sand specimens are unavoidable, regardless of the preparation method. Ishihara (1993), in the 33rd Rankine Lecture, emphasized that apart from the basic requirement to produce homogeneous specimens, a preparation method should also be able to cover a wide density range of reconstituted specimens. He reported that the widest range of void ratio can be achieved using the MT method, al-

lowing both the contractive and dilative behaviours of sand to be studied. More recently, Yoshimine and Koike (2005) reported that homogeneous and uniform sand specimens prepared in the laboratory by either method do not generally resemble natural soil deposits, because soil structures commonly observed in nature are layered and stratified rather than homogeneous.

Despite some discrepancies in artificial specimen preparation, it is undisputed to get advantage of the existing literature in optimizing the sample preparation techniques to get a more generalized procedure; which is capable enough in capturing the basic skeleton of naturally cemented materials.

2.4.2 Cemented specimen preparation

Preparation of cemented specimens comparable in properties to the natural cemented materials in uniformity and consistent density has always been a challenge for the researchers. Reproducibility of the samples, regarding density and eventual strength is of vital concern. Therefore, different techniques of sample preparation have been proposed in the past to address the subject more accurately. Traditionally, cementing of the soils have been modelled by mixing Portland cement or gypsum powder to the soil in an appropriate proportion to obtain a given strength (Ismail *et al.* 2000). Prior to the preparation of the composite, it is also worth noting to determine the properties of the cementing agents, which are essential in determining the behaviour of cemented sands eventually. Although the formation of cemented soils is complicated, general features regarding the cement content effects

on soil properties can still be observed in a collective way based on the experimental findings (Wang and Leung 2008).

From the comprehensive review of the literature (e.g. Amini and Sama 1999, Bradshaw and Baxter 2007, Wanatowski and Chu 2008, Yang *et al.* 2008), it is apparent that the general procedure of specimen preparation for both cemented and uncemented materials for comparative study could be moist tamping method (MT). The MT method is relatively more suitable for capturing the overall behaviour of cemented materials with varying degree of initial relative densities and cement contents.

In MT method, the oven-dried soil is mixed with the required percent of cement by dry weight of soil for the preparation of cemented specimen. Mixing of dry materials is continued until a uniform appearance of the sand-cement mixture is obtained. Water is then added to the optimum moisture content of the material. Further mixing is performed until a homogeneous appearance of the moist sand-cement mixture is achieved. The mixture is then stored in an airtight container to avoid any moisture loss before subsequent specimen preparation.

For uncemented specimens the sample is prepared directly on the pedestal of the triaxial apparatus. However, in case of cemented specimens, prior to the placement of the mixture, the mould is provided with a '*thin transparency sheet*' to avoid sticking of the cement materials with the wall of the mould. The mixture is then compacted in layers into the split mould to the targeted dry unit weight. To achieve uniformity of specimens the undercompaction method, proposed by Ladd (1978) is

used. After compaction, the specimens are allowed to cure inside the mould for 24 hours. The moulds are then dismantled and the specimens are stored in a humid room to cure for a proposed curing period (commonly 7-14 days) before testing.

2.5 Factors affecting the strength of cemented soils

The knowledge and understanding of the strength controlling parameters of the test specimens play an important role for the subsequent investigations of the mechanical behaviour of materials. According to Consoli *et al.* (2007), the influence of the amount of cement, the porosity and the moisture content on the strength of an artificially cemented sandy soil, as well as the use of water/cement and a voids/cement ratio supposed to be the key parameters for strength control of artificially cemented soils.

The amount of cement content has significant effect on the strength of soil-cement composite. A small addition of cement is enough to generate a considerable gain in strength. The effectiveness of the cement is greater in more compacted mixtures (Clough *et al.* 1981, Consoli *et al.* 2007). Cement content causes formation of weak to strong bonds between soil particles. The cement bonds strongly affect the mechanical behaviour of soil. The bond strength as a function of moisture content is observed to be increasing up to the optimum moisture content (OMC), after which the strength reduces again. The change of strength is probably related to the structure created at the time of moulding, and the amount of added water would have a fundamental role in the formation of the structure. However, there has been lack of

agreement on the relationship for the effect of water/cement ratio on the strength of the cemented materials.

In brief, the agreed upon points which affect the behaviour of cemented materials and the key parameters dictating the strength of a specimen are the cement content, initial density, moisture content, curing period, proper mixing, uniform compaction, and the method of sample preparation.

The preparation and analysis of cemented specimens with varying degree of cement content and dry density can give a reasonable framework for understanding the mechanics of naturally cemented materials having spatial degree of variation in density and cement content. Confining pressures equally significantly influence the stress-strain-strength and volume change behaviour of sand under triaxial compression test. The influence of confining pressure on the plastic properties of sand, mainly for friction and dilatancy angles are of great importance. The early work of Taylor (1948) and Bolton (1986) indicated that both effective stress and soil density affect the dilative behaviour of soils and their strength parameters. Ignorance of such dilative behaviour can lead to significant errors in predicting ultimate bearing stresses, deformation, or stability of geotechnical structures.

2.6 Micromechanics of cemented sand

It is widely recognised that the mechanical behaviour of sands can be directly related to its microstructure, i.e., the geometrical arrangement of the grain particles including the forces acting between them (Wan and Guo 2001). Microscopy analysis are generally, undertaken in order to characterize the grain shapes of the hosting sand

and identify the nature of cement content due to calcite and the other particulate cementing agents. For instance, Figure 2.4 can give a good picture of the microstructure of cemented sand. Both the cemented specimens shown in Figure 2.4 demonstrate evidences of cement content on the particle surface and at particle contacts. Moreover, microscopy analysis is used to investigate the effect of compression and shearing on cement bonding and particles crushing. Other than the common factors influencing the particle breakage (such as the grain size distribution, the size and shape of the particles, the state of packing and the mineralogical composition), particle crushing during isotropic compression and shearing is perhaps the most significant phenomenon occurring at high pressures that affects the overall soil behaviour.

At high pressures, the crushing of sand particles is widely reported by many researchers such as Lee and Farhoomand (1967), Tai (1970). Lade *et al.* (1996), Yamamuro and Lade (1996), and Yamamuro *et al.* (1996), Based on laboratory experiments, some general factors have also been related to the particle crushing. For example, some researchers, such as Lade *et al.* (1996), McDowell and Bolton (1998), directly related the crushing with particle strength. According to Lade *et al.* (1996), Lee and Farhoomand (1967), and McDowell and Bolton (1998), uniform granular materials composed of large particles crushes more readily than one composed of smaller particles of the same material. DEM analysis carried out for visualization of crushing in granular materials under compression by Sebastian *et al.* (2006) reported that the crushing does not develop uniformly throughout the sample, but rather concentrate in different regions.

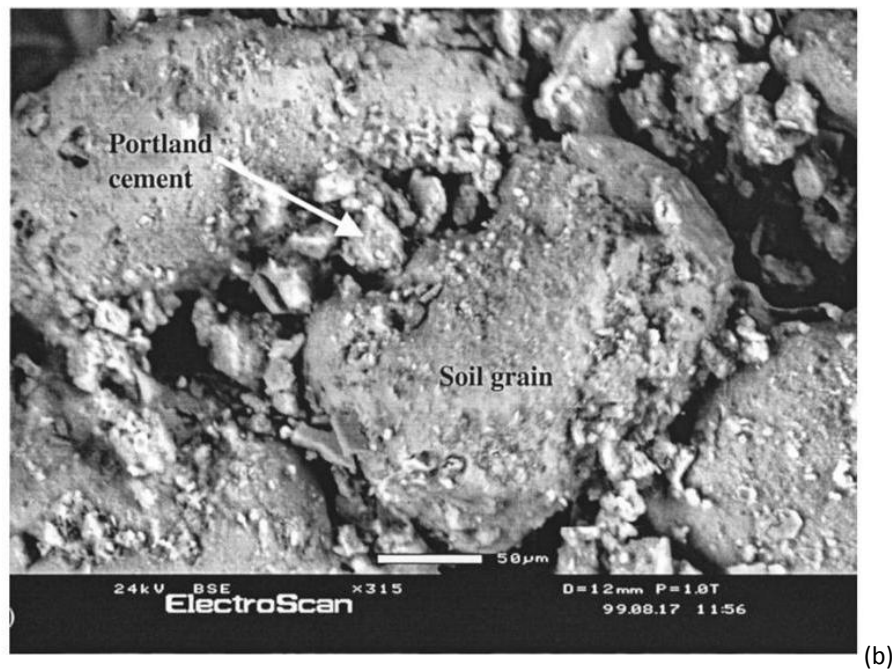
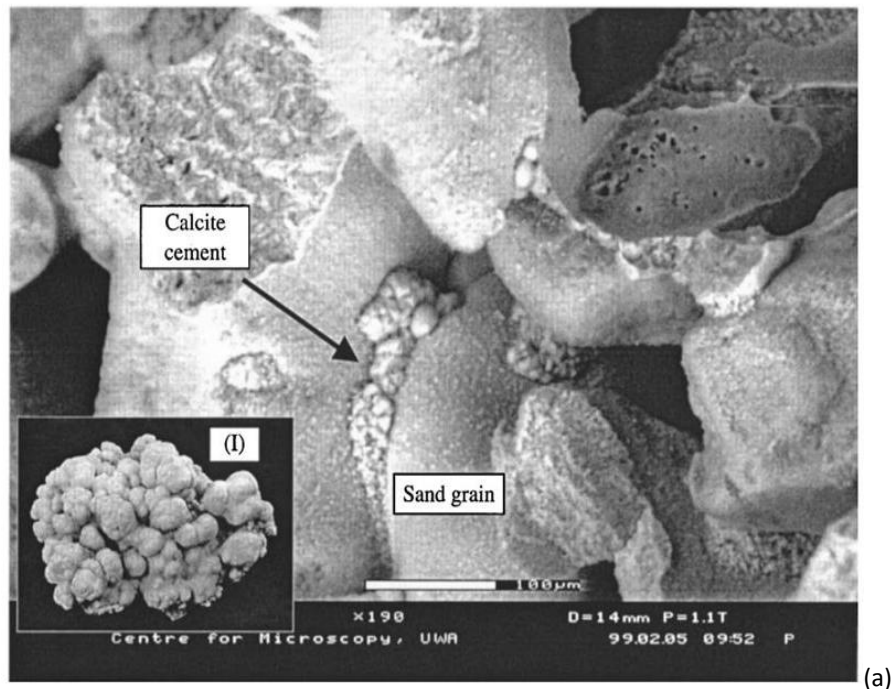


Figure 2.4 SEM micrograph of RT* sample cemented with (a) calcite; (b) Portland cement (after Ismail *et al.* 2002).

*This soil was dredged near shore from a location between Perth and Rottnest Island in Western Australia and referred to here as RT sand.

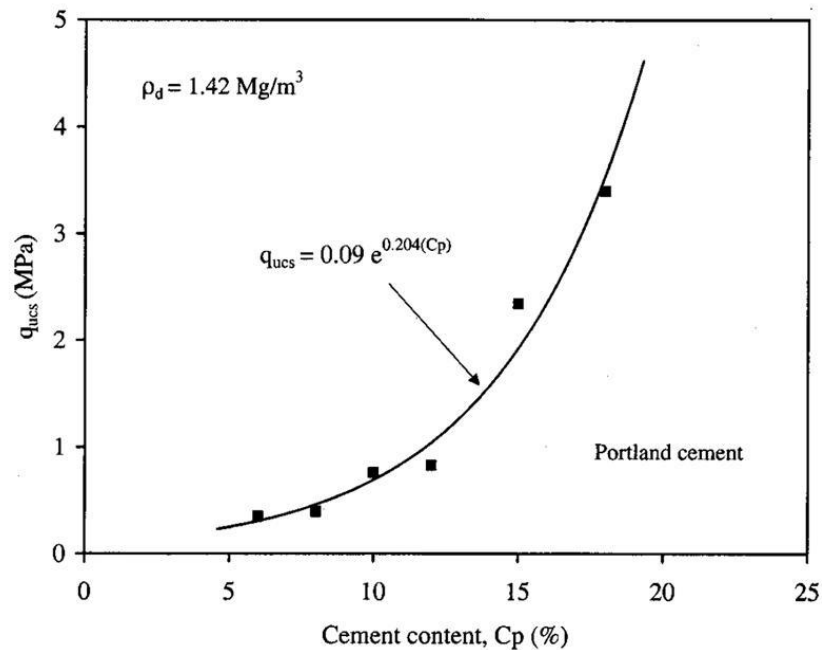


Figure 2.5 Relationship between unconfined compressive strength (q_{ucs}) and cement content for Portland cement (after Ismail *et al.* 2002).

For cemented sand, the amount, type, and location of inter-granular cements are a primary factor influencing the strength of cemented materials. Small amounts of inter-granular cement can have profound effects on bulk mechanical behaviour of the material. For instance, Figure 2.5 shows that the unconfined compressive strength can significantly increase by the increase in cement content.

However, the microscale interactions between individual constituents of the grain-cement network subjected to differential stresses and cement contents complicated with particle crushing and bond breakage at high pressures are poorly understood, inhibiting the development of a physically based link between microscopic phenomena and macroscopic behaviour. Detailed experimental characterization of these systems would improve constitutive models for the predictive modelling of geomechanical phenomena.

2.7 Isotropic compression behaviour

The compression behaviour of geomaterials has always been a topic of investigation in geotechnical engineering, because many field problems are analyzed solely based on soil properties obtained from compression tests (Pestana and Whittle 1995). For example, the great majority of settlement calculations for geotechnical structures are made based on the coefficient of compressibility of the soil layers beneath the foundations (Butterfield and Baligh 1996). In the compression characteristics, one of the major parameter is the structure of the material. Apart from that, natural calcarenite specimens were also found to have wide variations of dry density and degree of cement content (Airey 1993). These variations complicate interpretation of the test data (as shown in Figure 2.6). The engineering responses of non-carbonate and carbonate sands at same void ratios show similar behaviour when compared (Semple 1988), suggesting that the differences in engineering response are primarily related to the differences in their in situ void ratios and can be characterized from the normal compression line. The normal compression line (NCL) may be characterized by equation (2.1).

$$v = N - \lambda \ln p' \quad (2.1)$$

Where, N = volume intercept of isotropic normal compression line at $p'=1$ kPa; and λ = gradient of normal compression line.

2.7.1 Density and cement content effect on compression

Some researchers have reported that the isotropic compression curves of sand cannot be represented by straight lines in the space of specific volume v versus logarithm of mean stress $\ln p'$. However, these curves seem to approach an asymptotic

line at high stresses (Lee and Seed 1967). On the other hand, it has been reported that the specimens with different initial specific volumes converged to a unique normal compression line (NCL) in the v - $\ln p'$ plane at high pressures (Coop and Lee 1993, Dos Santos *et al.* 2009). However, the location of normal compression line changes with the inclusion of cements or fibres, as shown in Figure 2.7 and Figure 2.8. It can also be seen that the materials with different initial void ratios consolidated at high pressures converges to a unique void ratio as shown in Figure 2.9.

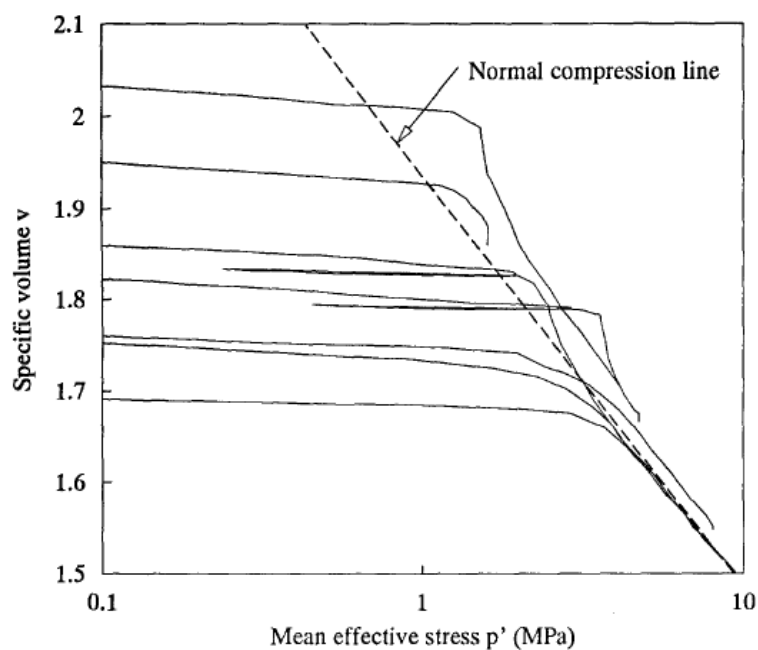


Figure 2.6 Isotropic compression responses (after Airey 1993).

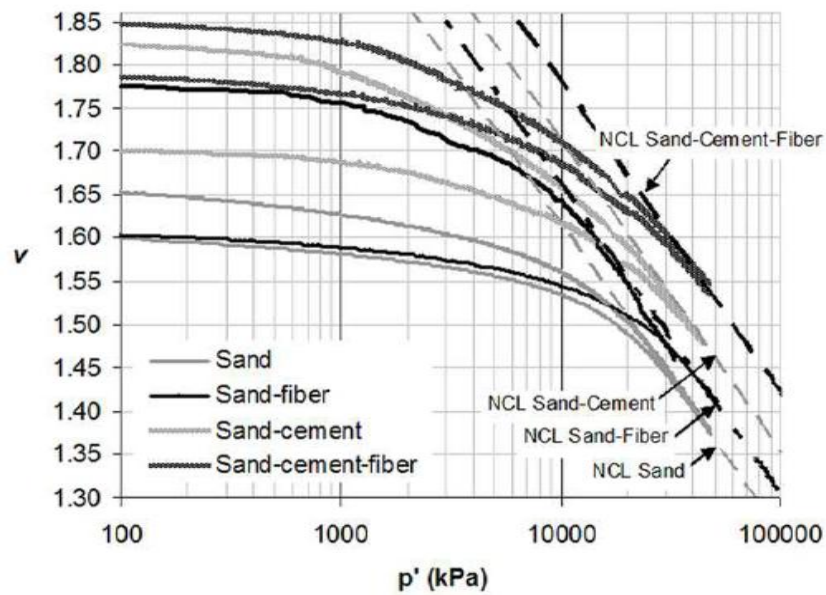


Figure 2.7 Isotropic compression lines for sand, fibre reinforced sand, cemented sand, and cemented fibre reinforced sand (after Dos Santos *et al.* 2009).

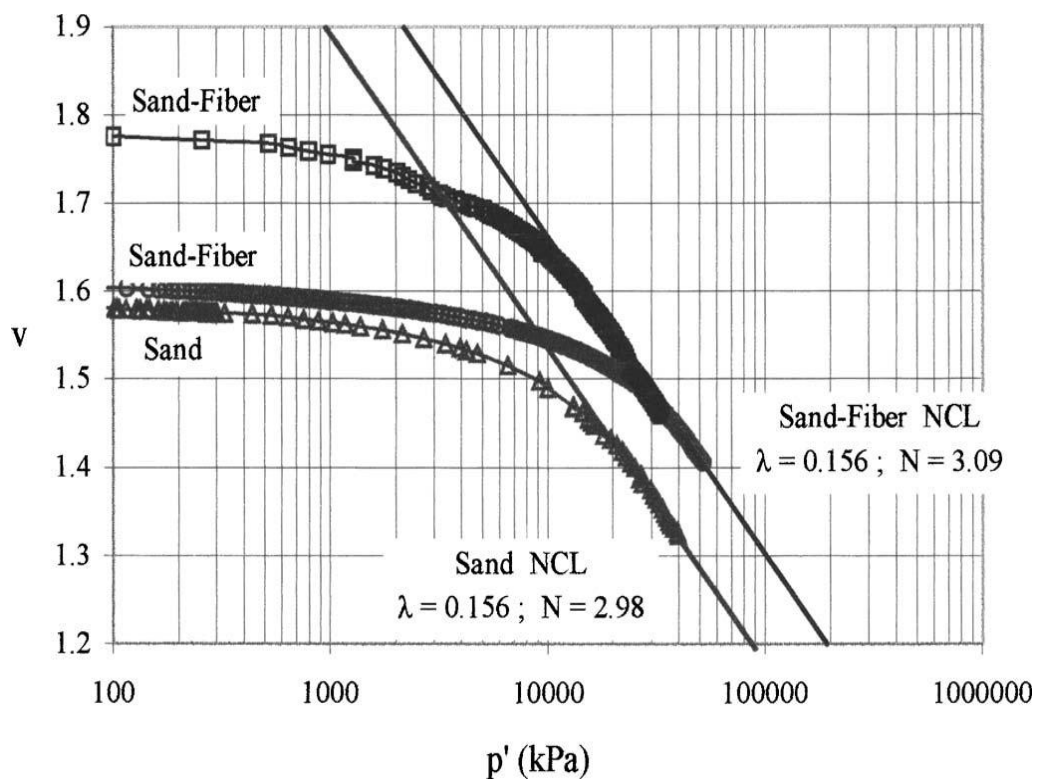


Figure 2.8 Isotropic compression data for sand and fibre-reinforced sand (after Consoli *et al.* 2005).

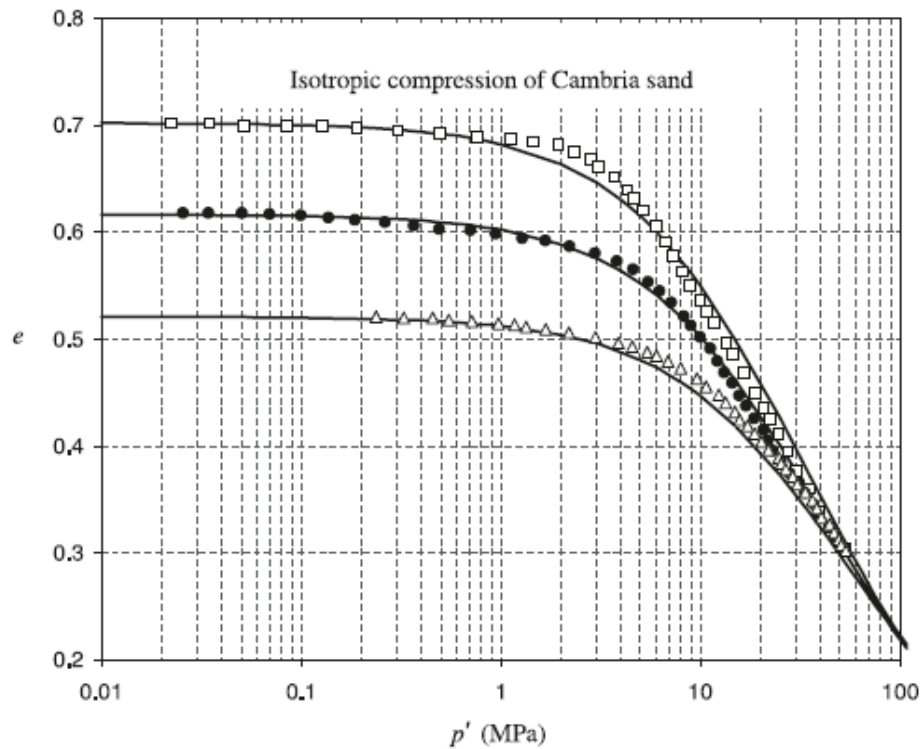


Figure 2.9 Isotropic compression curves of Cambria sand at different initial void ratios (after Bopp and Lade 2005).

2.7.2 Particles crushing and cement bond breakage during isotropic compression

It has been reported in the literature (e.g. Jefferies and Been 2000, Hyodo *et al.* 2002, Youwai and Bergado 2003, Cheng *et al.* 2003, Russell and Khalili 2004, Bopp and Lade 2005, Lade and Bopp 2005), that sand under isotropic loading is relatively incompressible at low stresses, and large volume changes only occur at very high stress levels, where, presumably particle crushing becomes dominant mechanism of volume change. According to Yamamuro and Lade (1996), the particle crushing during isotropic compression can be identified from the dip in the compression curve as shown in Figure 2.10. However, there is no other well-established technique suggested for the particle crushing during isotropic compression. Moreover, the effect

of cement content and density on particle crushing during isotropic compression is still not yet fully investigated.

Therefore, the behaviour of cemented sand under isotropic compression at high pressures in exploring the cement content effects on particle crushing would be significant. Moreover, comparison with uncemented sands including the effects of cement contents, dry density, and void ratio can give a reasonable framework in understanding naturally cemented materials with spatial degree of cement content and confining pressures. Scanning electron microscopy (SEM) analysis is also becoming a popular and emerging technique for the microscopic study of the granular materials, and can be better used for the microscopic study of the exhumed specimens after compression.

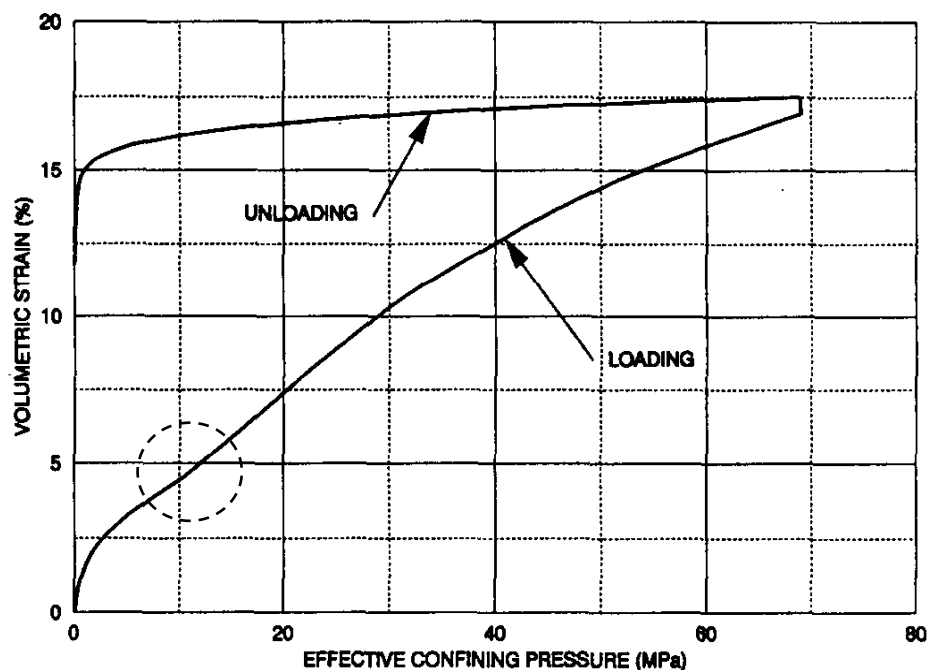


Figure 2.10 High-pressure isotropic compression test on dense Cambria sand (after Yamamuro and Lade 1996).

2.8 Triaxial compression behaviour

2.8.1 Drained behaviour

Isotropically consolidated drained triaxial compression tests provide data, which is useful in determining the strength, deformation, and volume change properties of soils. The determination of strength envelopes and the development of relationships to interpret and evaluate test results are quite significant for understanding the behaviour of cemented materials at high pressures.

The major characteristics of cemented materials vitally needed for any design, exploration, and construction on these materials, such as: compression, Shear strength, stiffness, softening, dilation, failure, critical state, and yielding can be investigated comprehensively through triaxial testing. The shear strength of soils under varying drainage conditions has also been a topic of significant interest for the last four decades.

There is general understanding that, for a given range of stresses, shear strength of naturally and artificially cemented sands can be represented by straight Mohr-Coulomb envelopes defined by the cohesion intercept (c). The Mohr-Coulomb envelope is a unique function of cement content, and the friction angle (ϕ'); and supposedly not affected by the amount of cement content. As for deformability concerned, cemented soils show a very stiff behaviour before yielding, which is governed by cement content.

The deformation and subsequent failure of cemented materials can be well characterized by the response of the material under compression. For instance, the mechanical property used to describe the extent to which materials can be deformed plastically without fracture is termed as ductile behaviour. Whereas, the characteristics of the material which is liable to fracture when subjected to stress i.e., it has little tendency to deform (or strain) before fracture and there is little or no evidence of plastic deformation before failure is called brittle behaviour. For cemented sand during compression the brittle behaviour changes to a ductile soil response as the stress level changes from low to high (Schnaid *et al.* 2001).

According to Leroueil and Vaughan (1990), the stress-strain behaviour of naturally and artificially cemented soils is basically, dependent on their initial state, yielding, and the critical state of the non-structured remoulded soil. Following the same concept, Coop and Atkinson (1993) described the idealized behaviour of cemented soils, which is divided into three different classes, as illustrated in Figure 2.11. The first class (1 in Figure 2.11) occurs when the soil reaches its yield stress during isotropic compression. In this case, shearing will produce a similar behaviour to that observed for an equivalent non-structured soil. The second class (2 in Figure 2.11) occurs for intermediate stress states, in which the bonds will be broken during shear; the strength is controlled by the frictional component of the equivalent non-structured soil and the stress-strain curve shows a well-defined yield point after an apparent linear behaviour. In the third class (3 in Figure 2.11), the soil is sheared at low confining stresses. A peak in the stress-strain curve occurs at small strains and stresses outside the limit state surface of the equivalent non-structured soil.

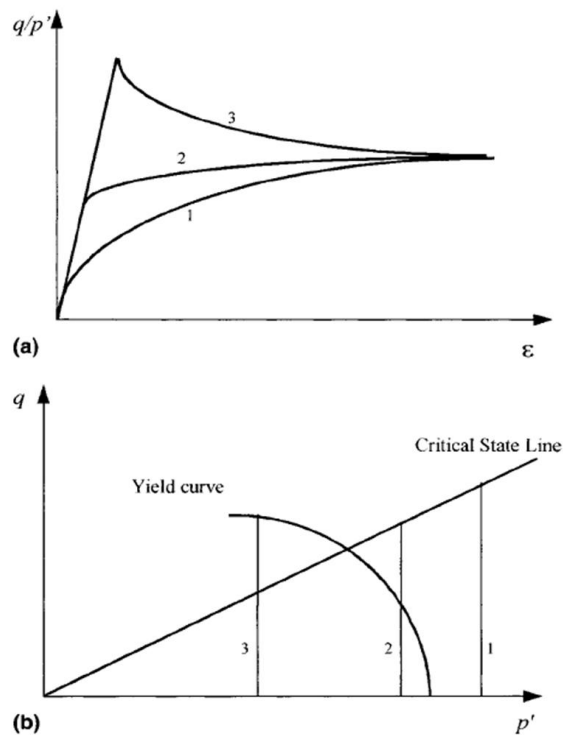


Figure 2.11 Idealized behaviour of cemented soil: (a) stress-strain curves; (b) effective stress paths (after Coop and Atkinson 1993).

So far, most of the investigations are conducted on samples with low cement contents and limited effective confining pressures. While normally, the cement content and pressure ranges are quite wider. For instance, the foundations of offshore structures laid on calcarenite can have spatial degree of cement content and could be experienced to high-pressure levels. Therefore, further experiments must be carried out at high pressures to cope with such challenges.

2.8.2 Undrained behaviour

The behaviour of granular materials can normally be accurately characterized for practical applications from results of drained tests, since in many problems the material can usually be considered fully drained. However, if the permeability of the material is relatively low, as in cemented sands, undrained condition can exist. The

undrained behaviour is of utmost importance for strength and deformation analyses in cemented sand under short-term conditions. Consideration of how the undrained shear strength of cemented sand is related to changes in pore pressure provides a more useful and practical framework for understanding the undrained strengths of these materials, and for characterizing undrained strengths for practical purposes.

The undrained strength in steady-state is simply defined as the state of deformation without any increment of stress components, then it may appear at two stages during undrained triaxial compression tests on loose sand under relatively low initial confining stress levels. The first is quasi steady state (QSS) following unstable deformation after peak stress state, and the other is ultimate steady state (USS) at the final stage of shear deformation. Quasi steady state appears at the state of phase transformation. Phase transformation is the state of minimum effective mean stress during undrained shear. At quasi steady-state not only mean stress but also shear stress components are minimum. When initial effective confining stresses are large enough, no hardening will develop after the reduction in strength and the minimum stress state becomes ultimate steady state. This state is called critical steady state (Yoshimine and Ishihara, 1998). Figure 2.12 indicates the definitions of Phase transformation, quasi steady state, critical steady state, and ultimate steady state.

The type of behaviour obtained from an undrained triaxial test depends on the relation between the initial void ratio of the sand tested, e_0 , and the critical void ratio, e_{cr} , which sets the boundary between strain hardening and strain softening behaviour of the sand under the given mean effective stress.

The stress-strain behaviour of uncemented sand under undrained conditions is void ratio dependent and may vary from strain softening to strain hardening type. Typical stress-strain behaviour of sand in an undrained triaxial test is presented schematically in Figure 2.13(a). It can be seen that for loose sand with $e_0 > e_{cr}$ (i.e. looser than critical void ratio) deviatoric stress reaches its peak and then decreases to an ultimate value with increasing axial strain. This type of behaviour is termed as the strain softening or the steady state of deformation where the soil is deforming continuously at constant volume and under constant stress state (Poulos *et al.* 1985). When $e_0 = e_{cr}$, the deviatoric stress maintains constant after the peak is attained, as shown in Figure 2.13(a). Once the void ratio of the soil, e_0 , is greater than, the critical void ratio, e_{cr} , the strain hardening behaviour is observed. Furthermore, the smaller the void ratio (i.e. the higher density), the stiffer stress-strain response is measured, as shown in Figure 2.13(a).

The corresponding effective stress paths of the stress-strain curves shown in Figure 2.13(a) are plotted in Figure 2.13(b) together with the critical state line (CSL) and the failure line (FL) obtained from drained triaxial tests on loose and dense sand, respectively. As shown in Figure 2.13(b), in the undrained test on loose sand with $e_0 > e_{cr}$ the effective stress path increases gradually towards the peak state and then traces down towards the CSL showing flow or strain softening behaviour.

The effective stress path of loose sand with $e_0 = e_{cr}$ also increases towards the peak state but then remains constant at the critical state. For loose sand with $e_0 < e_{cr}$, the

effective stress path of an undrained test increases towards the peak and then follows the CSL.

The effective stress path obtained from an undrained test on dense sand with e_0 much smaller than e_{cr} is also shown in Figure 2.13 (b). It can be seen that for dense (i.e. dilative) sand, the effective stress path of a CU test will increase monotonically and approach a constant stress ratio line (CSRL). In this case, a peak state and the critical state are no longer obtainable and strain-hardening behaviour is obtained throughout the entire undrained shearing.

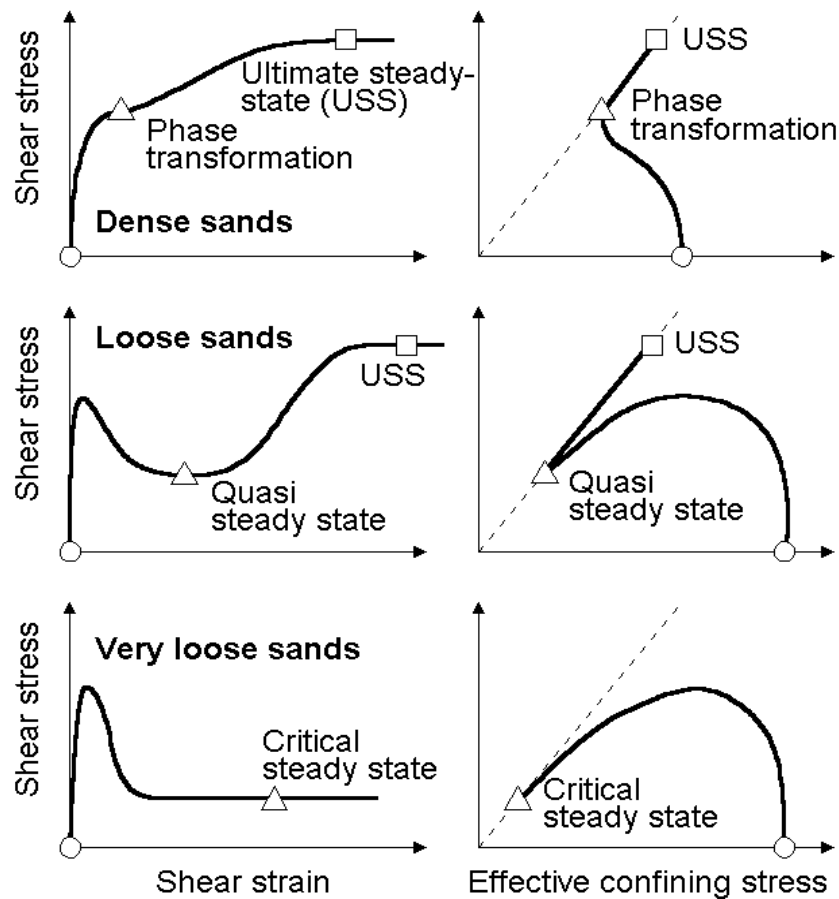
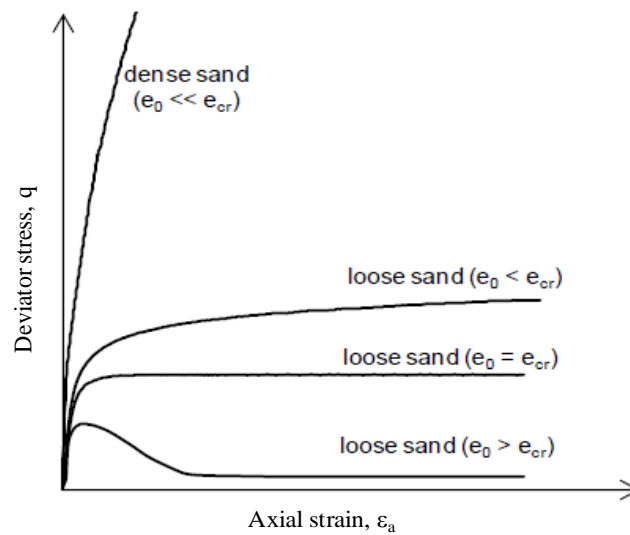
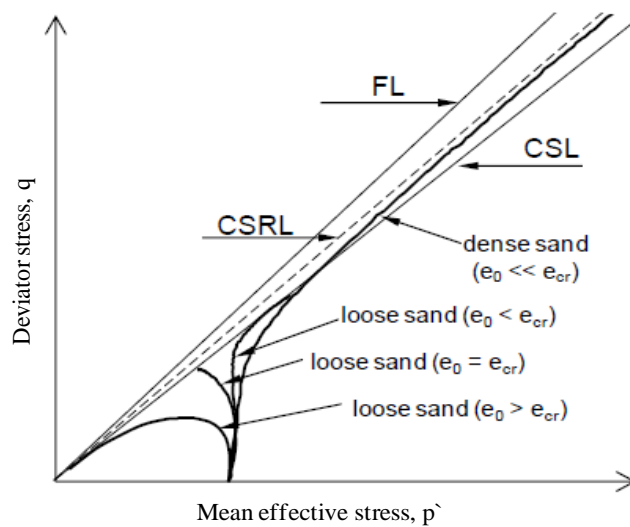


Figure 2.12 Illustration of undrained strength and stress paths (after Yoshimine *et al.* 1999).



(a)



(b)

Figure 2.13 Typical behaviour of loose and dense sand under undrained conditions: (a) stress-strain curves; (b) effective stress paths (after Tsai *et al.* 2010).

2.8.3 Comparison of drained and undrained behaviour

Normally, the stress paths from undrained tests define a similar failure envelope to that, which is defined by the drained tests. However, certain deviation in the drained and undrained stress paths was also reported by some researchers. For instance, in case of different depths of sampling as reported by Futai *et al.* (2004), it can be seen

that the undrained stress paths cross the failure envelope as shown in Figure 2.14. According to Asghari *et al.* (2003), in the cemented materials, the undrained tests cross the failure surface defined by the q_{\max} points from drained tests, showing that the material can attain higher stress ratios when sheared in undrained conditions as shown in Figure 2.15.

The difference between limiting stress ratios from undrained and drained tests is likely to be due to the fact that volumetric straining (as happens in the drained tests) will contribute to breakdown of the cemented bonds (Malandraki and Toll, 2001). When volume strains are prevented (in undrained tests), a higher stress ratio can be sustained before the bonds break down (Asghari *et al.* 2003). The mechanism of failure envelopes, dilation envelopes and critical state envelopes were investigated at conventional pressure. The progressive effect on these envelopes by the gradual increase in confining pressure for a wider range is significantly interesting. Therefore, it further elaboration with different amount of cement contents at high confining pressures.

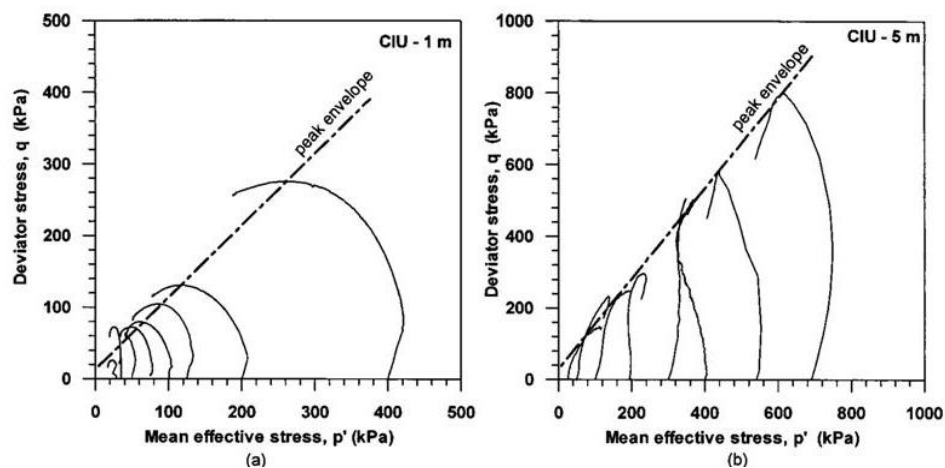


Figure 2.14 Undrained stress paths at a depth of: (a) at 1 m; (b) at 5 m (after Futai *et al.* 2004).

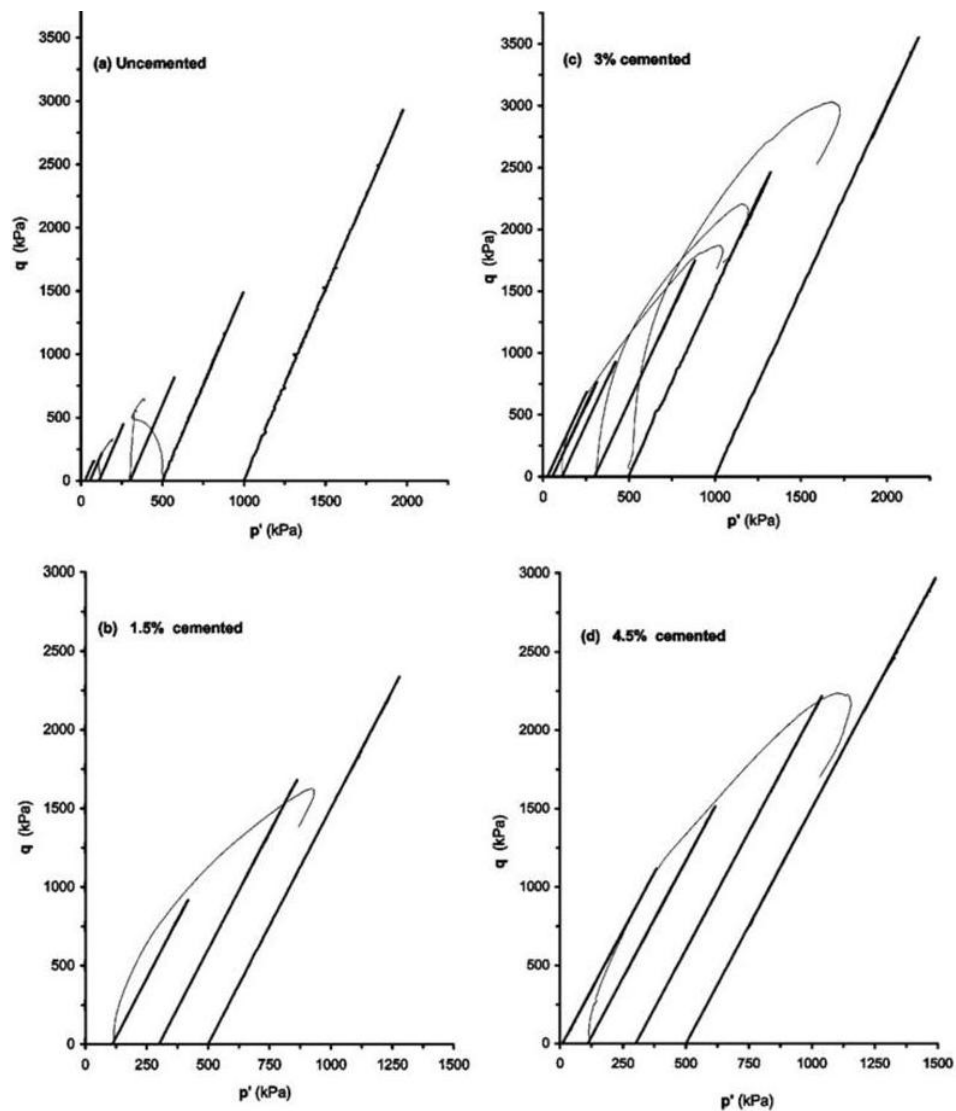


Figure 2.15 Effective stress paths for drained and undrained tests of Tehran alluvium with cement contents of: (a) 0%; (b) 1.5%; (c) 3%; (d) 4.5% (after Asghari *et al.* 2003).

2.9 Failure characteristics

The term failure is used to refer to the state of a specimen at its maximum load bearing capacity, which corresponds to the apparent peak average stress observed in a test (Huang *et al.* 2007). Failure may occur under uniform deformation conditions or localized deformation conditions. Typically the failure of a geotechnical materials can be categorized as Peak failure, localized failure and bulging failure. However, this has been controversial issue to the researchers for some reasons. The degree of cement

content and level of confining pressure affect the mechanism of failure in cemented materials. However, the effect of high confining pressure needs further investigations on the types and modes of failure.

2.9.1 Types and modes of failure

The major types of failure reported in the literature are peak, localized and bulging failure. The peak failure is indicated by a gradual degradation of the average strength after the peak is reached. The Localized failure is characterized by the development of shear bands around the apparent peak and is often indicated by a sudden reduction in the average strength. And the Bulging failure is primarily caused by friction on the top and bottom faces of a specimen acting in combination with a flexible lateral boundary (Huang *et al.* 2007). Rowe and Barden (1964) have highlighted the value of lubricated and enlarged end platens in preventing non-uniform deformation and the development of shear bands.

The main types of mode of failure can be characterized as the ductile and brittle modes of failure. The possible modes of failure are illustrated in Figure 2.16. Ductile behaviour is characterized by contractive response and gradual deformation to failure. Ductile response usually produces more diffused deformation, as typically evidenced by lateral expansion of cylindrical specimens loaded in shear, with less distinct shear failure surface. Brittle deformation is characterized by dilative response and sudden failure at a well-defined peak shear strength followed by strain softening down to residual shear strength. Brittle response can be accompanied by the formation of distinct shear failure surfaces (Nygard *et al.* 2006).

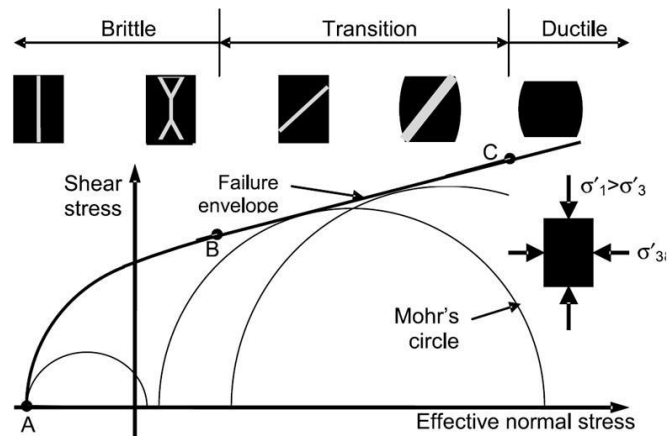


Figure 2.16 Mohr diagram showing possible modes of failure and fracturing (after Nygard *et al.* 2006).

2.9.2 Failure criteria

The purpose of failure criteria is to predict or estimate the failure/yield of soils. The Strength Parameters only allow defining the failure (strength) criterion for a material. For elastic materials, that returns to its original shape after the stress (e.g. external forces) that made it deform is removed the failure criterion parameters will only be used for the calculation and plotting of strength factor within the material. Although an elastic material cannot "fail", the failure envelope allows a degree of overstress to be calculated.

For plastic material, which describes the deformation of a material undergoing non-reversible change of shape in response to applied forces the strength parameters will be used in the analysis if yielding occurs. This is unlike Elastic materials, where the strength parameters are only used to obtain values of strength factor, but do not affect the analysis results (i.e. stresses and displacements are not affected).

For a plastic material depending on the strength criterion, residual strength parameters and a dilation parameter also need to be defined. If the residual strength pa-

rameters are equal to the peak parameters, then it is an "ideally" elastic-plastic material.

Mohr–Coulomb theory is a mathematical model, in geotechnical engineering; it is used to define shear strength of soils and rocks at different effective stresses. The Mohr–Coulomb failure criterion represents the linear envelope that is obtained from a plot of the shear strength of a material versus the applied normal stress. This relation is expressed as:

$$\tau = c + \sigma \tan (\phi) \quad (2.2)$$

Where, τ is the shear strength, σ is the normal stress, c is the intercept of the failure envelope with the τ axis, and ϕ is the slope of the failure envelope. The quantity c is often called the cohesion and the angle ϕ is called the angle of internal friction.

From Mohr's circle we have

$$\sigma = \sigma_m - \tau_m \sin \phi \quad (2.3)$$

$$\tau = \tau_m \cos \phi \quad (2.4)$$

Where,

$$\tau_m = \frac{\sigma_1 - \sigma_3}{2} \quad (2.5)$$

$$\sigma_m = \frac{\sigma_1 + \sigma_3}{2} \quad (2.6)$$

and σ_1 is the maximum principal stress and σ_3 is the minimum principal stress. Therefore, the Mohr–Coulomb criterion may also be expressed as:

$$\tau_m = \sigma_m \sin\phi + c \cos\phi \quad (2.7)$$

$$\text{Or} \quad \frac{\sigma_1 - \sigma_3}{2} = \frac{\sigma_1 + \sigma_3}{2} \sin\phi + c \cos\phi \quad (2.8)$$

This form of the Mohr–Coulomb criterion is applicable to failure on a plane that is parallel to the σ_2 direction. The criterion is shown in normal stress-shear stress space in Figure 2.17.

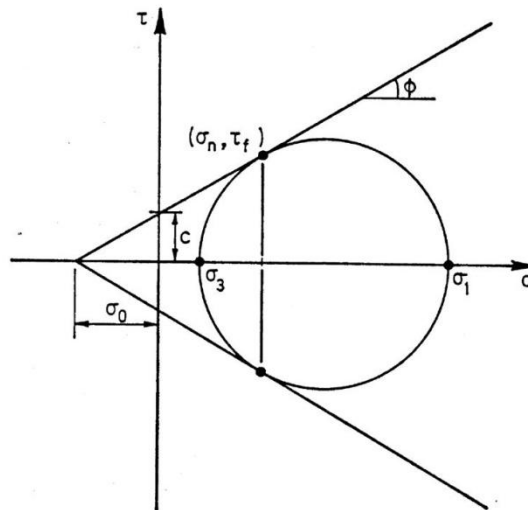


Figure 2.17 Failure criterion in normal stress-shear stress space (after Hously 1986).

In triaxial compression tests, the failure can be estimated from maximum stress difference ($\sigma'_1 - \sigma'_3$), or stress ratio (σ'_1 / σ'_3).

Various researchers explored the factors affect the failure mechanism in the past. The shear band thickness was found to increase as the surface roughness of the particles, particle size, and the particle angularity index increase while it tends to decrease as the particle sphericity, initial density and the confining pressure increase (Alsaleh *et al.* 2006). Yet, no well-formulated equations have been developed to quantify the effect of the surface roughness and grain shape on the thickness or/and

the inclination of the shear band (Alsaleh *et al.* 2006). Vardoulakis and Sulem (1995) emphasized that the surface roughness will affect the inter-particle slipping in granular materials. Huang *et al.* (2002), attempted to bring the surface roughness and shape of the grains into a hypoplastic numerical model to study their effect on the strain localization in granular materials.

In the failure state of cemented soil, the effects of cement content ought to make the strength of soil increase and extend the domain in which soil can exist. How the high confining pressure affect the failure mechanism of cemented materials is not yet fully investigated; because most of the previous investigations were limited to the conventional range of pressures. Therefore, investigations of cement content and high confining pressures effects on the failure of the material would be very interesting to explore.

2.9.3 Strain localization and shear band characterization

The process, which gives rise to shear bands, is known as “strain localization”. The local behaviour is considered to be inside the shear band and the global one is shear band patterning at the scale of the specimen (Desrues and Viggiani 2004). The strain localization is now generally recognized as a major factor governing the overall response of structures at or near failure. Strain localization manifests itself in the form of a shear band, a narrow zone of intense straining. It is now generally recognized that the intense deformation in the shear bands is primarily responsible for the accelerated softening response exhibited by most structures at post peak strength.

Strain localization is caused by the imperfections inherent in the medium, the boundary constraints, and non-uniform loading conditions. An ideal solution would capture all of these imperfections and irregularities, but this may not be possible since these defects and irregularities to a certain extent are usually unknown to the analyst. Sometimes this may cause due to high loading conditions. When a specimen subjected to high loading conditions, the initially smooth distribution of strain changes into a highly localized one, typically, the strain increments are concentrated in narrow zones while the major part of the specimen experiences unloading.

In case of strain localization during shear deformation, the deformation process diffuses at first, and then tends to concentrate in narrow zones called shear bands. Non-uniform deformation is supposed to be one of the main reasons for developing shear bands. Rowe and Barden (1964) have highlighted the value of lubricated and enlarged end platens in preventing non-uniform deformation and the development of shear bands. The main subjects of interest regarding shear bands are the orientation (Roscoe 1970, Arthur *et al.* 1977), the thickness (Roscoe 1970), and the initiation period.

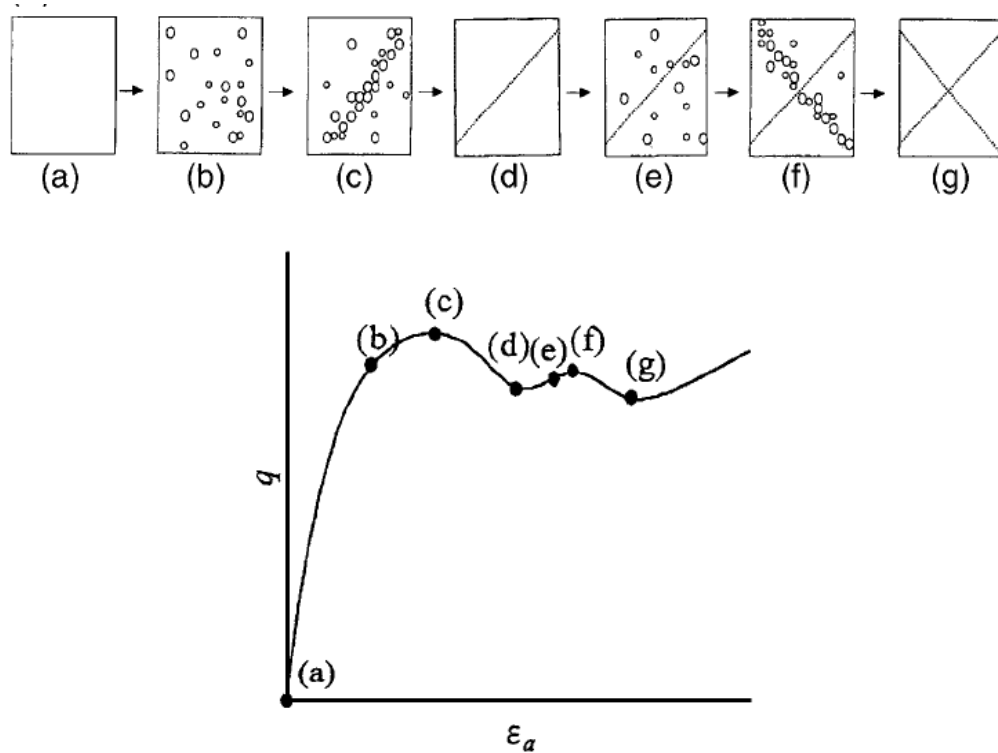


Figure 2.18 Illustration of progressive failure of sands in drained triaxial tests: (a) initial condition; (b) occurrence of dilative strain areas; (c) continuous linking of dilative strain areas; (d) fully developed shear band; (e) further occurrence of dilative strain areas; (f) continuous link of dilative strain areas; (g) “diagonally crossing shear bands;” and (h) q versus ε_a (after Suzuki and Yamada 2006).

For dense sands, several researchers have studied the local behaviour of shear bands using internal measurement techniques. Shear banding occurs with the strain-softening response. In addition, the appearance of shear banding becomes more visible with increasing cement content, and it cannot be observed at high confining pressures, which exhibits only a bulging type of failure. Because of the complex pattern of shear banding, it is difficult to accurately measure the angles of shear bands with respect to the horizontal axis. There is also no clear trend that the orientation is a function of the degree of cement content or confining pressure. This suggests high sensitivity of the shear band orientation with testing conditions.

2.10 Stress-dilatancy theory

The observed tendency of a compacted granular material to expand in volume as it is sheared is termed as dilatancy. The volume change plays an important role in the stability of frictional materials. For instance, it adds higher shear strength to the materials during shear, which is due to the apparent cohesion results from the tendency of soil to expand. The variation of dilatancy rate depends on the initial packing, with denser materials showing a more rapid decrease in dilatancy rate than loose materials. Ignorance of dilative behaviour can lead to significant errors in predicting ultimate bearing stresses, deformation, or stability of geotechnical structures.

The physical manifestation of dilatancy was first identified by Reynolds (1885), and long afterward, Rowe (1962) introduced a stress-dilatancy theory. The early work of Taylor (1948) and Bolton (1986) indicated that both effective stress and soil density affect the dilative behaviour of soils and their strength parameters. Lade and Yamamuro (1993) indicated that post peak softening requires volume dilation and it can be observed in drained tests on dense granular materials sheared under low effective confining pressures. Especially densely packed sands, tend to dilate during shear loading. The dilative behaviour of granular soils is important when analyzing critical or ultimate states and has significant influence on the apparent strength of granular soils (Chen *et al.* 2003).

There can be several factors that may instigate or influence the dilatancy into the granular materials. However, more frequently discussed factors in the literature are the initial relative density, cement content, and relative magnitude of confining pres-

sure. For instance, incorporation of cement component into the mechanical response of sand affects dramatically the stress–dilatancy behaviour of the sand. At a stress state remote from failure, a cemented soil has lower dilatancy relative to the parent soil because of the presence of significant bonding (Lo *et al.* 2003). However, bond breakage occurring at higher shear stress lead to a more dilatant soil fabric. Lade and Overton (1989) reported that the cemented specimens have higher dilatancy at failure as compared to the parent soil, and this higher dilatancy at failure is an important contributor to the higher shear strength. In most cases, granular soils would reach their maximum volume change at their peak strength stages, and start to exhibit plastic flow. It is also reported that there is decrease in the rate of dilation by the increase in confining pressure. Therefore, the progressive suppression of dilatancy with gradual increase in the confining pressure needs further investigations. The effect of cement content instigating dilatancy can be noticed from Figure 2.19, in which all of the samples are prepared with very similar void ratios and are in a loose state, all the Portland cement samples exhibiting volumetric dilation upon shearing even with 1% cement content; whereas, the uncemented sample is showing volumetric contraction. Therefore, in this case the volumetric dilation is completely due to the cement content effect and not to the density effect. However, such a general explanation requires further elaboration.

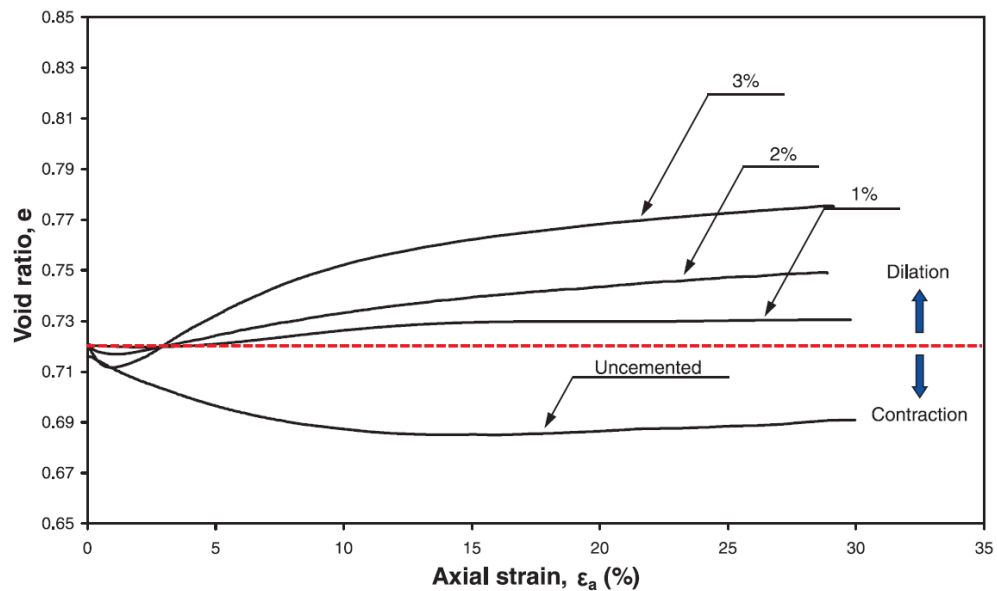


Figure 2.19 Void-ratio variations of Portland cement sand samples in response to shearing at 100 kPa confining pressure (after Wang and Leung 2008).

At high stresses, the suppression of dilatancy rate plays an important role in controlling the shear behaviour of cemented sand. The influence of the confining pressure on the plastic properties of sand, mainly for friction and dilatancy angles are of significant importance. Moreover, the progressive suppression of dilation in cemented materials by the gradual increase in confining pressures is quite important to incorporate into the design considerations and need further elaboration.

2.10.1 Dilatancy angle

On the bases of experimental investigations, it was reported that under high pressures there is significant decrease in the volumetric dilation and angle of internal friction due to the crushing of the particles (Vesic Clough 1968, Banks and MacIver 1969, Miura *et al.* 1984, Bolton 1986, Golightly and Hyde 1988, Lade and Yamamuro 1996, Yamamuro and Lade 1996). The test results obtained by Ponce and Bell (1971), Fykushima and Tatsuoka (1984), Tatsuoka *et al.* (1986), Maeda and Miura (1999)

demonstrate that the decrease in the cell pressure leads to a strong increase in both friction and dilatancy angles. Vermeer and de Borst (1984) first reported the typical values of dilation angles of various geological materials based on the empirical data. According to this empirical data the dilation angle of dense sand is 15° and for loose sand $<10^{\circ}$. The dilation angle values suggested by Vermeer and de Borst are presently used in most geotechnical numerical analysis software. Bolton (1986) proposed a theoretical solution of the maximum dilation angle in the plane strain condition, suggesting the typical dilation angle of granular soil is in the range of 10 to 20 degrees and discussing the effect of confining pressure only at the stress level where granular particles start being crushed. He introduced a simple relationship between the angle of friction and dilation, which is given in the following equation (2.9).

$$\phi'_p - \phi'_{cs} = 0.5\psi \quad (2.9)$$

where, ϕ'_p is the peak friction angle, ϕ'_{cs} is the critical state friction angle and ψ is the dilatancy angle.

To quantitatively describe the dilatancy of granular soils, the dilation angle defined by the following equation introduced the direct dilatancy measurement of granular soils. The peak dilation angle is defined as the dilation angle when granular soil has its peak strength (Chen *et al.* 2003) as given in equation (2.10). The effective angle of internal friction is given in equation (2.11). The fact that the friction angle depends on the confining stress is generally admitted in the literature. Eq. (2.11) clearly shows pressure dependency of the frictional angle.

$$\tan\psi' = -\left(\frac{\delta\varepsilon_v}{\delta\varepsilon_q}\right) \quad (2.10)$$

where, ψ' is the effective dilation angle, ε_v is volumetric strain, and ε_q is shear strain.

$$\phi' = \sin^{-1}\left(\frac{\left(\frac{\sigma'_1}{\sigma'_3}\right)_{\max} - 1}{\left(\frac{\sigma'_1}{\sigma'_3}\right)_{\max} + 1}\right) \quad (2.11)$$

where, ϕ' is effective friction angle.

Not many experiments were carried out to investigate the behaviour of granular materials for a wide range of confining pressures and initial densities. However, the experiments carried out for a wide range of pressures led to a similar conclusion (Lee and Seed 1967, Verdugo and Ishihara 1996). For engineering practice, dilation angles of soils are often estimated from direct shear test data by measuring the maximum upward angle of the vertical displacement versus horizontal displacement curve. Dilation angles of soils can also be obtained by measuring the slope angles of linear portion of the volumetric strain versus axial strain curve of consolidated and drained triaxial tests (CD) with volume change measurement.

2.10.2 Stress-dilatancy relation

A great deal of attention has been given to the stress-dilatancy relationship of soils (e.g. Rowe 1962, 1963, Nova 1982, Bolton 1986, Wood 1990, Been and Jefferies 2004). Although there are several stress-dilatancy relationships in the literature, they retain the general form of Rowe's original equation, derived from minimum energy considerations of particle sliding (Rowe 1962). Rowe's stress-dilatancy relationship is commonly expressed as $R=K_cD$, where R is the ratio of principal stresses, K_c is a constant and $D = (1 - d\varepsilon_v/d\varepsilon_q)$ is the rate of dilatancy related to volumetric and major

principal strain rates. Following the work of Rowe (1962), the following stress-dilatancy relationship can be used to describe the rate of dilatancy of a cemented (or bonded) soil as given in equation (2.12).

$$\frac{\sigma'_1}{\sigma'_3} \times \frac{1}{1 - \frac{\partial \varepsilon_v}{\partial \varepsilon_q}} = \tan^2 \left(\frac{\pi}{4} + \frac{\phi'_f}{2} \right) + \frac{2c}{\sigma'_3} \tan \left(\frac{\pi}{4} + \frac{\phi'_f}{2} \right) \quad (2.12)$$

$$D = \frac{\frac{\sigma'_1}{\sigma'_3}}{\tan^2 \left(\frac{\pi}{4} + \frac{\phi'_f}{2} \right) + \frac{2c}{\sigma'_3} \tan \left(\frac{\pi}{4} + \frac{\phi'_f}{2} \right)} \quad (2.13)$$

where, σ'_1 and σ'_3 are the major and minor principal stresses, respectively, $d\varepsilon_v$ and $d\varepsilon_a$ are the increments of volumetric and major principal strains, respectively, c is the inter-particle cohesion, and ϕ'_f is the friction angle. This equation is derived from minimum energy considerations of particle sliding and therefore is valid for both sands and clays. By rearranging the equation, the rate of dilatancy can be expressed as given in equation (2.13).

It can be seen from Eq. (2.13) that the dilatancy of a cemented soils is influenced by both the inter-particle cohesion c and the angle of friction ϕ'_f , which shows that dilatancy is inhibited by the presence of cohesion or bonding between the particles of a cemented soil. This has been illustrated by a number of laboratory data (Anagnostopoulos *et al.* 1991, Coop and Atkinson 1993, Cuccovillo and Coop 1999, Schnaid *et al.* 2001). For example, triaxial compression tests on artificially cemented sand carried out by Schnaid *et al.* (2001) demonstrated that the dilation of artificially cemented sand is also inhibited by inter-particle bonding.

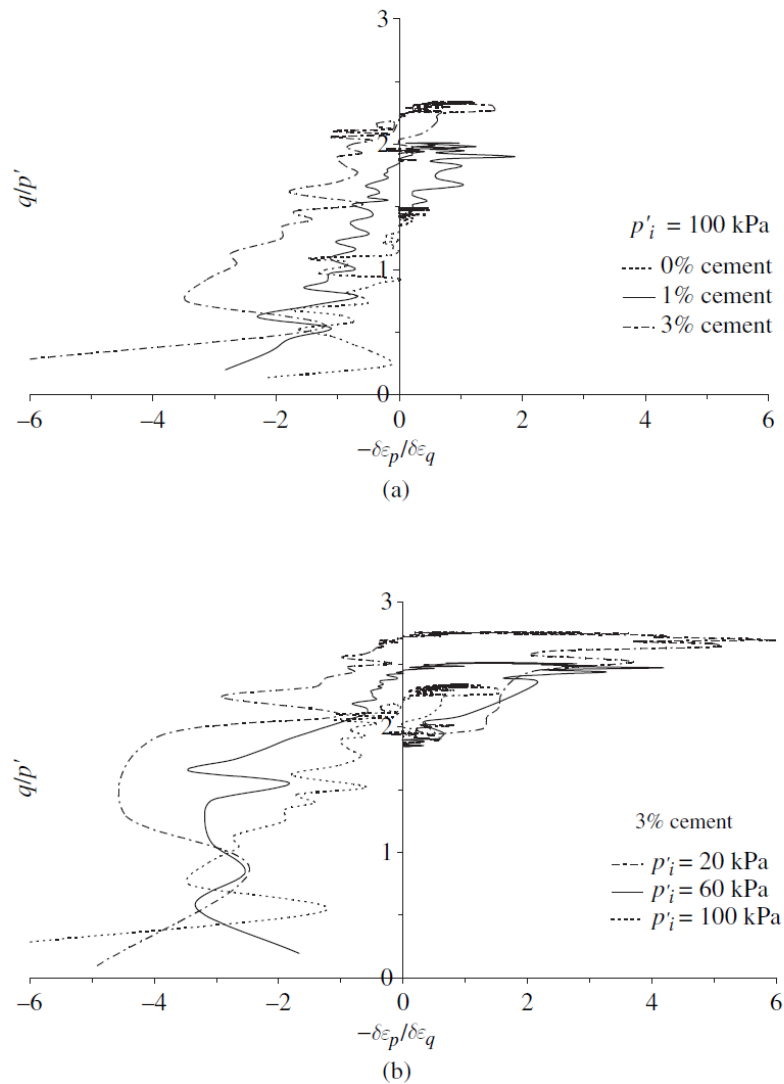


Figure 2.20 Stress-dilatancy behaviour of artificially cemented sands: (a) effect of cement content; (b) effect of initial mean effective stress (after Yu *et al.* 2007).

In addition, other experimental studies (Clough *et al.* 1981, Airey and Fahey 1991, Anagnostopoulos *et al.* 1991, Coop and Atkinson 1993, Lagioia and Nova 1995, Cucovillo and Coop 1999, Schnaid *et al.* 2001, Coop and Wilson 2003) have demonstrated that the stress-strain behaviour of bonded geomaterials changes from brittle to ductile as the confining stress increases. Since bonding tends to be brittle, this suggests that the behaviour of a cemented soil is mainly cohesive at very low confining stress, changing to purely frictional as the confining stress increases. This transi-

tion is believed to occur because the bonding bears some of the confining stress and thus “weaknesses” its effect on the soil skeleton. As shown in Figure 2.20 given by Yu *et al.* (2007), based on the data from Schnaid *et al.* (2001), the stress-dilatancy relationship in Eq. (2.13) can represent this “weakening” effect as the inter-particle bonding, c , is normalized by the minor principal stress σ_3 (which is also the confining stress in the conventional triaxial test). However, Schnaid *et al.* (2001) carried out all their triaxial tests at low confining pressures, $p'_c \leq 100$ kPa. This leads to the question that whether the stress-dilatancy relationship can capture the behaviour of a cemented soil at high pressures.

2.11 Yielding characteristics of cemented sand

The yield point is defined in engineering and materials sciences as the stress at which a material begins to plastically deform. Prior to the yield point the material will deform elastically and will return to its original shape when the applied stress is removed. Once the yield point is passed, some fraction of the deformation will be permanent and non-reversible. Yield point generally represents an upper limit to the load that can be applied. Moreover, it defines the onset of larger plastic deformations with further increases in applied stresses. In elastic-plastic, modelling the transition with increasing stress from pseudo-elastic to elasto-plastic behaviour occurs at the yield point. For the cemented sand larger stresses are necessary to yield the cementitious bonds between the particles (dos Santos *et al.* 2010). Lee *et al.* (2010) reported distinctive yielding for cemented sand due to the damage of cementation

bondage, while only a monotonic increase in the deformation without yielding for uncemented sand.

2.11.1 Identification of yield point

It is often difficult to precisely define yield due to the wide variety of stress-strain behaviour exhibited by real materials. In addition, there are several possible ways to define the yield point in a given material. The primary yield in Figure 2.21 represents a state where the $e-p'$ curve deviates from the initial linear behaviour (about 1700 kPa in the figure). The primary yield in Figure 2.21 is believed to represent the point at which breakage of the cement bonds commences (Rotta *et al.* 2003). Another suitable definition of yield for soils would appear to be the point of maximum curvature on a plot of voids ratio against the logarithm of stress, corresponding to the onset of grain fracture (McDowell 2002).

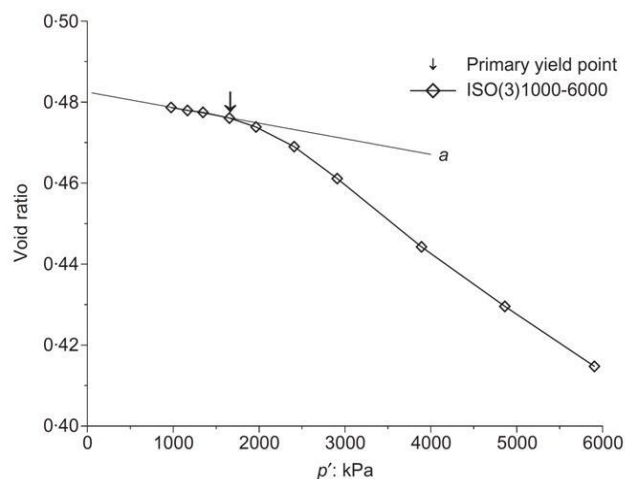


Figure 2.21 Determination of the primary yield point in isotropic compression (after Rotta *et al.* 2003).

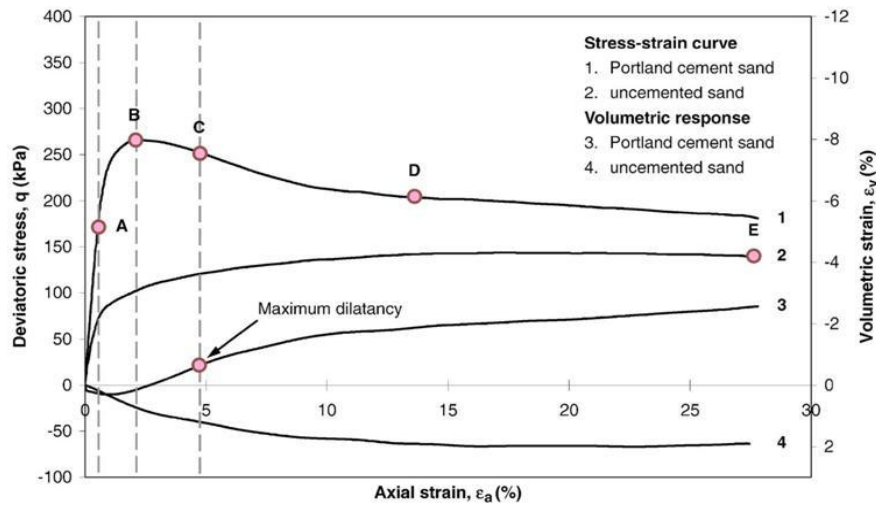


Figure 2.22 Location of yield point in stress-strain curve (after Wang and Leung 2008).

According to Moller *et al.* (2006), yield stress during shear is defined as the departure from linearity on stress-strain curve. Wang and Leung (2008) simply determined the yield point as the starting point of the transition from a stiff to a less-stiff response. Point A in Figure 2.22 locates the initial yield point. Typical yielding of granular quartz sand was illustrated by Karner *et al.* (2003) as shown in Figure 2.23.

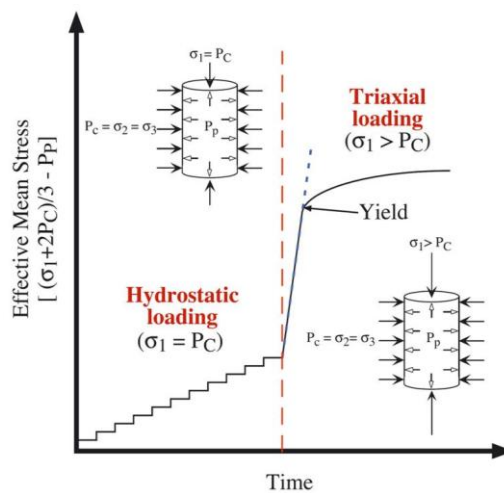


Figure 2.23 Typical location of yield point in stress-time curve for granular quartz sand (after Karner *et al.* 2003).

2.11.2 Yield stress in isotropic compression

The representative e - $\log p'$ curves of Toyoura sand (T-sand), Amami sand (A-sand), Dogs Bay sand (D-sand) and Quiou sand (Q-sand) are shown in Figure 2.24. The yielding stress p'_c obtained by the method of Casagrande as shown in Figure 2.24(a) suggests that the yielding stresses of carbonate sands (D-sand and Q-sand) are remarkably smaller than that of silica sand. As shown in Figure 2.24(b), ΔS is the amount of increasing surface area, which increased after the compression test. The value of ΔS is widely used to quantitatively estimate the amount of particle crushing and has good correlation with yielding stress p_c for all sands. Secondly, the higher the initial void ratio, the lower the yield stress can be observed. Therefore, it is believed that the yielding stresses can be utilized as a parameter related to soil crushability. According to Rotta *et al.* (2003), increasing the cement content causes an increase in the primary yield isotropic stress as shown in Figure 2.25. If this increase is correlated with particle crushing, then it can be concluded that the increase of cement content decreases the particle crushing.

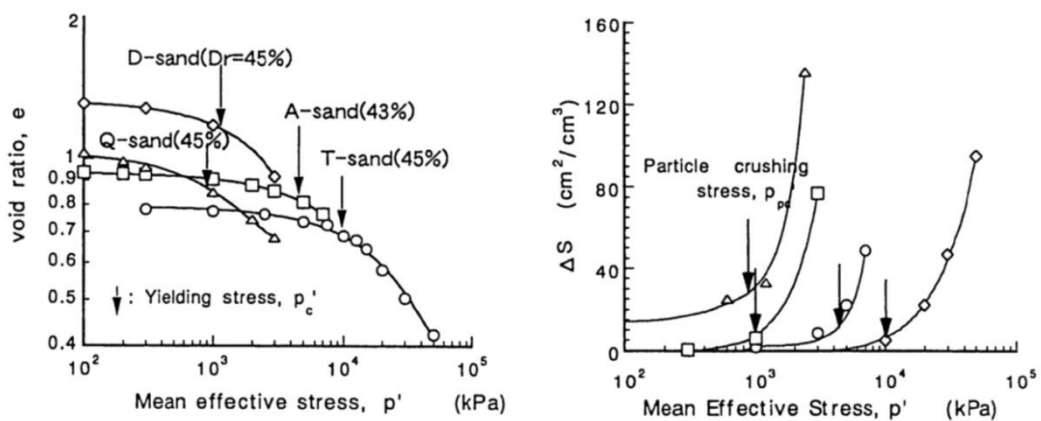


Figure 2.24 yielding stresses in isotropic compression (a) Representative e - $\log p'$ curves; (b) relationship between the crushability ΔS and mean effective stress p' (after Kwag *et al.* 1999).

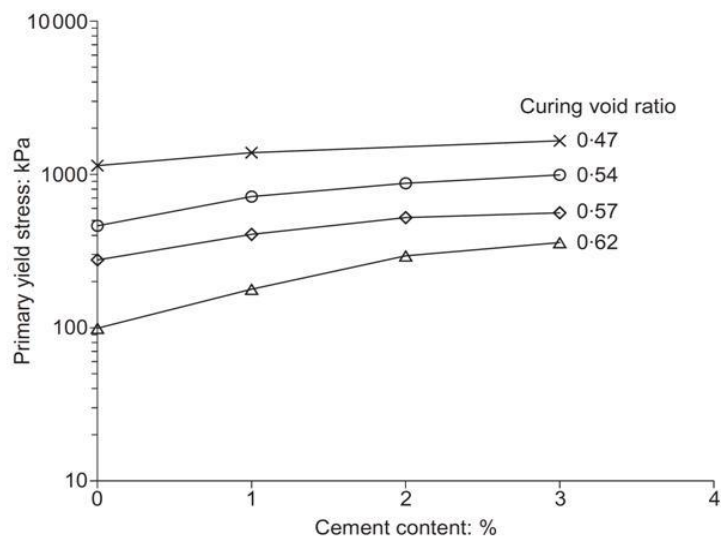


Figure 2.25 Variation of primary yield stress with cement content (after Rotta *et al.* 2003).

2.11.3 Yield stress in shearing

Previous studies on both naturally and artificially cemented soils have indicated that the stress-strain and volumetric change behaviour of cemented soils is governed by the relative magnitude of gross yield stress and confining pressure. These behaviours mainly depend on the nature of the soil particles, the void ratio, the cement content, and the strength of the cement (Reddy and Saxena 1992, Coop and Atkinson 1993, Cresswell and Barton 2003, Sharma and Fahey 2003, Chung *et al.* 2004, Hamidi and Haeri 2008). For cemented sand, it is believed that yield is approached when the bond created by the cementing agent gradually breaks, after which the stresses will be carried by the new destructed (uncemented) matrix of the host grains and broken cement (Coop and Atkinson 1993, Hamidi and Haeri 2008). However, no detailed investigations have been carried out to determine the yield locus of cemented granular materials at high pressures. The effect of high confining pressure on the alterations in the yield stress of the materials due to cement content needs further investigations.

2.12 Pre-failure deformation characteristics

Soil deformation modulus E_s is a parameter of soils ability to be deformed. If we have a relationship between stresses and strains for the soil, we can compute a stress-strain modulus E_s also called modulus of deformation or, more commonly (but incorrectly), the modulus of elasticity (Bowles 1997). The determination of deformation modulus in triaxial compression tests with internal and external instrumentation is illustrated in Figure 2.26.

It is quite appealing to measure the deformation modulus of the sand particles and cement bond at various percentages of cement contents by introducing different small-strain measuring devices to the high-pressure triaxial system. This will lead to evaluation of the initial maximum stiffness and stiffness degradation curves for different cement contents and densities at high pressures, which can provide guidelines for calculating ground movement and to prediction of large-scale behaviour in sand. Accurate measurement of soil deformation is fundamental to the success of geotechnical modelling and is an important parameter in traction prediction studies. The deformation moduli for granular materials are more commonly determined with small-strains measurements. On the other hand, for many geotechnical problems pre-failure and post-failure large strain deformations are equally significant. The large strain deformations are correlated with the initiation of yielding, and the yield point is coincided with the 'instigation and rate of dilation' of the material.

According to Leroueil and Vaughan (1990), when dilation is due to dense packing, the points of maximum dilation rate $(d\varepsilon_v/d\varepsilon_a)_{\max}$ coincide with maximum stress ratio

$(q/p')_{\max}$ but when the peak strength is controlled by cement content rather than density, the maximum rate of dilation takes place after the bonding has yielded as shown in Figure 2.27. Although the exact location of the point of yielding attributing to the threshold of deformation has always been challenging; however, the point of maximum rate of dilation can give a reasonably logical tip for the determination of deformation modulus as illustrated in Figure 2.28. Furthermore, it is well-established fact that all the materials first go under compression during shear, therefore the point of transition from compression to dilation can also be argued as the point of instigation of initial deformation.

All researches done on stiffness of soil have well adopted a plot between a stiffness parameter against logarithm of the corresponding strain, so-called stiffness degradation curve. This curve is generally used as a fundamental tool to exhibit the stiffness' strain dependency characteristics.

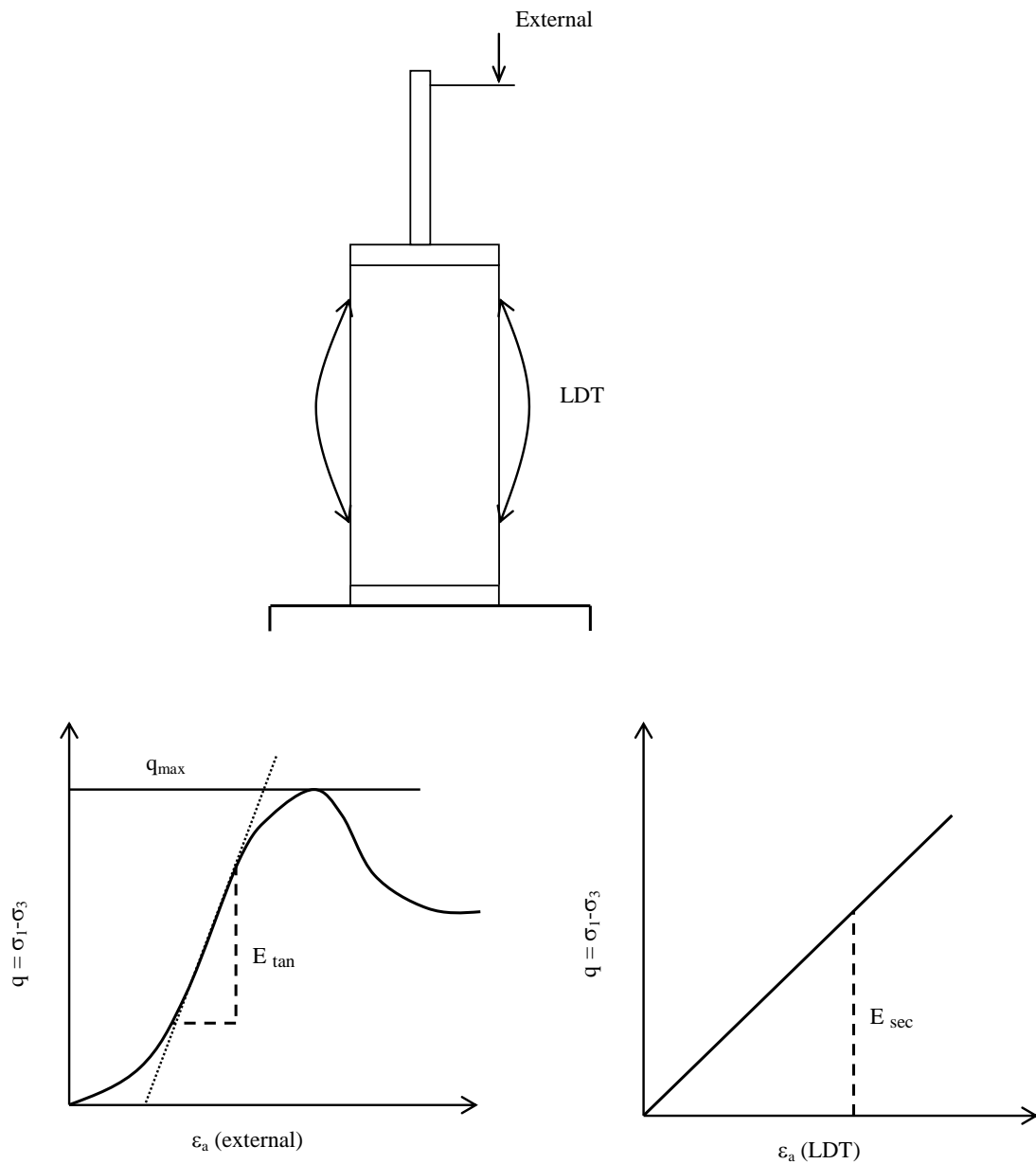


Figure 2.26 Illustration for the determination of deformation modulus with external load cell and internal local deformation transducers (LDT) during triaxial compression [redrawn from Goto *et al.* (1991) and Tatsuoka *et al.* (1994)].

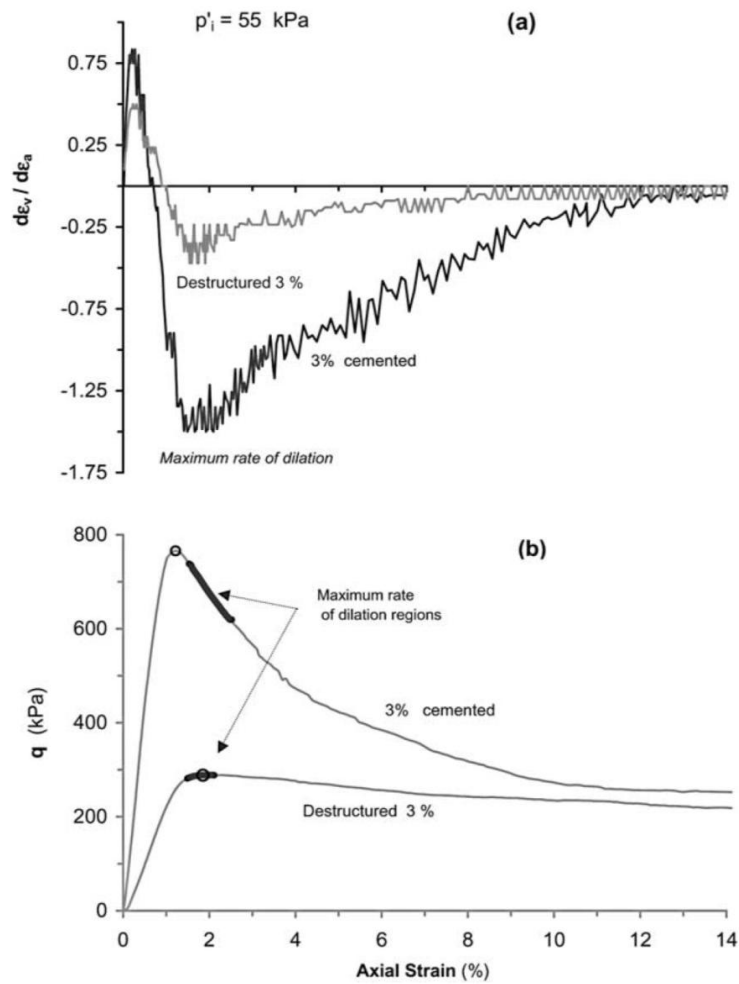


Figure 2.27 Initiation of dilation: (a) dilation rate-axial strain; (b) stress-strain curve with maximum rate of dilation regions (after Asghari *et al.* 2003).

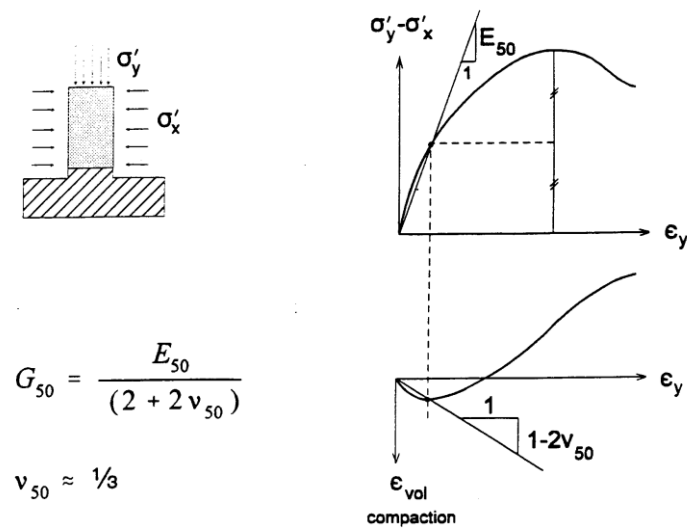


Figure 2.28 The onset of dilation correlated with deformation modulus (after Stein 2004).

The interpretation of measured values of the deformation modulus to general engineering applications is rather complex since the modulus varies as function of mean effective stress and shear strain amplitude [e.g., Jardine *et al.* (1984, 1986), Tatsuoka *et al.* (1993, 1994), Kim *et al.* (1994)]. On the other hand, Schnaid *et al.* (2001) argued that for the conventional pressure range, the deformation secant modulus of the cemented soil is not significantly affected by the initial mean effective stress; however, there is increase in the deformation modulus by the increase in the cement content. Either high confining pressures will also not affect the secant modulus of the cemented soils is not discussed in the literature. Therefore, it needs further investigations to see the effect of the high confining pressures on the deformation modulus of cemented sands.

2.13 Critical state behaviour

The term critical state is used to describe a condition at which plastic shearing of soil would continue indefinitely without changes in volume or effective stresses (Wood 1990). The critical state is an ultimate condition where all soils during shear will eventually attain a unique stress ratio (M) or critical state friction angle (ϕ_c) and reach a critical void ratio (e_c). This condition can be formulated as:

$$\frac{\delta p'}{\delta \varepsilon_q} = \frac{\delta q}{\delta \varepsilon_q} = \frac{\delta v}{\delta \varepsilon_q} = 0 \quad (2.14)$$

According to the critical state theory, there is a unique void ratio for each effective stress at critical state. Therefore, the critical state conditions can be described by a unique CSL in the e - p' - q space. The critical state concept has been found to be of

relevance for clays but its application for sands has been less successful and is still debated and it is same in the case for cemented materials.

A critical state concept has been used as a framework to illustrate the mechanical behaviour of the soils for many decades. Casagrande originally described the concept of critical state in 1936. In drained tests on a cohesionless soil, he observed that loose soils compress and dense soils expand under shear deformation and ultimately reach to a state where further deformation occurs at constant stress and without change in the volume as shown in Figure 2.29. This state was named as the critical state. Further, this was extended to undrained conditions for the study of liquefaction phenomena and was named as steady state. The rationale of critical state from drained to undrained condition is that, for a given soil, the volume change behaviour under drained conditions will transform to pore water pressure development in undrained shear. Loose soils which contract during drained shear at a constant confining pressure will under undrained conditions create positive pore water pressure and ultimately decrease the effective confining pressure. Likewise, dense soils, which dilate during drained conditions at a constant confining pressure, will under undrained conditions create negative pore water pressure and resulting to increase in the effective confining pressure. At critical state conditions, both drained and undrained tests move towards a unique line, which separates the dilative and contractive volumetric strain tendencies, produced during shearing. This line relates the critical void ratio and critical effective confining pressure, and it has been called critical state line or steady state line. The description of soil behaviour by the critical state line is the embodiment of all critical state concepts.

Extensive research work carried out at the University of Cambridge during the 1950's led to the concept of the critical state (Roscoe et al. 1958). According to Roscoe *et al.* (1958), the critical state shear strength is said to be intrinsic to the soil, and independent of the initial density or packing arrangement of the soil grains. In this state, the grains being sheared are said to be 'tumbling' over one another, with no significant granular interlock or sliding plane development affecting the resistance to shearing. At this point, no inherited fabric or bonding of the soil grains affects the soil strength. Different definitions of critical state for drained test with dilating sand are shown in Figure 2.30.

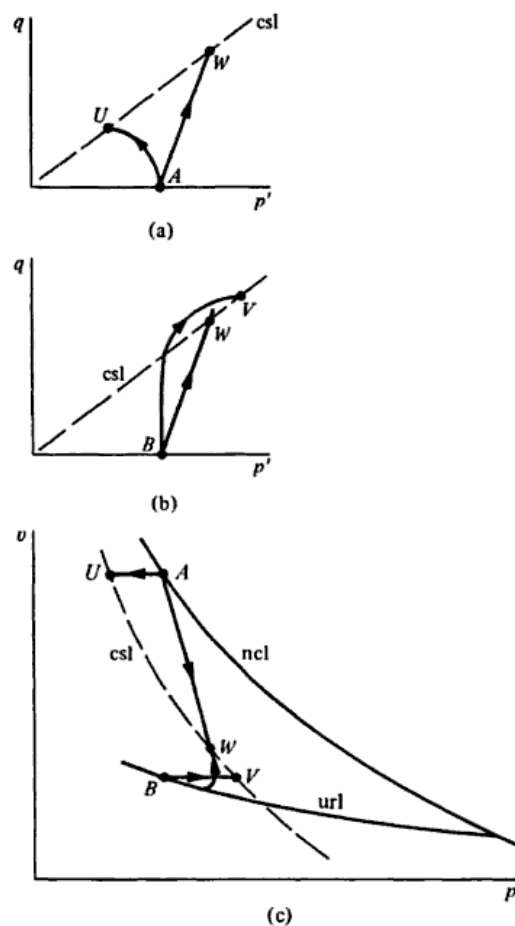


Figure 2.29 Critical state of soil (after Wood 1990).

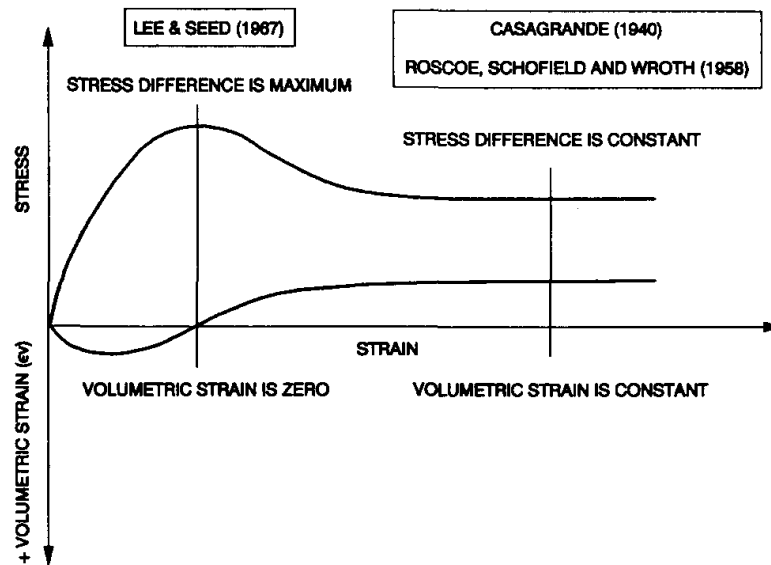


Figure 2.30 Different definitions of critical state for drained test with dilating sand.

2.13.1 Critical state concept in cemented materials

There are quite a number of papers and case studies available in literature regarding the critical state concepts in sandy soil. In the case of cemented soils, there are also some papers available in literature. Coop and Atkinson (1993) developed a framework for using critical state concepts in cemented sands. They used a double logarithmic space i.e. $\ln(q)-\ln(p')$ to define the critical state line. They showed that the critical state line for cemented sand is little lower than that of uncemented one in this space, that means a slightly lower friction angle in critical state for cemented soil in comparison to that of uncemented one. They used gypsum plaster as the cementing agent and a light silicon oil to saturate the samples to prevent degradation of cemented gypsum bonds. As they stated, the lower friction angle of cemented soil in critical state may result from cement adhering to the sand particles after yield. It should be noted that the friction angle of gravely sand, cemented with gypsum increases with cement content (Hamidi *et al.* 2004 and Haeri *et al.* 2005).

Coop and Atkinson (1993), also indicated the critical state line in $n: \ln(p')$ space for gypsum cemented sands. According to their results, the critical state line of cemented sand is lower than that for uncemented one in this space. Cuccovillo and Coop (1999) made a comparison between critical state lines of two intact and reconstituted cemented sandy soils. According to their results, both lines were coincided in $q: p'$ stress space. As a result, they concluded that the structure does not affect the critical state characteristics of the sandy soil at this space. This is in some contrast with that of Coop and Atkinson (1993). Obviously, there seems to be problems in identifying the real critical state for cemented materials. Therefore, it is needed to identify and highlight those problems and workout for their appropriate and reasonable solutions.

2.13.2 Problems in identifying the critical state for cemented sand

As mentioned earlier the critical state concept has been used as a framework to illustrate the mechanical behaviour of the soils for many decades. According to Roscoe *et al.* (1958), the critical state shear strength is said to be intrinsic to the soil, and independent of the initial density or packing arrangement of the soil grains. In the critical state framework, there are divided opinions of the researchers about the validity of critical state parameters for all types of soils. Some researchers argued that the critical state framework is reasonably applicable to all type of soils such as constitutive models based on critical state soil mechanics (CSSM) have been developed over the last four decades (e.g. Roscoe and Schofield 1963, Roscoe and Burland

1968, Yu 1998, 2006). Some researchers have shown, however, some significant departure from the original critical state theory. Triaxial tests performed on Botucatu sandstone by Ferreira and Bica (2006), have shown that the critical state line (CSL) is dependent on the initial void ratio of the sample: therefore the concept of a unique CSL does not apply. Studies by Leeson and Campbell (1983) have shown that the critical state boundaries of soils are related to the water content and soil structure; therefore, critical state parameters are also influenced by the method of specimen preparation.

Very few investigators have been working on the characterization of ultimate or critical states for cemented geomaterials [e.g., (Airey 1993, Coop and Atkinson 1993, Cuccovillo and Coop 1997, Cuccovillo and Coop 1999, Schnaid *et al.* 2001)]. The general agreement between the model predictions and experimental data on reconstituted soils is generally satisfactory, which is not surprising as these theories are derived from observing element testing of reconstituted soils in the laboratory.

It is believed that the investigations of the critical state line, as well as of the complete state boundary surface, play a fundamental role in establishing a general theoretical framework for the behaviour of cemented soils. The existence of such a critical state and the way it is affected by the degree of cement content need further investigation (Schnaid *et al.* 2001).

2.14 Summary

This literature review gives an overview of the published literature on laboratory testing of the mechanical behaviour of cemented granular materials over a wider

range of confining pressure, initial relative density, and degree of cement content. The mechanical behaviour of cemented sands was reviewed regarding the, compressibility, drained and undrained shear behaviour, strength-deformation, yielding, failure mechanism, stress-dilatancy, and critical state behaviour. This literature also includes the critical review of the specimen preparation techniques, testing procedures, and difficulties/ problems with high-pressure triaxial testing.

The key points are summarized as follow:

- 1) There has long been interest in studying uncemented soils at high pressures since the constructions of massive structures significantly increased the magnitude of foundation loads on soils under a variety of stress paths. However, in spite of indentifying the natural process of cementation into the soil due to silicates, amorphous silica, iron oxide, and calcium carbonate (Clough *et al.* 1981), very limited data is available in the literature regarding the mechanical behaviour of cemented sands at high pressures.
- 2) Previous studies suggest that the test data obtained from naturally cemented carbonate sediments are frequently highly scattered. Therefore, a general framework for the behaviour of cemented carbonated sands is very difficult to develop from the natural cemented materials. Therefore, artificially cemented soils were created in the laboratory to simulate natural soils. These studies have provided some useful insight into the influence of cement content on the mechanical behaviour of sands and the problems of variability in cement na-

ture and cement contents were avoided that are usually associated with naturally cemented materials.

- 3) Bearing in mind the varying degree of cement content and densities for capturing the overall behaviour of cemented materials, different sample preparation procedures were investigated. From these investigations, it was concluded that more preferable procedure of specimen preparation for both cemented and uncemented materials for comparative study could be moist tamping method (MT). This method can further be sophisticated by the undercompaction and density controlled vibratory tamping.
- 4) The compression behaviour of geomaterials has always been a topic of investigation in geotechnical engineering. However, the effect of cement content and density on particle crushing during isotropic compression is still not yet fully investigated. Moreover, comparison with uncemented sand including the effects of cement contents, dry density, and void ratio can give a reasonable framework in understanding naturally cemented materials with spatial degree of cement content and confining pressures.
- 5) Most of the research in the mechanics of cemented soil has focussed on soil behaviour at low or moderate pressures, where most of the geotechnical engineering problems tend to arise. However, many practical problems fall into the category of high pressures. For example, offshore piles and constructions on oil bearing strata. Understanding the behaviour of cemented soils subjected to high pressures is therefore fundamental to assisting in the solution to these types of geotechnical and geological problems. How initial dry and/or relative

density and bond strength responds at high pressures under drained and undrained conditions is important to investigate.

- 6) According to Asghari *et al.* (2003), the stress paths from undrained tests defined a similar failure envelope to that defined by the drained tests. However, in the cemented materials, the undrained tests cross the failure surface defined by the q_{\max} points from drained tests, showing that the material can attain higher stress ratios when sheared in undrained condition. This needs further elaboration at high confining pressures.
- 7) The previous studies on both naturally and artificially cemented soils showed that the stress-strain and volumetric behaviour of cemented soils is governed by the relative magnitude of gross yield stress and confining pressure. For cemented sand, it is believed that yield occurs when the bond created by the cementing agent breaks, after which the stresses will be carried by the new destructed (uncemented) matrix of the host grains and broken cement. A gradual breakdown of the cement content can be observed as yield is approached. However, no detailed investigation has been carried out to determine the yield locus of cemented granular materials at high pressures.
- 8) The failure envelopes for granular materials in the range of conventional pressure (<1 MPa) were more often reported as straight line, however, some researchers had reported it as curved shape, which needs further elaboration by including the effect of cement content and increasing the range of confining pressure.

- 9) The Dilative behaviour is important when analyzing critical or ultimate states and has significant influence on the apparent strength behaviour of granular soils. The volume change plays an important role in the stability of frictional materials. It is reported that there is decrease in the rate of dilation by the increase in confining pressure. Therefore, the progressive suppression of dilatancy with gradual increase in the confining pressure needs further investigations.
- 10) It is widely recognised that mechanical behaviour of sands can be directly related to its microstructure, i.e., the geometrical arrangement of the grain particles including the forces acting between them (Wan and Guo 2001). The micro-scale interactions between individual constituents of the grain-cement network subjected to differential stresses and cement contents complicated with particle crushing and bond breakage at high pressures are poorly understood, inhibiting the development of a physically based link between microscopic phenomena and macroscopic behaviour. Detailed experimental characterization of these systems would improve constitutive models for the predictive modelling of geomechanical phenomena.
- 11) It is apparent that there have not been many studies of cemented sand behaviour at high pressures. There appears to be some disagreement regarding specimen preparation procedures, shape of failure envelope, critical state framework validity, frictional angle, cement-sand bond breakage, particle crushing, and effect of cement contents at high pressures. A comprehensive understanding of the nature of shearing resistance and compression behaviour

of cemented sand is essential to adequate design of foundations. Research in these areas was largely performed at low stress levels. The maximum confining pressure was reported to be 0.1-5.0 MPa (Huang and Airey 1998). However, the maximum pressure at the tip of a pile foundation may reach around 350 MPa (Yamamuro and Lade 1996). In particular, the foundations of offshore constructions resting on naturally cemented sand.

METHODOLOGY

3.1 Introduction

The basic requirements for reliable triaxial testing are controlled specimen preparation to ensuring reproducible initial state, complete saturation of the specimen, well centred axial load, negligible friction on the loading ram, well-controlled cell and pore pressures, and accurate measurements of axial load, axial deformation, and volumetric change.

Because the triaxial test is an elemental test, performed to obtain mechanical properties, the specimen should be perfectly homogeneous. From a more technical point of view, the area correction that is necessary to take into account the radial variation of the specimen during the test in order to calculate the actual axial stress (and estimate the membrane action on the actual lateral pressure) can be obtained from axial and volumetric strains only as long as the specimen shape remains cylindrical. In other cases, additional assumptions must be made:

3.2 Materials

3.2.1 Portaway sand

Well-graded, medium quartz sand from Sheffield (England), so-called Portaway sand was used as the base material for the cemented specimens. Portaway sand was previously used at the University of Nottingham in two other experimental projects on evaluation and extension of a simple critical state model for sand (Yu *et al.* 2005) and

on validation of the shakedown concept for pavement design and analysis (Brown *et al.* 2008). The index properties of Portaway sand, determined by British Standard methods (BS1377), are given in Table 3.1. The particle size distribution of Portaway sand is shown in Figure 3.1. The sand grains were mainly sub angular and sub rounded in shape. It should be noted that the index properties of Portaway sand reported in this study are slightly different from those reported by Yu *et al.* (2005), because of different batches of the tested sand. Before the preparation of cemented specimens, the sand was passed through 2 mm sieve to remove gravel size particles and washed through 0.063 mm sieve under the running water to remove fines.

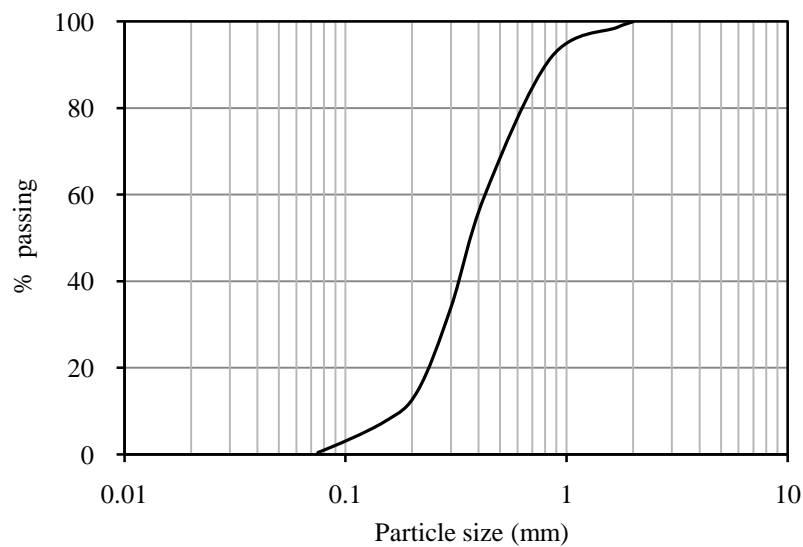


Figure 3.1 Grain size distribution curve.

Table 3.1 Index properties of Portaway sand.

Effective grain size D_{10} : mm	0.19
D_{30} : mm	0.295
Mean grain size D_{50} : mm	0.393
D_{60} : mm	0.42
Uniformity Coefficient D_{60} / D_{10}	2.21
Specific Gravity, G_s	2.65
e_{max}	0.79
e_{min}	0.46

The shape of the particles significantly influences the stress-strain behaviour of the material. The relation between directional porosity and the preferred orientation of granular particles and voids was found to be highly dependent on their angularity and elongation.

3.2.2 Particle shape and mineralogy

In order to understand the micromechanical behaviour of cemented sand, micro-scale observations of the intact and sheared specimens of the Portaway sand were carried out to see the particle shape, structure, sand-cement bond interaction (for cemented sand) and mineralogy of sand and sand-cement composition. Figure 3.2 illustrates the shape of sand particles together with clay platelets deposited on the particle surfaces.

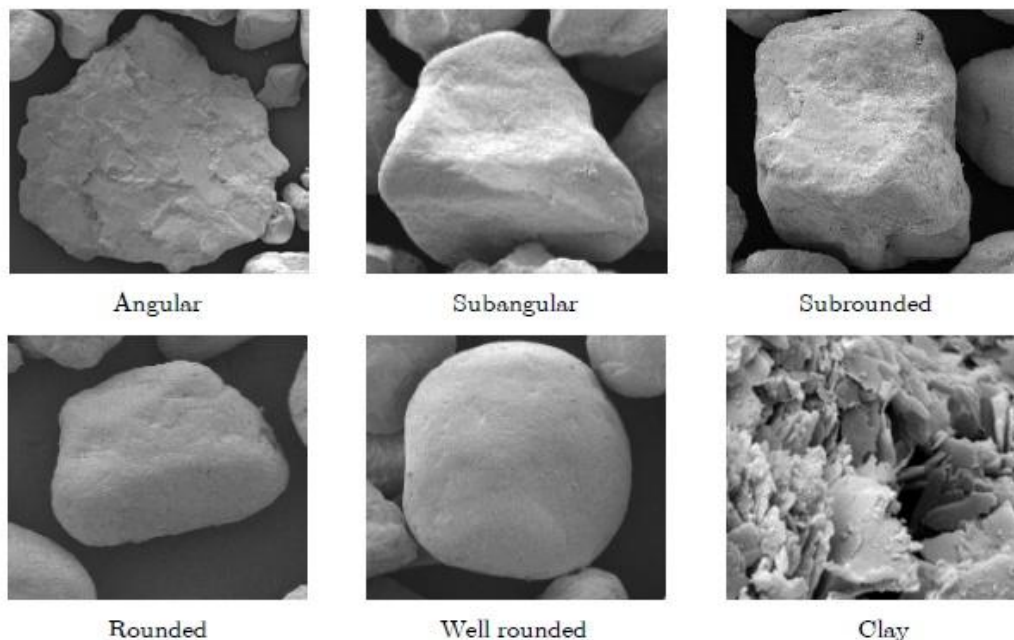


Figure 3.2 Shape of the Portaway sand particles (Wang 2005).

Portaway sand is uniform sand composed of angular, sub-angular, and rounded shape particles. Figure 3.3 and Figure 3.4 illustrates the mineralogical composition of

uncemented and cemented sand respectively. The most abundant mineral found in Portaway sand is quartz (Si) along with traces of aluminium (Al), magnesium (Mg), and potassium (K), etc.

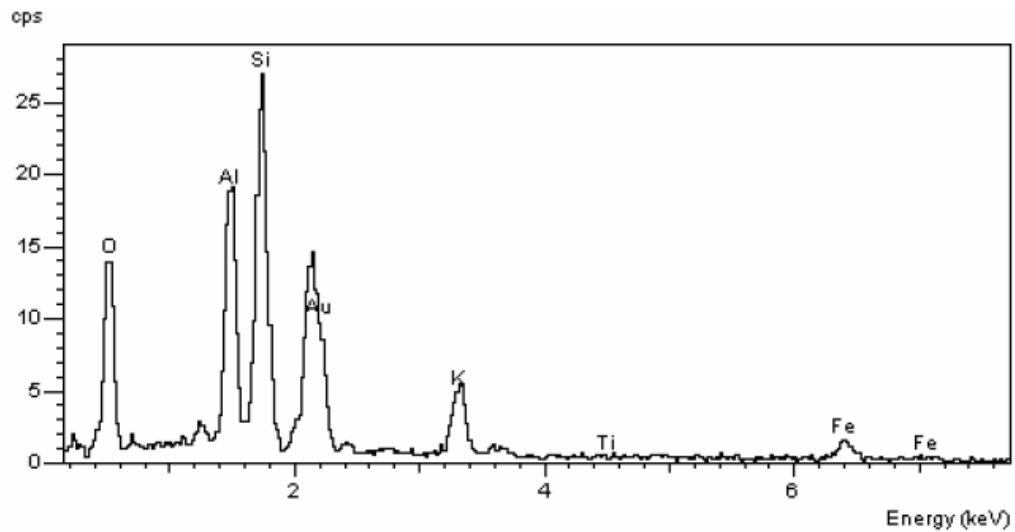


Figure 3.3 Energy dispersive spectrum (EDS) of uncemented sand (Wang 2005).

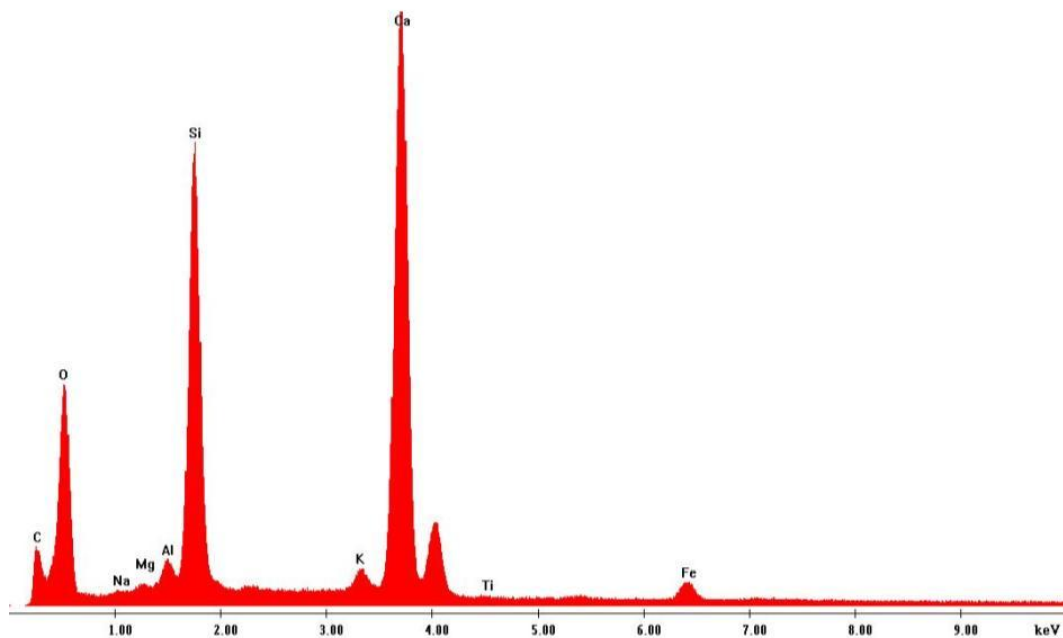


Figure 3.4 Energy dispersive spectrum (EDS) of cemented sand.

Element	C	O	Na	Mg	Al	Si	K	Ca	Ti	Fe
Wt%	11.74	51.56	0.10	0.28	1.04	13.31	0.72	19.87	0.00	1.38

3.2.3 Cement

Ordinary Portland cement (BS EN 197-1 CEM I 42, 5N) was used as cementing material. Its initial setting time is 80 to 200 minutes and the specific gravity of 3.15. The consistent strength meeting all the conformity criteria in BS EN 197-1.

3.3 Sample preparation procedures

An adequate amount of the base material (i.e., the Portaway sand) from the available batch of sand sufficient for all the proposed number of experiments has been washed and oven dried. The fraction of the material passing 2.0 mm and retaining on 63 μm was collected and stored in a bucket for subsequent usage in the preparation for cemented and uncemented materials for triaxial and other required testing. Portland cement bags were kept in airtight container in order to keep the cement dry during storage.

The materials were mixed thoroughly to get consistent test specimen. The targeted dry unit weight of the material for a standard size specimen was maintained by varying the weight of the moist sample using the following equation (3.1).

$$\gamma_d = \frac{\gamma}{1 + \omega} \quad (3.1)$$

where, $\gamma = \frac{\omega}{V}$

γ , is the bulk unit weight, γ_d is the dry unit weight, ω is the moisture content and V is the total volume.

The procedure incorporated a tamping method of compacting moist coarse-grained sand in layers. Each layer was compacted to a selected percentage of the required dry unit weight of the specimen by the method of undercompaction (Ladd 1978). Slight modifications were made in this method to avoid stratification into the specimens.

By the method of undercompaction, the following equation (3.2) can be used to calculate the percent undercompaction for each layer.

$$U_n = U_{ni} - \left[\frac{(U_{ni} - U_{nt})}{n_t - 1} \times (n - 1) \right] \quad (3.2)$$

U_{ni} = percent undercompaction selected for 1st layer

U_{nt} = percent undercompaction for final layer usually zero

n = number of layers being considered

n_i = first layer

n_t = total number of layer (final layer)

The correct value of U_{ni} can be determined by measuring the dry unit weight of the prepared test specimen as a function of its height. For dense specimen the U_{ni} is taken as 0%. The required height of the specimen at the top of the nth layer can be determined by applying the following formula (Eq. 3.3).

$$h_n = \frac{h_t}{n_t} \left[(n - 1) + \left(1 + \frac{U_n}{100} \right) \right] \quad (3.3)$$

Where,

h_n = Height of compacted material at the top of the layer being considered and h_t = Final (total) height of the specimen

n_t = Total number of layers, n = Number of the layer being considered

U_n = Percent undercompaction for layer being considered, for dense specimen the U_{ni} is taken as 0%.

The compaction of each succeeding layer can further densify the sand below it. The method uses this fact to achieve uniform specimens by applying the concept of undercompaction. In this case, each layer is typically compacted to a lower density than the final desired value by a predetermined amount, which is defined as percent undercompaction U_n . The U_n value in each layer is linearly varied from the bottom to the top layer, with the bottom (first) layer having the maximum U_n value.

Latex and neoprene membranes (Figure 3.5) were used to enclose the specimens. The thickness of the latex and neoprene membrane is 0.25 mm and 0.5 mm respectively. The elastic modulus E for latex is reported as 1100 kPa (Donaghe *et al.* 1988).

The ASTM standard D 4767 provides a membrane correction and recommends correcting for the strength of the membrane if the error in deviatoric stress due to strength of the membrane will be greater than 5%. However, the membrane effects were noticed well below the limit for the materials tested at high pressures.

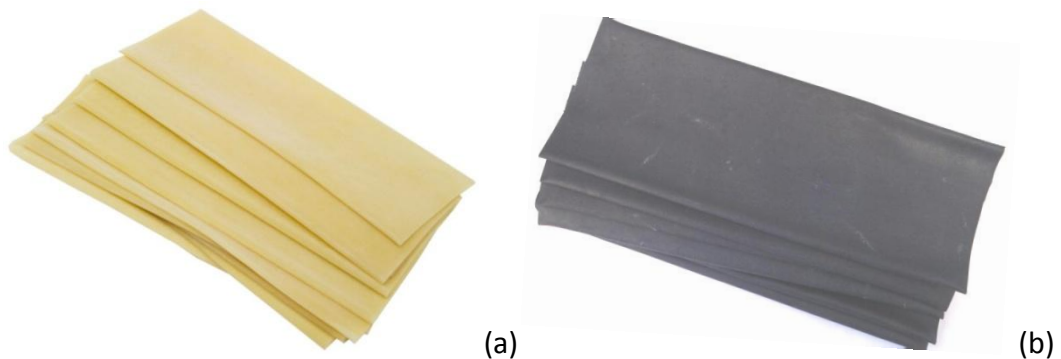


Figure 3.5 Rubber membranes: (a) Latex; (b) Neoprene.

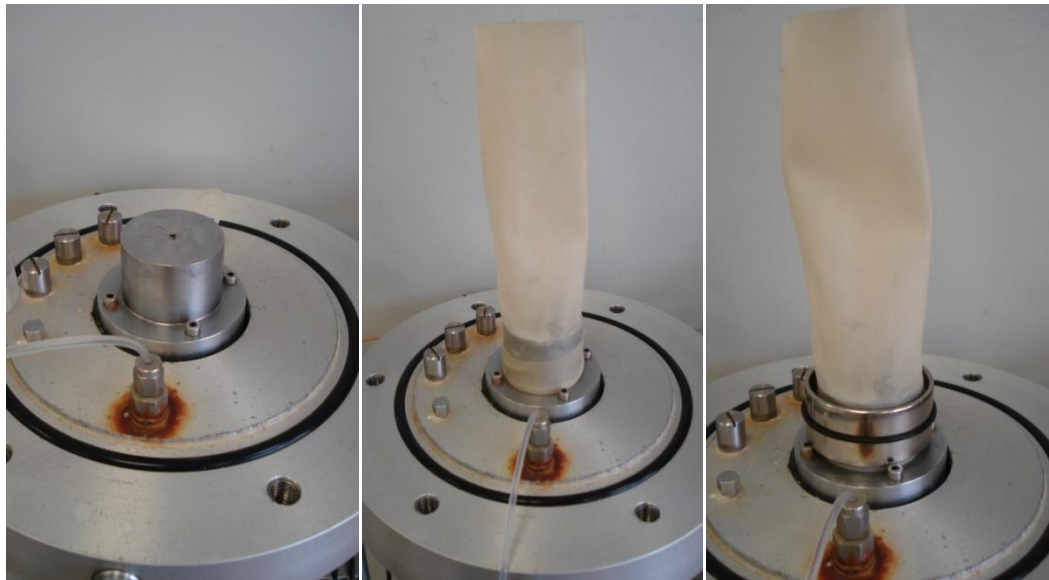
3.3.1 Preparation of uncemented specimens

Stepwise procedure of sample preparation for both conventional and high-pressure triaxial systems is described as follow:

1) Conventional pressure

In Figure 3.6 the photographs of various stages of sample preparation for uncemented sand for conventional triaxial testing system are given. The pedestal base as shown in (a) was lubricated with silicon grease to provide airtight connection with the latex membrane. The latex membrane was then provided on the pedestal base as shown in (b). With the help of o-ring stretcher, the o-rings were mounted to provide airtight grip as shown in (c) and (d). Split mould was then mounted and tightened with clamping ring as shown in (e) and (f). Top o-rings were slipped over the split mould with the help of o-ring stretcher and then the membrane was stretched carefully to release shrinks from inside to provide smoother inner surface as shown in (g), (h) and (i). Prior to pouring the moist sand into the mould, bottom porous stone and filter paper were placed and vacuum suction was applied to keep the membrane stretched and shrinks free as shown in (j). The moist sand was then filled in layers and each layer was tamped to a required number of blows as per the procedure of undercompaction. Prior to the placement of next layer, the surface was well scratched to avoid layering. After final layer, the surface was levelled prior the placement of top porous stone as shown in (k). Filter paper and top porous stone were put on the top as shown in (l). Top cap was lubricated with silicon grease and placed on the top as shown in (m). Folded membrane was then stretched over the top cap carefully and then the o-rings were glided over the top cap and membrane

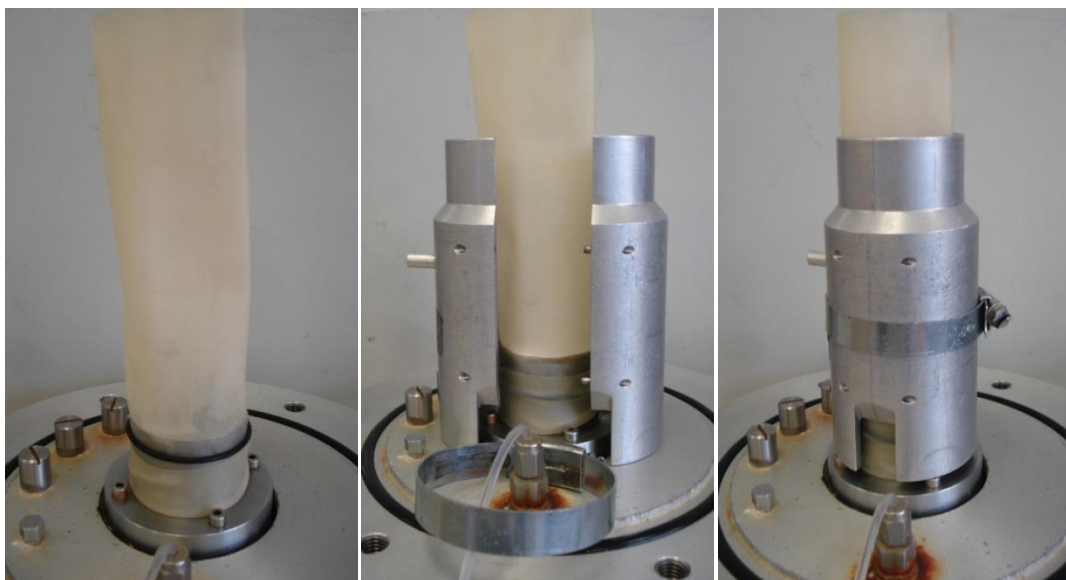
to create watertight connection as shown in (n). The top drainage wall was closed and a slight suction was applied through bottom drainage wall to keep the sample intact prior to the removal of split mould and then the mould was removed as shown in (o). Triaxial cell was mounted over the cell base and were provided with necessary connections as shown in (p).



(a)

(b)

(c)



(d)

(e)

(f)



(g)

(h)

(i)



(j)

(k)

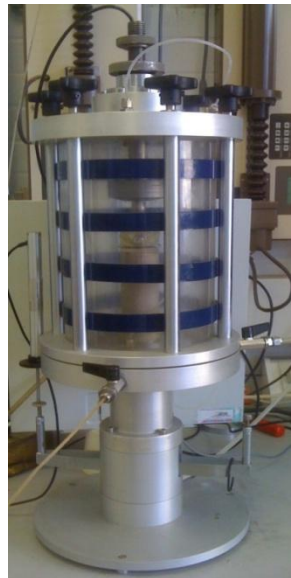
(l)



(m)

(n)

(o)



(p)

Figure 3.6 The sequential steps for the preparation of uncemented samples for conventional triaxial testing from: (a) to (p).

2) High-pressure

In Figure 3.7, the photographs of various stages of sample preparation for uncemented sand for high-pressure triaxial testing system are given. Most of the steps of high-pressure test setup were similar to that of conventional pressure triaxial testing system. Further brief description is given here. The pedestal base was lubricated with silicon grease to provide airtight connection with the neoprene membrane. The neoprene membrane was then mounted on the pedestal base as shown in (a). Split mould was then provided and tightened with clamping ring and the top extended portion of the membrane was stretched and rolled over the top portion of split mould as shown in (b). Prior to pouring the moist sand into the mould, bottom porous stone and filter paper were placed and vacuum suction was applied to keep the membrane stretched and shrink free. The moist sand was then filled in layers and each layer was tamped to a required number of blows as per the procedure of undercompaction. Prior to the placement of next layer, the surface was well scratched to avoid layering. Prior to the placement of filter paper and top porous stone, the surface was levelled.

In case of providing double membrane (At high-pressure triaxial testing more than one membrane is required to avoid membrane puncture), the split mould was removed and the second membrane was put on the first membrane with the help of membrane stretcher as shown in (d). Bottom o-rings were put with the help of o-ring stretcher. The top o-rings were left on the o-ring stretcher at the bottom of the sample. The mould was mounted again. The extended membrane was folded over the split mould. Filter paper and top porous stone were put on the top and top cap was

lubricated with silicon grease and placed on top porous stone. Folded membrane was then stretched over the top cap carefully as shown in (e). The split mould was then removed as shown in (f) and then the o-ring were glided over the top cap and membrane to create water tight connection as shown in (g), (h) and (i). The ready specimen to put into the cell is shown in (j).



(a)

(b)

(c)



(d)

(e)

(f)

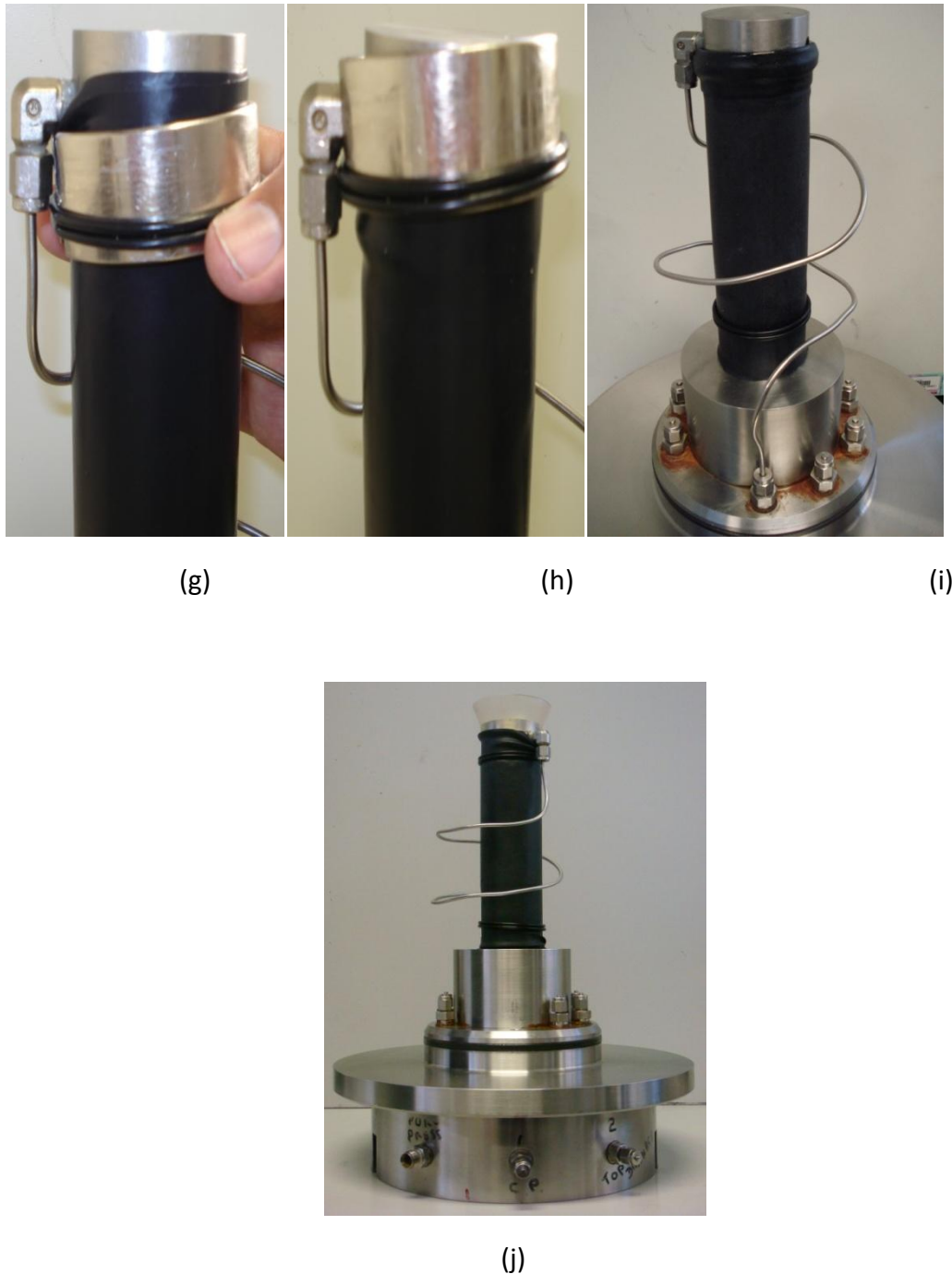


Figure 3.7 The sequential steps of the preparation of uncemented samples for high-pressure testing from: (a) to (j).

3.3.2 Preparation of cemented specimens

The specimens (50 mm diameter x 100 mm height) were prepared by initially mixing relevant amounts of dry Portaway sand and powdered ordinary Portland cement to obtained cement contents of 5%, 10%, and 15% by weight of dry sand. These

sand-cement mixtures are characterized as moderately to very strongly cemented soils (average unconfined compressive strength of 565, 2210, and 5540 kPa, respectively) using the classification criteria proposed by Rad and Clough (1985). Mixing of dry materials was continued until a uniform appearance of the sand-cement mixture was obtained. Water was then added to the mixture in accordance with the optimum moisture content of 10% and further mixing was performed until a homogeneous appearance of the moist sand-cement mixture was achieved. The mixture was then stored in an airtight container to avoid any moisture loss before subsequent compaction. Prior the placement of the mixture the mould was provided with a '*thin transparency sheet*' to avoid sticking of the cement materials with the wall of the mould. The mixture was then compacted in layers into the split mould (50 mm diameter and 100 mm height) to the targeted dry unit weight. To achieve uniformity of specimens the undercompaction method, proposed by Ladd (1978) was used. After compaction, the specimens were allowed to cure inside the mould for 24 hours. The moulds were then dismantled and the specimens were stored in a humid room to cure for 14 days before testing.

The assembling of the specimen on triaxial base is shown in Figure 3.8. Prior to the placement on the base pedestal of the high-pressure triaxial cell, the specimen was dried, weighed and dimensions were taken. The surface of the specimen was covered with a thin film of a mixture of clay and fine sand to minimize membrane penetration effects. Two 0.5 mm thick neoprene membranes (double membranes with an average thickness of 0.5 mm were used to prevent membrane being punctured by sharp edges of coarse grains when the samples were tested at high pressures) and

two O-rings were fitted around the specimen and the pedestal. The top cap was then placed on the specimen surface. The membrane was carefully wrapped around the top cap and secured to it with two O-rings.

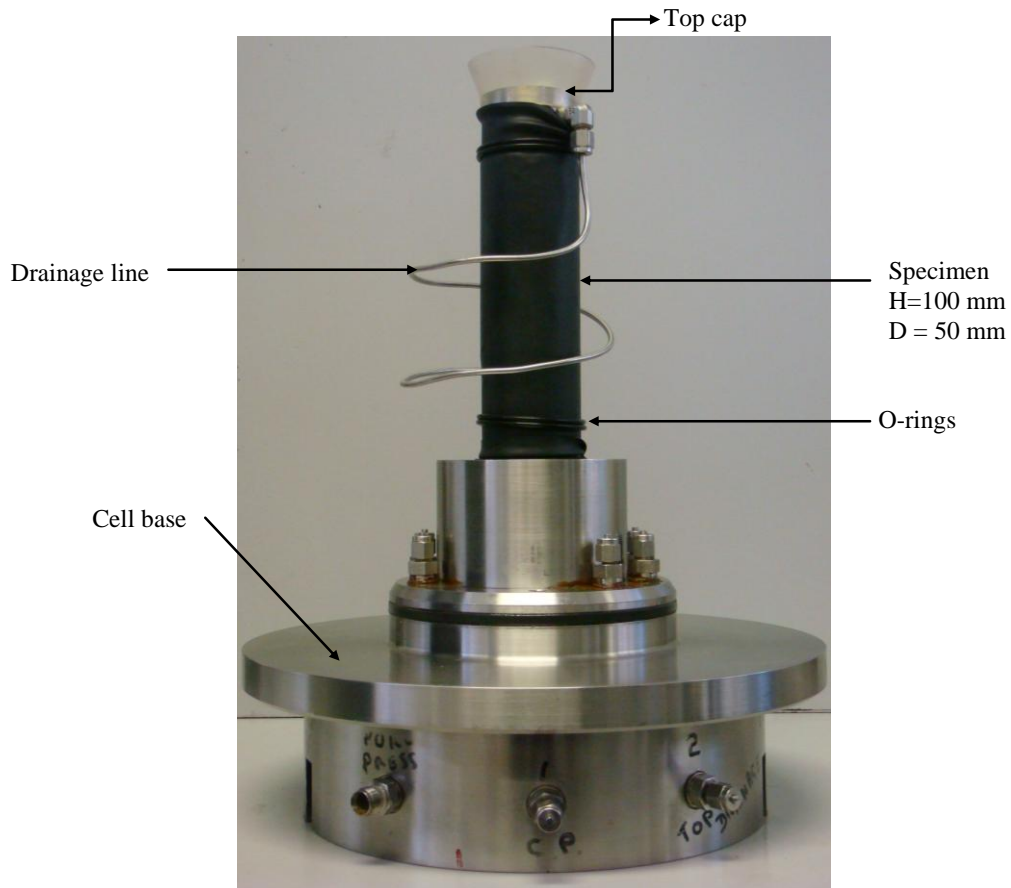


Figure 3.8 Specimen placed on the cell base.

3.4 Testing setup

Bishop-Wesley Conventional pressure and GDS high-pressure triaxial apparatus were used for triaxial testing. The detail silent features, working mechanism and test setup of these apparatus are described here in detail.

3.4.1 Bishop-Wesley triaxial system

The triaxial testing system is intended for performing conventional triaxial tests, namely a constant rate of axial strain compression test. A Schematic diagram of

Bishop and Wesley stress path cell is shown in Figure 3.9. In the GDS controller, liquid (normally de-aerated water) in a cylinder is pressurized and displaced by a piston moving in the cylinder. The piston is actuated by a ball screw turned in a captive ball nut by an electric motor and gearbox that move rectilinearly on a ball slide. Pressure is measured by an integral solid-state transducer. Control algorithms are built into the onboard microprocessor to cause the controller to seek to a target pressure or step to a target volume change. Volume change is measured by counting the incremental steps of the motor. The controller can be set and read manually by an integral keyboard and display. An important provision for automated testing is the computer communications interface by which a desktop computer could direct the controller and also take readings of pressure and volume change. The computer-controlled mechanism is shown in Figure 3.10.

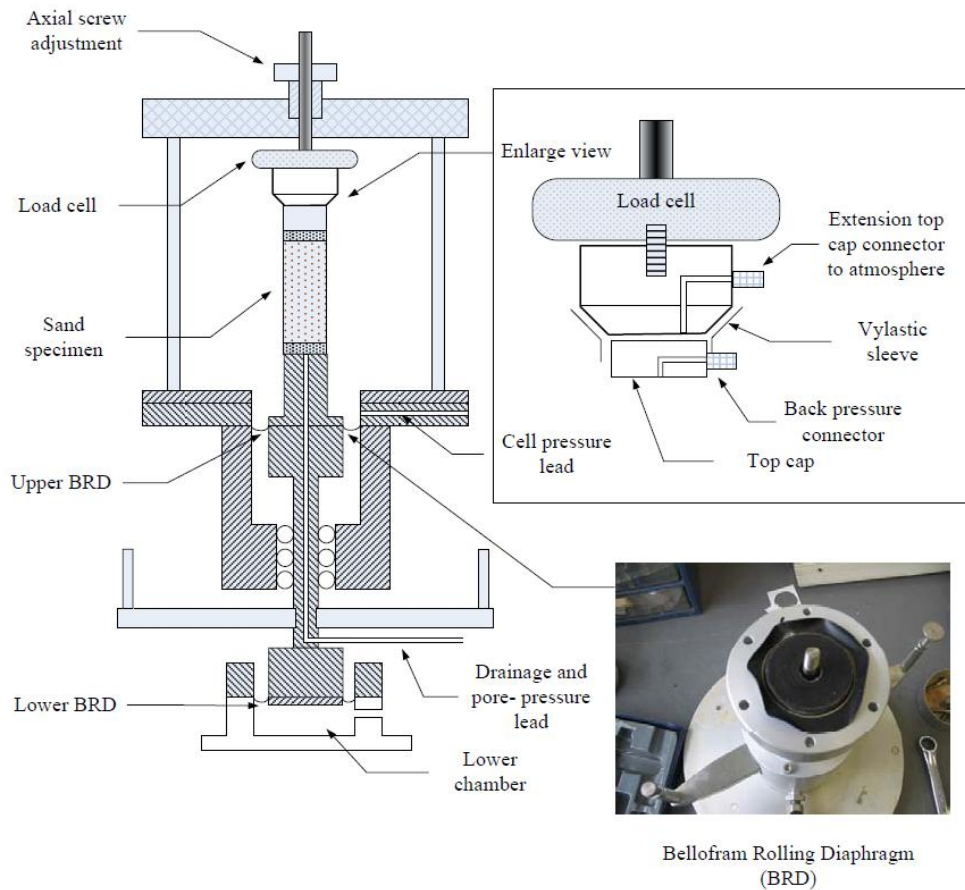


Figure 3.9 Bishop-Wesley triaxial setup and working mechanism (after Wang 2005).

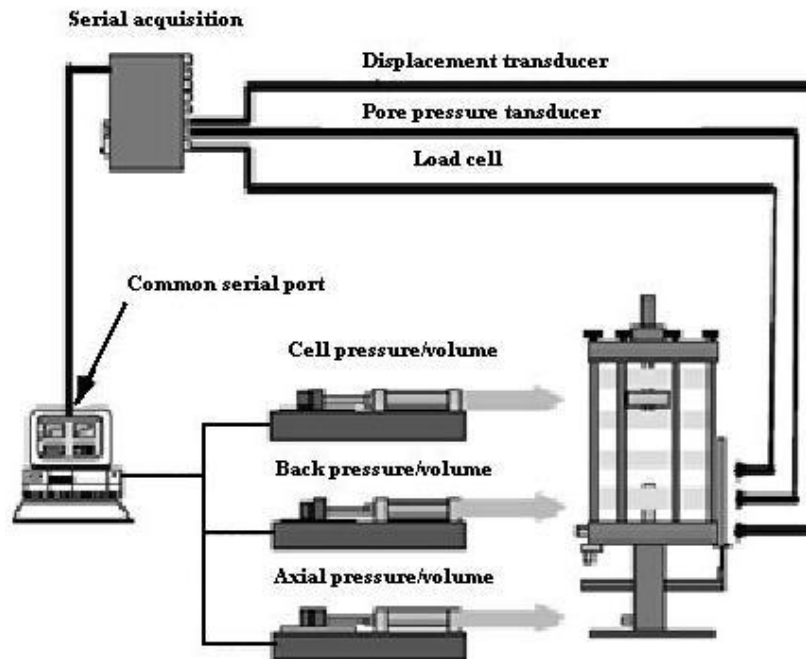


Figure 3.10 The modified experimental set up for conventional pressure triaxial testing system.

3.4.2 High-pressure triaxial system

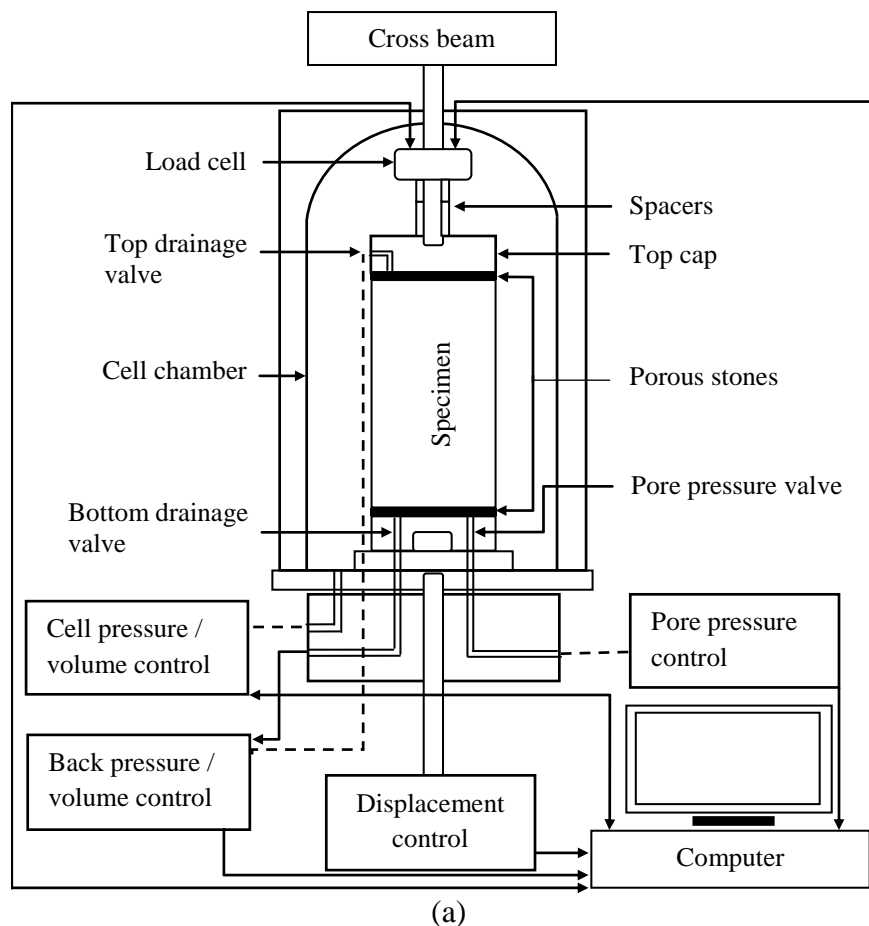
A high-pressure testing system, developed at the University of Nottingham, United Kingdom in conjunction with GDS Instruments Ltd. was used for the experiments at high confining pressures. A schematic cross-section and a photograph of the assembled high-pressure triaxial cell are shown in Figure 3.11, and the technical specifications of the system are given in Table 3.2. The main components of the system consist of a loading frame, high-pressure triaxial cell, digital displacement/load controller, two digital/pressure volume controllers, load cell, pore pressure transducer, data acquisition box, and a computer.

A 100 kN loading frame that can also be used as an independent compression machine was used in this study (Figure 3.11b). As shown in Figure 3.11 (a), displacement (or load) in the high-pressure system was applied from the bottom of a loading frame via a digital hydraulic force actuator. The actuator was controlled by a computer via a digital load/displacement control box. The control box adjusted the movement of the base pedestal to achieve a desired rate of load or rate of displacement so that the triaxial apparatus could be used under either deformation-controlled or load-controlled loading mode. A 100 kN submersible load cell was used to measure the vertical load at the top of specimen. The cell pressure was applied through a GDS digital pressure/volume controller (DPVC). Another DPVC was used to control the backpressure from the top of the specimen and measure the volumetric change in a drained test, or to control the volumetric change and measure the pore water pressure in an undrained test. The DPVCs used in this study had a ca-

capacity of 64 MPa. A high capacity pressure transducer was also used to measure the pore water pressure at the bottom of the specimen.

Table 3.2 Technical specifications of GDS high-pressure triaxial apparatus.

Parameters	Values
Nominal size	2.3 m×1.0 m×0.96 m
Computer interface	IEEE-488 standard
Load range	100 kPa(10 ton)
Load resolution	±1 in 10,000
Load cell accuracy	±0.03%
Displacement range	100 mm
Displacement resolution	0.1 μm
Displacement accuracy	0.05%
Max: displacement rate	3.75 mm/min Target
Ramp	1.2 mm/mm
Ramp target load control	1.0 mm/min





(b)

Figure 3.11 High-pressure triaxial testing system: (a) schematic diagram; (b) photograph of the cell in the loading frame.

3.4.3 Cell base connections

Pressure and electrical connections were made into the cell through the base of the cell. The cell base is shown in Figure 3.12 in standard form with pressure connectors in 7 out of 8 connections. All cable feed through are slotted on the outside of the cell to allow cable exit. The cell base has five pressure lines and five cable feed through holes. All pressure lines are provided with connectors on the outside of the cell. All cable feed through holes are slotted on the outside of the cell to allow cable exit. Therefore, all the necessary pressure and electrical connections could be made into the cell through the base of the cell.

To change the pedestal the four bolts must be removed on the outside of the cell base. The pedestal can then be removed. Care should be taken when placing the

new pedestal to ensure that the pore pressure ports in the pedestal and the base line up and that all of the O-rings are in place. The bolts should then be replaced and tightened. All pressure lines are provided with a Swagelok connector on the outside of the cell.

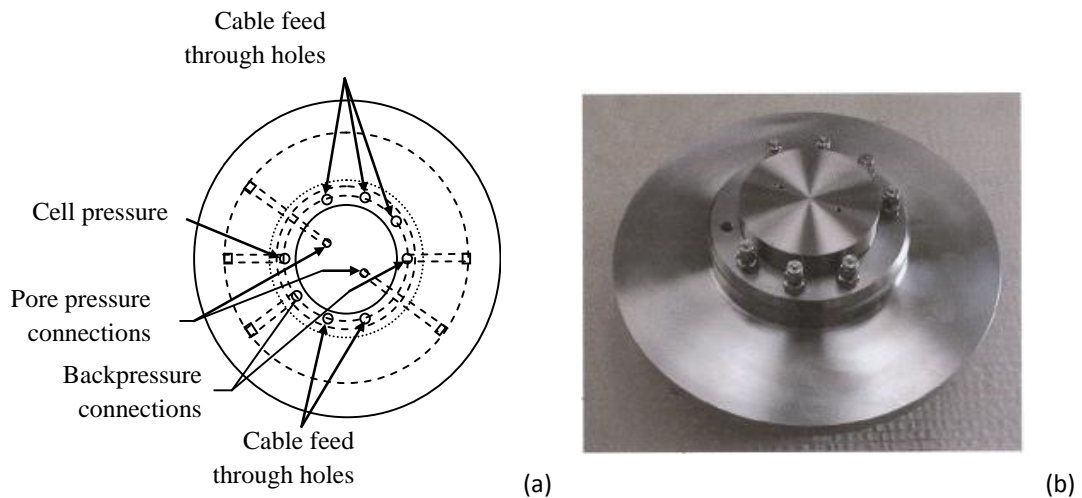


Figure 3.12 High-pressure triaxial cell: (a) Schematic cross-section and Cell photograph; (b) cell base schematic diagram and Cell base photograph.

3.4.4 Cell usage

For conventional pressure triaxial apparatus, before placing the cell on the cell base the load cell rod was raised enough making sure that it will not touch the specimen during cell placement to cause any damage or disturbance to the specimen. (The top drainage pipe folded accordingly so that it may not touch the cell walls that ultimately cause the specimen tilting). In addition, the bottom drainage pipe avoided of any pinching during the cell placement). After the cell positioned properly it was tightened with the screw rods. The load cell ram was then lowered just to touch the top cap of the specimen.

For high-pressure triaxial apparatus, the bolts in the balanced ram assembly were checked for sufficient tightness. Using an Allen Key, the bolts were tightened to the required torque. Prior to assembling the cell each time all the components were made clean and free of debris, as single sand particle can even stop the cell assembling correctly. The base plates were attached to the load frame using the bolts supplied. The bolts were tightened to correct torque and then the base platen permanently left in place. The balanced ram connection was made using the supplied stainless steel tube. The tube is connected between ports A-B as shown in Figure 3.13. The second A and B ports were sealed with the provided end stops. Port C end cap was removed and kept open to atmosphere. With the cell base on a flat, level surface the cell top assembly was lowered slowly into place using the two provided lifting eyes, taking care to manually guide it over the seal and to ensure it descends vertically. Once the cell top was in place the three-clamp ring parts were placed (as shown in Figure 3.14(a)) carefully not to damage the parts on assembly. Next, the retaining ring (as shown in Figure 3.14(b)) was placed over the loading frame. The cell is now ready to be placed into the loading frame. To open the cell the last four steps were reversed.

The cell is made of stainless steel, has a pressure capacity of 64 MPa and a working axial load capacity of 250 kN. The cell is designed to accept specimens with a diameter of up to 100 mm and a height of 200 mm without local strain instrumentation and up to a diameter of 70 mm and a height of 140 mm with local strain instrumentation. The high-pressure cell consists of three main parts, the cell base, the cell top, and the balanced ram assembly. The cell base is assembled to the cell top by using a

three-part split clamping ring, which is secured with the retaining ring. The high-pressure cell has the balanced ram assembly, installed at the top of cell the pressure chamber, which ensures zero uplift force and zero volume/pressure change inside the cell when the specimen is loaded at high cell pressure. The loading ram has a piston halfway along it, whose area is as twice as that of the ram itself. Furthermore, the chamber inside the balanced ram assembly is linked to the cell pressure chamber using the stainless steel tube connected to ports A and B, shown in Figure 3.13(a). As a result, when the cell pressure was applied during the triaxial test, the uplift pressure on the end of the ram was equal to the downward pressure applied by the upper chamber pressure on the top of the piston. Due to the balanced pressures acting on the triaxial cell ram, the vertical force applied to the loading frame was reduced significantly and the loading frame with relatively low capacity of 100 kN could be used in all the high-pressure tests. It should also be pointed out that the balanced ram helped controlling the cell volume/pressure during the test. When the vertical load was applied and the ram entered the cell, water from the pressure chamber was piped to the upper chamber. As the upper chamber inside the balanced ram assembly had the same swept area as the ram, there was no volume change in the cell fluid system. In this way, the DPVC could control the cell pressure more quickly and more accurately.

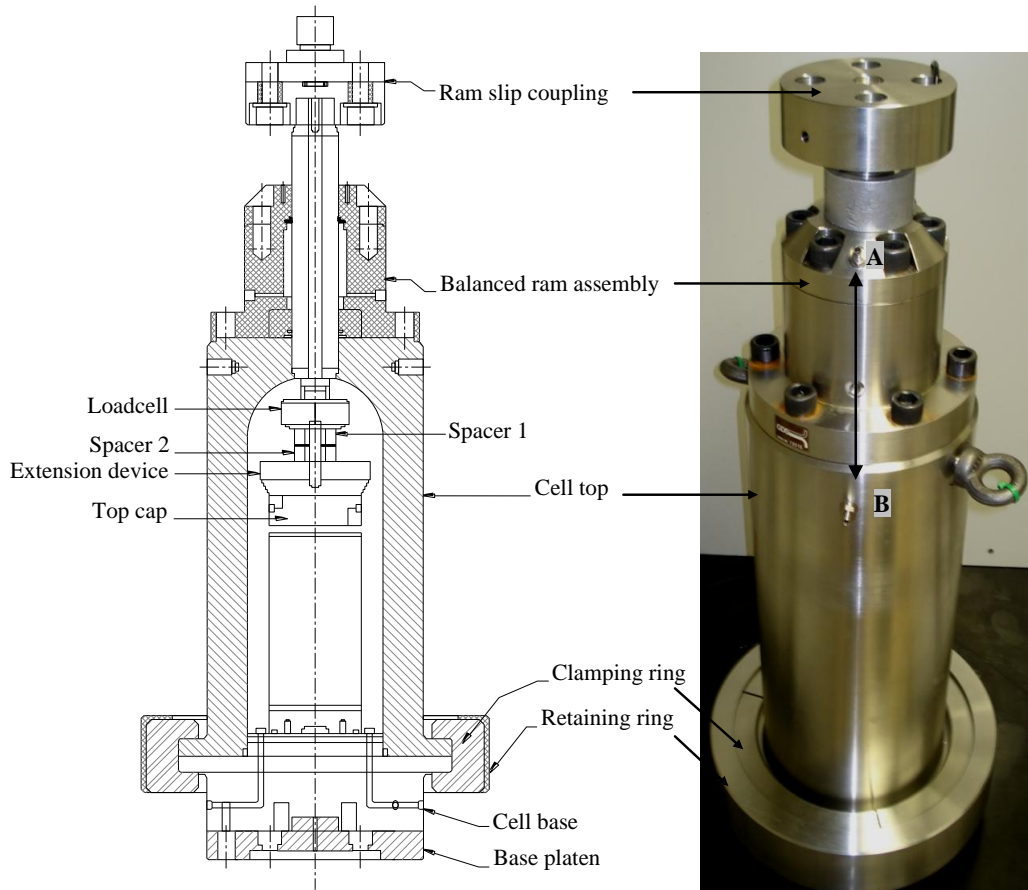


Figure 3.13 High-pressure triaxial cell.

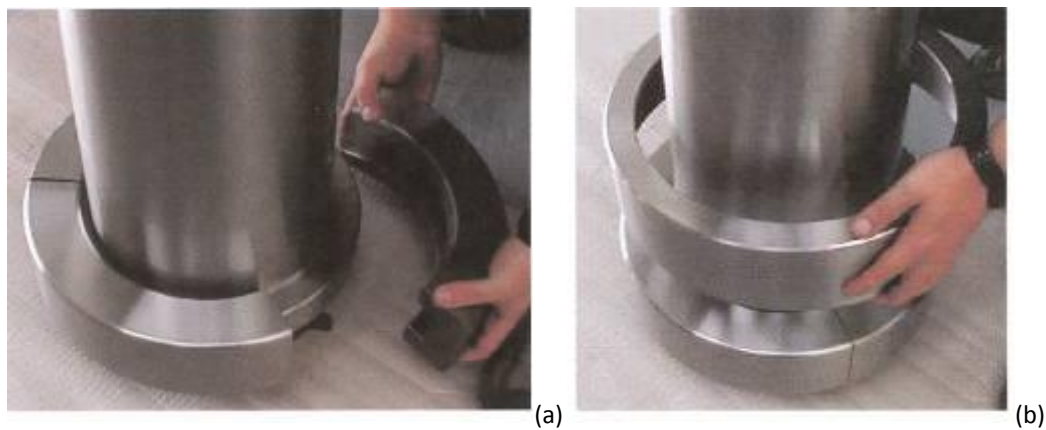


Figure 3.14 High-pressure triaxial cell: (a) Placement of clamp rings; (b) Placement of retaining ring.

3.4.5 Digital controller

The GDS digital controller (as shown in Figure 9) is a microprocessor controlled hydraulic actuator for the precise regulation and measurement of liquid pressure and liquid volume change. The GDS digital controller generates measures and logs both liquid pressure and volume change. The hydraulic fluid may be de-aerated water or oil. De-aerated water or oil in cylinder is pressurized and displaced by a piston moving in the cylinder. The piston is activated by a ball screw turned in a captive ball nut by a stepping motor and gearbox that move rectilinearly on a ball slide. Pressure is detected by means of an integral solid-state pressure transducer. Control algorithms are built into the programmable memory to cause the motor to seek to a target pressure or step to a target volume change. Volume change is detected by counting the steps of the stepping motor.

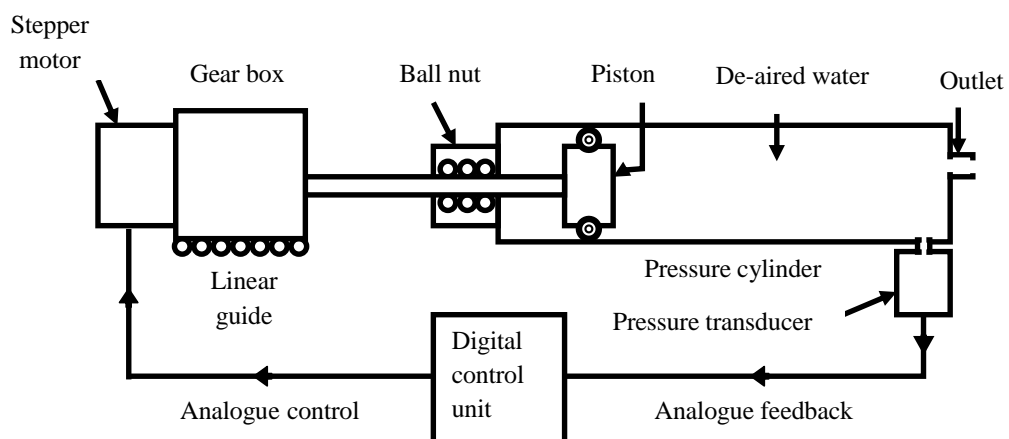


Figure 3.15 Digital controller of high-pressure triaxial testing system.

3.5 Salient features of high-pressure triaxial testing system

A high-pressure testing system, developed at the University of Nottingham, United Kingdom in conjunction with GDS Instruments Ltd. The loading frame is linked to a computer via the IEEE-488 standard interface and allows a continuous feedback con-

trol of axial load and displacement. The loading frame has a unique GDS virtual infinite stiffness (VIS) system that improves accuracy of soil and rock stiffness measurement. This is because the system minimizes compliance errors of the loading system and the load measuring system. Such equipment compliance errors add to variety of specimen bedding effects that tend to reduce the stiffness of tested materials compared to that measured in-situ (Jardine *et al.* 1984; Lo *et al.* 1989).

In the VIS axial loading system, both the measurement and control of platen displacement are automatically corrected so that it corresponds to the deformation that occurs between the base platen and the load button of the load cell. In this way, the displacement of platens is corrected for strain in the load cell and side columns of the frame, bending flexure of the crossbeam, and distortion within the motorized mechanical transmission. Therefore, the vertical displacement can be measured without additional external LVDT. However, in order to improve accuracy of the displacement measurement, local strain instrumentation can also be used.

The VIS system is calibrated by a computer to provide precise data on the load-deformation relationship of the entire load application measurement. The calibration data is loaded into the read only memory (ROM) of the system, which constantly monitors the axial load and uses the calibration to apply a correction to the platen displacement. It therefore appears to the controlling computer that the measurement of platen displacement is derived from a loading frame with “infinite” stiffness.

3.6 Scanning electron microscope

Micromechanical analysis can offer an insight into the nature of a soil and the way in which the structure changes in response to the stress and strain imposed on the soil mass. Several researchers have applied this technique for the investigation of micromechanical behaviour of soil; some of which have been reviewed in the literature.

Attention in the current study has been extended to the effects of density and cement content on the microstructure i.e., soil mineralogy, cement bonding, uniformity of the mix, bond breakage and particle crushing. Cemented sand sections at various densities and cement contents have been made and this has enabled the effects of density and cement content on the pre-deformation soil structure to be examined. The specimens with varying density and cement contents after isotropic compression, drained shearing and undrained shearing were examined to exhume the effect of compression and shearing on post-deformation particle and bonding structure.

The techniques used include scanning electron microscopy and energy dispersive spectrum (EDS) analysis. The analyses were carried out using EDAX Quanta 600 scanning electron microscope as shown in Figure 3.16. Attempt has been made to see the effect of cement content and density on the deformation characteristics of the material; both from microscopic and macroscopic approach. Our approach extends micromechanical analysis using the Scanning Electron Microscope equipped with Energy Dispersive X-ray Spectroscopy and Electron Backscatter Diffraction origi-

nally developed within the field of materials science for characterizing the properties of thin films and nano-scale materials.

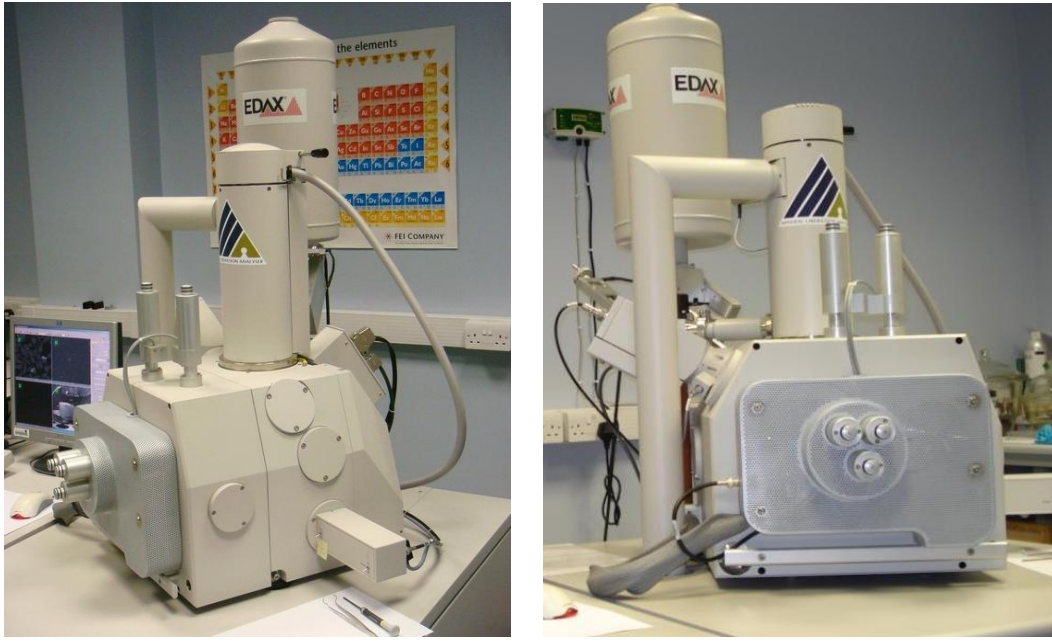
An SEM is essentially a high magnification microscope, which uses a focussed scanned electron beam to produce images of the sample, both top-down and, with the necessary sample preparation, cross-sections. The primary electron beam interacts with the sample in a number of key ways:-

- Primary electrons generate low energy secondary electrons, which tend to emphasise the topographic nature of the specimen.
- Primary electrons can be backscattered which produces images with a high degree of atomic number (Z) contrast.
- Ionized atoms can relax by electron shell-to-shell transitions, which lead to either X-ray emission or Auger electron ejection. The X-rays emitted are characteristic of the elements in the top few μm of the sample.

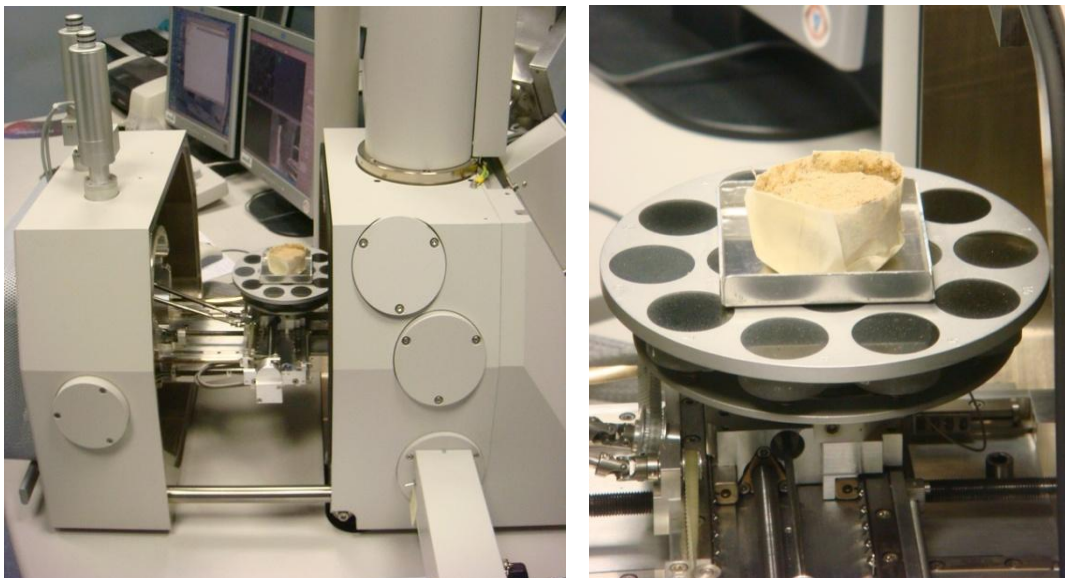
The SEM instrument has many applications across different industry sectors. The extremely high magnification images together with localised chemical information mean the instrument is capable of solving a great deal of common industrial issues such as particle analysis, defect identification materials and metallurgical problems.

Microscopic study of uncemented and cemented specimens of Portaway sand was carried out with the help of scanning electron microscopy (SEM). The specimens were investigated before and after the triaxial testing's. Before triaxial testing, particle shape, structure, sand-cement bond interaction (for cemented sand), and mineralogy of sand and sand-cement composition and homogeneity of the sand-cement

mix were examined. And after isotropic compression, consolidated drained shearing and consolidated undrained shearing, the specimens were investigated for subsequent deformations and change in the composite due to compression and shear.



(a)



(b)

Figure 3.16 Scanning Electron Microscope: (a) outside views; (b) inside views.

3.7 Testing procedure

The testing producers and the computer controlled software usage for conventional and high-pressure triaxial system similar except with slight differences in some of the steps. The detail procedure for both conventional and high-pressure testing is described below:

3.7.1 Saturation

For conventional triaxial testing system, water was flushed into the cell from cell valve and the top overflow valve was kept open to exit air from the cell. After filling the cell, first the cell pressure valve and then the top overflow valve was closed; assuring that there is no air entrapped in the cell and in the pipes. The cell valve was then connected with cell pressure panel. A typical cell pressure of 10-20 kPa was applied to keep the uncemented sample intact prior to the release of suction pressure. Once the cell pressure was established suction pressure was released by opening the bottom and bottom drainage valves.

For high-pressure triaxial system water was pumped into the cell through the cell pressure port in the base of the cell. Air was allowed to escape through the unused port "A" in Figure 3.13 shown in previous section. Once water is flowing uninterrupted from port, "A" it was then be sealed using the stop end provided. Testing was then carried out as required. To drain the cell after completion of the testing; pressure was first reduced to atmospheric pressure using a GDS pressure controller. Once atmospheric pressure has been achieved a drain tube was fitted to the cell pressure port in the cell base. The unused port "A" was opened. To speed drainage a

short large diameter tube was be used for the drain tube and if required a foot pump could be attached to port A to provide a small positive pressure to force the water out of the cell. It was assured that all pressure has dissipated before proceeding to next step. The cell was then opened. Once the cell was emptied the valves, the load cell and top loading frame were disconnected by unlocking the screws.

The bottom drainage valve was connected with backpressure panel and de-aired distilled water was used to saturate the specimen, which was flushed by a small pressure difference of 5–10 kPa for uncemented materials and 20-50 kPa for cemented materials. The flushing was continued for about an hour to ensure sufficient amount of water driven through to remove air entrapped. The flushing was maintained by pushing water through bottom drainage valve of the specimen that was connected with backpressure panel. The top drainage valve of the specimen was kept open for air removal from the specimen.

After flushing was completed, the pressure panels were checked to assure that these were refilled. Both top and bottom drainage valves were connected with the backpressure panel. After flushing the rest of the experimental steps were controlled through the computer control GDS software.

The cell pressure, and backpressure panels were ensured that these are filled with water (if not these should be refilled before commencing to the next step). GDS software was opened and a new file was created for each test. The initial essential (such as diameter, height) and supplementary (such as specific gravity, mass, density, sample date etc) values were put in the software window. In the satcon: satura-

tion ramp stage was created with a specified targeted cell and backpressures to reach the target pressures in given time (usually overnight time for proper saturation).

Backpressure saturation of typically 700 kPa for uncemented sand and 1000-2000 kPa for cemented sand was held until to ensure that the B -value was greater than 0.95 and 0.9 for uncemented and cemented sand respectively. The specimen saturation ramp was applied by rising the cell pressure and backpressure simultaneously, keeping the effective stresses constant typically 50-100 kPa.

After saturation ramp completion, to ensure the required saturation of the specimen, B -value check was applied. A new stage of B -check was created. During B -check the backpressure was kept constant and cell pressure was increased. Typically the cell pressure change was kept 100 kPa and the change in pore pressure was measured. B -value was calculated as is given in the following equation:

$$B = \frac{\Delta u}{\Delta \sigma_3} \quad (3.4)$$

For uncemented materials B -value above 0.95 and for cemented materials 0.9 was assured (if not the saturation ramp was applied again).

The excess cell pressure was then released by targeting the cell pressure to the original value from control panel.

3.7.2 Consolidation

The consolidation stage was created from satcon: the target backpressure was kept same and the target cell pressure was set to the required value to that the speci-

mens need to be consolidated. Before starting, the consolidation stage back volume was set zero.

The specimens were isotropically consolidated to the desired confining pressures and the volume changes were measured exactly at the end of consolidation. In isotropic loading only one-way drainage was permitted and the consolidation stage was continued until the back volume change approached to zero. A pore pressure transducer at the undrained end of the specimen was used to detect the end of primary consolidation.

3.7.3 Drained shearing

For standard triaxial drained compression, shearing commenced at the end of primary consolidation. From triaxial acquisition, consolidated drained (CD) stage was created. Prior to starting the shear stage axial displacement and axial strain were set to zero. All the CD tests were carried out under a deformation-controlled loading mode at a constant rate of 0.02 mm/min (1.2%/h) with constant control maintained for the cell pressure and backpressure. The load was applied at such a slow strain rate that particle readjustments in the specimen do not induce any excess pore pressure. GDS computer data logger was used throughout for test control and data acquisition.

3.7.4 Undrained shearing

For standard triaxial undrained compression, shearing commenced at the end of primary consolidation. From triaxial acquisition, consolidated undrained (CU) stage was created. Prior to starting the shear stage axial displacement and axial strain were set to zero. All the CU tests were carried out under a deformation-controlled

loading mode at a constant rate of 0.2 mm/min with constant control maintained for the cell pressure and backpressure. GDS computer data logger was used throughout for test control and data acquisition.

3.8 Strength control

Dry density of the compacted soil is one of the main factors that influence the strength of the cement-sand. In addition, the water is essential to achieve maximum density and to aid in hydration of the cement. Cement-sand samples prepared using the standard Proctor compaction tests with cement contents of 0%, 5%, 10%, and 15%. The average optimum moisture content of around 10% was observed to be giving the maximum dry density for the Portaway sand. Samples with aforementioned cement contents were prepared at the constant maximum dry unit weight of 17.4 kN/m³ (approx :), and were cured for 14 days in moisture control room. The average values of unconfined compression test parameters are given in Table 3.3.

Table 3.3 Average values of unconfined compression test parameters.

No.	samples	H (mm)	D (mm)	γ (kN/m ³)	Cement	Load (kN)	UCS (kN/m ²)	Cohesion
1	3	100	50	17.4	5	1.11	564	282
2	3	100	50	17.4	10	4.35	2213	1106
3	3	100	50	17.4	15	10.88	5541	2770

Unconfined compressive strength (UCS) tests were conducted on these samples. The typical failure mode of cemented specimen in unconfined compression test is as shown in Figure 3.17. The average results are presented in Figure 3.18. The UCS is observed to be increasing exponentially with the increase in cement content. For the specified dry unit weight, the UCS can be correlated with the cement content by the following equation.

$$q_u \cong 20C^2 \quad (3.5)$$

Where,

q_u = unconfined compressive strength

C = cement content in percent



Figure 3.17 Typical failure mode of cemented specimen in unconfined compression test.

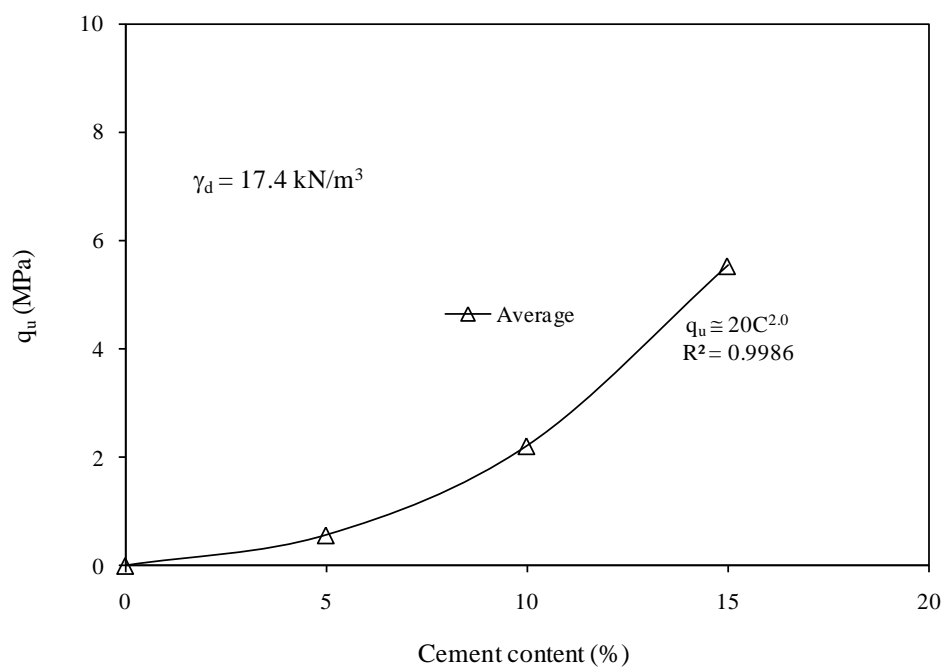
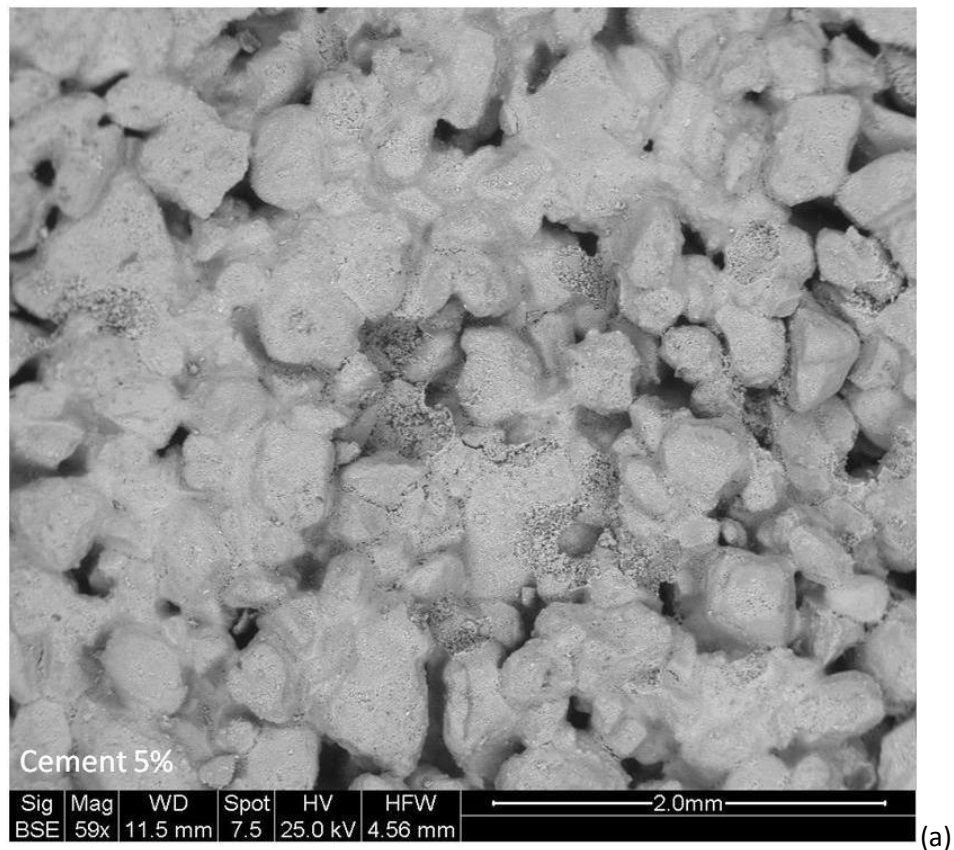


Figure 3.18 Effect of cement content on unconfined compressive strength of Portaway sand.

3.9 Homogeneity of the cemented specimens

Even though prior to the specimens preparation the materials were thoroughly mixed until acquiring a homogeneous and quite consistent mix in visual observations; however, yet there can be seen some poor bonding and cement deposition on the surface of the sand grains. Microstructure of the composite (cement + sand) as shown in Figure 3.19 reveals that the homogeneity of the composite at microstructure level is not ideally consistent. Repeatedly tested specimens eventually demonstrated that the perfect homogeneity is relatively hard to achieve at micro-scale level.



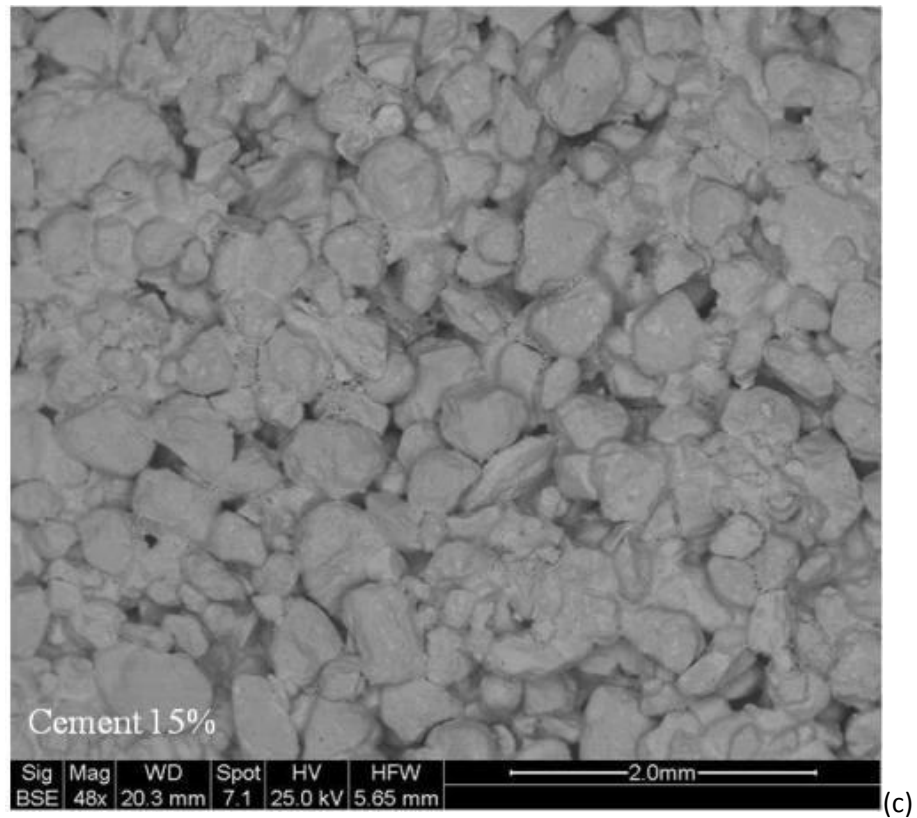
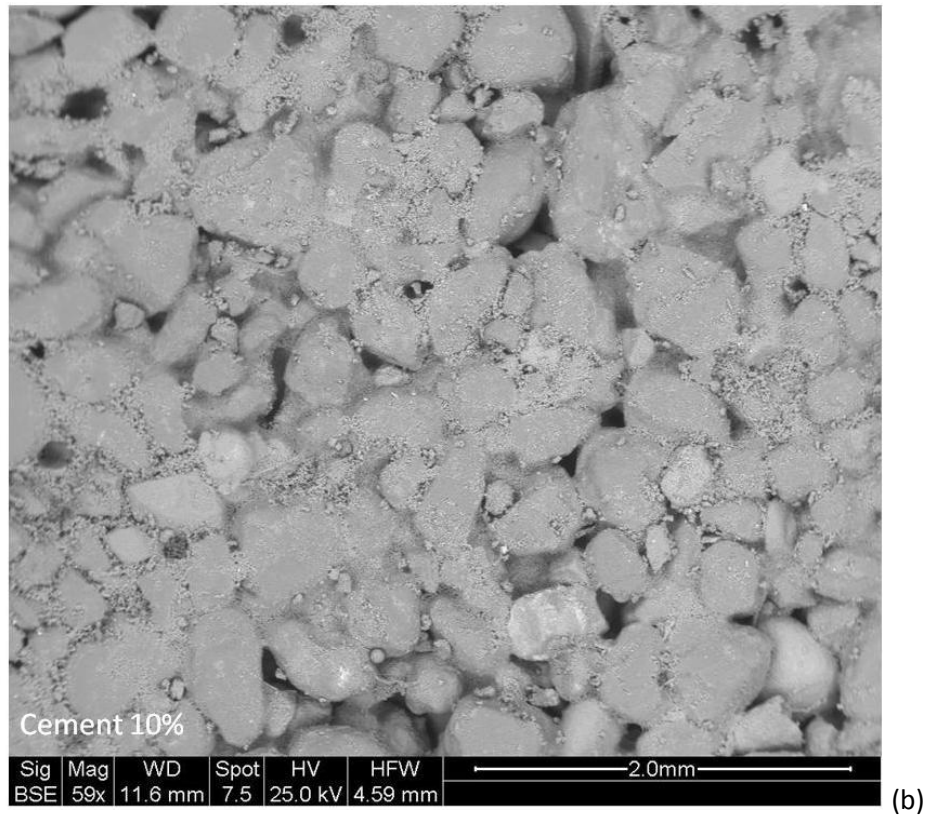


Figure 3.19 Microstructure of dense cemented sand with cement content of: (a) 5%; (b) 10%; and (c) 15%.

3.10 Effect of cement content on specific volume

According to the (Coop and Atkinson 1993) the addition of gypsum, fines result in samples of considerably smaller specific volume. However, it is in contrary for Portland cement. This is due to the specific weight of the cementing materials as compared to the base material. For example, the specific weight of Portaway sand is 2.65 and that of an average value of the specific weight of the gypsum is approximately 2.3. On the other hand, the specific weight of Portland cement is 3.15. Therefore, increase in gypsum content results of decreasing the specific volume and increase in cement content results an increase in specific volume of the composite (Figure 3.20). Differences in the specific gravities of the gypsum/cement and the sand also affect the density and thus even if the void ratios are identical, the densities will be different, possibly leading to differences in behaviour.

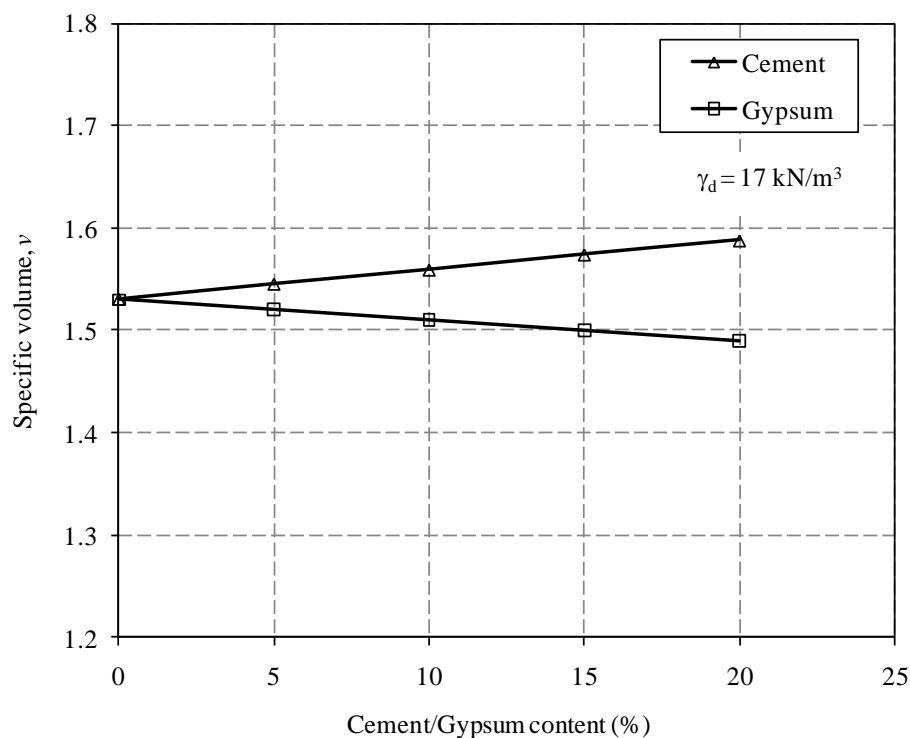


Figure 3.20 Effect of Portland cement and gypsum content on the specific volume of cemented sand

3.11 Calculations of derived parameters

3.11.1 Constant dry unit weight

For a constant dry unit weight with different cement contents, as the volume of the mould is same let suppose V ; therefore, to get a constant dry unit weight (γ_d), the dry mass should also be constant for different percentages of cement. If M_{total} is the total mass of sand + cement and C is the percent of cement by dry weight of sand then, the mass of sand M_{sand} and mass of cement M_{cement} can be calculated as follows:

$$M_{sand} = \left(\frac{100}{100 + C} \right) M_{total} \quad (3.6)$$

$$M_{cement} = \left(\frac{C}{100 + C} \right) M_{total} \quad (3.7)$$

Where, C is taken in percentage

3.11.2 Void ratio

Inter-granular void ratio- is the void ratio of the coarser grain matrix. The term “volume of voids” in the definition of void ratio refers to the space that is not occupied by the mineral grains. When a sandy soil or a reconstituted mixture with some amount of fines is examined, the volume of voids can further be subdivided into two categories as voids due to skeleton particles sand grains and voids due to finer grains.

Similarly, the grain matrix can also be categorized as coarser grain matrix and finer grain matrix. These matrices are expected to influence each other and the overall macro behaviour. The void ratio of each sample was calculated from the initial dry

unit weight. Following procedure was adopted for the determination of the void ratio of a cemented specimen and establishing a relationship between cement content and specific volume.

Determine

1. The specific gravity of sand G_{sand}
2. The specific gravity of cement G_{cement}
3. The dry mass of specimen, M_{dry} i.e., the mass of solid, M_{solid}
4. Specimen dimensions i.e., height, H and diameter, D

Calculate

1. The average specific gravity of the specimen G (taking cement content = C %)

$$G = \frac{100 - C}{100} \times G_{sand} + \frac{C}{100} \times G_{cement} \quad (3.8)$$

2. The volume of solid (i.e., sand + cement) V_{solid}

$$V_{solid} = \frac{M_{solid}}{G \times \rho_w} \quad (3.9)$$

3. The total volume of the specimen V_{total}

$$V_{total} = \frac{\pi}{4} D^2 H \quad (3.10)$$

4. The volume of voids V_{voids}

$$V_{voids} = V_{total} - V_{solid} \quad (3.11)$$

5. The initial void ratio of the specimen e

$$e = \frac{V_{voids}}{V_{solids}} \quad (3.12)$$

Void ratio during consolidation

$$e_{ci} = \frac{V_{voids} - (V_{Bvol})_{ci}}{V_{solids}} \quad (3.13)$$

where $(V_{Bvol})_{ci}$ is the back volume during consolidation

Void ratio during shear

$$e_{si} = \frac{V_c - (V_{Bvol})_{si}}{V_{solids}} \quad (3.14)$$

where V_c is the volume of voids at the end of consolidation and $(V_{Bvol})_{si}$ is the back volume during shear. V_c can be calculated as:

$$V_c = V_{voids} - (V_{Bvol})_{cf} \quad (3.15)$$

$(V_{Bvol})_{cf}$ is the back volume at the end of consolidation

3.11.3 GDS software calculated parameters

The computers controlling the operation of conventional and high-pressure triaxial apparatus are provided with GDS software. This software has capability of creating and saving data files. Many of the basic parameters of triaxial test results are automatically calculated. The formulation of these background calculations is briefly described here:

1) Axial force, F (kN)

$$F = \text{Load cell reading} + \text{radial pressure (area of specimen- area of ram)} \quad (3.16)$$

2) Axial stress, σ'_1 (kPa)

$$\sigma'_1 = \frac{F}{A} \quad (3.17)$$

$$p = \frac{\sigma_1 + 2\sigma_3}{3} \quad (3.18)$$

$$p' = p - u = \frac{\sigma'_1 + 2\sigma'_3}{3} \quad (3.19)$$

$$\varepsilon_r(\%) = \frac{\Delta D}{D_0} \times 100 \quad (3.20)$$

3) Specimen corrected area

$$A_{corrected} = \frac{\frac{\pi}{4} D_0^2 H_0 + \Delta V}{H_0 - \Delta H} \quad (3.21)$$

4) Shear strain

$$\varepsilon_s = \frac{2}{3} (\varepsilon_a + \varepsilon_r) \quad (3.22)$$

where ΔD is the average diameter change and D_0 is the initial diameter.

3.12 Problems involved with triaxial testing of cemented soils

Evaluation of errors should be an important aspect of all experimental investigations. However, based on the common belief that soil variability dominates most measurement errors and hence negate these aspects, nevertheless the testing system and experimental data should be checked for certain basic concepts regarding different sources of errors, both for improving testing practice and for general perspective.

During the sample preparation and testing there is likelihood of certain errors due to several means and reasons, some of these can be avoided by careful handling, and some are unavoidable. Therefore, for a good quality results it is important to be cautious about such type of errors and apply necessary corrections for unavoidable errors before subsequent investigations and analysis.

An exploratory series of test were run to identify and fix the problems before the commencement of investigatory testing.

3.12.1 Stratification of the samples

For the preparation of the samples, the method of undercompaction is theoretically quite reasonable as compared to normal compaction methods of compacting, each layer with equal number of blows. However, controlling height and uniformity of the blows have always been bit tricky. A suitably height and base rotation controlled device might bring some consistency. Secondly, the more objectionable point is to avoid layering. Even carefully scarifying the surface of each layer prior to the placement of subsequent layers, the layering effect could not be avoided. Although at conventional pressure it is not noticeable; however, at high confining pressures the layering effect can be seen clearly (Figure 3.21).



Figure 3.21 Stratification of cemented materials prepared by the method of undercompaction compressed at high confining pressures: (a) before isotropic compression; (b) after isotropic compression.



Figure 3.22 Homogeneity check of cemented materials prepared by density controlled vibratory tamping method compressed at high confining pressures (a) before isotropic compression; (b) after isotropic compression.

On the other hand, by 'density controlled vibratory temping', it can be seen that there is no layering effect even compressed at high confining pressures (Figure 3.22). However, it further needs to be investigated for any other effects, such as bleeding and segregation and uniformity of cement bonding (in particular for loose cemented specimens) etc.

3.12.2 Membrane puncture

During experimentations, it was noticed that the membranes were more prone to damage and puncture at high pressures. In particular, the maximum likelihood of the membranes to be damaged and punctured were noticed at contact points of porous stone with the specimen edges (Figure 3.23), sharp edges of the grains pointing outward on the surface of the specimen and deformation along the shear plane (Figure 3.24). The loose and porous cemented specimens resulted to the membrane puncture due to penetration (Figure 3.25) ultimately resulting to the test failure.

In order to avoid testing failures due to membrane damage and puncture at high pressures, double membranes were provided to the specimens. The top and bottom edges were covered with thin strips of membrane (Figure 3.26) and the pores on the surface of the specimens (in case of porous samples) were filled with clay-sand mixture. The mentioned remedial measures were resulted to a successful completion of testing (Figure 3.28).



Figure 3.23 membrane puncture along the edge of the specimen.

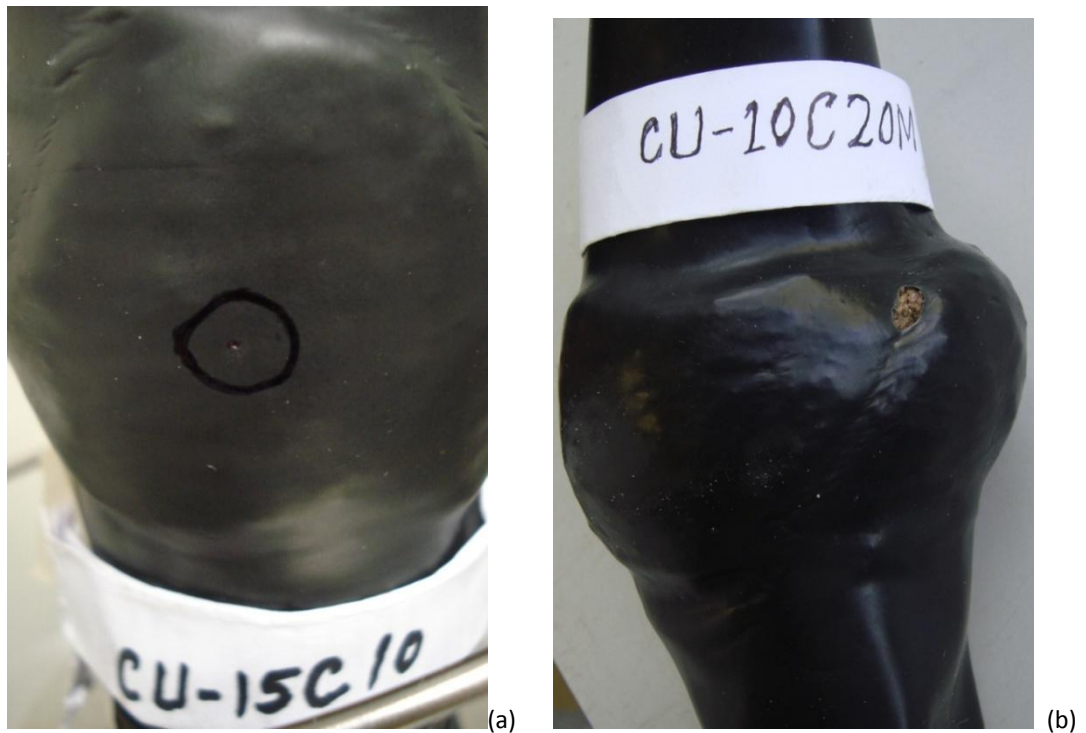


Figure 3.24 Membrane damage and puncture: (a) due to sharp edges of particles; (b) along shear plane.

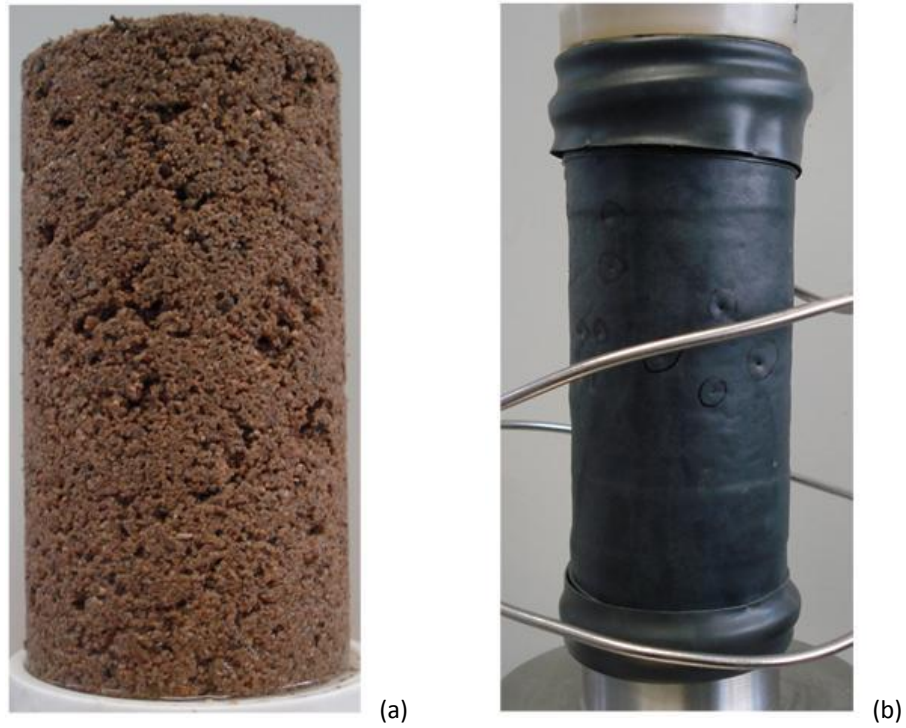


Figure 3.25 Membrane puncture: (a) Loose and porous cemented specimen resulting; (b) the membrane punctures due to penetration.

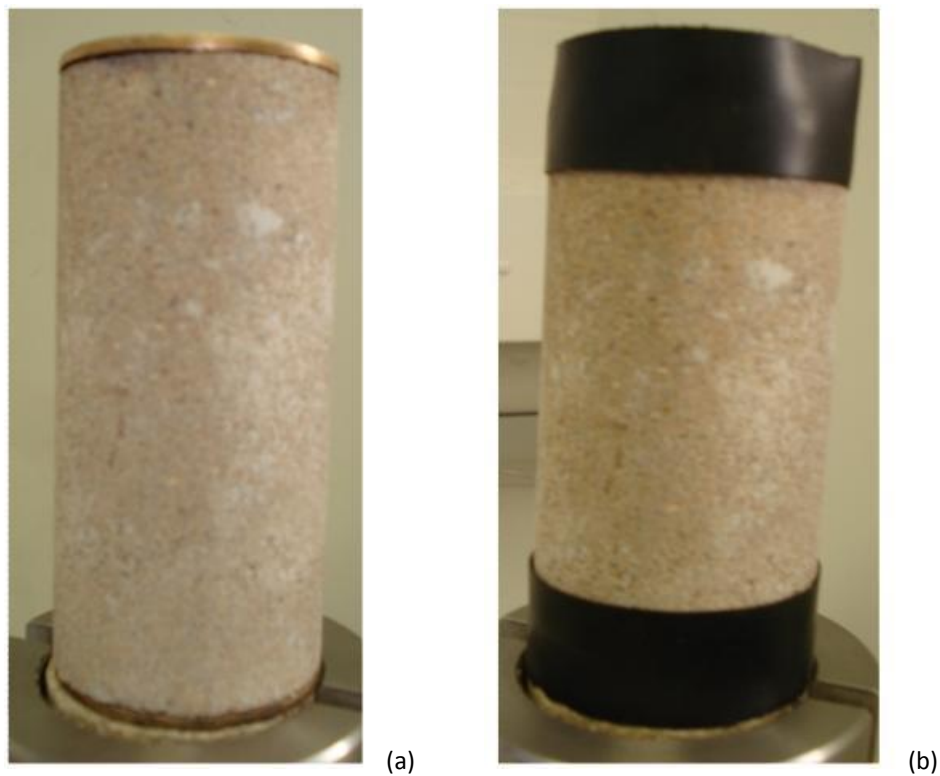


Figure 3.26 Avoiding membrane puncture: (a) the top and bottom edges of the specimen; (b) Membrane strip provided to avoid penetration and puncture at sharp edges.

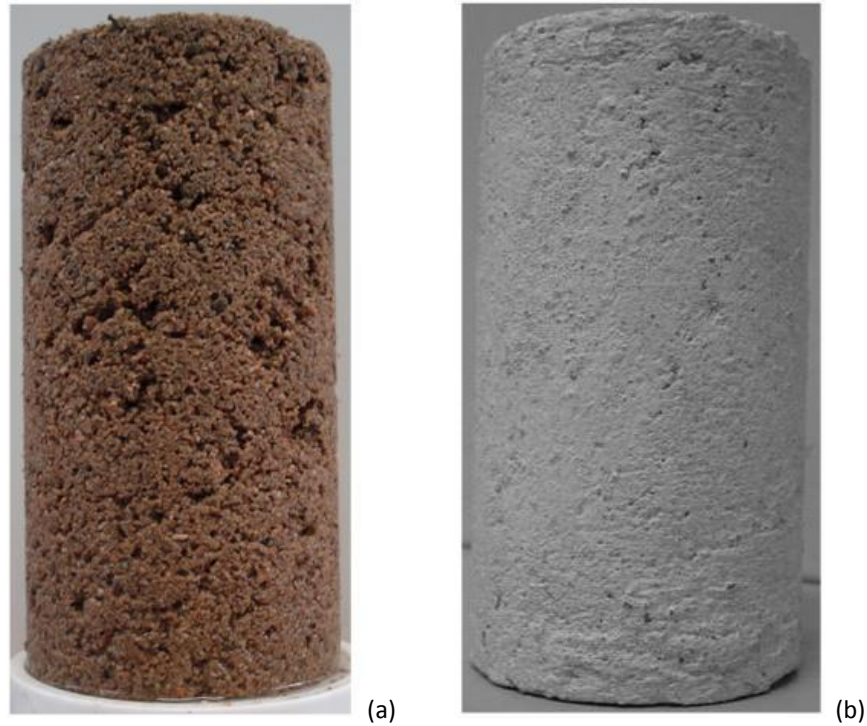


Figure 3.27 Avoiding membrane puncture: (a) Pores on the surface of the sample (b) Pores are filled with clay sand mixture to avoid membrane punctures.

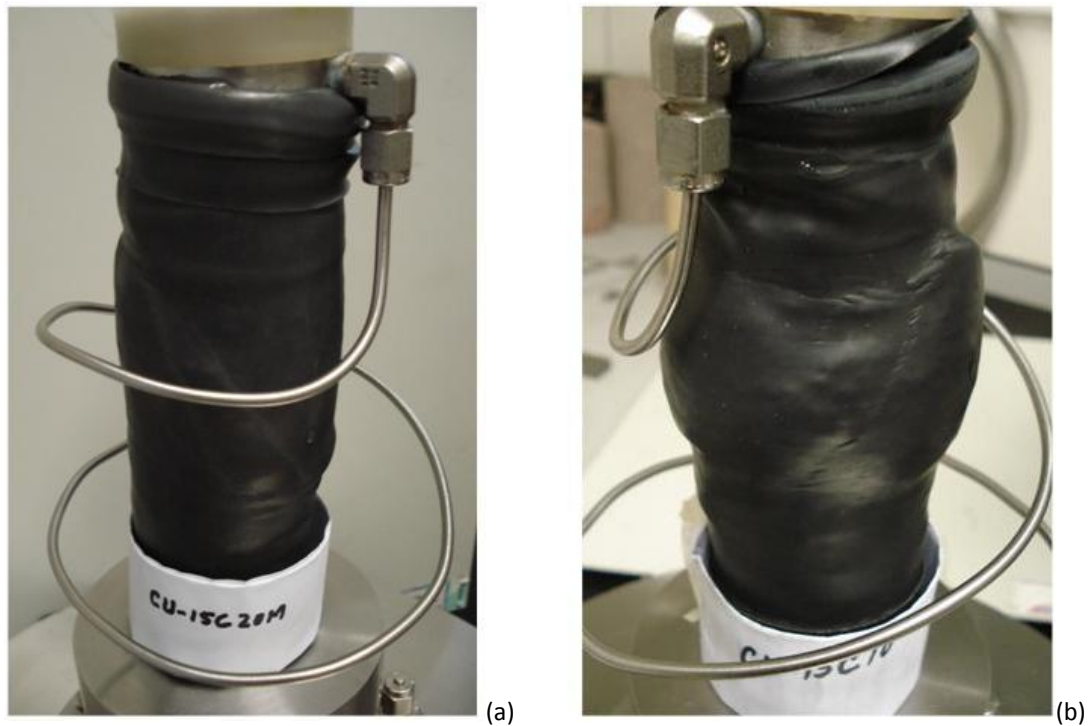


Figure 3.28 Successfully completed experiments after remedial measures against punctures: (a) sample with diagonal shear band; (b) sample with conjugate shear band.

3.13 Repeatability of test results

Repeatability of test results was verified by the results of experiments performed on Portaway sand.

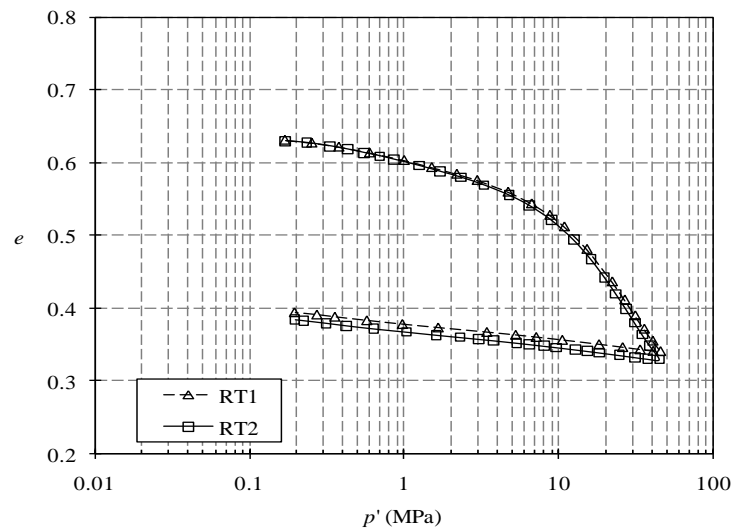


Figure 3.29 Repeat tests on Portaway sand during isotropic loading and unloading.

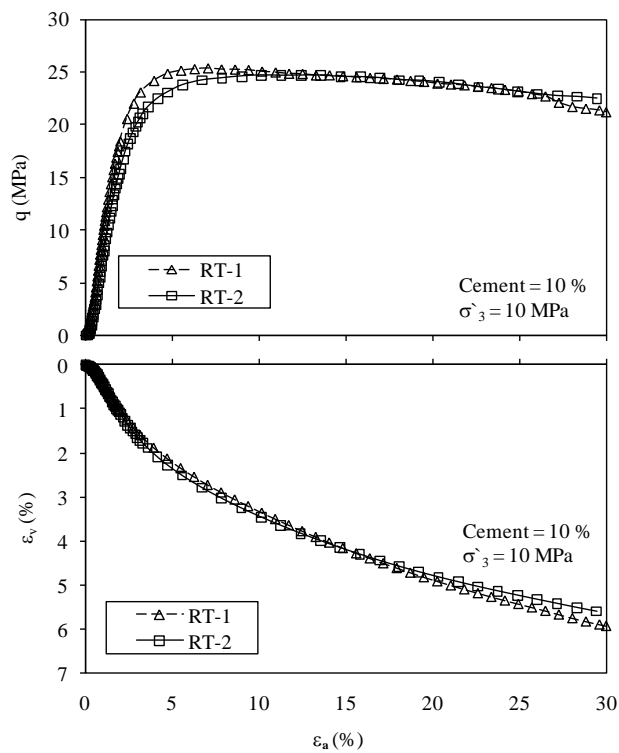


Figure 3.30 Repeat tests on cemented Portaway sand during consolidated drained compression.

The isotropic compression tests were run under isotropic loading and unloading and drained compression tests were performed on dense cemented sand by “repeat tests” at selected effective confining pressures, σ'_3 . Good agreement was obtained for both isotropic (Figure 3.29) and drained compression tests (Figure 3.30).

3.14 Summary

Well-graded, medium quartz sand from Sheffield (England), so-called Portaway sand was used as the base material for the cemented specimens. The index properties of Portaway sand were determined by British Standard methods (BS 1377). The sand grains were mainly sub angular and sub rounded in shape. Before the preparation of cemented specimens, the sand was passed through 2 mm sieve to remove gravel size particles and washed through 0.063 mm sieve under the running water to remove fines. Ordinary Portland cement was used as cementing material. Its initial setting time is 80 to 200 minutes and the specific gravity of 3.15.

Method of undercompaction using moist soil was adopted for the preparation of both cemented and uncemented sand specimens to achieve varying degrees of initial relative densities, void ratios, and dry unit weights. Bishop-Wesley Conventional pressure and GDS high-pressure triaxial apparatus were used for conventional and high pressure triaxial testing respectively.

The first stage of each test was the sample saturation. This was done by applying a small positive effective stress and then raising simultaneously both the cell and backpressures keeping the effective stress constant. The backpressure was increased typically to around 700 kPa, for uncemented sand and to around 2000 kPa for ce-

mented sand, when the pressures were kept constant and the sample was allowed to saturate for at least 24 h or longer if required, until a B value of 95% was achieved.

An exploratory series of tests were run to identify and fix the problems before the commencement of investigatory testing. Specimen stratification and membrane punctures were noticed at high pressures. Suitable arrangements were made to avoid these errors.

The effect of cement type having different specific unit weights was examined. For example, by the increase in gypsum content having specific unit weight less than the Portaway sand resulted to decrease in the specific volume of the composite; on the other hand the addition of Portland cement resulted to increase in the specific volume of the composite.

Microscopic study of uncemented and cemented specimens of Portaway sand was carried out with the help of scanning electron microscopy (SEM). Particle shape, structure, sand-cement bond interaction (for cemented sand), and mineralogy of sand and sand-cement composition and homogeneity of the sand-cement mix were examined. Moreover, the specimens were investigated for subsequent deformations, change in the structure due to compression, and shear.

ISOTROPIC COMPRESSION TESTS

4.1 Introduction

This chapter is aimed at a fundamental understanding of the behaviour of cemented sand under isotropic compression, when compared with uncemented sand. High-pressure isotropic compression tests were carried out on samples of uncemented and cemented Portaway sand at different initial void ratios, initial relative densities, and cement contents. The list of typical isotropic compression tests discussed is given in Table 4.1.

Table 4.1 Summary of typical isotropic compression tests.

Test	σ'_3 (MPa)	C (%)	γ_d (kN/m ³)	D_r (%)	e_0	e_c
IC-0C20M	20	0	17.4	90	0.493	0.383
IC-5C20M	20	5	17.4	87	0.504	0.403
IC-10C20M	20	10	17.4	83	0.517	0.467
IC-15C20M	20	15	17.4	78	0.531	0.494
IC-0C20M	20	0	17.4	90	0.493	0.383
IC-5C20M	20	5	17.6	90	0.493	0.394
IC-10C20M	20	10	17.7	90	0.493	0.444
IC-15C20M	20	15	17.9	90	0.493	0.459
IC-0C50M	50	0	17.4	89	0.495	0.277
IC-0CL50M	50	0	16.2	48	0.631	0.341
IC-5C50M	50	5	17.4	87	0.503	0.366
IC-10C50M	50	10	17.4	81	0.523	0.453
IC-10CMD50M	50	10	16.7	62	0.584	0.464
IC-10CL50M	50	10	16.0	40	0.657	0.453

The effects of different initial void ratios, initial relative densities, and cement contents on the compression characteristics of Portaway sand were investigated. The ef-

fects of high confining pressure on particle crushing and cement bond breakage were examined in further detail with the help of scanning electron microscopy analysis of the specimens retrieved after isotropic compression. Effects of cement content and confining pressure on the yield stress during isotropic compression were also investigated.

4.2 Effect of initial void ratio

In order to observe the effect of initial void ratio on the isotropic compression characteristics of uncemented and cemented sands, high-pressure isotropic compression tests were carried out on samples of uncemented and cemented Portaway sand at different initial void ratios (e_0). The cement contents of 0%, 5%, 10%, and 15% were used and the resulting isotropic compression e - $\ln(p')$ curves are plotted. From the compression curves of uncemented sand as shown in Figure 4.1, it can be noticed that by the progressive increase in the confining pressure there is tendency of convergence in the compression curves of the sand specimens prepared with different initial void ratios. At the end of isotropic compression, the curves tend to approach to a unique void ratio at high-pressures.

Similarly, from Figure 4.2, which shows the e - $\ln(p')$ curves of cemented sand, it can be observed that the cemented sand also demonstrates similar trend of convergence in the compression curves and having tendency to approach a unique void ratio at high-pressures as is noticed for uncemented sand. This suggests that by the increase in confining pressure during isotropic compression, there is tendency of convergence in the compression curves for both uncemented and cemented sands, which are

prepared at different initial void ratios. The only difference that can be noticed in the compression curves of uncemented and cemented sands is the difference in the compression path and the compression index. For instance, at the end of compression the final void ratio for uncemented sand is less than the final void ratio for cemented sand, i.e., the cemented sand is relatively less compressible as compared to the uncemented sand. The numerical values of the final void ratio at the end of consolidation (e_c) for uncemented and cemented sand are given in Table 4.1.

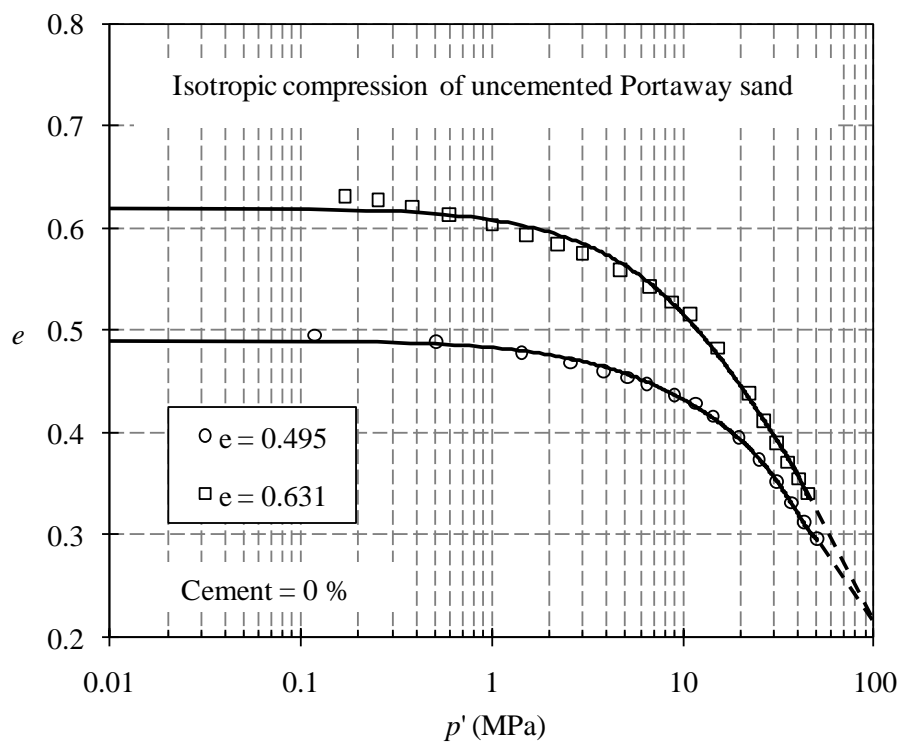


Figure 4.1 Isotropic compression curves of uncemented Portaway sand at different initial void ratios.

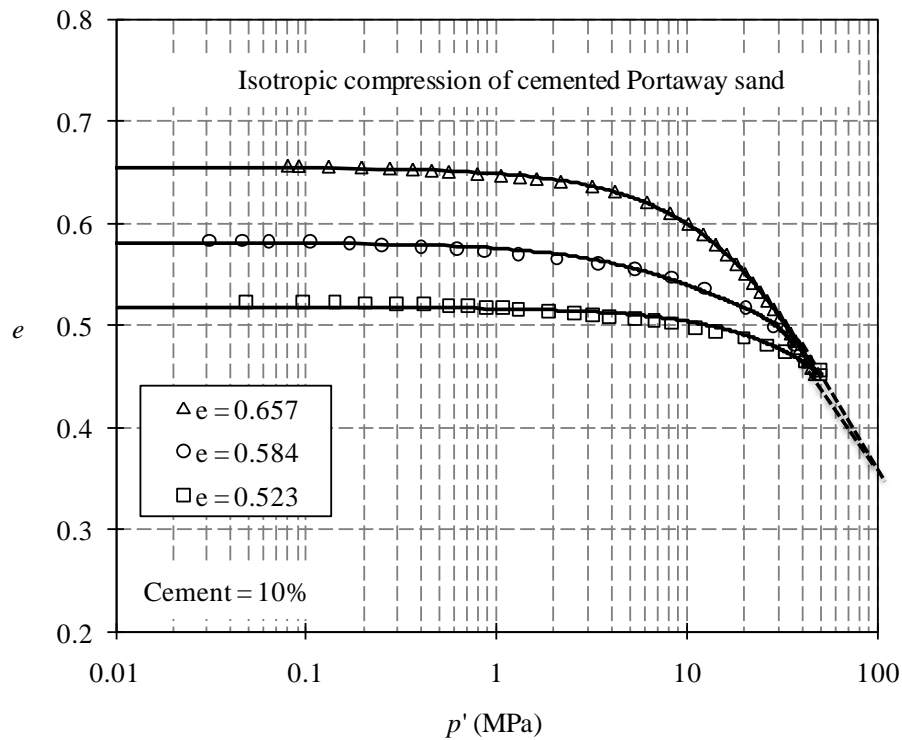


Figure 4.2 Isotropic compression curves of cemented Portaway sand at different initial void ratios.

4.3 Effect of cement content

The parametric relationship of the variation of void ratio at the end of consolidation with effective confining pressure at different cement contents is shown in Figure 4.3. The specimens with cement contents of 0% (i.e. uncemented), 5%, and 10% were prepared at constant dry unit weight of 17.4 kN/m^3 . It is to be noted that due to different cement contents there is slight difference in the initial void ratios of the specimens in spite prepared at same dry unit weight as shown in Table 4.1. The relationships of the variation of void ratios taken at the end of isotropic compression versus effective confining pressures suggest that the increase of cement content results to decrease in the sand compression. Therefore, for the specimens prepared at constant dry unit weight with different cement contents, the void ratios will be hav-

ing tendency of more divergence by the progressive increase in the confining pressures.

The effect of cement content on the compressibility was also investigated by keeping the dry unit weight constant as shown in Figure 4.4. It can be seen that at the constant dry unit weight of 17.4 kN/m^3 , there is slight difference at the beginning of the tests due to the change in cement content. Moreover, it can be observed that the rate of compression of sand is decreasing with the increase in cement content and therefore, at the end of compression the difference in the void ratio is more pronounced. The difference in initial void ratios due to cementation and final void ratios due to confining pressure for the specimens with initial dry unit weight of 17.4 kN/m^3 are shown in Table 4.1. Similar investigations were made to observe the effect of cement contents on the compressibility of sand by keeping the initial void ratio constant ($e_o = 0.493$) as shown in Figure 4.5. Trend of increase in the difference of void ratio by the increase in confining pressure for different cement contents can be seen even the initial void ratio is constant. This might be due to the reduction in particle crushing because of increase in the cement content, as the large volume change can only occur when particle crushing becomes dominant. Therefore, the specimens with different cement contents but prepared at same initial void ratios (e_o) show different final void ratios (e_c) at the end of compression. The numerical values of final void ratio (e_c) having constant initial void ratio $e_o = 0.493$ are given in Table 4.1.

State paths during isotropic compression may be plotted on a graph of specific volume, v versus logarithm of mean effective stress, $\ln(p')$. For soils compressed for the

first time, there is a unique relationship between specific volume and mean normal effective stress p' , which is represented by a straight line on the graph of v against $\ln(p')$, known as the isotropic normal compression line (NCL).

$$v = N + \lambda \ln (p') \quad (4.1)$$

where, λ is the compression index and for sands it is relatively large due to particle crushing.

Soil cannot usually be at a state outside the normal compression line unless it is bonded or structured. The effect of cement content on the normal compression line of uncemented sand (0% cement) and cemented sand (10%) is shown in Figure 4.6. It can be seen that when the cemented Portaway sand with different initial void ratios is compressed, the compression curves appear to approach the same NCL, however, different from the normal compression line approached by the uncemented Portaway sand. The addition of cement to the sand appears to have no appreciable effect on the slope of NCL but moves it outside the NCL of uncemented sand i.e., increase in cement content shifts the NCL to the right. This suggests that cementitious bonds are sufficiently strong relative to the particles to allow the cemented samples to reach states outside the NCL of the uncemented soil. This shift in NCL is in accordance with the previous reports (Consoli *et al.* 2005, Dos Santos *et al.* 2009).

However, the assumption that high confining pressure would cause the cement bond breakage and progressively diminish the cement content effect; ultimately, resulting to a destructed material, which would result to a similar trend as that for uncemented sand might not be validated for NCL. From the experimental results, there ap-

pear to be negligible convergence and for effective confining pressures up to 50 MPa, the normal compression lines are still essentially parallel. The effect of cement content on the cement bond-strength and particle crushing might be a crucial factor and need further investigation.

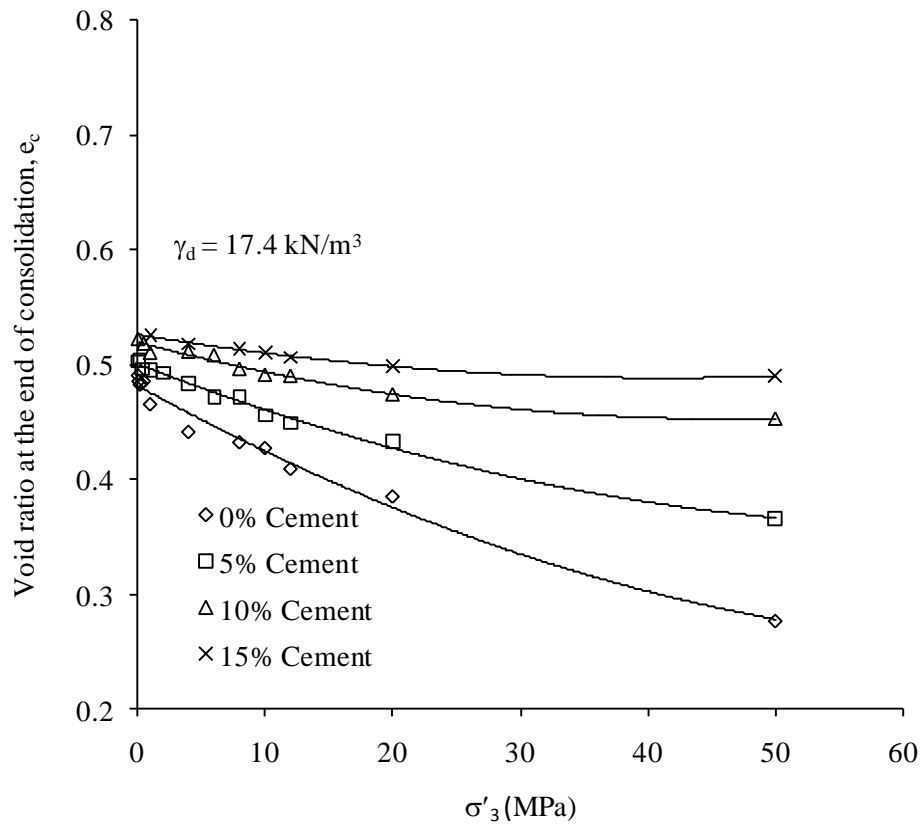


Figure 4.3 Variation of void ratio at the end of consolidation with effective confining pressure at different cement contents.

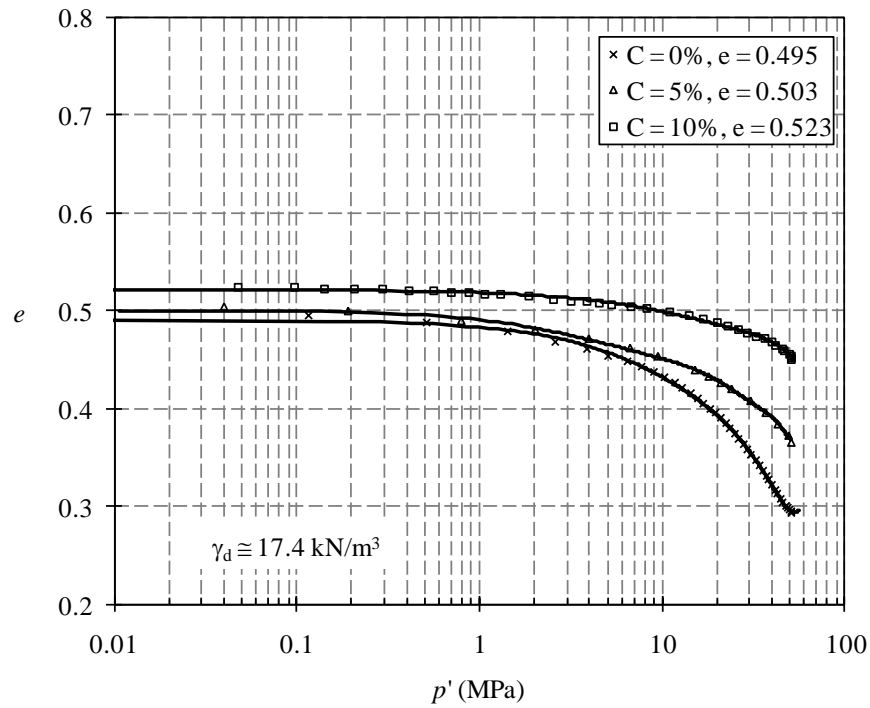


Figure 4.4 Effect of cement content on isotropic compression curves of dense Portaway sand at constant dry unit weight.

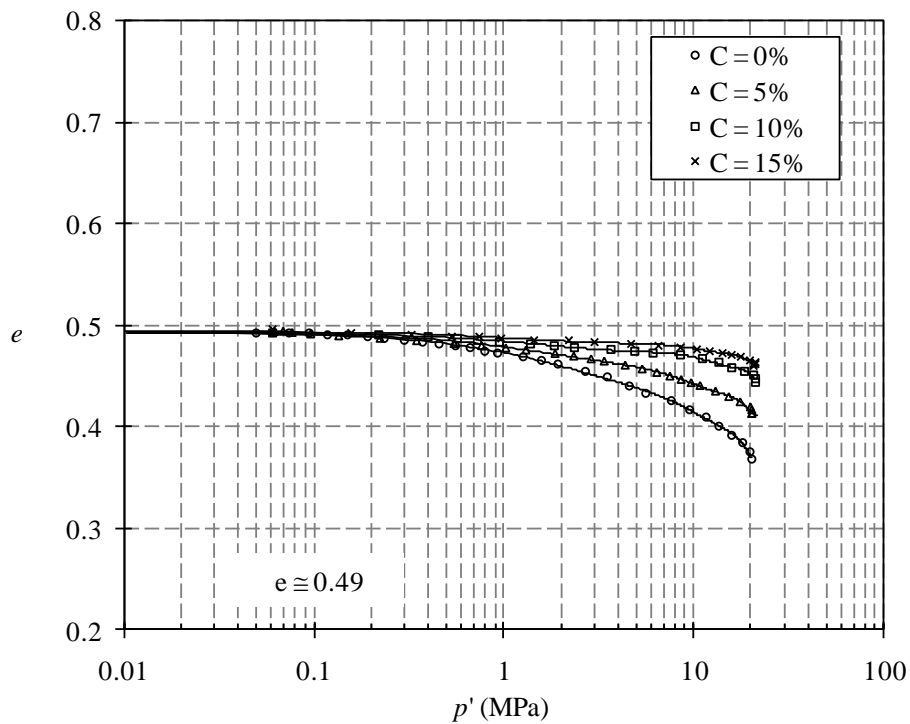


Figure 4.5 $e-\ln(p')$ curves of Portaway sand with different cement contents prepared at constant initial void ratio.

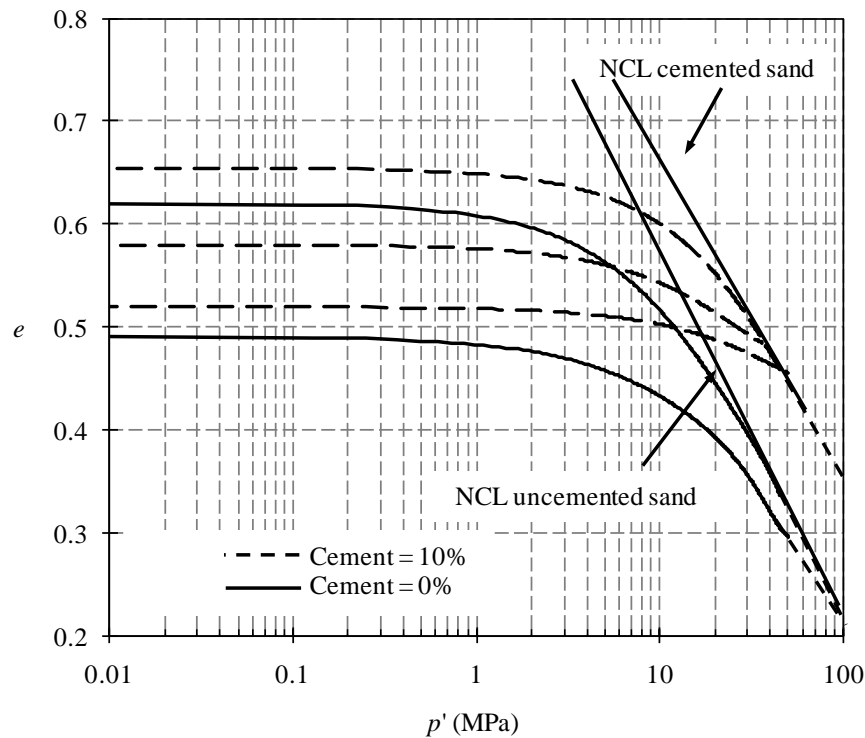


Figure 4.6 Normal compression lines for uncemented and cemented Portaway sand.

4.4 Deformation of cemented sand during compression

Isotropic compression tests were carried out to explore the effect of initial relative density and cement content on the deformation characteristics of uncemented and cemented sand. The tests were carried out on uncemented and cemented Portaway sand with varying degree of cement contents and initial relative densities (D_{r0}) to high-pressures. After completing the isotropic compression process, the samples were examined visually and microscopically using scanning electron microscopy (SEM). The effects of cement content and initial relative density on the particle crushing were thoroughly investigated.

4.4.1 Effect of cement content on particle crushing

In order to investigate the effect of cement content on the particle crushing, isotropic compression tests were performed on uncemented and cemented sand

specimens. The curves for volumetric strain versus mean effective stress with loading and unloading cycle of the test are presented. A close look on the compression curve for uncemented sand shown in Figure 4.7 indicates a slight dip at a mean effective confining pressure of about 10 MPa. Yamamuro and Lade (1996) reported similar type of dip for Cambria sand during isotropic compression to a high-pressure. The cause of this dip was previously, reported as being related to the particle crushing by Yamamuro and Lade (1996). However, for relating the dip to the particle crushing no any other conformity reason was given. Therefore, in this study, the isotropically compressed specimens were further investigated with the help of SEM analysis. For this purpose, both cemented and uncemented samples were taken. The results of isotropic compression tests carried out on cemented sand with the cement contents of 5% and 10% are shown in Figure 4.8. The assessment of compression curves of cemented sand specimens show no any noticeable dip in the compression curves. Therefore, it can be said that the particle crushing, which were seen for uncemented sand is being resisted by the effect of cement bonding in the cemented specimens.

Moreover, the comparison of compression curves with different cement contents, shown in Figure 4.9, suggests that the rate of volume change decreases with the increase in cement content. The slope of compression curve represents the rate of volume change. The decrease in the rate of volume change suggests that the compressibility of the material decreases by the increase in cement content.

The SEM analyses were carried out on two groups of samples; ones, which were showing dip in the compression curves and others without any noticeable dip on the

compression curves. The SEM photographs exposed noticeable particle crushing for those specimens, which were showing dip on the compression curves (as shown in Figure 4.10(a)) and no significant particle crushing were seen for the specimens, which were showing no significant dip on the compression curves as shown in Figure 4.10(b)). Therefore, it is further confirmed that the dip on the compression curve can be attributed to the particle crushing. However, it is still needed to carry out more SEM analysis of the specimens immediate after the stage of compression at which the dip is seen on the compression curve.

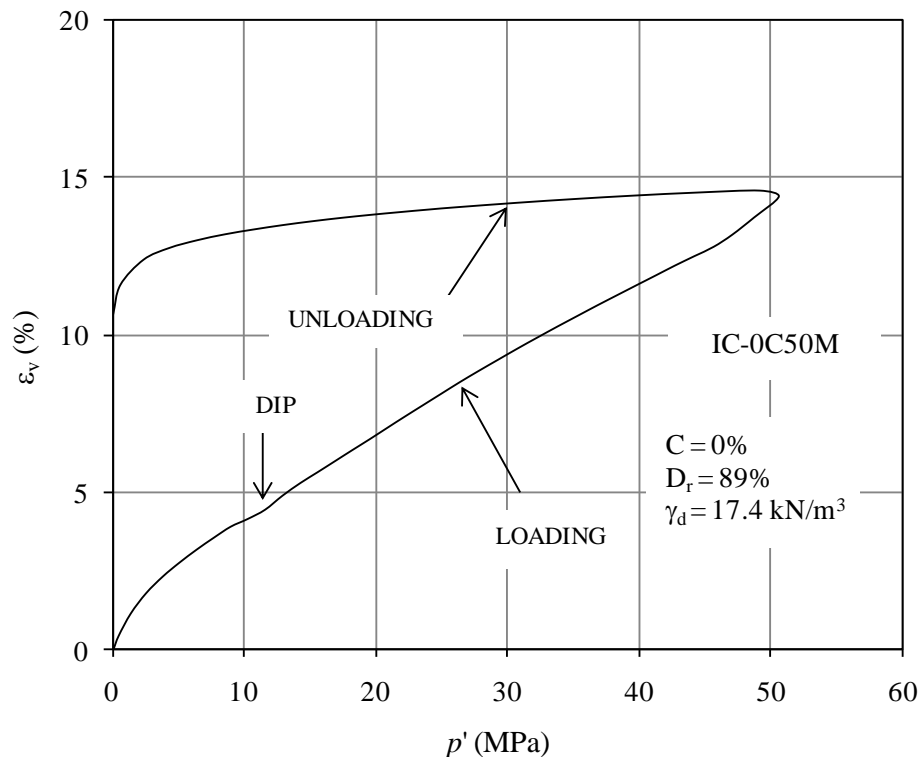


Figure 4.7 High-pressure isotropic compression test on dense Portaway sand.

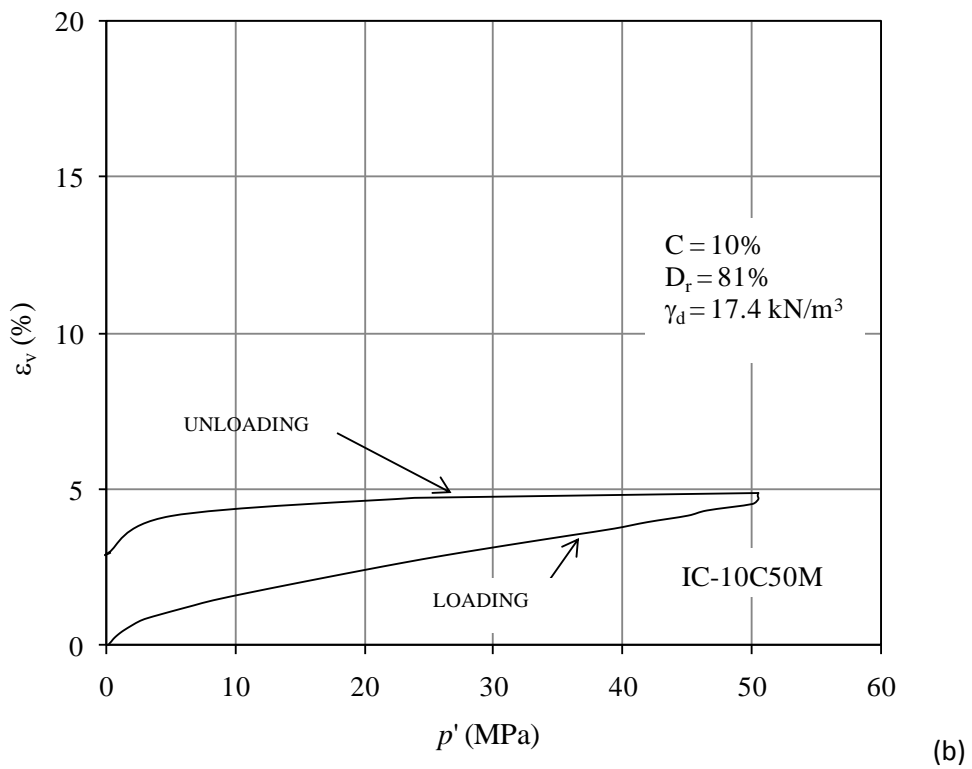
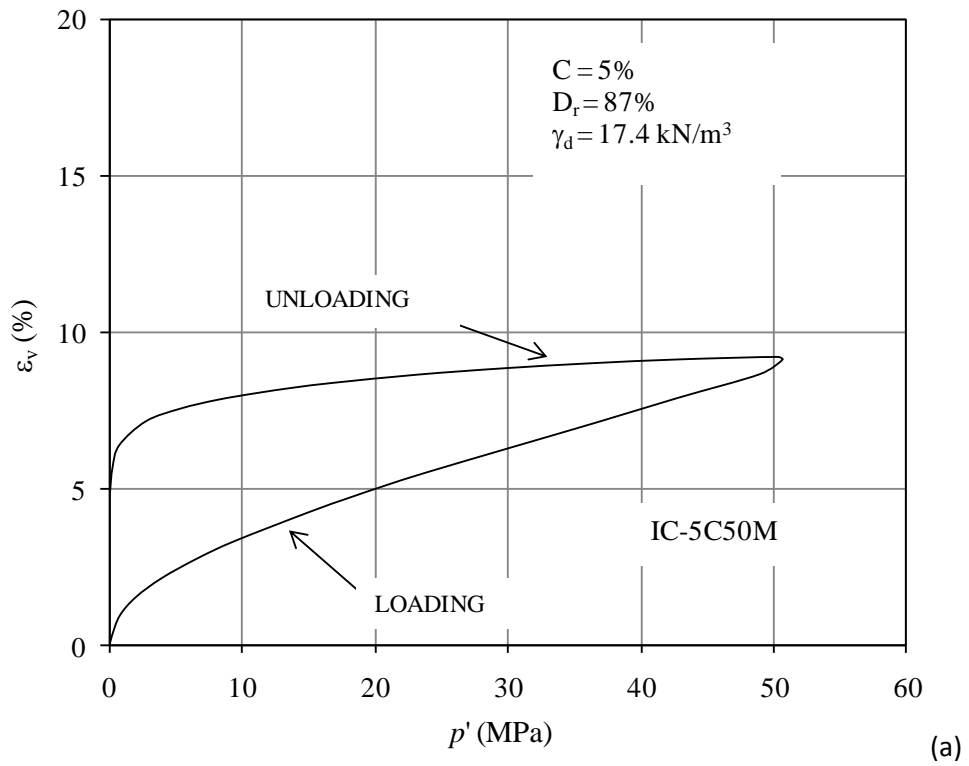


Figure 4.8 High-pressure isotropic compression test on cemented Portaway sand with: (a) 5% cement content; (b) 10% cement content.

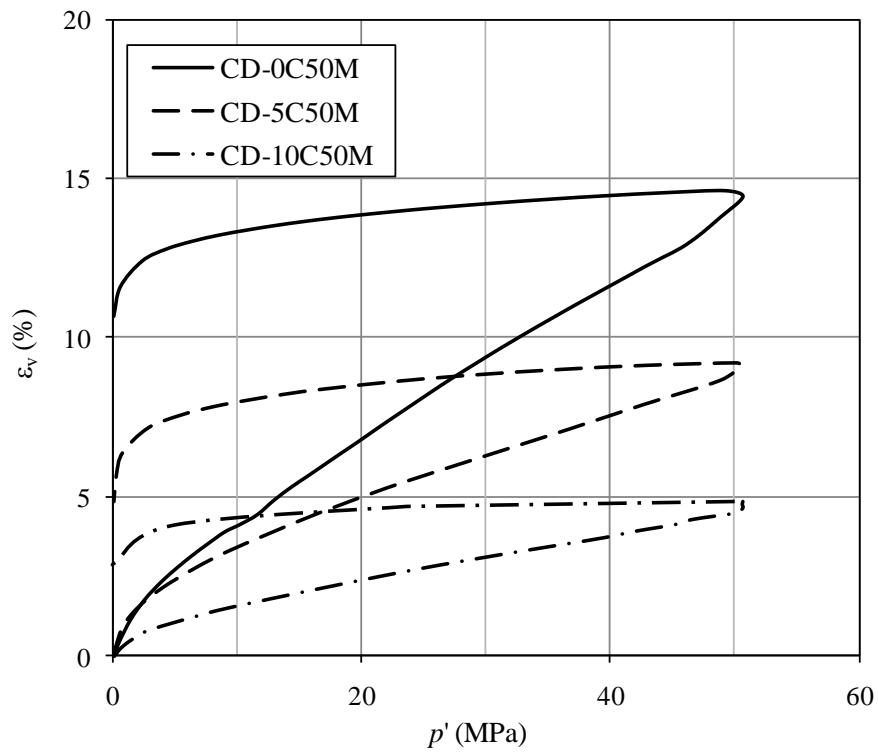
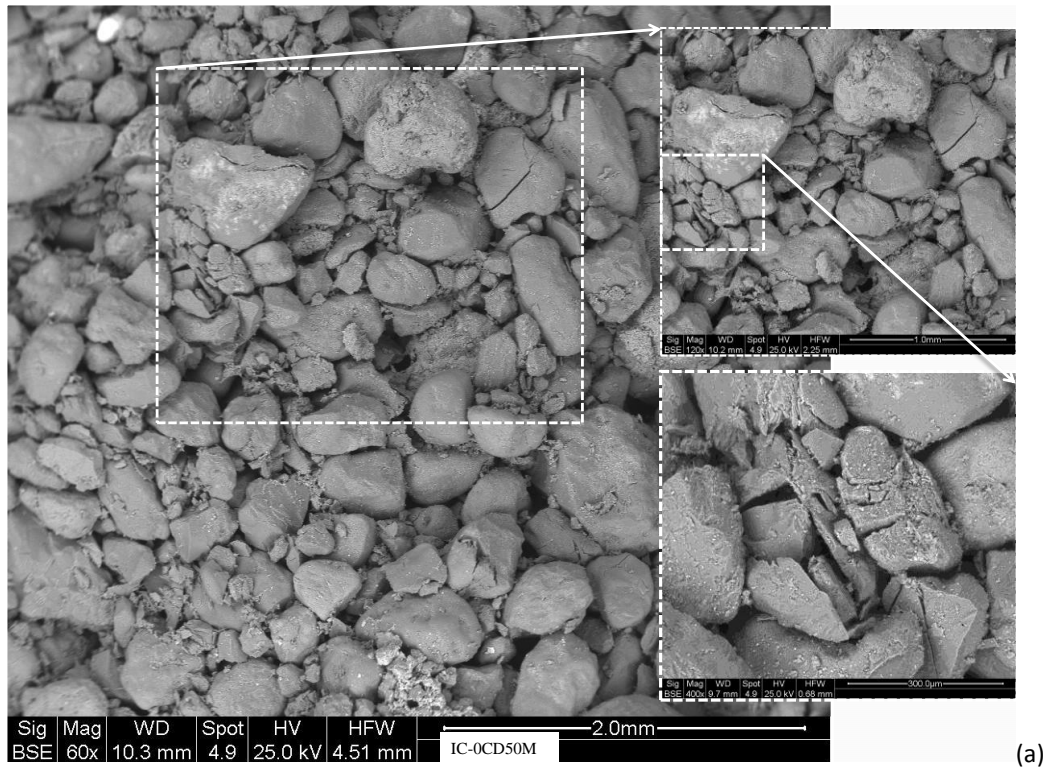


Figure 4.9 Effect of cement content on isotropic compression at high-pressure.



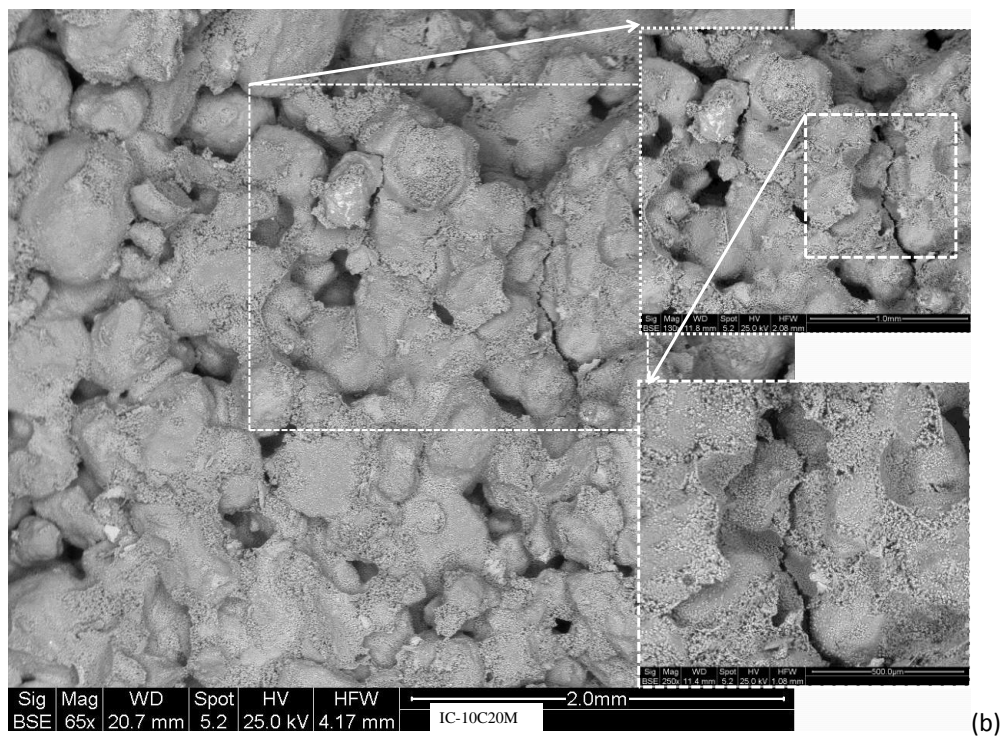


Figure 4.10 SEM photographs of specimens after isotropic compression at high pressures: (a) specimen showing crushing of particles and had dip on the compression curve (b) specimen showing no significant crushing of particles and had no dip on the compression curve.

4.4.2 Effect of dry density on particle crushing

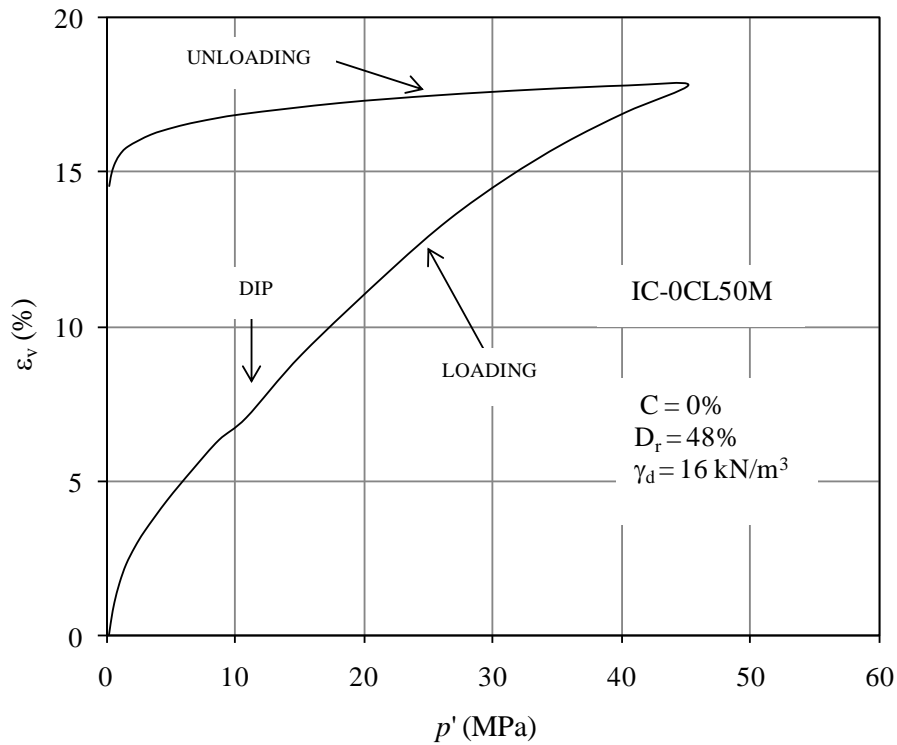
In order to investigate the effect of the initial dry density on the compression characteristics of Portaway sand, different density sand samples were isotropically consolidated to the effective confining pressure of 50 MPa. The density parameters are shown in Table 4.1. The loading-unloading curves with respect to the volumetric strain versus mean effective stress are shown in Figure 4.11(a) and (b), it can be noticed that at the mean effective confining pressure of about 10 MPa a dip appears on the compression curves. The initial dry density appears to have no significant effect on the location of dip with respect to the compression curves. However, as was expected, the relatively less dense sand specimen shows more volumetric change during compression. The dip in the compression curve can be attributed to the particle

crushing. Moreover, it was also confirmed from SEM analysis of the exhumed isotropically consolidated specimens (see Figure 4.12). From Figure 4.12, it can be seen that the sand particles are fractured and crushed during compression for both relatively loose ($D_r = 48\%$) and dense samples ($D_r = 89\%$).

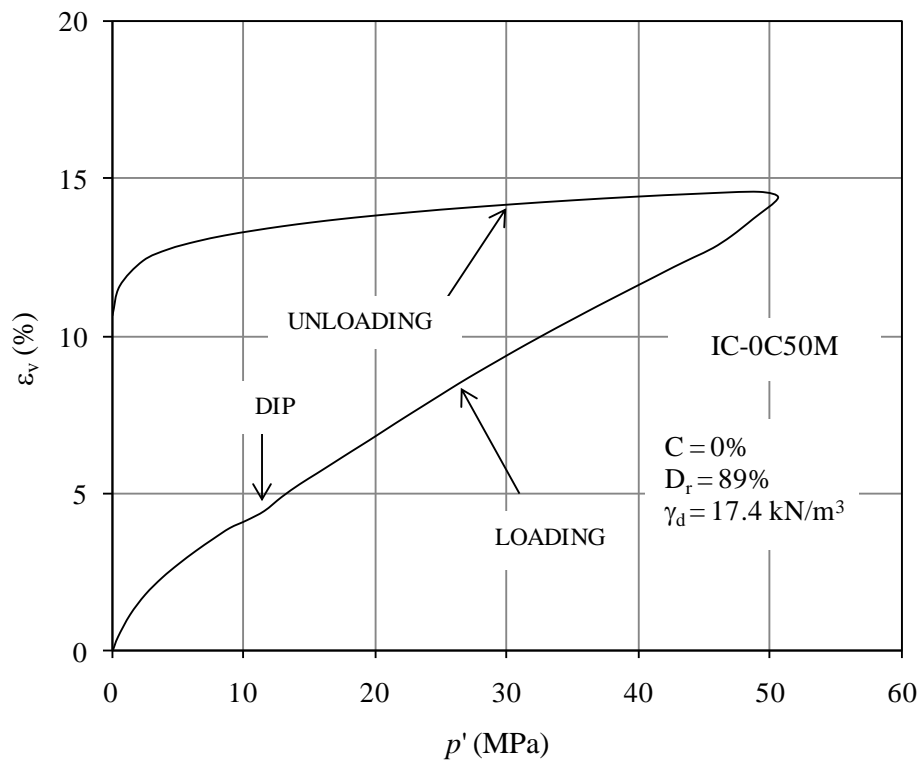
The density effects were also investigated for cemented sands at high-pressure during isotropic compression as shown in Figure 4.13. From Figure 4.13(a) it can be seen that for relatively loose cemented sand specimen ($D_r = 40\%$), there are two dips appearing on the compression curve. The first dip (DIP1) is presumably due to cement content bond breakage. The second dip (DIP2) is attributed to the usual particle breakage as were noticed for uncemented sands as shown in Figure 4.7. For relatively less dense cemented soil, it appears that the cement matrix initially bears the confining stress, preventing particle breakage, once the matrix fractures; load is shed to the particles. For dense cemented sand there cannot be seen any noticeable dip in the compression curve for $p'-\varepsilon_v$ which is an indication of no significant particle breakage. It was further confirmed from the SEM photographs of the exhumed specimens after compression as shown in Figure 4.14. From the figure, it can be seen that the extent of deformation is relatively high at loose state (see Figure 4.14a) and gradually is diminishing by the increase in density (see Figure 4.14b), and subsequently it is becoming insignificant at dense state (see Figure 4.14c).

It was presumed that continued loading would cause the cement bond breakage and progressively diminishes the cement content effect; ultimately would result to a similar trend as that for uncemented sand. However, the experimental results are

not fully agreeing with this hypothesis of Coop and Atkinson (1993), and the effect of cement content during isotropic compression is evident.



(a)



(b)

Figure 4.11 Effect of initial dry density on isotropic compression at high-pressures: (a) relatively loose sand with $D_r = 48\%$; (b) relatively dense sand with $D_r = 89\%$.

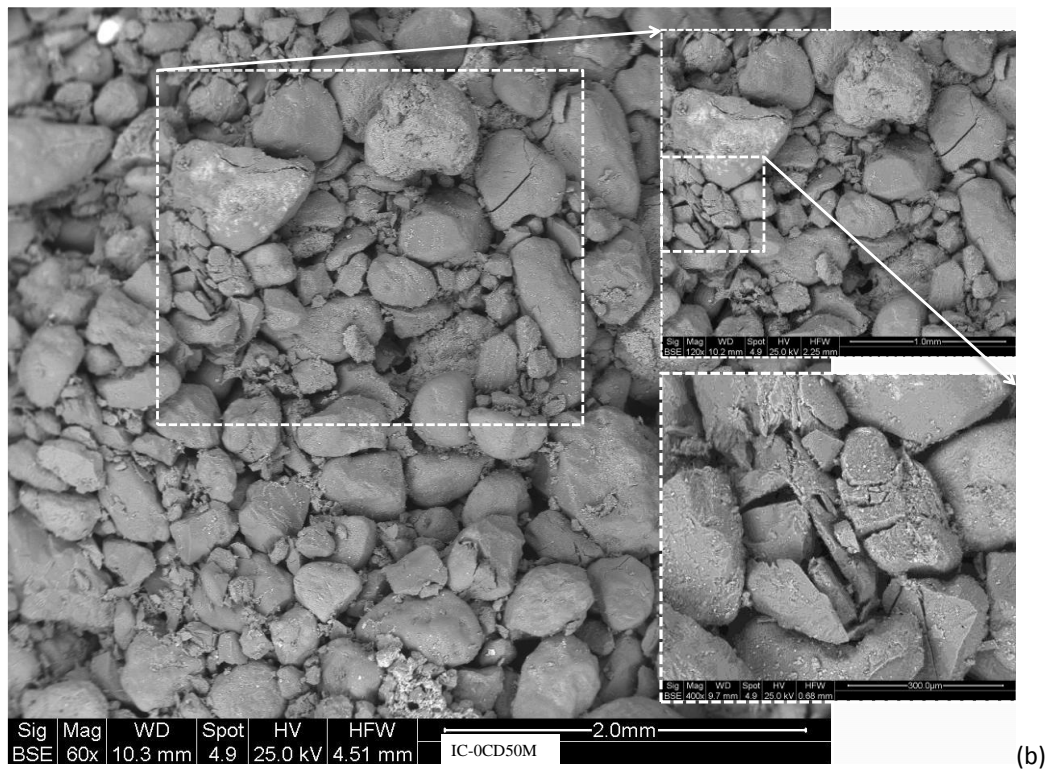
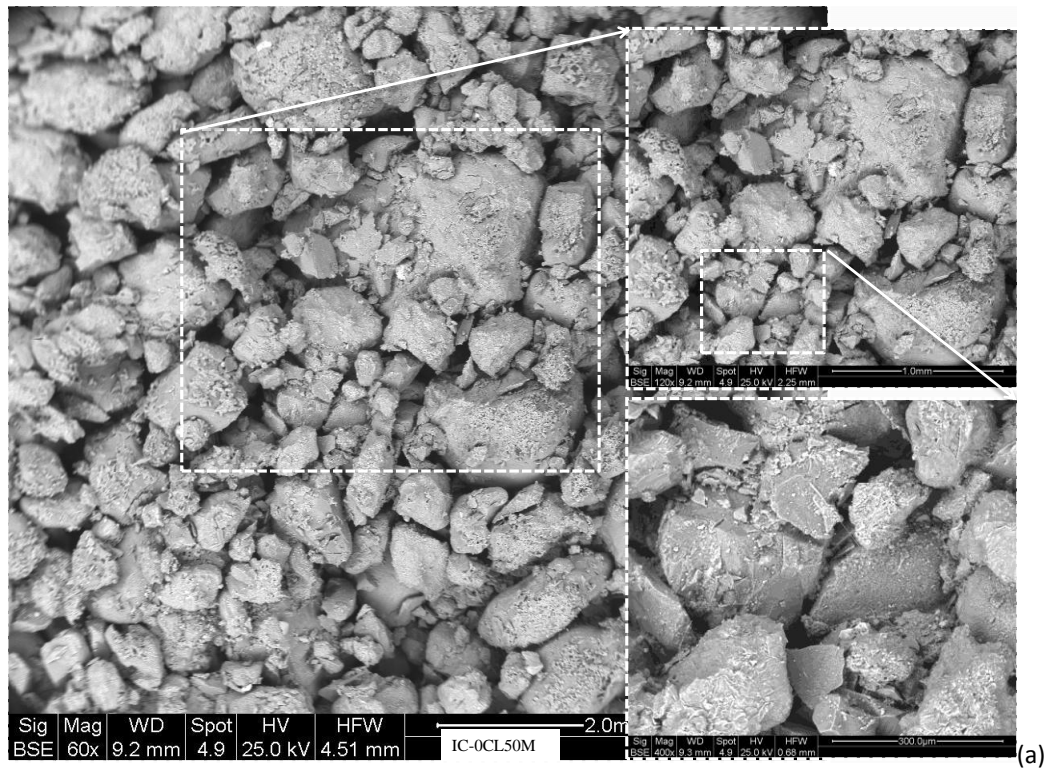


Figure 4.12 SEM photographs of uncemented sand after isotropic compression at $\sigma'_3 = 50$ MPa: (a) relatively loose sand with $D_r = 48\%$; (b) relatively dense sand with $D_r = 89\%$.

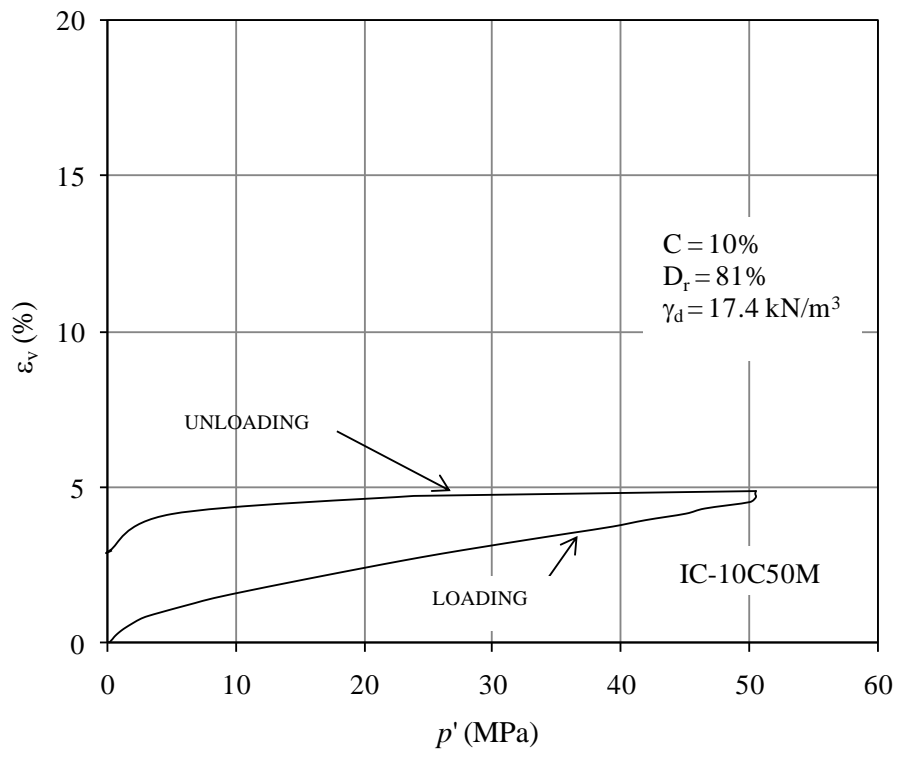
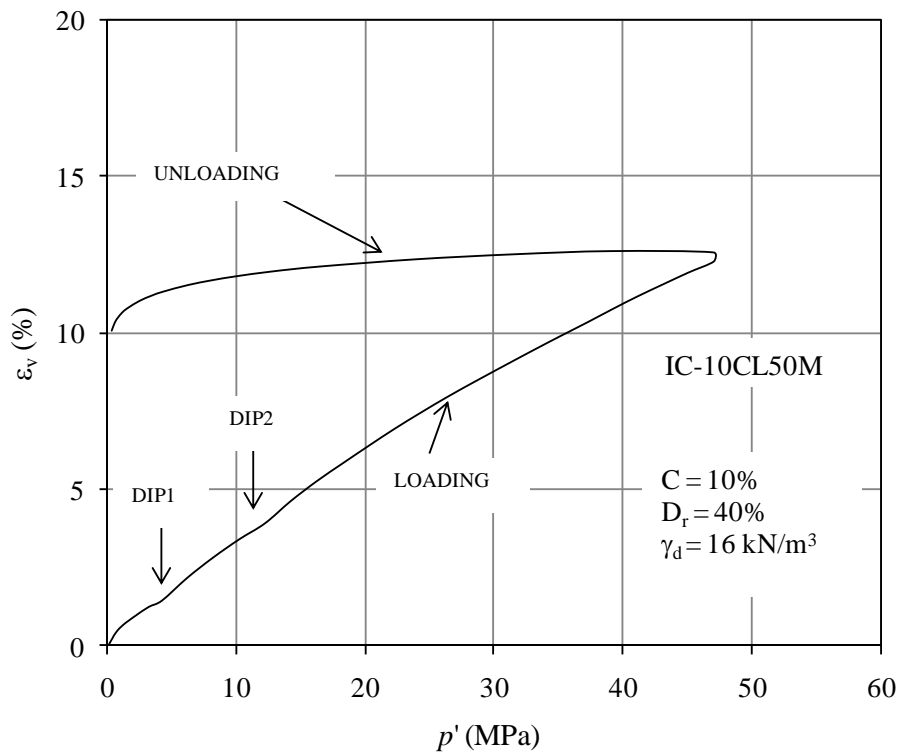
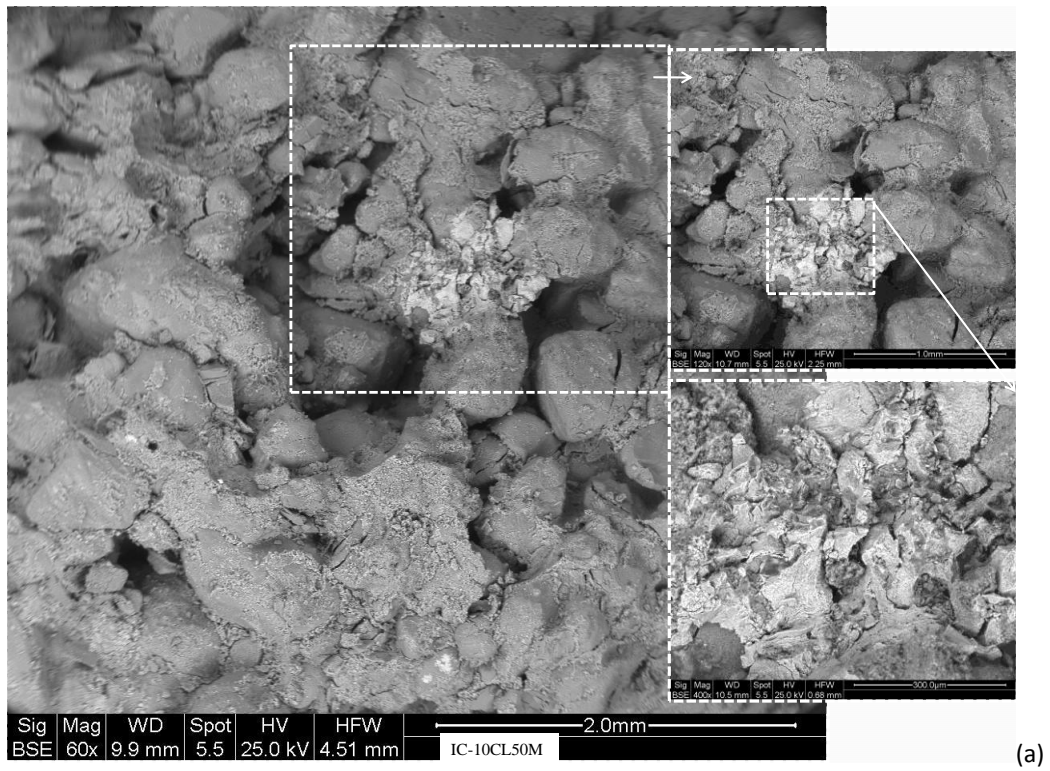
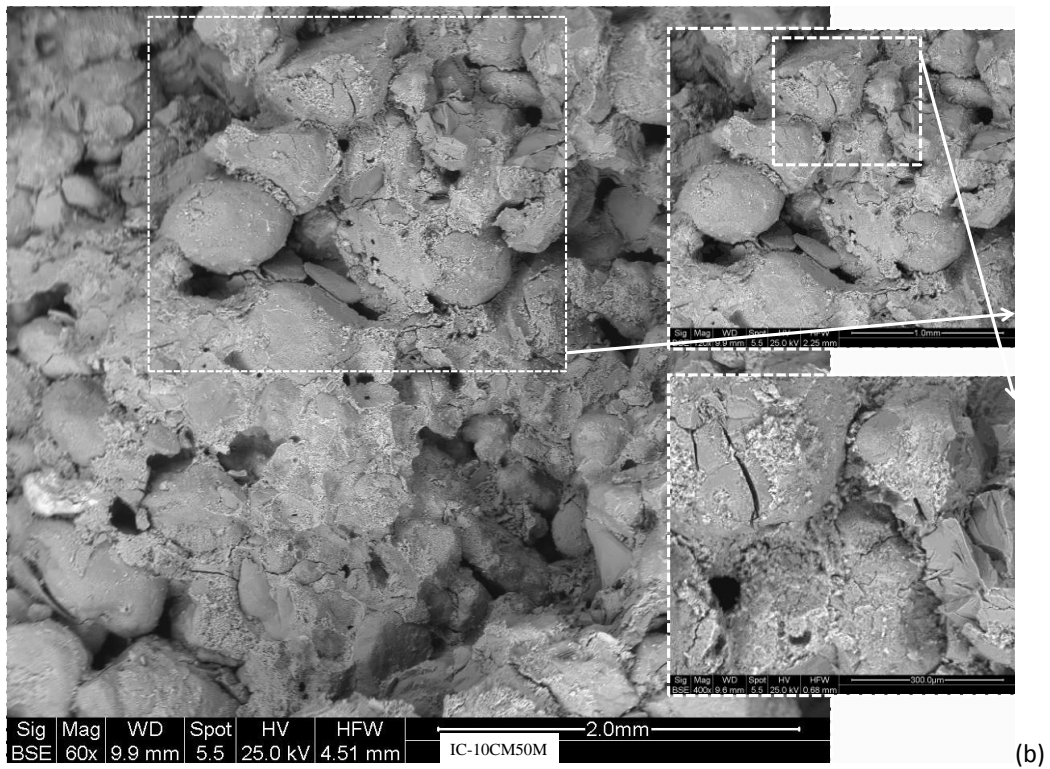


Figure 4.13 Effect of initial dry density on isotropic compression at high-pressures: (a) relatively loose cemented sand with $D_r = 40\%$; (b) relatively dense cemented sand with $D_r = 81\%$.



(a)



(b)

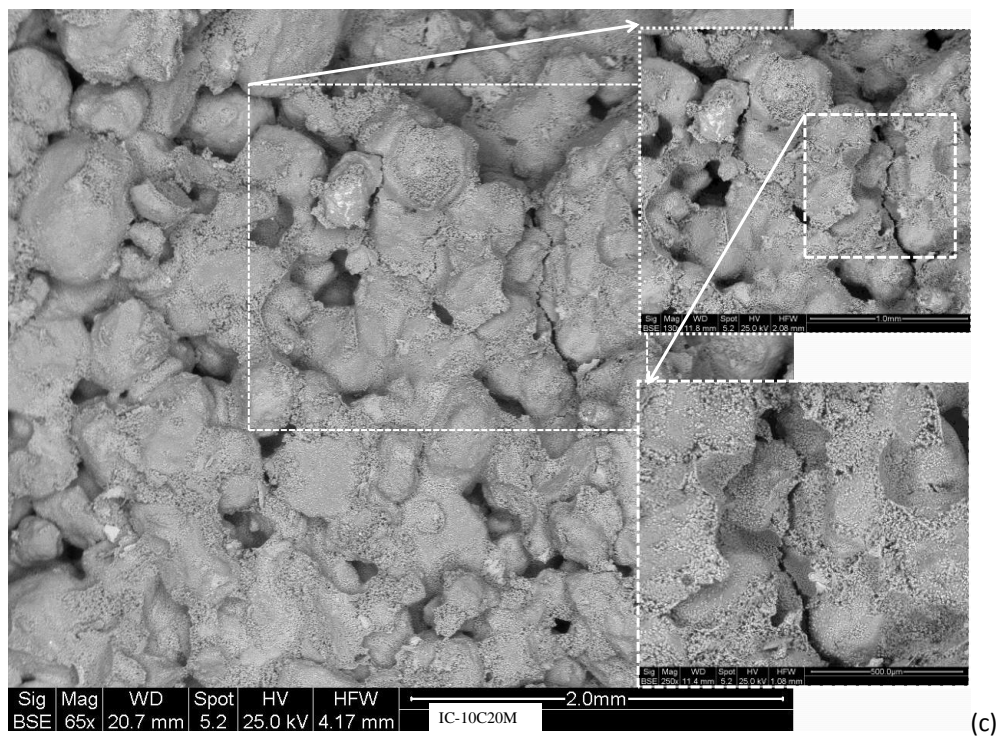


Figure 4.14 SEM photographs of cemented sand specimens after isotropic compression at high-pressures with initial relative densities of: (a) $D_r = 40\%$; (b) $D_r = 62\%$; (c) $D_r = 81\%$.

4.5 Summary

This chapter was aimed at a fundamental understanding of the behaviour of cemented sand under isotropic compression, when compared with uncemented sand. High-pressure isotropic compression tests were carried out on samples of uncemented and cemented Portaway sand at different initial void ratios, initial relative densities, and cement contents.

From the experimental investigations, it was observed that the effect of initial void ratio for both cemented and uncemented sands appear to diminish at high pressures and there is convergence in the isotropic compression curves. Similar to uncemented sand, the cemented sands with different initial void ratios converge towards a

unique final void ratio when compressed at high pressures. Therefore, the variation of initial void ratio has less significance at high confining pressures.

Keeping the initial void ratio constant the effect of cement content were also examined and it could be seen that the effect of cement content is even more profound at high pressures. For instance, the sand samples with different cement contents prepared at the same initial void ratio showed different final void ratios at the end of compression. Comparison of isotropic compression curves indicates that the variation of cement content as compared to conventional pressure is more significant at high pressures (Figure 4.3). This can be due to the increase in the cement content of the materials, which ultimately results to decrease in the compression.

The addition of cement to the sand appears to have no appreciable effect on the slope of normal compression line (NCL). There appears to be negligible convergence and for effective confining pressures up to 50 MPa, the normal compression lines are still essentially parallel. However, increase in cement content shifts the NCL to the right, which can be attributed to the increase in cohesion component due to increase in the cement content.

From the isotropic compression of relatively loose cemented sands with initial relative density of 40%, it can be observed that there is double dip in the compression curve. The first dip, which appeared around 5 MPa of mean effective confining pressure, can be attributed to the cement bond breakage. This was further confirmed with SEM microphotographs, which were showing cement bond breakage. The second dip, which appeared around 10 MPa of mean effective confining pressure, can

be due to the bulk of particle crushing and was confirmed from SEM microphotographs as well as from previous literature, which was reported by Lade and Yamamuro (1996). The amount of particle crushing during the isotropic compression at high pressures was observed to be decreasing by the increase in cement contents. This can be noticed from the dip in the isotropic compression curve and SEM analysis of the exhumed specimens.

Regarding the particle and bond breakage, standalone neither density nor cement content was found to resist the deformation due to higher confining pressures. For instance, in both cases of uncemented sand and loose cemented sand, both the compression curves and SEM photographs indicated significant deformation. However, in the case of dense cemented sand both the compression curves and SEM photographs indicated significant reduction in the deformation bond breakage and particle crushing during isotropic compression.

TRIAXIAL COMPRESSION TESTS

5.1 Introduction

The stress–strain and volume change behaviour of cemented sand can be well understood from triaxial compression tests. The shear strength of cemented soils under varying drainage conditions has been a topic of significant interest for the last four decades. There is a wealth of experimental data that has been published in the literature (e.g. Clough *et al.* 1981, Coop and Atkinson 1993, Abdulla and Kiousis 1997a, Abdulla and Kiousis 1997b, Consoli *et al.* 2000, Dano *et al.* 2004, Haeri *et al.* 2006, Consoli *et al.* 2007). These experimental data has contributed significantly to the understanding of the important factors that control the shear strength behaviour of cemented and uncemented sands under drained conditions (e.g. volumetric dilation, drained strength parameters i.e., c and ϕ' , incorporation of cohesion components into the stress-dilatancy, strength and deformation etc).

Despite the concerns about the effects of the artificial agents, evidences from experiments on a range of cemented geomaterials suggest that the most important parameters controlling the mechanical responses are the initial relative density and the strength of the bonding (Leroueil and Vaughan 1990). Thus, it is believed that all artificial specimens with essentially similar mineralogy and densities should give a useful indication of the mechanical behaviour of natural soils.

Most of the research in the mechanics of cemented soil has focussed on soil behaviour at low or moderate pressures, where most of the geotechnical engineering problems tend to arise. However, many practical problems fall into the category of high pressures. For example, offshore piles and constructions on oil bearing strata. Understanding the behaviour of cemented soils subjected to high pressures is therefore fundamental to assisting in the solution to these types of geotechnical and geological problems. How initial dry and/or relative density and bond strength responds at high pressures under drained and undrained conditions is important to investigate. For instance, a soil with a tendency to compress during drained loading will exhibit an increase in pore water pressure during undrained loading, resulting in a decrease in effective stress. And a soil with a tendency to expand or dilate during drained loading will exhibit a decrease in pore water pressure during undrained loading, resulting in an increase in effective stress.

The present work evaluates the mechanical behaviour of artificially cemented Portaway sand using triaxial drained and undrained compression tests. Some typical tests are presented in Table 5.1. The behaviour of cemented samples is compared with that of the uncemented sand to examine the influence of cement content. The degree of cement content and the effective stress level are two major variables examined.

Table 5.1 Summary of isotropically consolidated drained compression tests
(failure parameters).

Test	σ'_3 (MPa)	C (%)	D_r (%)	e_0	e_c	p'_{peak} (kPa)	q_{peak} (kPa)	ϕ'_{peak} ($^\circ$)	$(q/p')_{peak}$	I_B
CD-0C0.05M	0.05	0	90	0.49	0.49	109	180	40.4	1.7	0.32
CD-0C0.1M	0.1	0	89	0.50	0.49	205	318	38.1	1.5	0.34
CD-0C0.2M	0.2	0	89	0.50	0.48	411	624	37.3	1.5	0.32
CD-0C0.3M	0.3	0	89	0.50	0.48	592	881	36.6	1.5	0.33
CD-0C0.5M	0.5	0	90	0.49	0.49	964	1395	35.6	1.4	0.23
CD-0C1M	1	0	89	0.50	0.47	1836	2363	32.4	1.3	0.10
CD-0C4M	4	0	89	0.50	0.44	7779	9815	31.9	1.3	0.00
CD-0C8M	8	0	90	0.49	0.43	13690	17188	31.3	1.3	0.00
CD-0C10M	10	0	90	0.49	0.43	18450	22505	30.6	1.2	0.00
CD-0C12M	12	0	90	0.49	0.41	20093	24361	30.4	1.2	0.03
CD-0C20M	20	0	91	0.49	0.39	32924	38945	29.4	1.2	0.12
CD-5C0.05M	0.05	5	85	0.51	0.50	331	779	58.2	2.4	2.13
CD-5C0.1M	0.1	5	85	0.51	0.50	445	954	52.6	2.1	2.15
CD-5C0.3M	0.3	5	85	0.51	0.50	763	1385	44.2	1.8	0.82
CD-5C1M	1	5	85	0.51	0.50	2288	3800	40.6	1.7	0.51
CD-5C2M	2	5	85	0.51	0.49	4118	6244	37.2	1.5	0.34
CD-5C4M	4	5	85	0.51	0.48	7537	10637	34.8	1.4	0.14
CD-5C6M	6	5	86	0.51	0.47	11086	15265	34.1	1.4	0.13
CD-5C8M	8	5	85	0.51	0.47	14470	19367	33.2	1.3	0.05
CD-5C10M	10	5	85	0.51	0.46	17775	23360	32.6	1.3	0.02
CD-5C12M	12	5	85	0.51	0.45	21192	27662	32.1	1.3	0.01
CD-5C20M	20	5	84	0.51	0.43	33282	39896	29.7	1.2	0.18
CD-10C0.05M	0.05	10	81	0.52	0.52	701	1949	71.9	2.8	6.16
CD-10C0.5M	0.5	10	81	0.52	0.52	2585	6125	59.0	2.4	2.12
CD-10C1M	1	10	81	0.52	0.51	3887	8484	52.4	2.2	1.36
CD-10C4M	4	10	81	0.52	0.51	8972	14882	40.5	1.7	0.50
CD-10C6M	6	10	82	0.52	0.51	11616	16990	36.0	1.5	0.22
CD-10C8M	8	10	82	0.52	0.50	14880	20750	34.5	1.4	0.11
CD-10C10M	10	10	82	0.52	0.49	18242	24726	33.6	1.4	0.10
CD-10C12M	12	10	82	0.52	0.49	21886	29630	33.3	1.4	0.14
CD-10C20M	20	10	82	0.52	0.47	33946	41868	30.5	1.2	0.23
CD-15C1M	1	15	77	0.54	0.53	4943	11124	56.6	2.3	2.28
CD-15C4M	4	15	78	0.53	0.52	10943	20776	46.2	1.9	0.60
CD-15C8M	8	15	78	0.53	0.51	16585	25857	38.2	1.6	0.24
CD-15C10M	10	15		0.54	0.51	17566	25655	36.5	1.5	0.21
CD-15C12M	12	15	78	0.53	0.51	22221	30715	35.2	1.4	0.11
CD-15C20M	20	15	78	0.53	0.50	34584	43761	31.2	1.3	0.25

$\gamma_d = 17.4 \text{ kN/m}^3$ for the above test data

5.2 Drained behaviour

In order to understand the drained behaviour of cemented sands at high pressures, isotropically consolidated drained (CD) tests were conducted on Portaway sand with the cement content 0% (i.e., uncemented), 5%, 10%, and 15%. The specimens were isotropically consolidated to mean effective stresses, $p'_c = 1, 4, 8,$ and 12 MPa and sheared under drained conditions with σ'_3 maintained constant. The deviatoric stress (q), the effective stress ratio (q/p'), and the volumetric strain (ε_v) are plotted versus the axial strain (ε_a) using the same scales for horizontal and vertical axes. In this way, the effects of confining pressure and cement content on the stress-strain behaviour of cemented sand could be easily illustrated. This was essential for analyzing the stress-strain behaviour of cemented sand, in which the degree of cement content and the effective stress level are the two major variables.

5.2.1 Effect of confining pressure

The effect of the confining pressure on the stress-strain behaviour of uncemented Portaway sand is shown in Figure 5.1(a). The increase in confining pressure increases the peak deviatoric stress, the axial strain to the peak and the amount of contraction during shearing. Therefore, the stress-strain behaviour becomes increasingly ductile with increasing confining pressure. It can be seen that there is contractive behaviour, which can be observed in all the tests. Both the deviatoric stress and the volumetric strain increased gradually with the axial strain and approached (or were approaching) a constant ultimate value at the end of each test. Furthermore, all the tests approached the same failure stress ratio at the end of test $(q/p')_f = 1.19$. This ratio is

consistent with the slope of the critical state line, M_{CS} , obtained by Yu *et al.* (2005), and based on drained and undrained triaxial tests on loose Portaway sand. Therefore, it can be assumed that the ultimate state reached by all the dense specimens of Portaway sand at high pressures is the same as the critical state, determined by triaxial tests on loose sand at conventional pressures. This is consistent with observations made by Yamamuro and Lade (1996), who observed diminishing effect of void ratio on the stress-strain behaviour of dense Cambria sand at high confining pressures.

It can be observed from Figure 5.1 (b), (c) and (d) that for almost all the tests carried out at σ'_3 of 1 and 4 MPa, there is an initial volumetric contraction, which is followed by a subsequent volumetric dilation, except for the specimen with 5% cement content sheared at $\sigma'_3 = 4$ MPa, which exhibited only volumetric contraction. Regardless of the cement content, the higher the p'_c , the more contractive behaviour of the specimens was obtained from the tests. It can also be observed from the ε_v - ε_a curves shown in Figure 5.1, that the volumetric strain curves were approaching a constant value at the end of each test. Therefore, the ultimate state obtained from the q - ε_a and q/p' - ε_a curves could also be considered to be very close to the critical state for the cemented sand tested.

5.2.2 Effect of cement content

The results of consolidated drained compression tests (CD) carried out on specimens with different cement contents at confining pressures of 1, 4, 8, and 12 MPa are plotted in Figure 5.2. An examination of the q - ε_a and q/p' - ε_a curves shows that the

behaviour of cemented sand is dependent on the cement content. In general, the increase in the peak deviatoric stress and the reduction in the axial strain corresponding to peak deviatoric stress can be observed with the increase in cement content. In other words, the increased amount of cement content changes the stress-strain behaviour of cemented specimens from ductile to brittle. However, it can be observed that the effect of cement content is suppressed by the increase in confining pressure. For example, the specimen with 15% cement content sheared at $\sigma'_3 = 1$ MPa exhibited stiff stress-strain behaviour up to the peak deviatoric stress, then softened and approached a constant ultimate state at the end of test, as shown in Figure 5.2 (a). On the other hand, the peak deviatoric stress followed by strain softening was not observed for the specimen with the same cement content sheared at $\sigma'_3 = 12$ MPa, as shown in Figure 5.2 (d).

It can be seen from the q - ε_a curves that during shearing at $\sigma'_3 = 1$ MPa, the deviatoric stress firstly reached a peak, and then reduced gradually to a constant ultimate value for all three cement contents. However, for the tests carried out under confining pressures of 4, 8, and 12 MPa, the peak deviatoric stress could not be clearly defined and there was practically no strain softening observed. The deviatoric stress in all the tests conducted at 4 to 12 MPa increased gradually to maximum value and remained constant until the end of test (i.e. $\varepsilon_a = 30\%$). Therefore, the ultimate state was reached in all the tests. It can be seen from the q - ε_a curves that the higher the p'_c , the higher the deviatoric stress at the ultimate state. Similar behaviour was also observed for the specimens with 15% cement content (Figure 5.2(d)). However, peak

deviatoric stresses followed by strain softening were clearly observed for confining pressures of 1 and 4 MPa, whereas very little or no strain softening occurred in tests carried out at confining pressures of 8 and 12 MPa.

The $q/p' - \varepsilon_a$ curves in Figure 5.2 illustrate that the cement content does not affect significantly the ultimate stress ratios, which are in a narrow range for a given confining pressure. It can be seen that the peak stress ratios for given cement content are generally different. This suggests that the failure envelope for cemented sand is a curve and depends on the confining pressure. The q/p' versus ε_a curves in Figure 5.2 also shows that similar ultimate stress ratios were obtained for sand with 0% and 5% of cement content. However, the stress ratios at ultimate states for cement content of 10 and 15% displayed some variation. These observations again suggest that ultimate state of cemented sand may depend on both cement content and confining pressure.

The $\varepsilon_v - \varepsilon_a$ curves presented in Figure 5.2 also show that increasing the cement content reduces the contraction of the cemented sand for a given confining pressure. However, the effect of cement content on the volumetric strain behaviour reduces at higher confining pressures, where all the specimens' exhibit contractive behaviour and the volumetric strain curves are getting closer to each other. The increase in cement content increases the peak deviatoric stress but reduces the axial strain to the peak and the amount of contraction during shearing (i.e. increases the amount of dilatation). In other words, the stress-strain behaviour changes from ductile to brittle with increasing cement content. The effects of confining pressure and cement con-

tent on the stress-strain behaviour of soil, agree well with other experimental data published in the literature (Clough *et al.* 1981, Lagioia and Nova 1985, Lade and Overton 1989, Airey and Fahey 1991, Coop and Atkinson 1993, Yamamuro and Lade 1996, Cuccovillo and Coop 1999, Schnaid *et al.* 2001, Haeri *et al.* 2005).

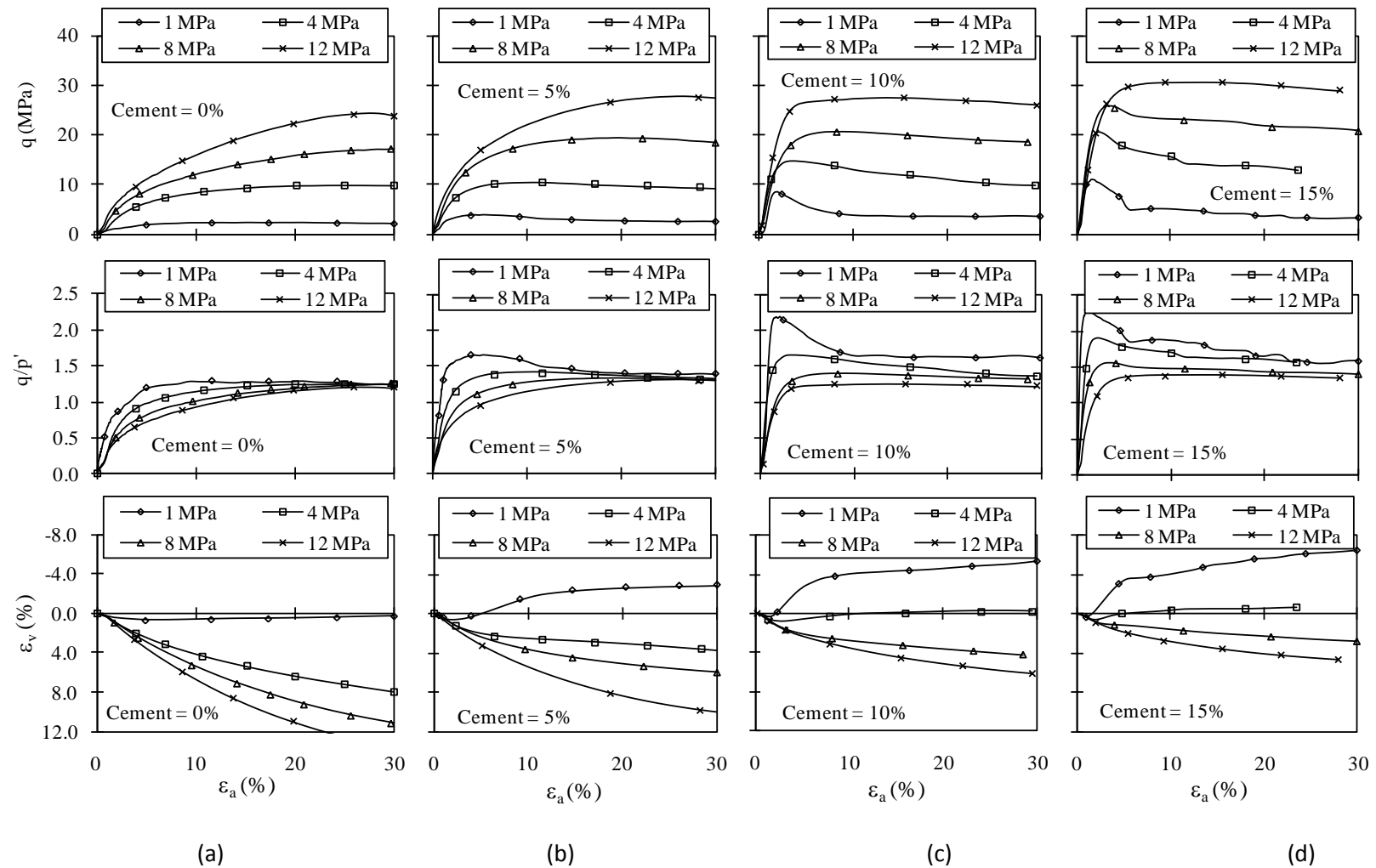


Figure 5.1 Effect of confining pressure on the stress-strain behaviour of sand with different cement contents: (a) 0%; (b) 5%; (c) 10%; and (d) 15%.

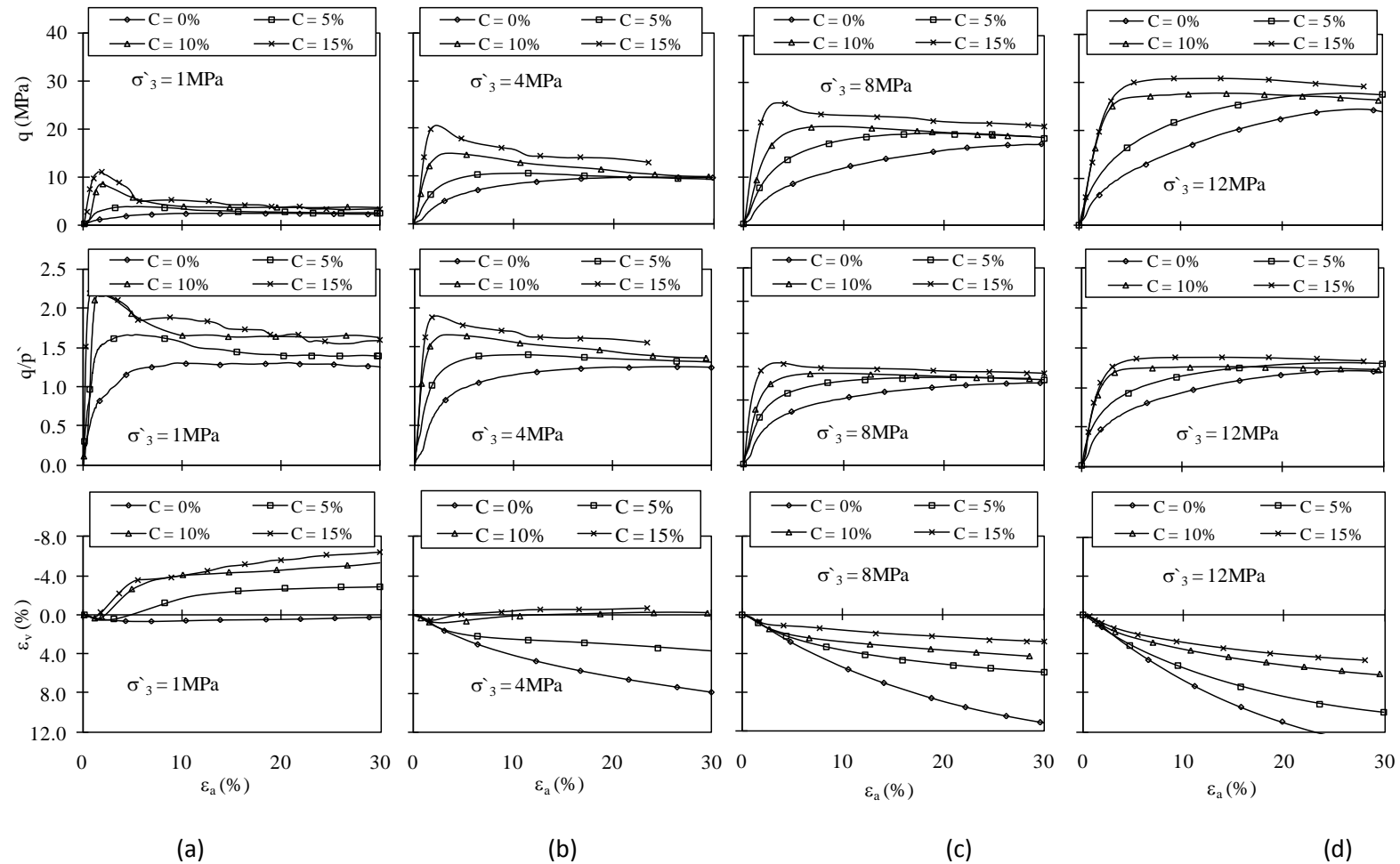


Figure 5.2 Effect of cement content on the stress-strain behaviour of sand with different confining pressures of: (a) 1 MPa; (b) 4 MPa; (c) 8 MPa; and (d) 12 MPa.

5.2.3 Drained shear strength

The peak failure data obtained from the tests results carried out on isotropically consolidated drained compression tests with different cement contents for a wide range of confining pressure are plotted on the $q-p'$ plane, as shown in Figure 5.3. Best-fit failure envelopes were plotted from the data obtained. The failure envelopes were also extrapolated to zero confinement. It can be seen from the figure (see Figure 5.3) that all the failure envelopes are curved. However, it appears that the curvature of the failure envelopes increase slightly with increasing cement content. It can also be observed that the failure envelopes move to higher stress levels with increasing cement content. As a result, extrapolated deviatoric strength at zero confinement also increases with increasing cement content. This in turn suggests that the cohesion intercept (and an inter-particle cohesion) of Portaway sand would also increase with the cement content.

From Figure 5.3 It can also be seen that the slope of the failure envelopes decreases with the increase in confining pressure, which shows that the curvature of failure envelopes is also affected by confining pressure. This indicates that the strength of cement content is significantly reduced when specimens are sheared at high pressures. Such a reduction occurs because of the breakage of cementing bonds by consolidation and shearing at high pressures, as reported by Lade and Overton (1989), Malandraki and Toll (2000), and Asghari *et al.* (2003). This means that the influence of cement content is greater at low confining stresses and this effect reduces with an increase in confining stress. Therefore, it is expected that the failure envelopes of

uncemented and cemented sand would merge at very high confining pressures. However, the confining pressures applied in this study were not high enough to confirm it.

A summary of failure states obtained from CD triaxial tests on uncemented and cemented Portaway sand is shown in Figure 5.4. Plots of the effective stress ratios at failure $(q/p')_f$ and friction angle at failure, ϕ'_f , for different cement contents, are given in Figure 5.4 (a) and (b), respectively. In addition, the critical state stress ratio ($M_{cs} = 1.19$) and the friction angle at the critical state ($\phi'_{cs} = 29.8^\circ$) determined for Portaway sand by Yu *et al.* (2005) are indicated in Figure 5.4 (a) and (b). It should be pointed out however, that these critical state parameters were determined by drained and undrained triaxial tests on loose Portaway sand at relatively low mean effective stresses $p'_c < 1$ MPa. Figure 5.4 shows clearly that both cement content and confining pressure affects the failure state of cemented sand. The $(q/p')_f$ and ϕ_f both increase with increasing cement content but reduce with increasing confining pressure, as shown in Figure 5.4 (a) and (b), respectively. Therefore, the differences between the peak strength of specimens with different cement contents are large at low confining pressures and reduce significantly at high pressures. In other words, the influence of cement content is greater at low confining stresses and this effect reduces with an increase in confining stress. It can also be observed from Figure 5.4 that the failure parameters of uncemented sand determined at the confining pressure, $\sigma'_3 = 20$ MPa coincide with the critical state parameters determined for loose specimens at low pressures.

The effects of cement content on the shear strength parameters are summarized in Figure 5.5. The failure envelopes are considered as straight lines to obtain overall cohesion intercept and frictional angle of Portaway sand with different cement contents. The most striking conclusions from Figure 5.5 are that cement content increases the cohesion in a non-linear way (see Figure 5.5 a). It can also be noticed that there is some cohesion observed for the uncemented sand as well. This cohesion is assumed to be, the effect of liquid between the grains in the granular media. In cemented sand, for the given range of confining pressures (see Figure 5.5 b), there can be seen that the friction angles are significantly higher than the uncemented sand. While in general, there is marginal decrease in the friction angles due the increase in the cement content. The decrease in the frictional angle might be due to the convergence of failure envelopes of cemented sand towards the critical state of uncemented sand at high pressures i.e. the slope of the failure envelopes decreases with the increase in confining pressure as mentioned before. The higher frictional angles for cemented sand and in particular at relatively lower confining pressures might be due to the shearing of the specimen in larger pieces rather than the individual grains. The deformation in pieces might be due to cement bonding that could hold several particles together.

It is worth noting that the effect of confining pressure observed on the failure characteristics of artificially cemented sand during this study is consistent with the findings of previously published reports. For instance, similar observations were made by Yamamuro and Lade (1996) for a clean sand, Toll and Malandraki (1993) and Malandraki and Toll (2000) for an artificially cemented soil, Asghari *et al.* (2003) for a

cemented coarse-grained alluvium, Rampello *et al.* (1993) for a natural clay, and Lo and Wardani (2002) and Lo *et al.* (2003) for a silt stabilized by a cement and fly ash mixture. However, there is no general agreement regarding the effects of cement content on the peak friction angle. Whereas some researchers reported increase of the friction angle due to cement content (Saxena *et al.* 1988, Lade and Overton 1989). Others (Wissa *et al.* 1971, Clough *et al.* 1981) reported a parallel movement of the failure envelope (i.e. no change in frictional angle) caused by increase of cement content. And in present study there could be seen slight decrease in the frictional angle by the increase in cement content. It is important to note that the effect of cement content on frictional angle in previous studies were carried out at conventional pressures and in this study it has been elaborated to high confining pressures.

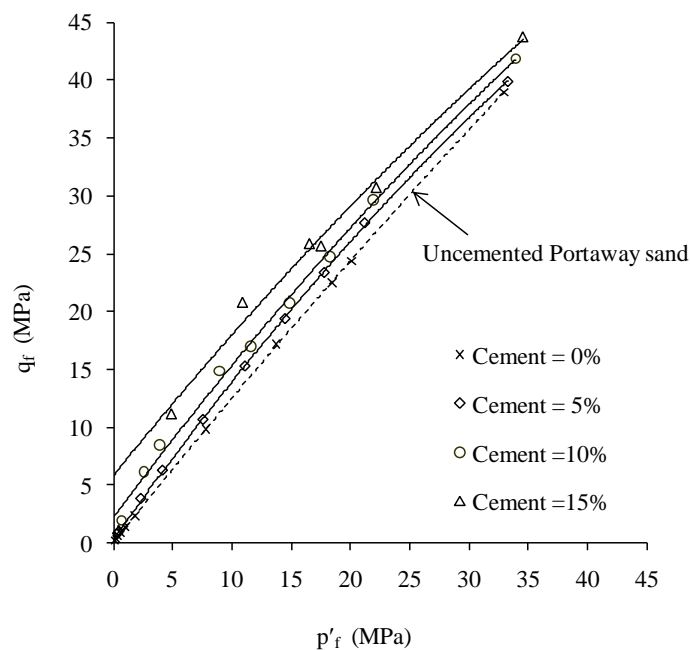


Figure 5.3 Failure envelopes of specimens with different cement contents during drained compression.

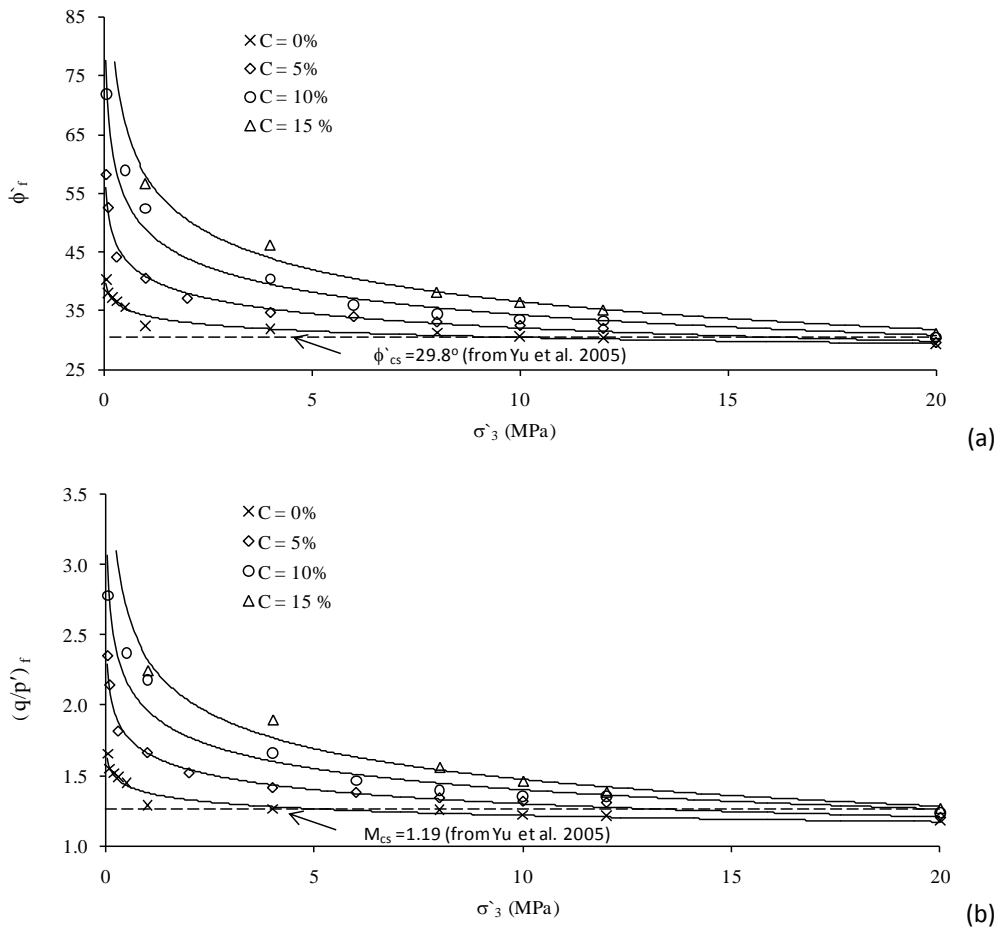
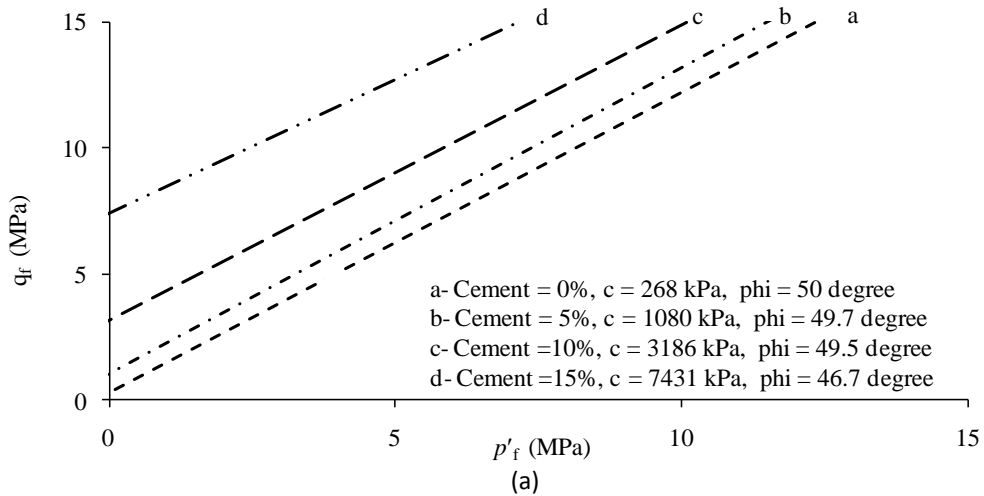
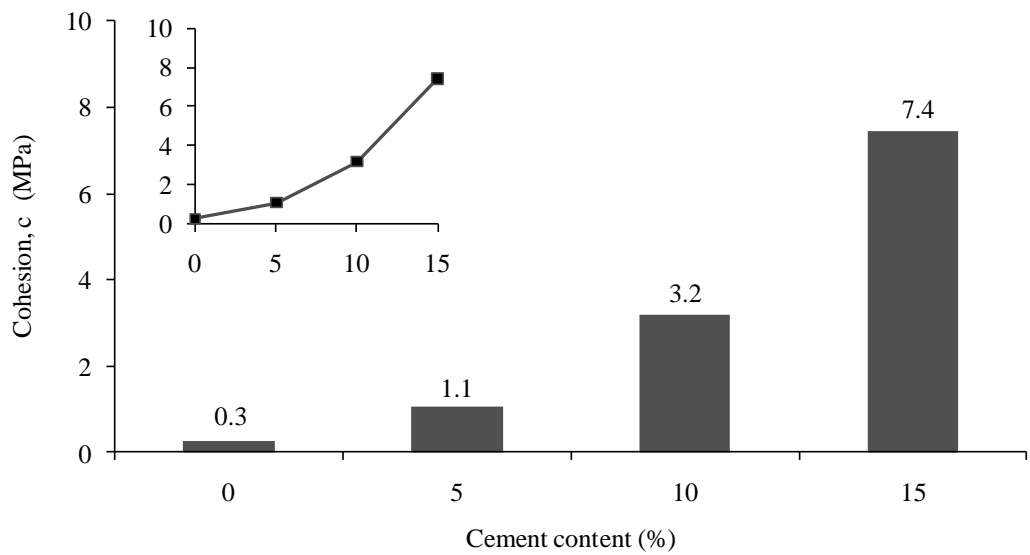
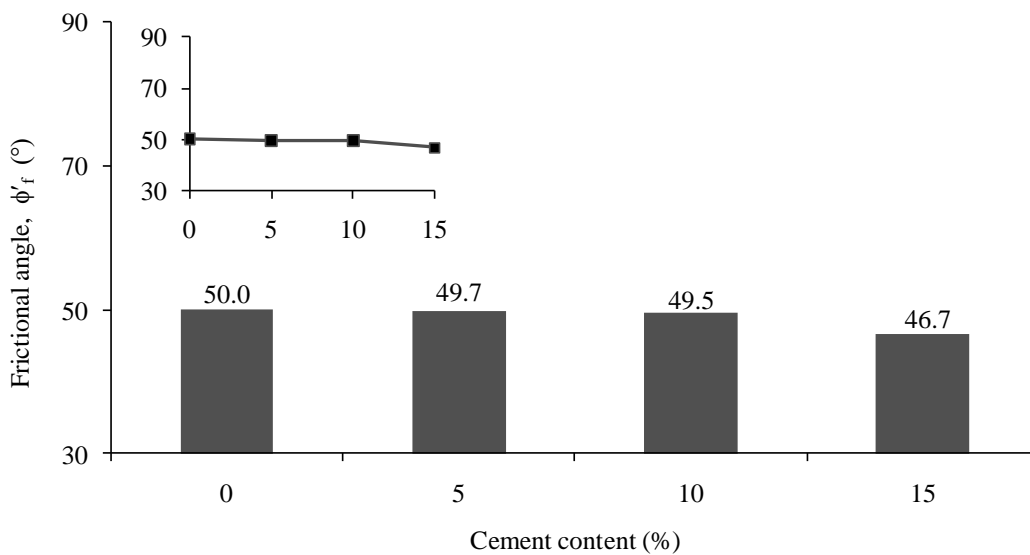


Figure 5.4 Effect of confining pressure for a wide range of cement contents at failure state on: (a) stress ratio (q/p'); (b) frictional angle.





(b)



(c)

Figure 5.5 Effect of cement content on: (a) failure envelopes; (b) cohesion; and (c) frictional angle.

5.3 Undrained behaviour

An attempt to illustrate the typical engineering characteristics of cemented sand, undrained triaxial compression tests were performed with initial confining pressures between 100 kPa and 20 MPa. The role of cement content and confining pressure on the mechanisms controlling the undrained shear behaviour of uncemented and ce-

mented sand was investigated. The tests consisted of drained isotropic compression followed by undrained shearing under strain control. The total confining pressure was maintained constant throughout shearing. The specimens were sheared at strain rate of 0.2 mm/min. Induced pore pressure was measured with a pressure transducer attached to the base of the triaxial cell. List of the undrained tests carried out with initial conditions is given in Table 5.2. The typical stress-strain (q - ϵ_a), excess pore pressure (Δu - ϵ_a) and stress paths (q - p') for uncemented sand during undrained tests are shown in Figure 5.6. Different stages during the progress of consolidated undrained compressions tests are indicated by numbering (e.g., 1, 2, 3, 4 etc) on various parametric relationships. From Figure 5.6, it can be seen that the mechanism of undrained compression is significantly dominated by the change in pore water pressure. For instance, by the continuous increase in the pore water pressure, as is in the case of loose sand. It can be seen that after peak stress there is significant post peak decrease in the principal stress difference. The stress path follows a curved pattern with gradual post peak decrease in the deviatoric stress tending towards zero as shown in Figure 5.6(a). It suggests that there is throughout dominance of compression during consolidated undrained shearing of loose sand at the given confining pressure.

Figure 5.6(b) shows consolidated undrained shearing of dense sand. It can be seen that after reaching to a peak excess pore water pressure there is quick decrease and then flatter rate of reduction in the excess pore water pressure towards larger axial strains. This suggests that after initial elastic compression there is significant dilation in the dense sand during undrained shearing. It can be seen from stress-strain curve

that there is post peak hardening depending on the dissipation of excess pore water pressure. The undrained stress path changes its direction after reaching to the point of maximum excess pore water pressure and shows a tendency of constant increase inclined towards the right.

Figure 5.7(a) shows undrained response of cemented sand. It can be seen that after maximum excess pore water pressure there is slight dissipation in pore water pressure that can be due to slight dilation in the material. However, this dilation is suppressed by high confining pressure and there is further deformation without significant change in pore water pressure. However, from Figure 5.7(b) it can be seen that after elastic compression, the initiation of dilation is suppressed and there is further post peak compression resulting to a progressive increase in the excess pore water pressure. At this stage, it would be interesting to compare the undrained compression curves for loose sand as discussed in Figure 5.6(a) and dense cemented sand as shown in Figure 5.7(b). In general, the undrained response of dense cemented sand at high pressures is similar to, loose sand at conventional pressure. However, the post peak softening of cemented sand is mild as compared to sharp post peak softening of loose sand at conventional pressure. The stress path of cemented sand at higher pressures shows a sharp turn at peak stress point as compared to smoother stress path of loose sand. The cemented sand is not reaching to state of liquefaction as compared to, loose sand. These particular differences might be due to the cement bonding.

Table 5.2 Summary of isotropically consolidated undrained compression tests (failure parameters).

Test	σ'_3 (MPa)	C (%)	D_r (%)	e_0	e_c	p'_{peak} (kPa)	q_{peak} (kPa)	ϕ'_{peak} (°)
CU-0C0.2M	0.2	0	89.4	0.495	0.477	4062	5529	35.3
CU-0C0.5M	0.5	0	90.0	0.493	0.467	1939	2632	34.6
CU-0C4M	4	0	89.4	0.495	0.453	4902	6502	33.6
CU-0C10M	10	0	89.4	0.495	0.399	10005	7097	33.4
CU-0C20M	20	0	90.3	0.492	0.367	19946	9423	33.3
CU-5C0.5M	0.5	5	85.8	0.507	0.489	2244	4409	42.3
CU-5C4M	4	5	84.5	0.511	0.483	5011	7599	39.1
CU-5C10M	10	5	84.8	0.51	0.466	9749	13279	36.2
CU-5C20M	20	5	85.2	0.509	0.427	19891	16565	34.1
CU-10C4M	4	10	80.9	0.523	0.508	10081	15808	44.5
CU-10C10M	10	10	80.9	0.523	0.496	13497	20907	41.5
CU-10C20M	20	10	80.9	0.523	0.479	20586	25071	36.7
CU-15C4M	4	15	76.7	0.537	0.517	10385	17304	47.9
CU-15C10M	10	16	77.9	0.533	0.507	14563	23954	45.0
CU-15C20M	20	15	78.2	0.532	0.499	19970	28419	39.1

$\gamma_d = 17.4 \text{ kN/m}^3$ for the above test data

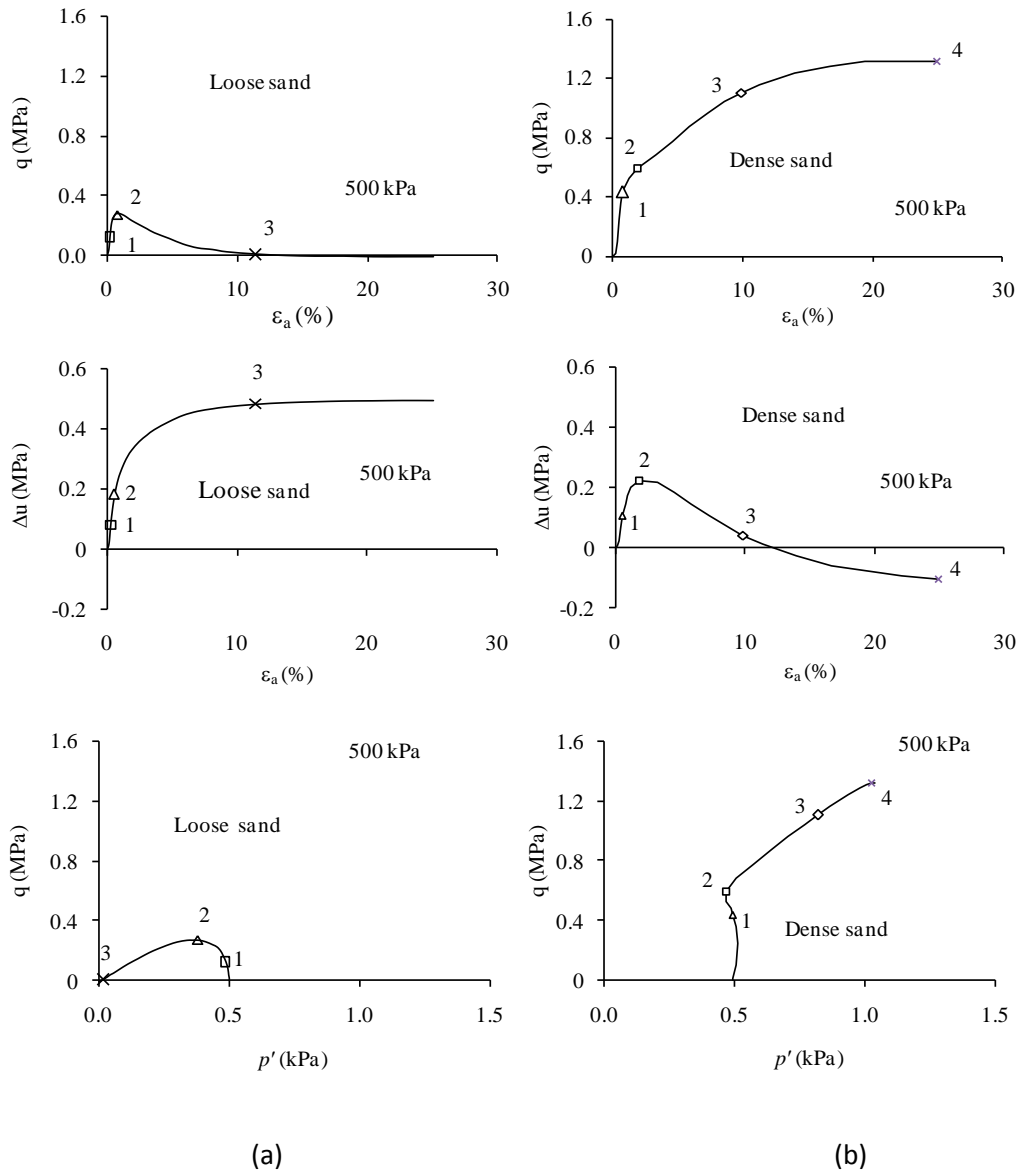


Figure 5.6 Typical undrained response of uncemented sand: (a) loose sand; and (b) dense sand.

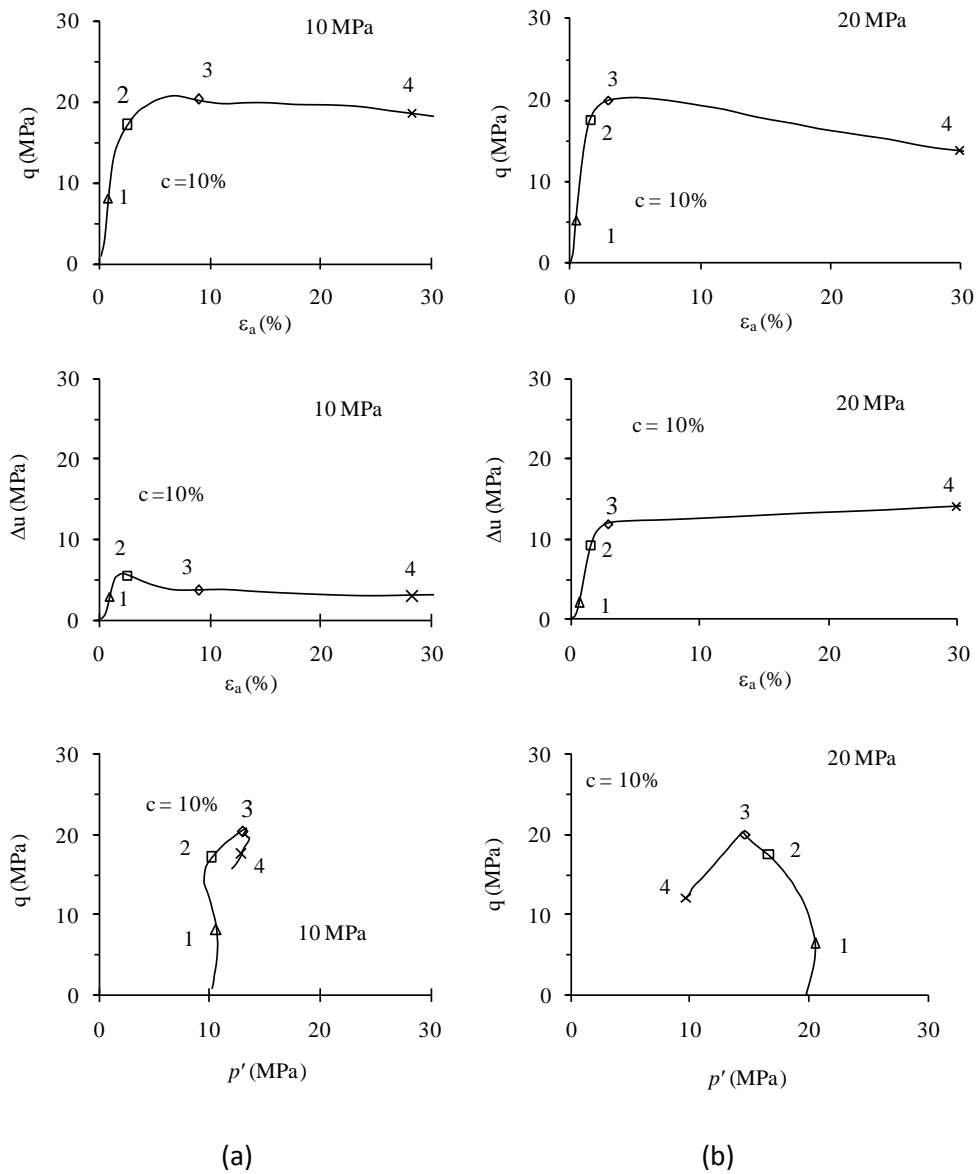


Figure 5.7 Typical undrained response of cemented sand at: (a) 10 MPa; and (b) 20 MPa.

5.3.1 Effect of confining pressure

The results of isotropically consolidated undrained (CU) tests on Portaway sand are illustrated in Figure 5.8. The stress-strain ($q-\varepsilon_a$), the effective stress paths ($q-p'$), and pore pressure-axial strain ($\Delta u-\varepsilon_a$), obtained from the undrained tests are plotted. The specimens were prepared at same initial dry density and consolidated to mean effective confining pressures of 0.5 MPa, 4 MPa, 10 MPa, and 20 MPa, respectively. As shown in Figure 5.8(a), the peak deviatoric stress increases with increasing mean effective stress. After the stress-strain curves reached a peak stress, strain softening occurred in every test. However, the strain softening observed in the tests carried out from $p'_c = 0.5$ MPa and 4.0 MPa is different from that in the test carried out from $p'_c = 10$ MPa and 20 MPa. Firstly, it can be observed from Figure 5.8(a) that at the lower confining pressures (0.5 MPa and 4 MPa) the peak deviatoric stress occurred at a relatively large axial strain ($\varepsilon_a = 9.5\%$ and 11.8%) compared to that at the highest confining pressure ($\varepsilon_a = 2.5\%$). Secondly, the strain softening in the first two tests was accompanied by the formation of shear bands. In other words, a banding softening was observed. However, in the test carried out from $p'_c = 20$ MPa the peak stress occurred before shear band development, which occurred when the effective stress path reached the failure.

From the stress path curves as shown Figure 5.8(b), the strain hardening, limited strain softening and strain softening were obtained for the specimen sheared from p'_c of 0.5 MPa to 20 MPa. It can be seen that the initial confining pressure affects the effective stress paths obtained from the tests. The behaviour changes from the

strain hardening at low confining pressure to the limited strain softening at high confining pressure. It should also be pointed out that shear bands were developed at the peak stresses in all the tests. Therefore, similarly to the tests on uncemented sand, the banding softening was observed in the tests on cemented sand regardless of the initial strain hardening response of each specimen.

From the excess pore water pressure versus axial strain curves as shown in Figure 5.8(c), it can be seen that in the specimen sheared from $p'_c=10$ MPa and 20 MPa the excess pore water pressure increased continuously throughout shearing and approached a constant value at the end of test. The Δu - ε_a curves obtained from the other two tests (i.e., 0.5 MPa and 4 MPa) showed an initial pore water pressure build-up and a distinct peak (i.e. Δu_{max}). After the Δu_{max} , a gradual reduction in pore water pressure was observed in the two tests. In the test commenced from $p'_c = 0.5$ MPa, the change in pore water pressure ceased when the shear band had occurred. As a result, the pore pressure became constant in the post-peak region. The pore water pressure in the specimen sheared from $p'_c = 4$ MPa increased slightly in the post peak region. Overall, it can be seen that the behaviour of sand under undrained conditions significantly depends on the confining pressure. From the excess pore water pressure versus axial strain curves the higher the p'_c the higher the Δu measured in the test.

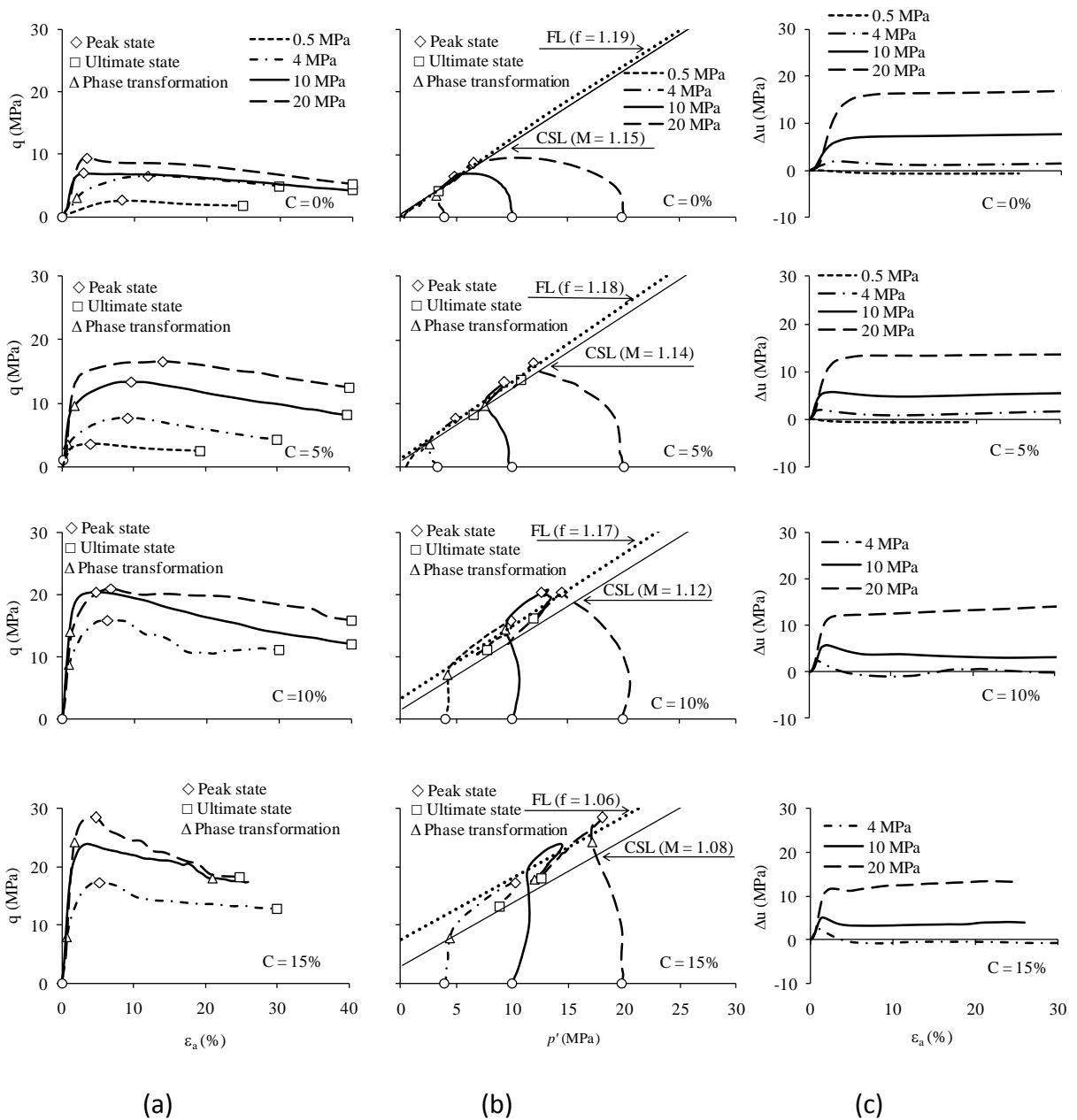


Figure 5.8 Undrained test responses under the effect of confining pressure at cement content of: (a) 0%; (b) 5%; (c) 10% and (d) 15%.

5.3.2 Effect of cement content

Cement content plays an important role in the stress-strain and strength behaviour of frictional materials (Lade and Overton 1989). Marri *et al.* (2010) showed that the drained behaviour of Portaway sand at high confining pressures is strongly affected by the cement content. The question then arises whether similar effect of the ce-

ment content will be observed under undrained conditions. Therefore, cement content effects were studied in undrained triaxial compression tests on uncemented and cemented samples. Artificially cemented samples with cement contents of 5, 10, and 15% of the weight of dry sand were prepared. All the specimens were isotropically consolidated before undrained shear. The results of CU tests are shown in Figure 5.9. From the figure, it can be seen that the stress-strain curves, the effective stress paths, and the excess pore water pressures are all affected by the cement content irrespective of the magnitude of confining pressure. For instance, at 4, 10, and 20 MPa of effective confining pressures, the cement content effect is obvious. It suggests that the effect of cement content during undrained compression tests is relatively less suppressed as compared to drained tests by the increase in confining pressure.

From stress-strain curves as shown in Figure 5.9(a), it can be seen that by the increase in the degree of cement content there is increase in peak strength and for a given confining stress, the strain associated with peak strength decreases with an increase in cement content.

The stress paths of undrained tests along with drained failure envelopes for various cement contents at the effective confining pressure of 4, 10, and 20 MPa are shown in Figure 5.9(b). From the figure, it can be noticed that the shape of the stress paths is cement content and confining pressure dependent. For higher cement contents it could also be seen that the stress paths crossing the drained failure envelopes.

As shown in Figure 5.9(c), by the increase in cement content, there can be seen post peak decrease in the excess pore water pressure, however, it is more pronounced at

relatively lower pressures. At high pressures the excess pore pressure dissipation is suppressed by the confining pressures and there can be noticed an approximate constant excess pore water pressure towards the ultimate state.

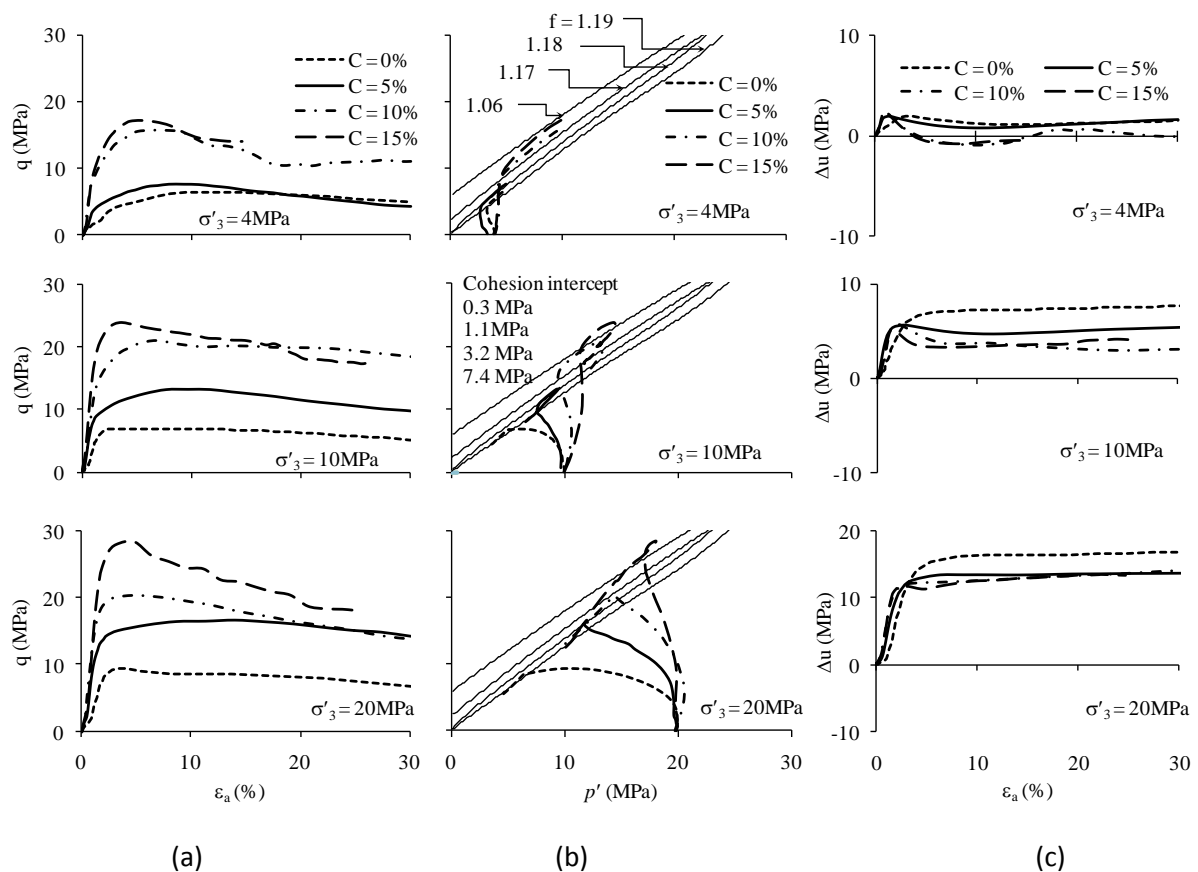


Figure 5.9 Effect of cement content on the undrained behaviour of Portaway sand: (a) stress-strain curves; (b) effective stress paths; (c) excess pore water pressures.

5.3.3 Undrained shear strength

A series of consolidated-undrained triaxial compression (CU) tests were performed on comparable uncemented and cemented specimens of Portaway sand to evaluate the undrained frictional properties of cemented sands. Figure 5.10 suggests that increase of cement contents increases the angle of internal friction values as compared to values for uncemented soil. A comparison of the Mohr-Coulomb strength parameters for the uncemented and cemented sand specimens reveal that cementa-

tion has a significant effect in improving the effective stress friction angles. Horpibulsuk et al. (2004) also reported increase in the undrained friction angle in clay due to cement content.

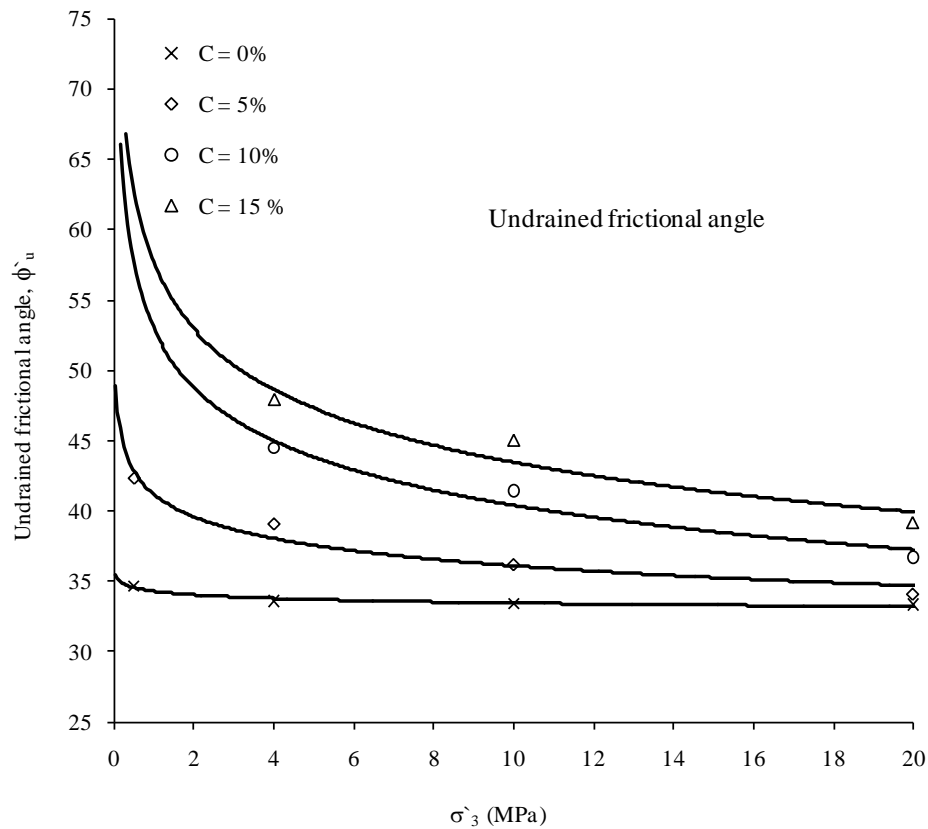


Figure 5.10 Effect of confining pressure for a wide range of cement contents at undrained frictional angle.

5.4 Comparison of drained and undrained behaviour

Effective stress paths for uncemented and cemented samples are shown in Figure 5.11. The stress paths for drained tests are a straight line with a slope 3/1 in q - p_0 space. The highest point on that line is the failure point for uncemented and cemented samples. However, for cemented samples the test continues with strain softening behaviour where the stress condition decreases along the same stress path to reach a lower ultimate stress.

Some previous studies that have been carried out on artificially and naturally cemented sands at conventional pressure, reported that the failure envelopes of both the cemented and uncemented sands are essentially straight lines with nearly the same slope. For instance, according to Clough *et al.* (1981), the cohesion intercept increases with increasing amount of cement and the friction angle is not affected by cement content. However, in the present studies carried out on uncemented and cemented sands at high pressures (see Figure 5.11) indicating that the failure envelopes are rather curved for both cemented and uncemented sands. In addition, there is decrease in the slope of the failure line by the increase in cement contents. The effect of cement content on frictional angle is quite significant at conventional pressures; however, cement content effect is suppressed at high pressures.

For the uncemented material, the stress paths from undrained tests define a similar failure envelope to that defined by the drained tests as shown in Figure 5.11. However, in the cemented material, the undrained tests cross the failure surface defined by the q_{\max} points from drained tests, showing that the material can attain higher stress ratios when sheared in an undrained condition as shown in Figure 5.11 (c) and (d) and is in accordance with Asghari *et al.* (2003). This is likely to be due to the fact that volumetric straining as happened in the drained test will contribute to the breakdown of the cemented bonds (Malandraki and Toll 2001). When volume strains are prevented in undrained tests, a higher stress ratio can be sustained before the bonds break.

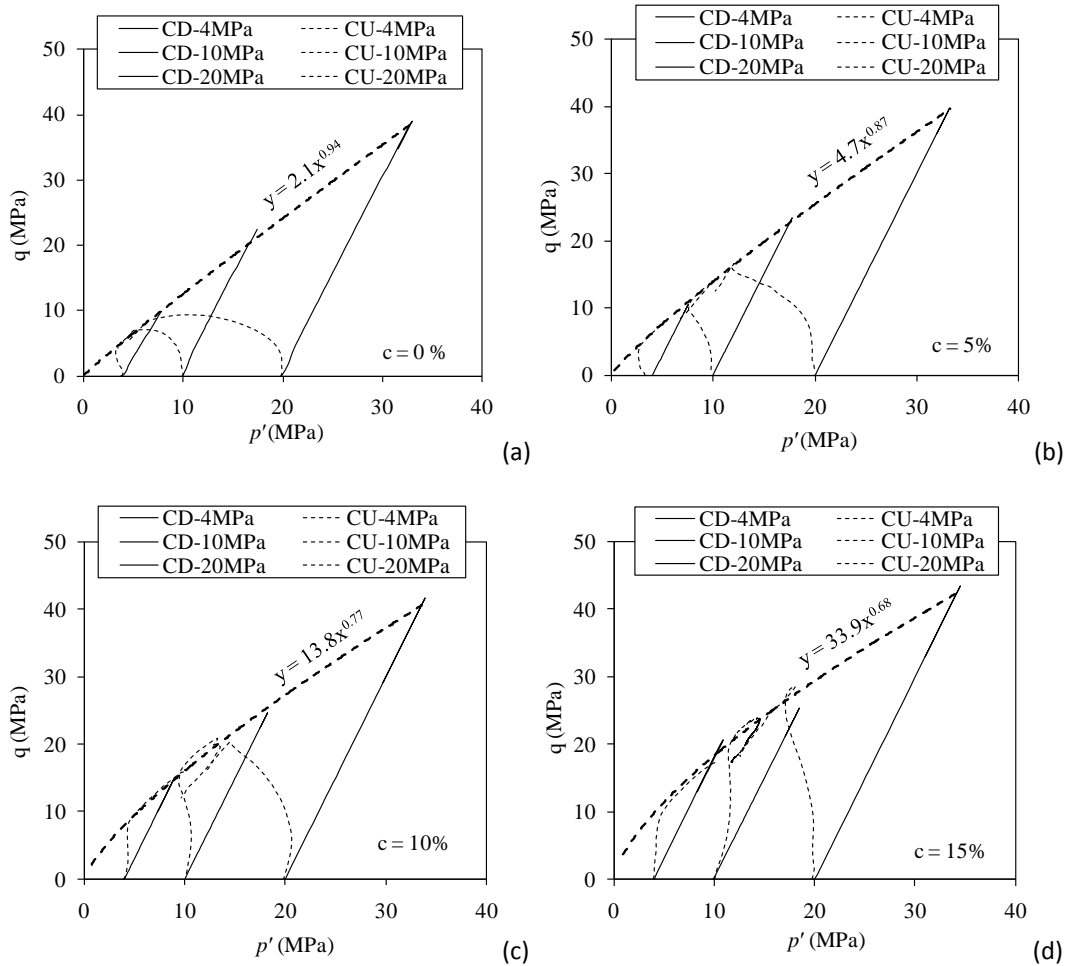


Figure 5.11 Drained and undrained stress paths and failure envelopes for cemented Por-taway sand with the cement content of: (a) 0%; (b) 5%; (c) 10%; and (d) 15%.

Figure 5.12 indicates that the effective stress friction angle from the CU tests are slightly higher than those from the CD tests, whereas for the effective stress cohesion intercepts of cemented sand specimens from the CU tests, low confining pressure tests are required for getting a well-defined cohesion intercept to compare with those from the CD tests.

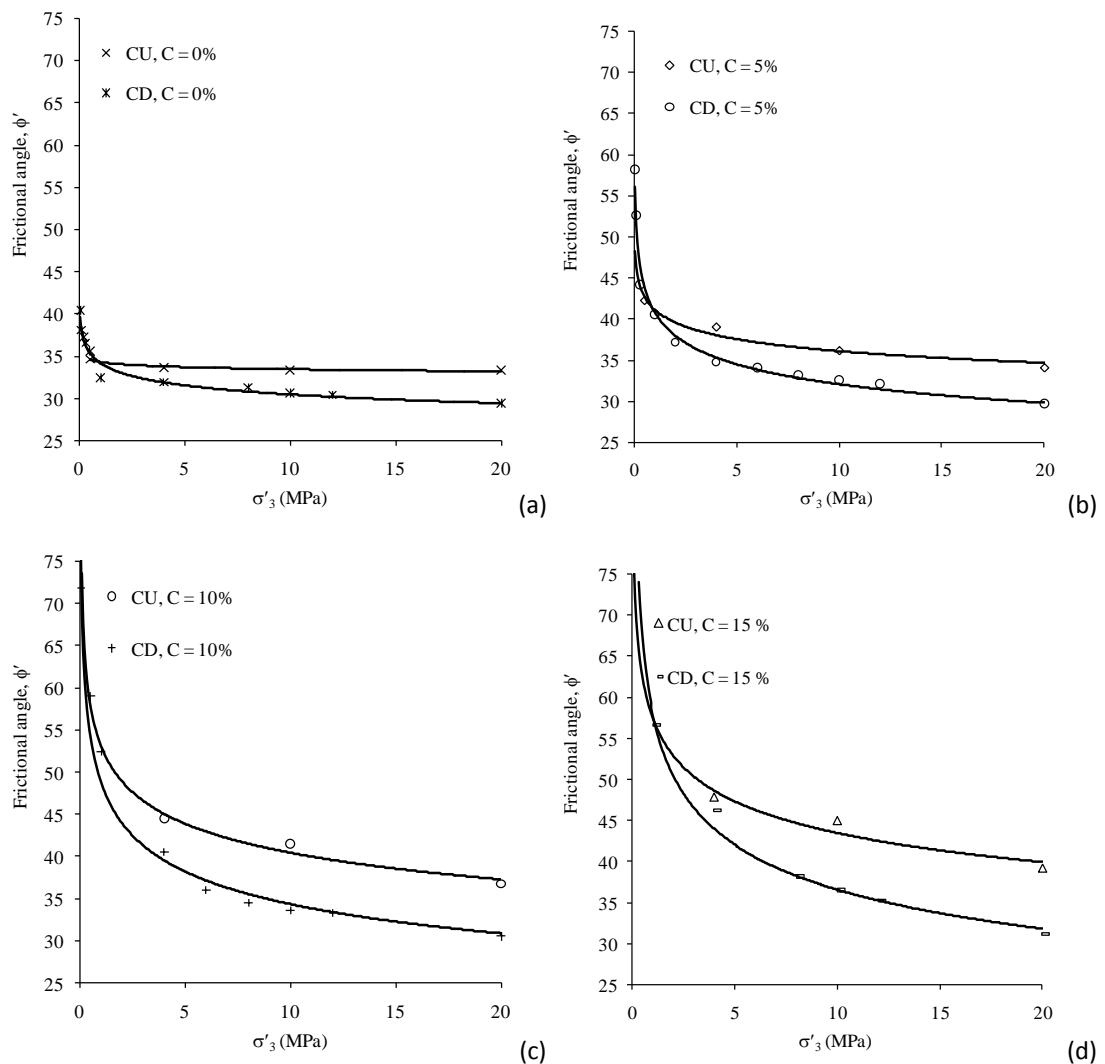


Figure 5.12 Comparison of the effective frictional angles for undrained and drained compression tests with cement contents of: (a) 0%; (b) 5%; (c) 10%; and (d) 15%.

5.5 Failure characteristics

In considering the failure mechanism of cemented sand, two aspects are relevant: the peak strength and the mode of failure. It is well known that the failure mechanism of cemented granular soils is influenced by the friction angle (ϕ_f) and the cohesion intercept (c) because of the cohesive-frictional nature of the cemented soil. These failure characteristics can be determined from the peak state (i.e. failure state) data obtained from CD triaxial tests.

In the failure state of soil with cement content, the effects of cement content ought to make the strength of soil increase and extend the domain in which soil can exist. How the high confining pressure does affect the failure mechanism of cemented materials is not yet fully investigated. Most of the previous investigations were limited to the conventional range of pressures could be one of the reason. Therefore, investigations of the effects of cement content and high confining pressures on the failure mechanism would be very interesting to explore.

The failure mechanism and the mode of failure of the specimens was examined through stress-strain behaviour, photographs of the exhumed specimens after shearing and scanning electron microscopy (SEM) pictures. The brief description of the experimental data used for the investigations of failure mechanism of cemented sand for a wider range of cement content and confining pressure is given in Table 5.2, which summarizes the typical testing program undertaken to evaluate the undrained behaviour of uncemented and cemented specimens. The undrained test data is used to compare both drained and undrained behaviour of artificially cemented sand and analyze the undrained strength parameters of the materials.

5.5.1 Failure criteria

There are different criteria that define failure. The maximum deviatoric stress, q_{\max} , is an indicator of the soil, and has been used as a failure criterion. An alternative failure criterion is the effective stress ratio defined as $(q/p')_{\max}$. In an undrained test, the maximum deviatoric stress and maximum effective stress ratio may not occur at the same axial strain. (The maximum effective stress ratio is a function of the pore-water

pressure measured during the undrained test. On the other hand, the maximum deviatoric stress is not a direct function of the pore pressures). The limiting strain failure criterion is sometimes used when large deformations are required in order to mobilize the maximum shear stress. In general, the different failure criteria produce similar shear strength parameters.

The Mohr-Coulomb failure criterion is the most common empirical failure criterion used in soil mechanics. Most published research concentrates on testing cemented soils, and developing appropriate simple Mohr-Coulomb-type failure criteria. However, only limited information on experimental details has been reported, and the intricacies of brittle material testing seem to have been ignored (Abdulla and Kiousis 1997). The mechanisms that lead to failure in composite materials are not yet fully understood.

In an attempt to understand the failure mechanism and failure characteristics of cemented sand, triaxial drained and undrained compression tests were carried out on Portaway sand with a wider range of cement content and confining pressures. Considering the effect of cement content and confining pressures, the failure criteria were examined on the bases of the laboratory investigations. From the drained compression tests (shown in Figure 5.13) it can be seen that for varying range of cement contents and confining pressures the maximum deviatoric stress q_{\max} and the maximum stress ratio defined as $(q/p')_{\max}$ occurs at the same axial strain. This experimental evidence validates the assumption of co-occurrence of q_{\max} and $(q/p')_{\max}$. However, by the increase in confining pressure it is evident that the cited failure cri-

teria occurs at very large strains, as large as 25% (see Figure 5.13(c)), while such large strains are rarely tolerable for various geotechnical structures. For such a case, the limiting strain failure condition could be an alternative criterion.

In the case of undrained triaxial compression tests as shown in Figure 5.14, it is noticeable that the maximum stress difference, q_{\max} does not coincide with maximum effective stress ratio $(q/p')_{\max}$. It can be observed that by the increase in cement content the maximum deviatoric stress position shifting towards left i.e., at smaller axial strain (see Figure 5.14 (a)) and by the increase in confining pressure it's position shifts towards right i.e., it occurs at larger axial strains (see Figure 5.14 (b)). However, in either case it is limited with 15% of axial strain.

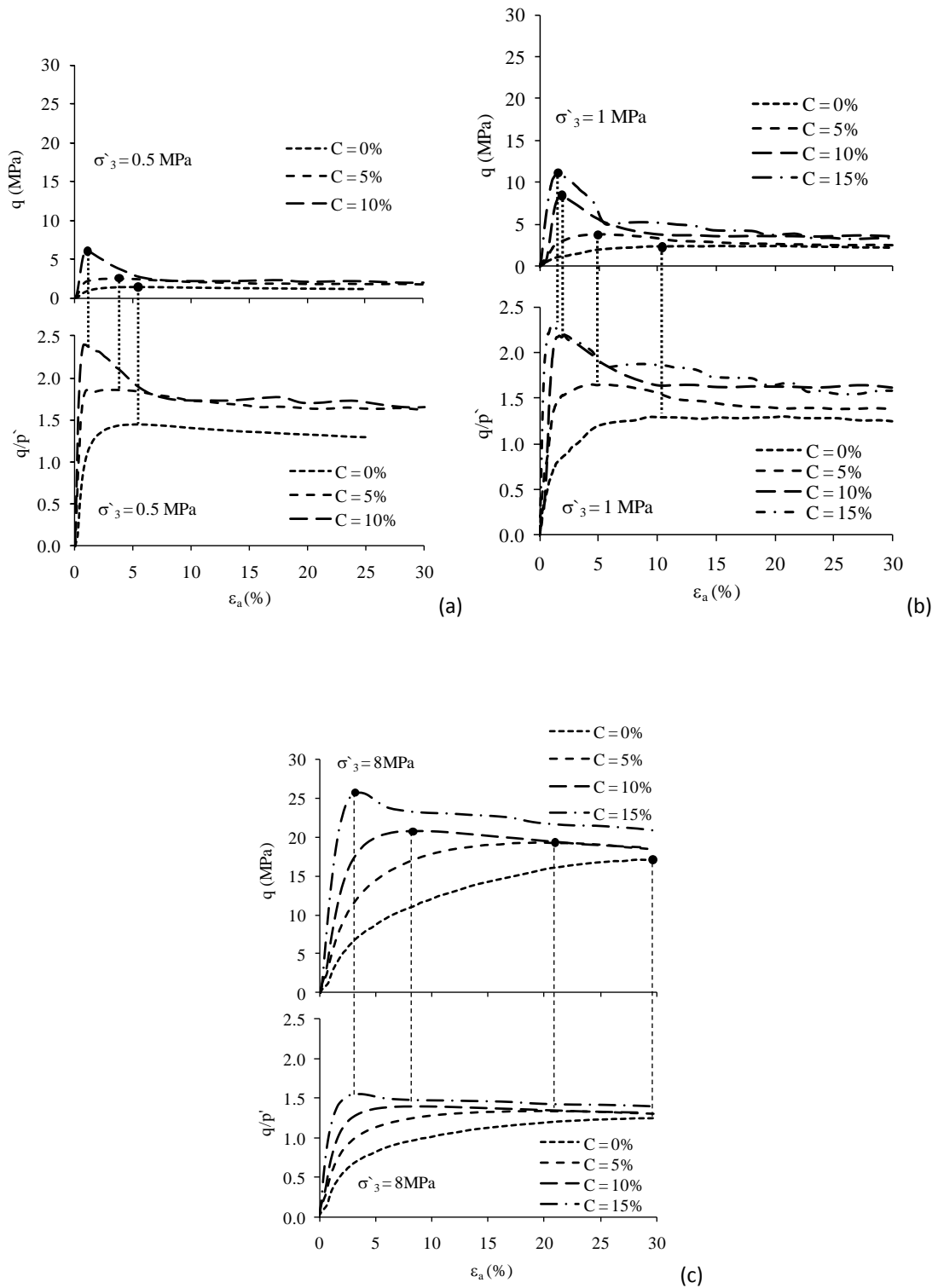


Figure 5.13 Comparisons of failure criteria based on the effect of cement content and confining pressures during drained compression tests at effective confining pressures of: (a) 0.5 MPa; (b) 1 MPa; and (c) 8 MPa.

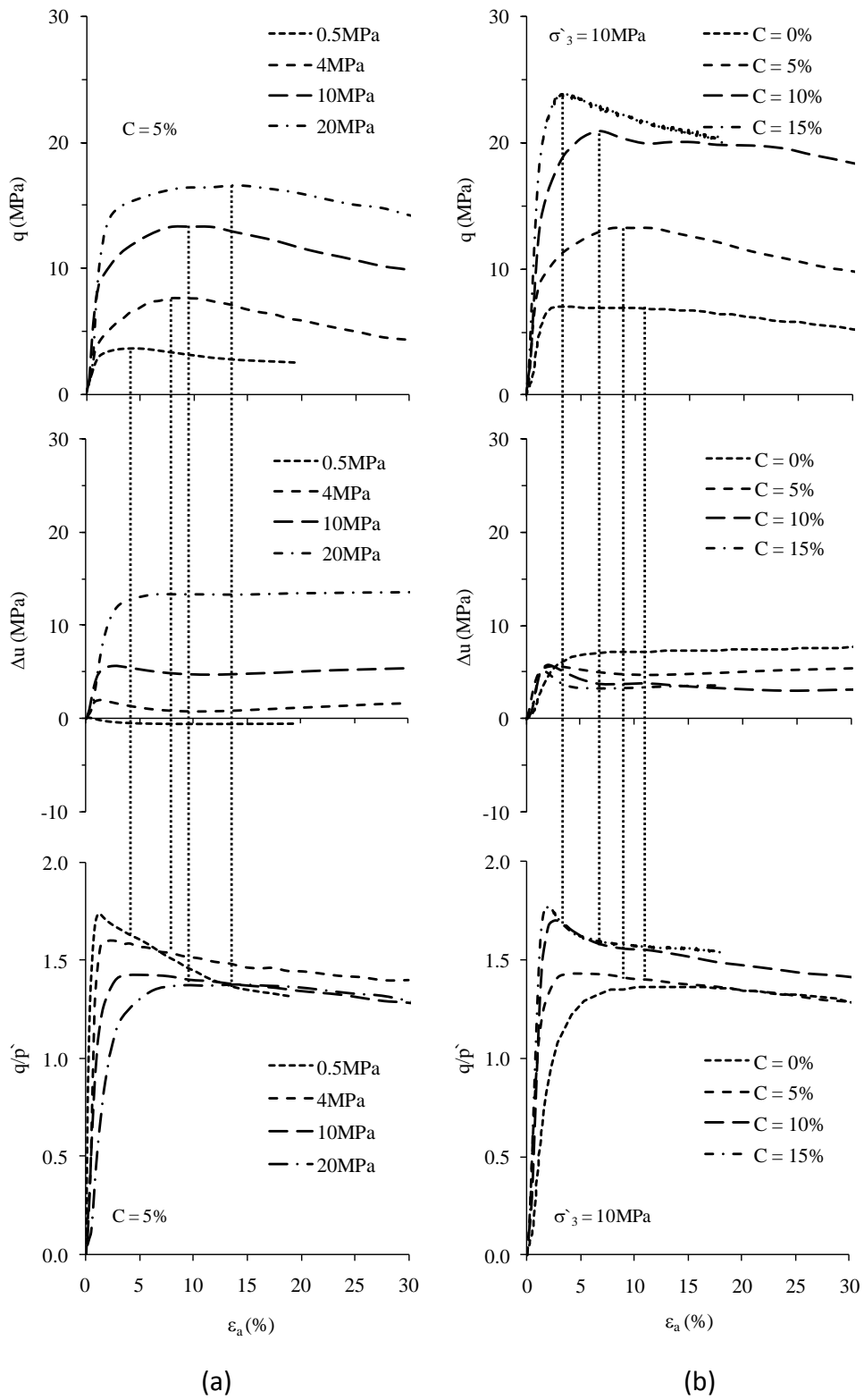


Figure 5.14 Comparisons of failure criteria based on the effect of: (a) confining pressure; and (b) cement content during undrained compression tests.

5.5.2 Modes of failure

Failure mode is the manner whereby the failure is observed. Generally, it describes the way in which the failure happens. Traditionally cemented sand failure in compression is categorized in two modes. In first, a sample may show strain localization and fail by strain softening and brittle failure under relatively low confining pressure. Moreover, in second, it may show delocalization and fail by strain hardening under elevated confining pressure. While at intermediate pressures, a transitional regime is sometime observed, with failure modes involving complex localized features such as conjugate shear bands.

As reported by Coop and Atkinson (1993), Schnaid *et al.* (2001), Haeri *et al.* (2005), and others, the mode of failure is also important in analyzing the failure behaviour of cemented sand. This because it affects significantly the strength parameters determined from the tests. The mechanical properties of the materials are essential for understanding the behaviour of cemented sand to provide a useful method of predicting failure mode. An absolute measure of such behaviour is provided by brittleness index (I_B) defined by the following expression given by Consoli *et al.* (1998). And the physical manifestation can be captured by the pictures of the exhumed specimens after shearing and SEM photographs.

$$I_B = \frac{(\sigma'_1 - \sigma'_3)_f}{(\sigma'_1 - \sigma'_3)_u} - 1 = \frac{q_f}{q_u} - 1 \quad (5.1)$$

where, q_f , and q_u are the deviatoric stress at failure and ultimate state respectively.

Triaxial compression tests were conducted on cemented specimens. Confining pressure ranging from 0.1 MPa to 30 MPa was applied to observe the transition from the brittle to ductile mode of failure. All uncemented specimens tested at high confining pressures (i.e. > 1 MPa) showed barrelling failure modes. Failure of the uncemented specimens sheared at lower confining pressures (i.e. ≤ 1 MPa) was accompanied by shear band formation.

In cemented specimens sheared at confining pressures lower than 1 MPa, shearing was accompanied by a shear band without significant barrelling. At higher confining pressures, however, the specimens displayed clear barrelling accompanied with shear bands. It was observed that the brittle behaviour increased with increasing cement content and decreased with an increase in confining stress. This is consistent with observations made for cemented gravelly sand by Asghari *et al.* (2003).

1) The brittle regime

From Figure 5.15, it can be observed that the brittleness index is high at relatively lower confining pressure and higher cement contents; which is indicating a stronger, stiffer, and more brittle material. The mode of failure, which indicates clear shear banding during consolidated drained compression, can be seen in Figure 5.16(a), having cement content of 15% and sheared at an effective confining pressure of 6 MPa.

2) The transitional regime

An intriguing feature of the cemented sand as shown in Figure 5.16 (b) is that over a broad range of intermediate pressures the failure mode cannot be unambiguously

categorized as strictly "brittle" or "ductile". Moreover, instead of a single shear band, the cylindrical surface of the failure sample is marked by several conjugate shears. This type of transitional failure mode is referred as "quasi-brittle" by Klein et al. (2001). From brittleness index, the transitional range can be between 6 MPa to 12 MPa.

3) The ductile regime

The brittleness index above the confining pressure range of 12 MPa for cement contents up to 15% can be characterised by ductile attributes with an overall strain-hardening trend. The mode of failure for a specimen with cement content of 10% and an effective confining pressure of 12 MPa is captured as shown in Figure 5.16(c), which is showing a bulging pattern during consolidated drained shearing.

Overall, in cemented samples, the peak strength and the associated strain-softening response become more distinct as the cement content increases or confining pressure decreases. Adding cement is markedly increasing the strength and altering the stress-strain behaviour. Increase of confinement causing to reduce the softening tendencies, and generally resulting in a more ductile response. These findings are in accordance with previously published results, for example, Wang and Leung (2008), Ismail *et al.* (2002), Schnaid *et al.* (2001), and Clough *et al.* (1981).

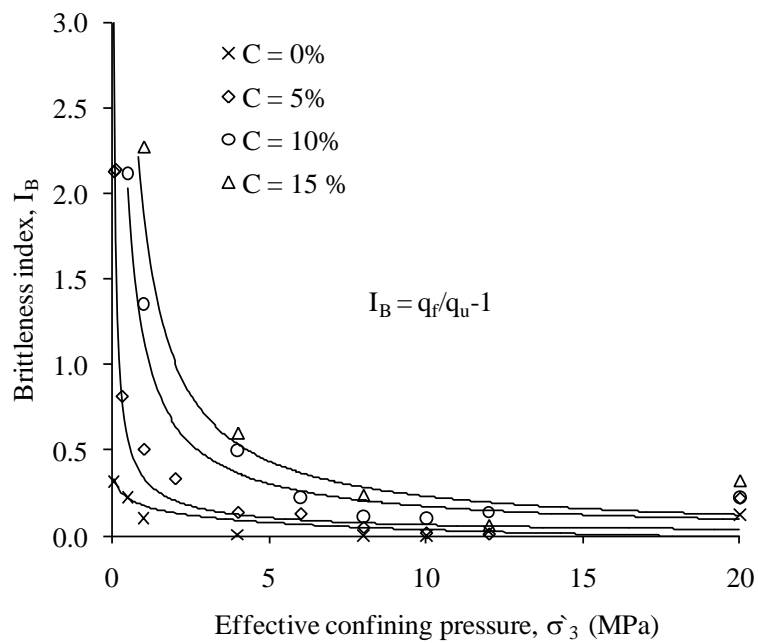


Figure 5.15 Effect of confining pressure on brittleness index.

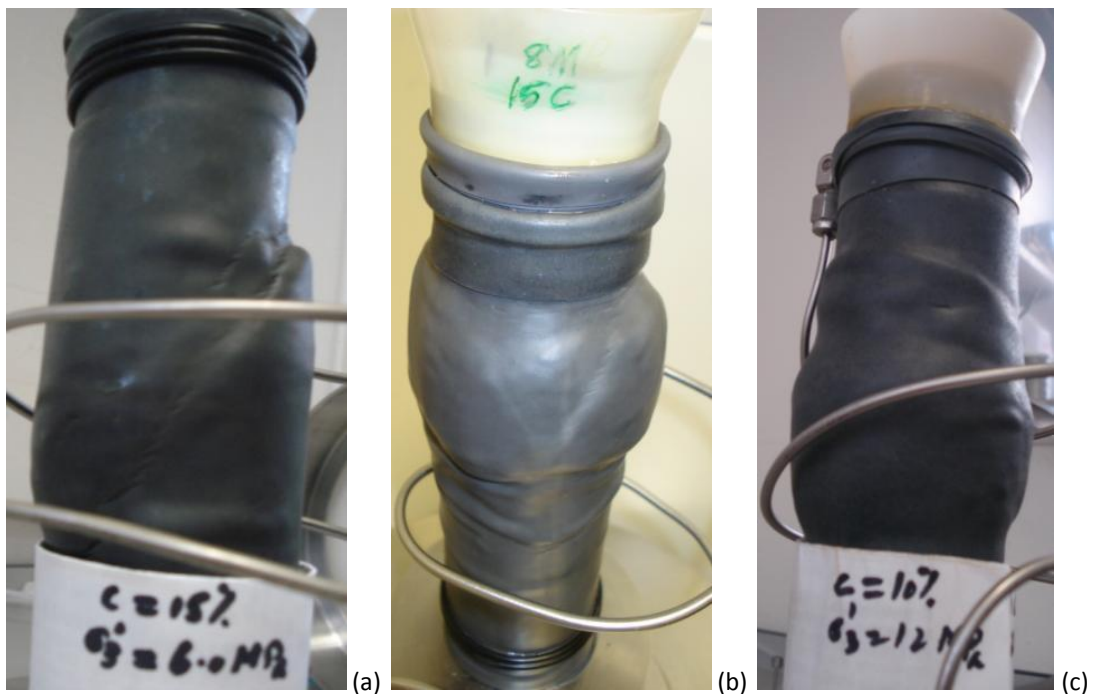


Figure 5.16 Mode of failure of cemented Portaway sand: (a) brittle; (b) Transitional; (c) Ductile.

5.5.3 Strain localization and shear band characterization

The process, which gives rise to shear bands, is known as “Strain localization”. Strain localization manifests itself in the form of a shear band, a narrow zone of intense straining. It is now generally recognized that the intense deformation in the shear bands is primarily responsible for the accelerated softening response exhibited by most structures at post peak strength.

In case of strain localization during shear deformation, the deformation process diffuses at first, and then tends to concentrate in narrow zones called shear bands. In order to illustrate the strain localization and shear band formation, typical sketches of isotropically consolidated drained sheared specimens are as shown in Figure 5.17. On the basis of visual assessment of the specimens’ photographs, the shear band shape patterns can be divided into the following categories: (a) weakly developed shear band; (b) fully developed shear band; and (c) fully developed shear bands that cross diagonally (“diagonally crossing shear bands”).



Figure 5.17 Illustration of shear band pattern after shearing, sketched from the tested samples.

The effect of confining pressure on shear banding and relative stress-strain and volumetric response of cemented Portaway sand is illustrated in Figure 5.18. Because of the complex pattern of shear banding, it is difficult to accurately measure

the angles of shear bands with respect to the horizontal axis. There is also no clear trend that the orientation is a function of the degree of cement content or confining pressure.

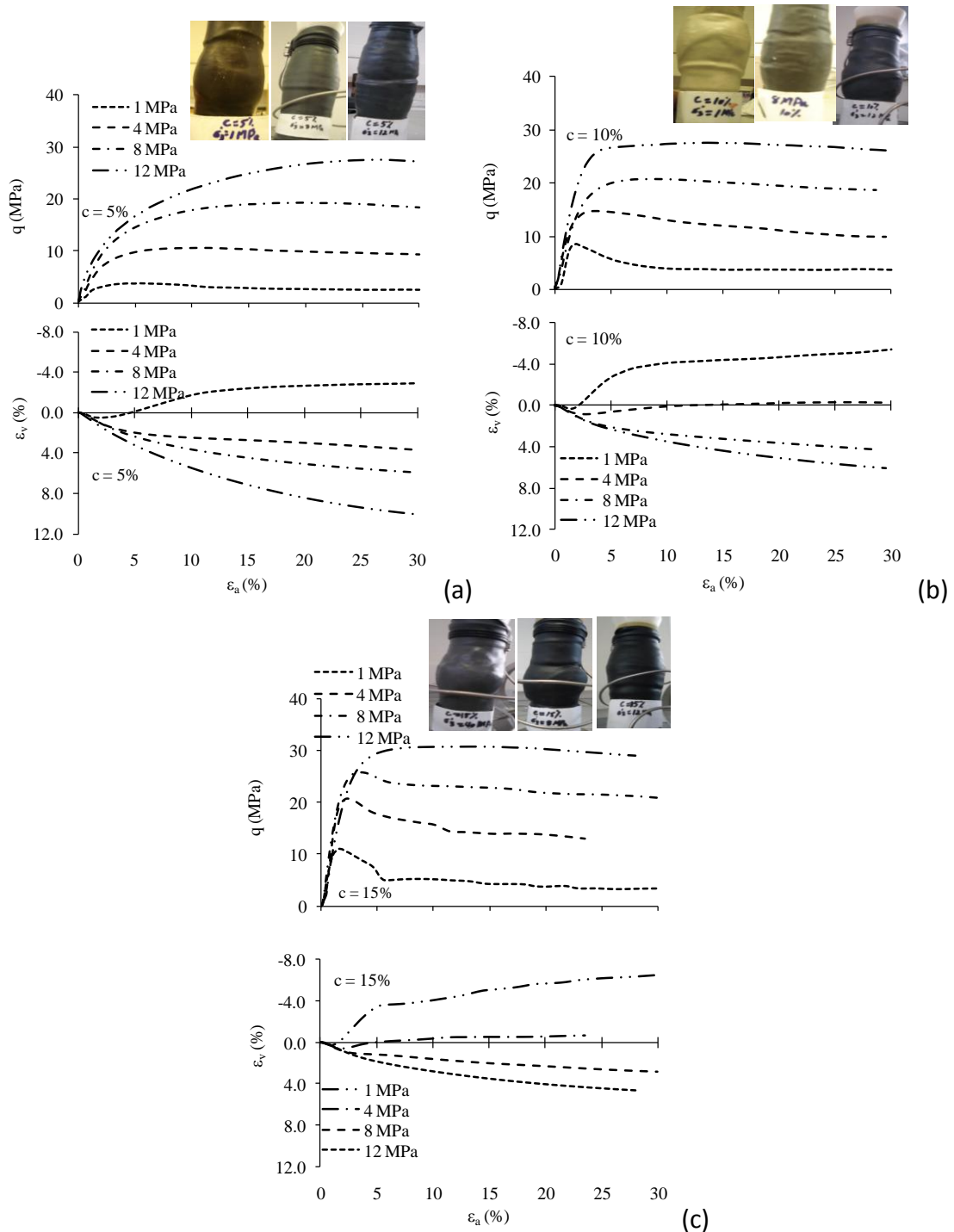


Figure 5.18 shear band characterization of sand at the cement contents of: (a) 5%; (b) 10%; and (d) 15%.

This suggests high sensitivity of the shear band orientation with testing conditions. It seems that when a shear band intersects a specimen, deformation is concentrated within the localized zone and is essentially absent elsewhere. Consequently, the characterization of continued deformation is focussed efforts towards shear band behaviour. It can be seen that Shear banding occurs with the strain-softening response. In addition, the appearance of shear banding becomes more visible with increasing cement content. The gradual increase in the confining pressure suppressing the shear band pattern resulting to exhibits only a bulging type of failure.

5.6 Summary

The stress-strain behaviour of Portaway sand for a wide range of cement content and confining pressure was investigated for both drained and undrained conditions. From the experimental results, it could be seen that the cement content and confining pressure significantly influences the mechanical response of sand. For instance, increasing the amount of cement content in the sand can markedly augment the strength and enhance the associated strain-softening response. The results show strength enhancement, volumetric dilation, and the shear banding associated failure mode. These features become more pronounced with increasing cement content and prevail only under low confining pressure. However, at high pressures strain-hardening behaviour and a bulging type of failure are observed and shear banding is rarely visible. Greater volumetric contraction, identical to the loose sand can be measured.

The failure characteristics and different failure criteria were investigated through laboratory testing. The effect of cement content and confining pressures were examined on the peak strength and mode of failure of the artificially cemented Portaway sand. The shear banding and progressive failure mechanism were closely investigated under the effects of cement content and confining pressures.

The preliminary investigations of cemented sand under drained and undrained conditions emphasizes the significance of density, cement content and confining pressure during triaxial compression and ultimately compelling to further detail studies of stress-dilatancy, yielding, and micromechanics of the material.

From the triaxial compression behaviour of cemented sand the following conclusions can be drawn:

- 1) In any case, either by the increase in cement content and/or confining pressures there is increase in the peak strength of the sand. The position of peak stress changes with the change in cement content and confining pressure. Increase of cement content resulting to a brittle behaviour and causing the peak strength to occur at smaller strain levels. On the other hand, increase in confining pressures resulting to induce ductility and causing the peak strength to occur at larger strain levels depending upon the magnitude of confining pressure.
- 2) The specimens exhumed after shearing were observed to be showing brittle, transitional and ductile mode of failure, depending upon the percentage of cement content and the amount of confining pressure applied. The quantita-

tive analysis of the mode of failure was made with the help of brittleness index (I_B).

- 3) During the brittle mode of failure usually occurring at relatively higher cement contents and lesser confining pressures strain localization was in abundance.
- 4) Cemented specimens show a brittle failure mode at low confining pressure accompanied by shear banding with a transition to ductile failure mode at higher confining pressures. This is in accordance with the previous findings.
- 5) The results of the triaxial tests performed on cemented and uncemented Portaway sand show that addition of the cement content could improve the strength of soils under undrained and drained loading conditions. Shear strength parameters of effective stress cohesion intercept and friction angle increase significantly in the CU and CD tests, due to the addition of cement. The effective stress friction angles from the CU tests are slightly higher than those from the CD tests.
- 6) Both cement content and confining pressure affect the stress-strain behaviour of cemented sand under undrained conditions.
- 7) An increase in the initial effective confining pressure increases the peak deviatoric stress, the axial strain to the peak and the excess pore water pressure developed in the test. Furthermore, the stress-strain behaviour of cemented sand changes from the strain hardening at low confining pressures to the strain softening at high confining pressures.
- 8) Cement content affects the effective stress paths. Increase in cement contents shifts the effective stress paths upward, increase the peak deviatoric stress,

and reduce the excess pore water pressure developed during consolidated undrained compression tests.

- 9) The behaviour of the cemented soil is found to be more brittle in drained conditions as compared to the undrained conditions.
- 10) In case of the formation of shear bands, the maximum deformation of cement bonding and particle crushing is likely along the shear plane. The particles in the bonding network jointly share the loading and cement addition significantly reduces the level of particle crushing.

STRESS-DILATANCY RESPONSE OF CEMENTED SAND

6.1 Introduction

After compression the subsequent phenomenon for dense granular materials is often, the expansion in volume of the materials which is usually called dilation. It is a measure of how much volume increase occurs when the material is sheared. Dilation occupies a central role in explaining phenomena such as the reduction of angle of friction with increasing stress level. The dilation usually takes place after a small initial compression. Zero rate of dilatancy corresponds to critical state of soil. The dilatancy of cemented specimens can be identified from non-linearity in either the volumetric strain versus axial strain or the differential stress versus volumetric strain curves as recorded during laboratory testing of cemented specimens and is discussed in the literature.

Various researchers have suggested evaluating dilatancy from the parameter, D which is called the dilatancy rate and is equal to the ratio of the increments in bulk strain $d\varepsilon_v$ to the increments in shear strain $d\varepsilon_q$ (i.e. $D = d\varepsilon_v / d\varepsilon_q$). The detail review of the literature regarding the dilatancy of uncemented and cemented materials reveals that the previous studies on soil dilatancy mostly concentrated on theoretical or analytical solutions of the dilation angle, as well as on its influence on soil strength. According to Chen *et al.* (2003), not many real test data of dilation angles

were reported in the past. The past research did not investigate in detail the influence of condition factors; such as the initial relative density, cement content, and confining pressure for a wider range of confining pressures and cement contents. The dilation angles of granular soils were found to be much higher than the empirical or theoretical values suggested in the previous literature and guidelines of numerical analysis computer codes. How dilatational behaviour and high peak friction angles at low stresses are gradually suppressed by higher and higher stresses would be one of the interesting aspects of the study of dilatancy characteristics of cemented sands. In triaxial drained compression, the dilatancy concept provides the key for understanding the deformation behaviour and strength reduction in dependence on pore pressure.

To capture the dilative properties of cemented Portaway sand, specimens with varying degree of cement contents and initial dry densities were prepared and tested for a wider range of confining pressures. The investigations were mainly based on the effect of cement content, initial dry density, and confining pressures. As the density of sand can vary depending on the grain size and moisture content and how tightly it is compacted; the initial relative density (D_{r0}) is used here to categorize the density of materials into loose, medium dense and dense. A number of experiments were run to capture the dilative behaviour of uncemented and cemented Portaway sand. The relationships between the friction angle, dilation angle, density, and confining pressure in cemented sand are explored. Some typical test data is given in Table 6.1. In this table initial mean effective stress (σ'_3), cement content (C %), initial dry unit weight (γ_d), initial relative density (D_{r0}), initial void ratio(e_0), void ratio at the end of

consolidation (e_c), ultimate/critical state void ratio (e_{cr}), ultimate/critical state friction angle, maximum frictional angle (ϕ'_p), and maximum dilatancy angles (ψ'_p) are given.

Table 6.1 Summary of isotropically consolidated drained compression tests (dilatancy parameters).

Test	σ'_3 (MPa)	C (%)	D_r (%)	e_0	e_c	ϕ'_{peak} (°)	ϕ'_{ult} (°)	* ψ'_{peak} (°)	** ψ'_{peak} (°)
CD-L0.3M	0.3	0	21	0.72	0.65	32.8	31.0	3.6	2.7
CD-MD0.3M	0.3	0	55	0.61	0.59	34.7	31.8	5.8	12.5
CD-D0.3M	0.3	0	80	0.53	0.51	36.6	32.6	8.0	18.1
CD-0C1M	1	0	89	0.50	0.47	32.4	30.9	3.0	2.3
CD-0C4M	4	0	89	0.50	0.44	31.9	30.5	2.8	-7.5
CD-0C8M	8	0	90	0.49	0.43	31.3	30.3	2.0	-6.6
CD-0C10M	10	0	90	0.49	0.43	30.6	30.0	1.2	-8.5
CD-0C12M	12	0	90	0.49	0.41	30.4	29.8	1.2	-6.4
CD-0C20M	20	0	91	0.49	0.39	29.4	28.1	2.6	-1.8
CD-5C1M	1	5	85	0.51	0.50	40.6	33.5	14.2	16.5
CD-5C2M	2	5	85	0.51	0.49	37.2	32.9	8.6	7.7
CD-5C4M	4	5	85	0.51	0.48	34.8	32.6	4.4	0.0
CD-5C6M	6	5	86	0.51	0.47	34.1	32.0	4.2	-1.2
CD-5C8M	8	5	85	0.51	0.47	33.2	31.7	3.0	-1.5
CD-5C10M	10	5	85	0.51	0.46	32.6	31.2	2.8	-1.6
CD-5C12M	12	5	85	0.51	0.45	32.1	31.0	2.2	0.0
CD-5C20M	20	5	84	0.51	0.43	29.7	28.5	2.4	-1.2
CD-10C1M	1	10	81	0.52	0.51	52.4	38.5	27.8	35.8
CD-10C4M	4	10	81	0.52	0.51	40.5	33.8	13.4	7.9
CD-10C6M	6	10	82	0.52	0.51	36.0	33.1	5.8	0.0
CD-10C8M	8	10	82	0.52	0.50	34.5	32.7	3.6	-1.4
CD-10C10M	10	10	82	0.52	0.49	33.6	32.4	2.4	-1.0
CD-10C12M	12	10	82	0.52	0.49	33.3	32.0	2.6	0.0
CD-10C20M	20	10	82	0.52	0.47	30.5	29.1	2.8	0.0
CD-15C1M	1	15	77	0.54	0.53	56.6	39.5	34.2	39.7
CD-15C4M	4	15	78	0.53	0.52	46.2	36.2	20.0	12.0
CD-15C8M	8	15	78	0.53	0.51	38.2	34.5	7.4	7.7
CD-15C10M	10	15	78	0.54	0.51	36.5	34	5.0	3.0
CD-15C12M	12	15	78	0.53	0.51	35.2	33.2	4.0	0.0
CD-15C20M	20	15	78	0.53	0.50	31.2	30.0	2.4	0.0

$$*\psi'_{peak} = (\phi'_{peak} - \phi'_{ult})/0.5, **\psi'_{peak} = (\delta\varepsilon_v / \delta\varepsilon_q)$$

6.2 Effect of initial relative density

Figure 6.1 shows typical test results obtained from uncemented sand with the loose, medium dense and compacted states. The figure shows that there is dilatancy in the material during the process of shearing at a rate that increases with increasing relative density (D_{r0}). For the given effective confining pressure of 300 kPa there can be seen that the loose sand is in compression zone. However, the medium dense and dense sand specimens after initial compression are showing dilation during triaxial compression. This suggests that there is a tendency of dilation in the granular materials which depends upon the initial relative density of the material. The effect of initial relative density was also examined on artificially cemented sand by preparing the cemented specimens at different initial relative densities. Figure 6.2 shows that for a given effective confining pressure of 1 MPa the specimen with zero cement content (i.e. uncemented) in its dense state of relative density is in compression. However, the cemented specimens with 10% cement contents at relative density of 44% and 81% after initial compression are showing dilation and there can be seen a higher rate of dilatancy for relatively more dense sand. This suggests that the increase of initial relative density induces dilatancy into the cemented specimens.

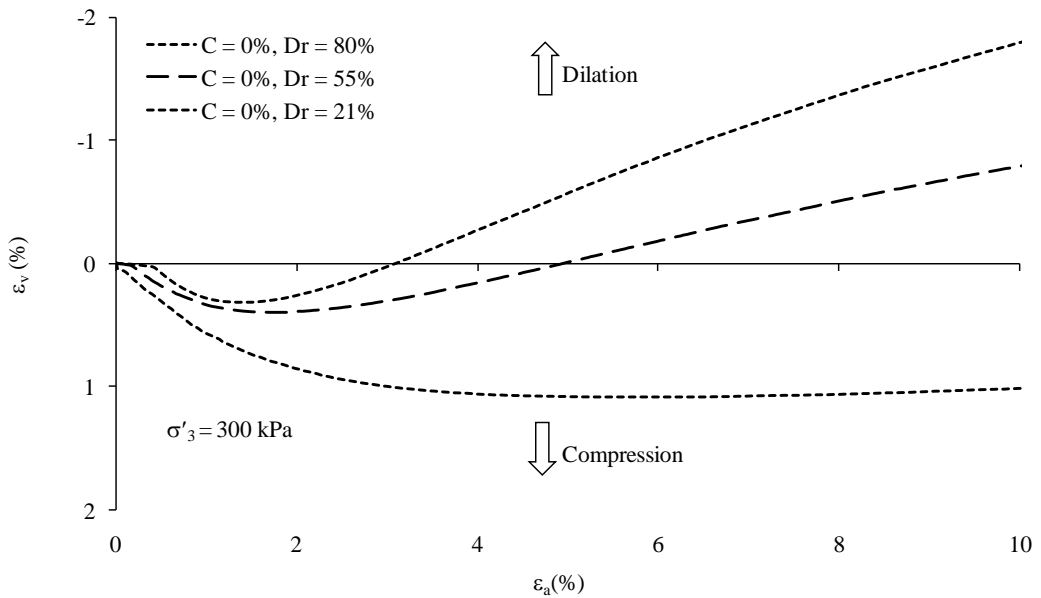


Figure 6.1 The effect of initial relative density on the dilatancy of uncemented sand.

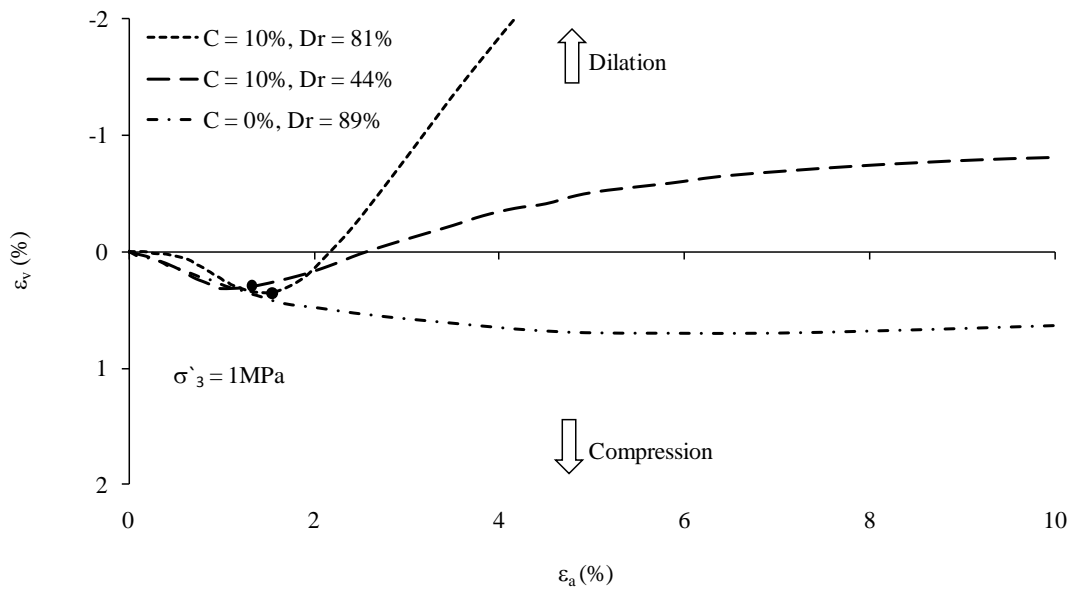


Figure 6.2 The effect of initial relative density on the dilatancy of cemented sand.

6.3 Effect of cement content

The reliance of dilatancy phenomenon on cement content is explored on the bases of laboratory experimental data. Figure 6.2 shows that for a given effective confining pressure of 1 MPa the specimen with zero cement content (i.e. uncemented) in its

dense state of relative density is in compression. However, the cemented specimens with 10% cement contents at similar density and even at relatively lower density after initial compression are showing dilation. As there is no dilation for uncemented sand at similar density, therefore this dilation could be attributed to the cementation only. This suggests that the cementation equally significantly induce dilatancy into the sand specimens as well.

As shown in Figure 6.3, the experimental observations reveal that cement content can effectively alter the volumetric response from contraction to dilation, and such a change is enhanced with increasing cement content. The dilative response, as expected, is suppressed by high confining pressure and this is obvious from Figure 6.3.

Figure 6.4 shows the points of maximum dilatation in the stress-strain, volumetric response, and stress-dilatancy relationships. The points of maximum rate of dilation were selected from stress ratio (q/p') vs. dilatancy (D) relationship and located on stress-strain and volumetric strain curves. It can be observed that after the peak state, the bond breakages lead to a decrease in the resistance to deformation but create subsequent volumetric dilation. The point of maximum dilatancy with respect to the peak stress is being delayed by the increase in cement content. For instance, at zero cement content the point of maximum dilatancy appears before peak stress point; however, by the increase in cement contents it gradually shifts towards the right of the peaks stress point. On the other hand, the increase of cement content (i.e., the cohesion effect) shifts the point of maximum dilatancy towards left with respect to the axial strain.

Figure 6.5 illustrates the cement bond breakage during consolidated drained triaxial compression test. Test results indicate that, besides the relative density, the dilation of granular soils is also very sensitive to cement content and confining pressure.

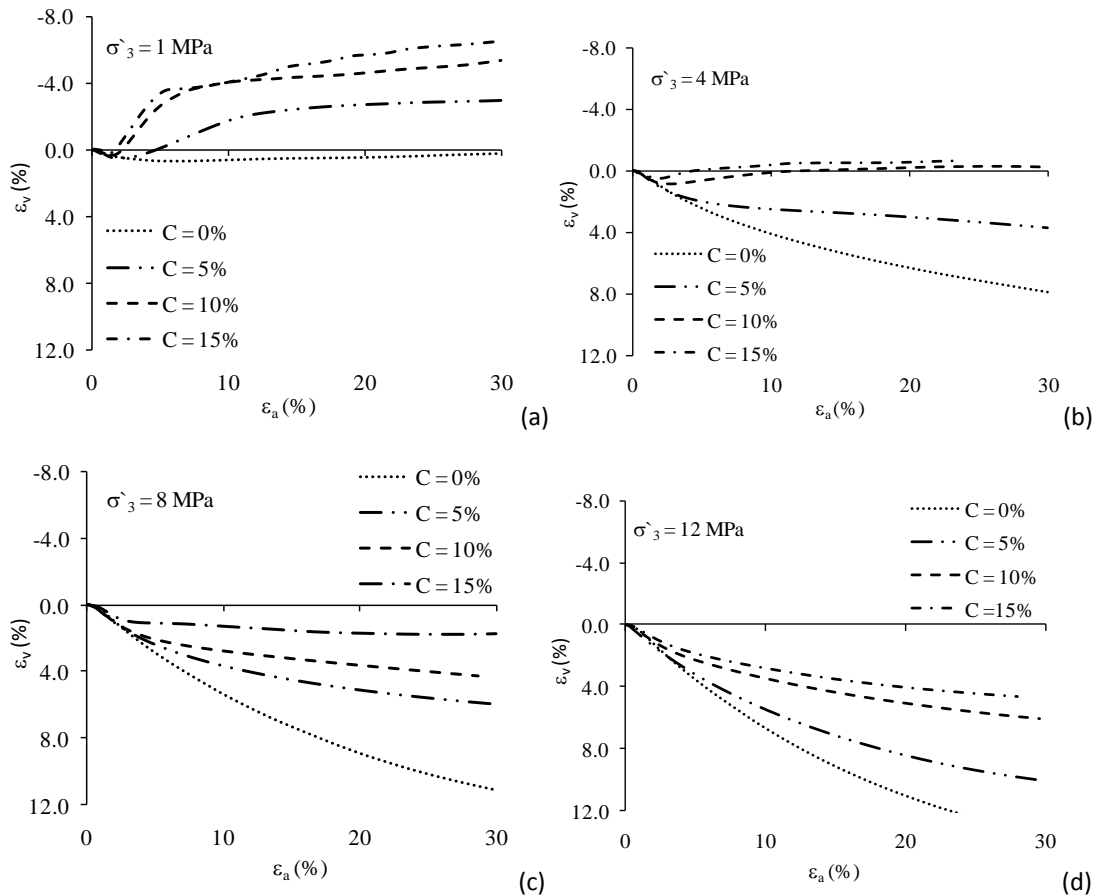


Figure 6.3 Volumetric responses of cemented sand at high pressures with cement contents 0 to 15% at effective confining pressures of: (a) 1 MPa; (b) 4 MPa; (c) 8 MPa; and (d) 12 MPa.

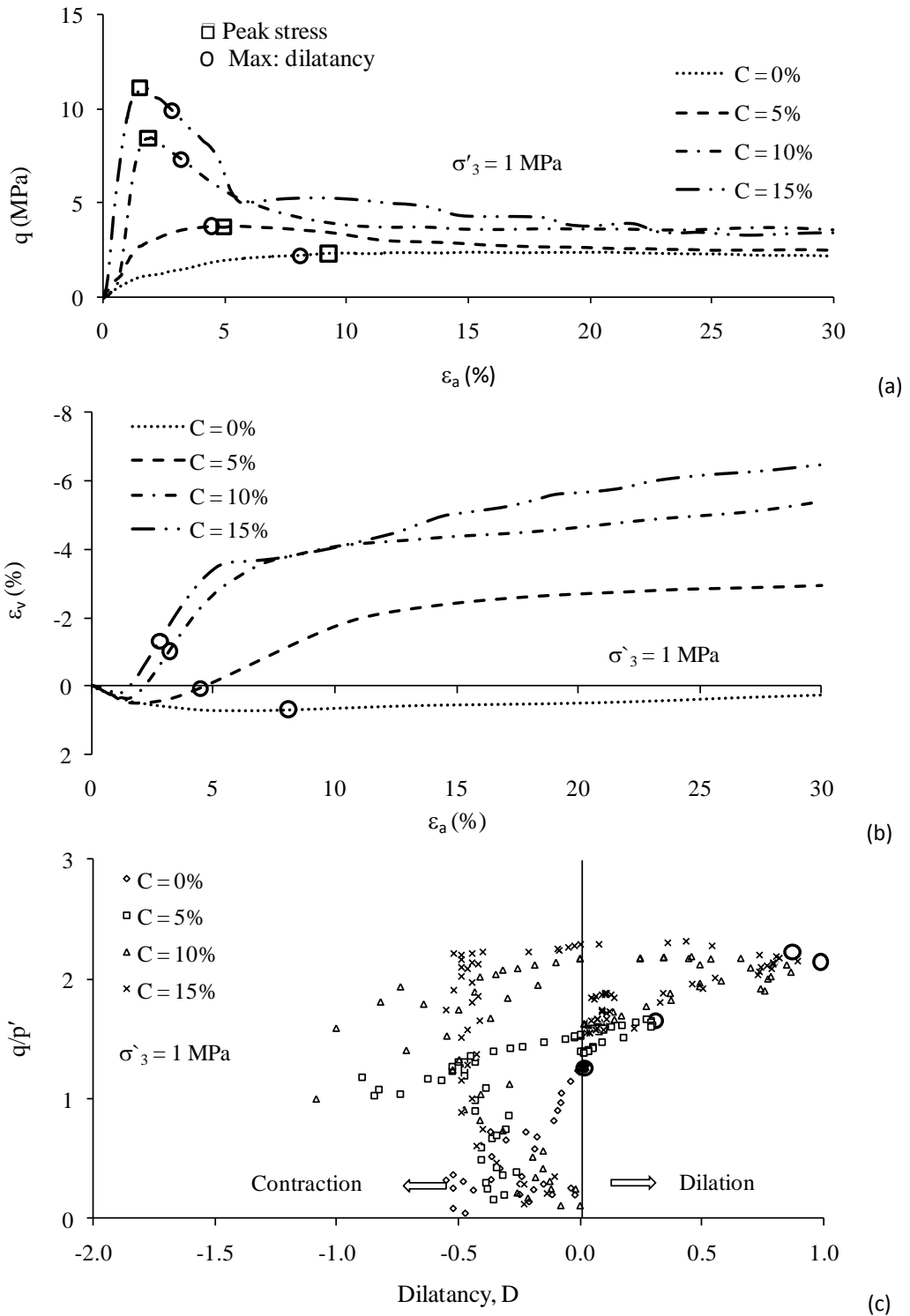


Figure 6.4 Location of the point of maximum dilation in the (a) stress-strain; (b) volumetric response; and (c) stress-dilatancy relationship.

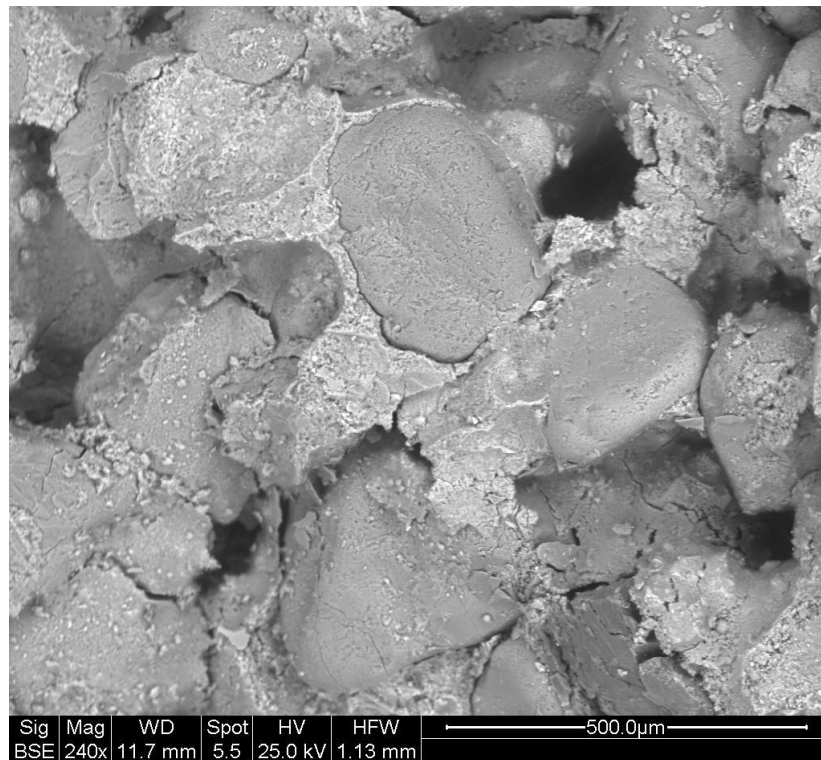


Figure 6.5 Typical SEM micrograph demonstrating the cement bond breakage during consolidated drained triaxial compression.

6.4 Effect of confining pressure

How dilatational behaviour and high peak friction angles at low stresses are gradually suppressed by higher and higher stresses is an interesting aspect of the dilatancy characteristics study of cemented sands. Portaway sand specimens were prepared at constant dry unit weight of 17.4 kN/m^3 . The dry unit weight was kept the same for uncemented and cemented sand specimens. The specimens were isotropically compressed and sheared at confining pressures ranging from 50 kPa to 20 MPa. The effect of confining pressure was investigated on the dilatational behaviour of the material as shown in Figure 6.6. From the figure, it can be seen that for the cement content range from 0% to 15%, at low stresses there is more dilation in the materials during shear. The dilatational behaviour is gradually being suppressed by the in-

crease in confining pressure. At high confining pressures, the materials show compression characteristics such as that of the behaviour of loose sand. From these experimental results, it is obvious that at high pressures the effect of dilation is diminishing. It can be presumed that the application of confining pressure causes both the propagation of micro cracks and the opening of voids within cemented sand to be suppressed, and so as the confining pressure increases, the dilatant deformation reduces. It is to be noted that at 20 MPa of confining pressure, the high-pressure triaxial cell reached to its maximum load cell capacity prior to reaching the terminal axial strain. Because of the reason there can be seen a constant volume change at the later part of the volumetric curve of 20 MPa confining pressure.

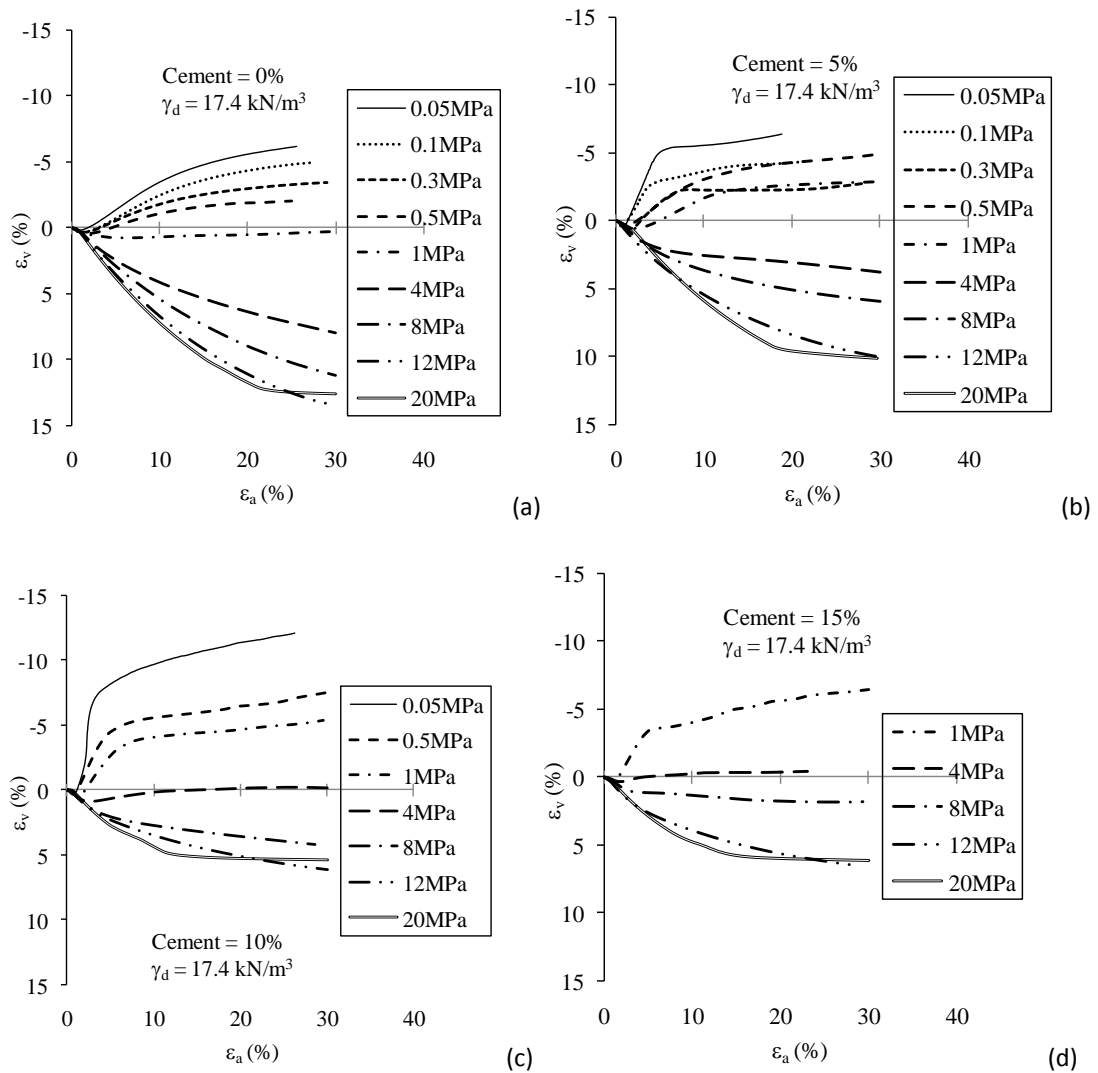


Figure 6.6 Suppression of the dilatancy by the gradual increase in confining pressure for the specimens with cement contents of: (a) 0%; (b) 5%; (c) 10%; and (d) 5%.

6.5 Dilation angle

The angle of dilation controls an amount of plastic volumetric strain developed during plastic shearing and is assumed constant during plastic yielding. The value of zero dilatancy angles corresponds to the volume preserving deformation while in shear. The peak friction angle of sand depends on its critical-state friction angle and on dilatancy.

The data points of dilatancy angle (ψ') determined from the rate of dilatancy ($\delta\varepsilon_v/\delta\varepsilon_q$) given by Eq. (6.1) are plotted versus the effective confining pressures for different cement contents are shown in Figure 6.7. The figure suggests that the peak dilation angle for cemented sand is significantly high at low confining pressures; however, by the progressive increase in the confining pressures, there is gradual decrease in the dilatancy and the dilation angle approaches to the negative values at high pressures.

$$\tan\psi' = -\left(\frac{\delta\varepsilon_v}{\delta\varepsilon_q}\right) \quad (6.1)$$

To develop an empirical relationship between the angles of shearing and dilation, triaxial compression test data with cement contents of 5%, 10%, and 15% is plotted between ψ_p vs. $(\phi_p - \phi_{cr})$ with trend lines were passed through the origin as shown in Figure 6.8. The slope of the lines range from 0.4 to 0.5 approximately, and therefore, the empirical relationship could be developed as given in Eq. (6.2).

$$\phi'_p - \phi'_{cr} = (0.4 \text{ to } 0.5)\psi_p \quad (6.2)$$

For triaxial compression of sand, Bolton (1986) established the relationship given in Eq. (6.3), which is re-reported by Chakraborty and Salgado (2010). The comparison of Eq. (6.2) and (6.3) suggests that there is close approximation to the empirical relations.

Triaxial compression:
$$\phi'_p - \phi'_{cr} = 0.5\psi_p \quad (6.3)$$

However, it has been difficult to acquire the true critical state for cemented sand during consolidated drained compression tests. The problems in identifying the critical state for cemented sand will be discussed in the next chapters.

The estimation of the dilatancy angle and general trend of its suppression by the gradual increase in confining pressures using Eq. (6.3) are plotted as shown in Figure 6.9 and Figure 6.10. There can be noticed that at low confining pressure, the dilation angles of cemented sand are much higher than the empirical or theoretical values suggested by the previous literature and guidelines of numerical analysis computer codes. However, at high pressures, the dilation angles are being suppressed. As the effect of dilation is significantly suppressed at high pressures, therefore the incorporation of dilatancy factor working at high pressures may not be of high consequences.

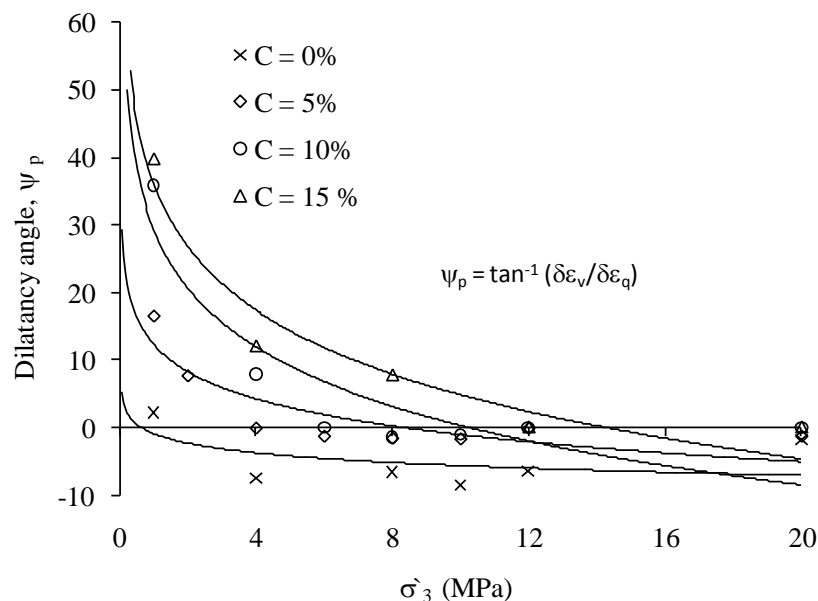


Figure 6.7 Effect of confining pressure on peak dilatancy angle derived from the rate of dilatancy.

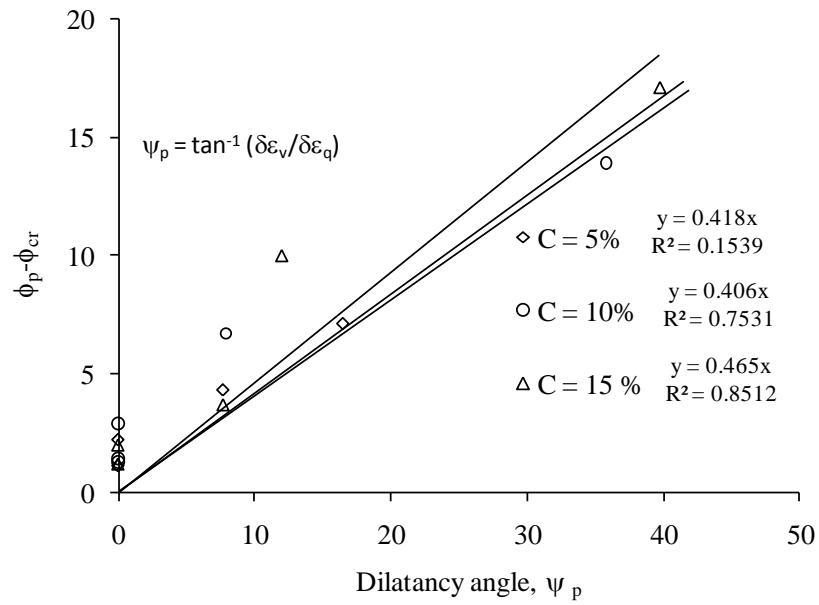


Figure 6.8 Angles of shearing resistance and dilatancy in triaxial compression for different cement contents

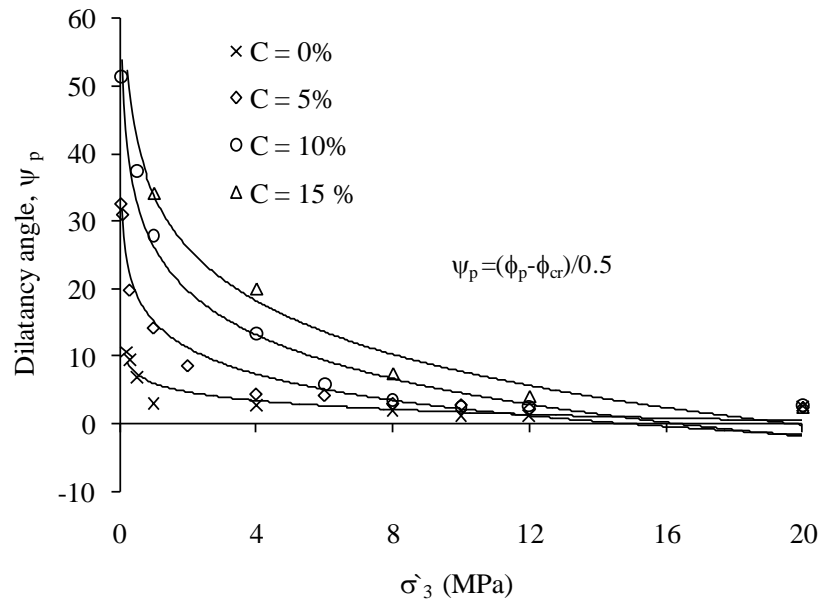


Figure 6.9 Effect of confining pressure on peak dilatancy angle derived from peak frictional and critical state/ultimate state angle.

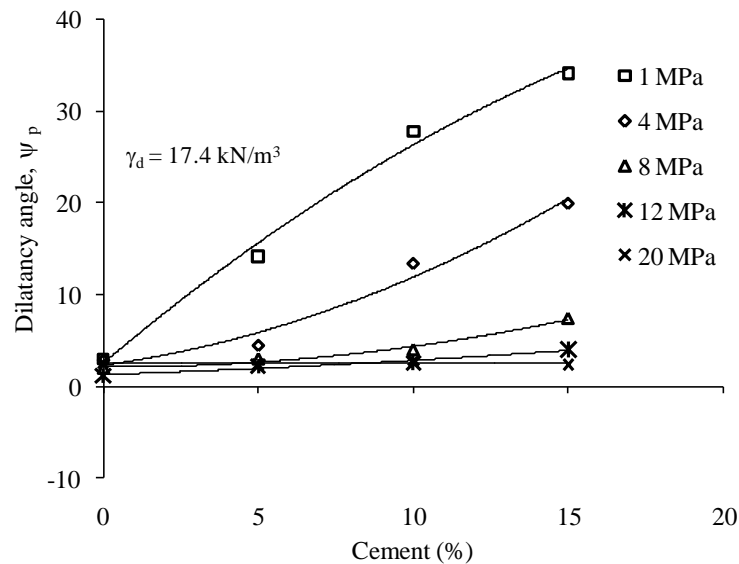


Figure 6.10 Effect of cement content on maximum dilatancy angle.

6.6 Stress-dilatancy relation

When a sand body is sheared, an increase in volume (dilation) ensues due to the geometrical constraints imposed by the fabric against applied stresses. This important phenomenon, coined as stress-dilatancy. The incorporation of cohesion component into the stress-dilatancy relationship enhances the capability of any soil model capturing the bonding effect on the stress-strain behaviour of cemented materials. Addition of cement into the granular materials develops inter-particle bonding (see Figure 6.11) and incorporates the cohesion component (see Figure 6.12). Consideration of the contribution of cohesion to plastic flow allows the modelling of delayed dilatancy and softening—contraction behaviour, which are two interesting phenomena observed in bonded geomaterials (Yu *et al.* 2007). Triaxial compression tests on artificially cemented sand carried out by Maccarini (1987) and Schnaid *et al.* (2001) confirmed that the dilation of artificially cemented sand is also inhibited by inter-particle bonding.

The stress-dilatancy relationships of Portaway sand are plotted in Figure 6.13. For the sake of clarity, only selected results are shown to illustrate typical behaviour at high pressures. Figure 6.13 shows that most specimens sheared at high pressures displayed a compressive behaviour with the rate of compression reducing to reach zero at ultimate state indicated by the vertical axis. Some specimens with cement contents of 10% and 15% also exhibited dilative behaviour. Figure 6.13 (a) shows plots of stress-dilatancy behaviour for specimens with different cement content sheared at confining pressures σ'_3 of 4 MPa, 8 MPa, and 12 MPa, respectively. For specimens with the same cement content sheared at different σ'_3 , the plot is generally shifted to the left as the effective confining stress increases (Figure 6.13(a)). This means that the effect of confining pressure is to reduce or prevent dilatancy at a given stress.

Figure 6.13(b) presents plots of stress-dilatancy relationships for specimens with cement contents of 5%, 10%, and 15% respectively sheared at different confining pressures. It can be seen from Figure 6.13(b) that for specimens sheared at the same effective confining stress, the effect of cement content is to move the plot of q/p' versus $(-d\varepsilon_v/d\varepsilon_q)$ upward. As a result, the stress-ratios at the peak and ultimate states increase with increasing cement content. This means that the effect of cement content, which introduces the component of cohesion into the stress-dilatancy relationship, is to increase bonding between particles at a given stress.

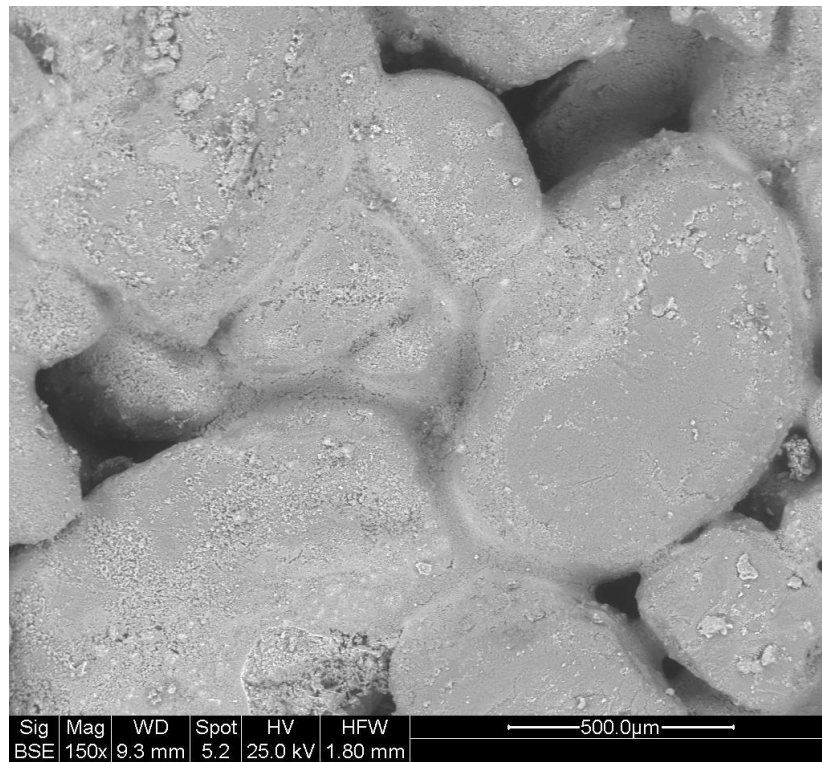


Figure 6.11 Inter-particle bonding due to cement content.

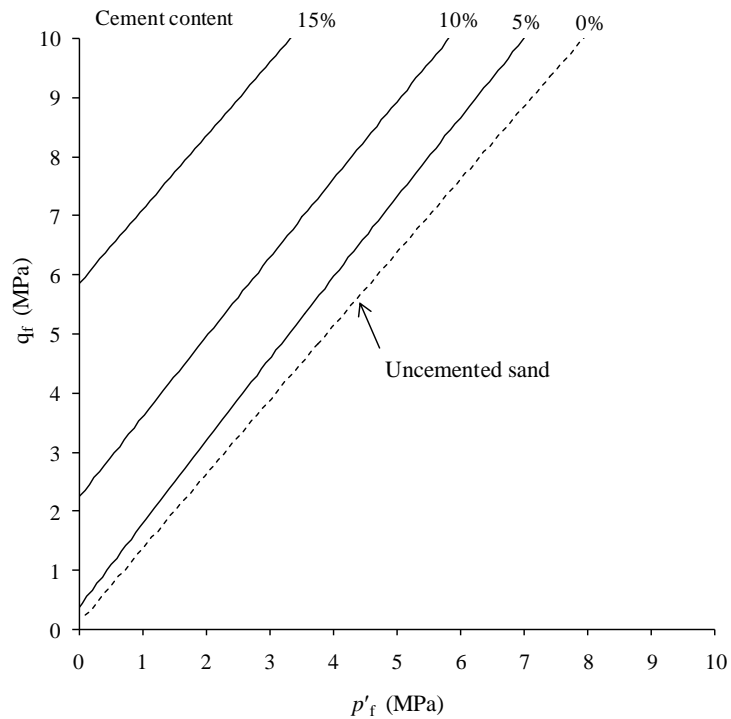


Figure 6.12 Incorporation of cohesion component due to cement content.

The patterns illustrated in Figure 6.13 are somewhat consistent with experimental data reported by Schnaid *et al.* (2001) and the computed behaviour using CSSM model (Yu 1998) reported by Yu *et al.* (2007) at low confining pressures. However, differences in stress-dilatancy behaviours at high pressures are much smaller compared to low pressures. This again shows that effect of cement content is diminished when specimens are sheared at high confining pressures.

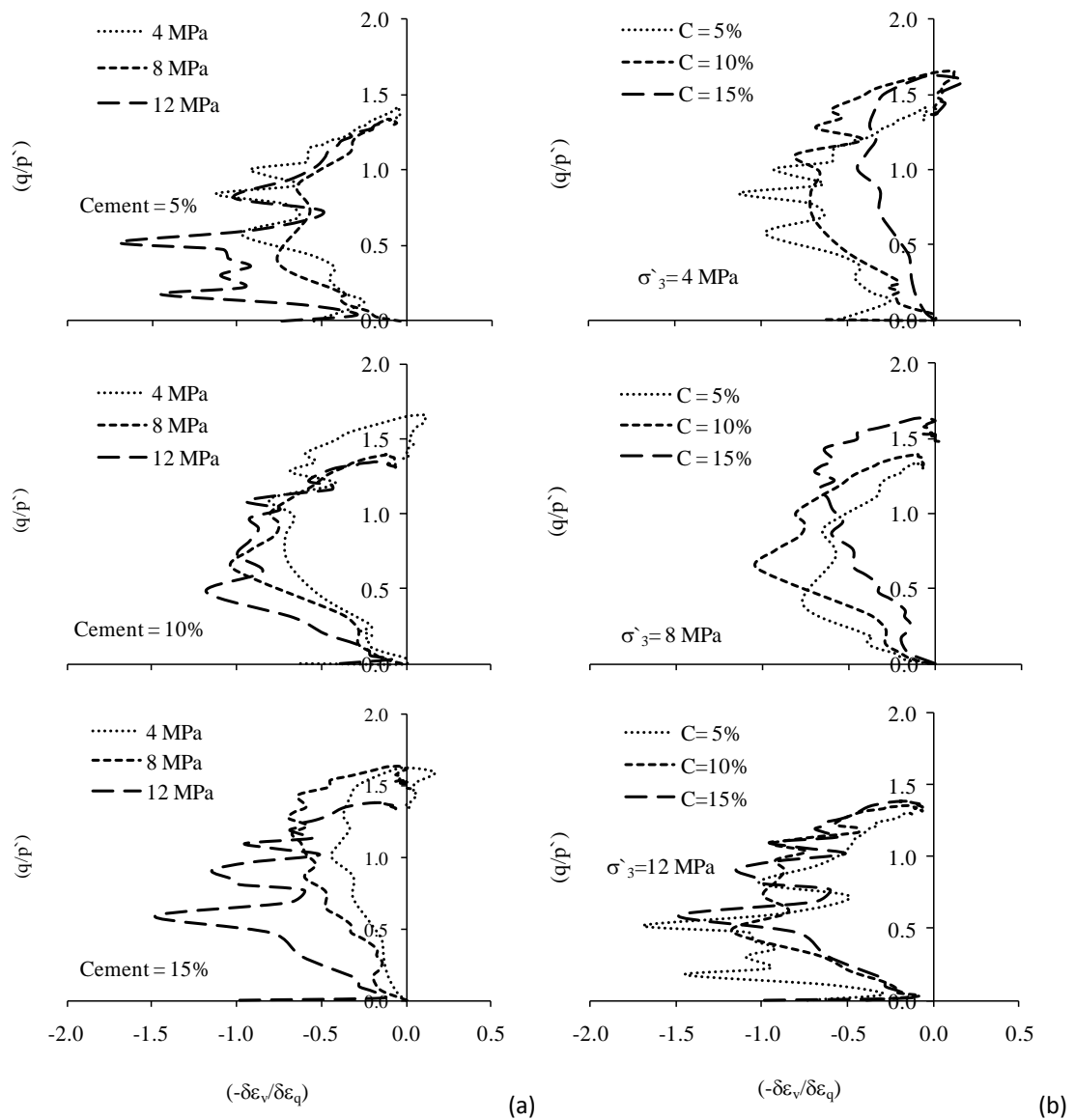


Figure 6.13 The stress-dilatancy relationships of Portaway sand: (a) effect of confining pressure; (b) effect of cement content.

6.7 Idealization of dilatancy phenomenon

The reliance of dilatancy phenomenon on cement content, confining pressure and initial relative density is further explored on the bases of laboratory experimental data. In particular, the onset of dilation is focussed. From Figure 6.14(a), it can be seen that the dilatancy commencement and rate are dependent on the magnitude of applied confining pressure and cement contents. By the increase in confining pressure, the onset of dilatancy is being delayed and hence more elastic contraction is being experienced. On the other hand, cement content is prompting early onset of dilation. Moreover, the rate of dilatancy is increasing with increasing cement content and reducing with increasing confining pressure. Figure 6.14 (b) shows the stress-strain and volumetric change behaviour of uncemented sand and cemented sand with respect to initial relative density. For the dense uncemented and dense cemented sand specimens with relative density $D_r \geq 80\%$ during consolidated drained shearing at 1MPa of effective confining pressure, from the comparison it can be seen that the cemented material showing significant dilation and on the other hand uncemented material is showing compression. The loose cemented sample with relative density $D_r = 44\%$ showing dilation during shear. This dilation behaviour can be attributed to cement content effects only.

From Figure 6.14 (c), it can be revealed that the commencement, rate, and post-peak dilatancy are cement content, density and stress dependent. The volumetric dilation commences after the sample passes over the initial elastic limit (also known to be the yield point) and the rate of dilation increases immediate after bond breakage.

Based on the experimental results and review of the literature an idealized deformation curve illustrating the phenomenon of dilatancy is shown in Figure 6.15. Although such a simplification is a close approximation to actual data; nevertheless, it gives an idea of underlying mechanism of the dilatancy. Irrespective of the initial density, cement content, and confining pressure, it has been observed that there is volumetric compression at the start of shearing. However, the subsequent pre-peak onset of dilation, increased rate of dilation and post peak dilation are reliant. Following an initial period of elastic contraction, the volumetric response tends to become dilatant as the material enters to an inelastic stage, which can be characterised by the development and coalescence of micro-structural damage. The micro-structural damages can be seen from the SEM photographs after shearing process of the bonded materials as shown in Figure 6.16.

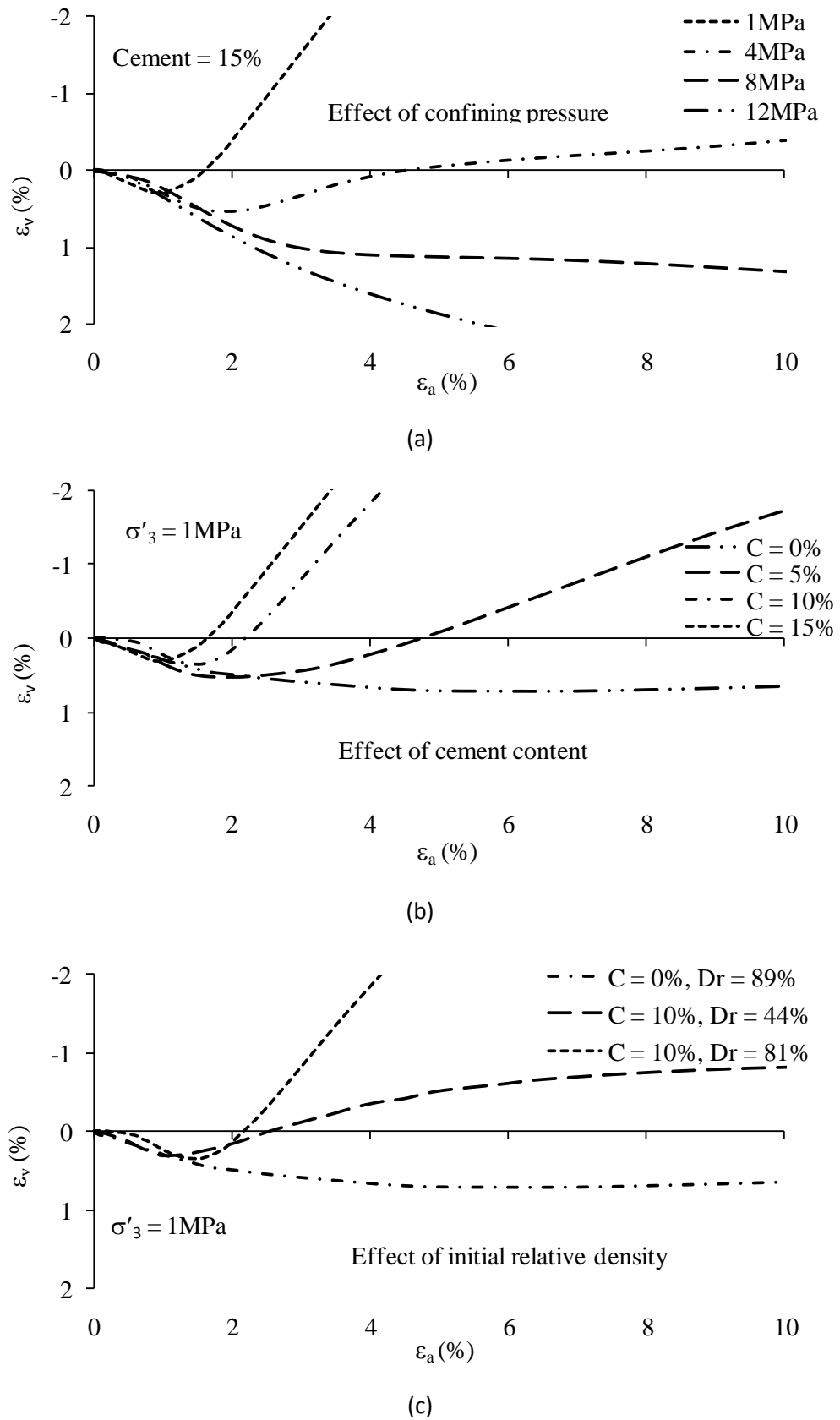


Figure 6.14 Typical results demonstrating how the onset of dilation is affected by: (a) confining pressure; (b) cement content; and (c) initial relative density.

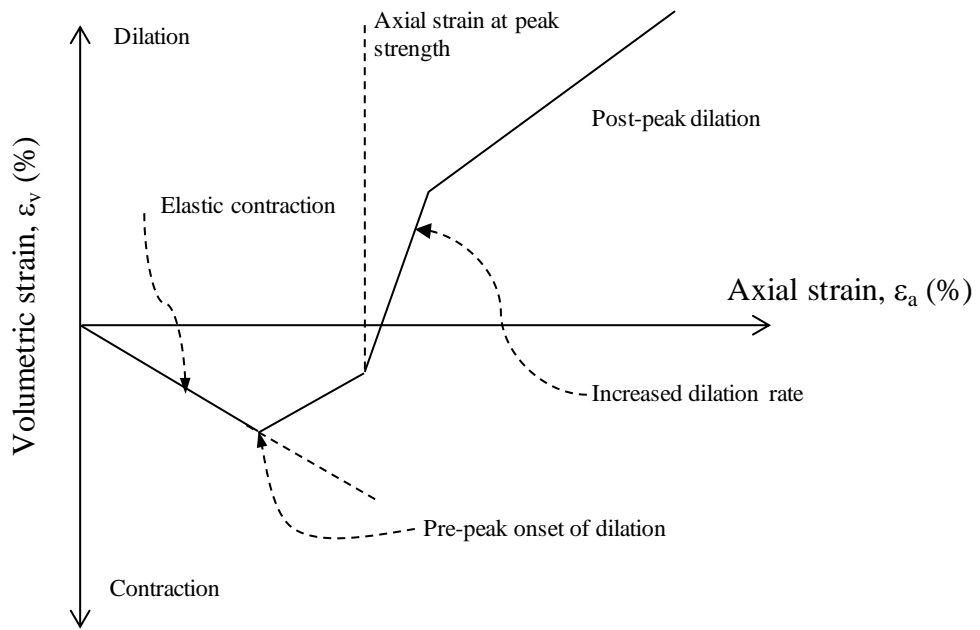


Figure 6.15 Illustration of dilatancy from multi-linear idealized deformation curve.

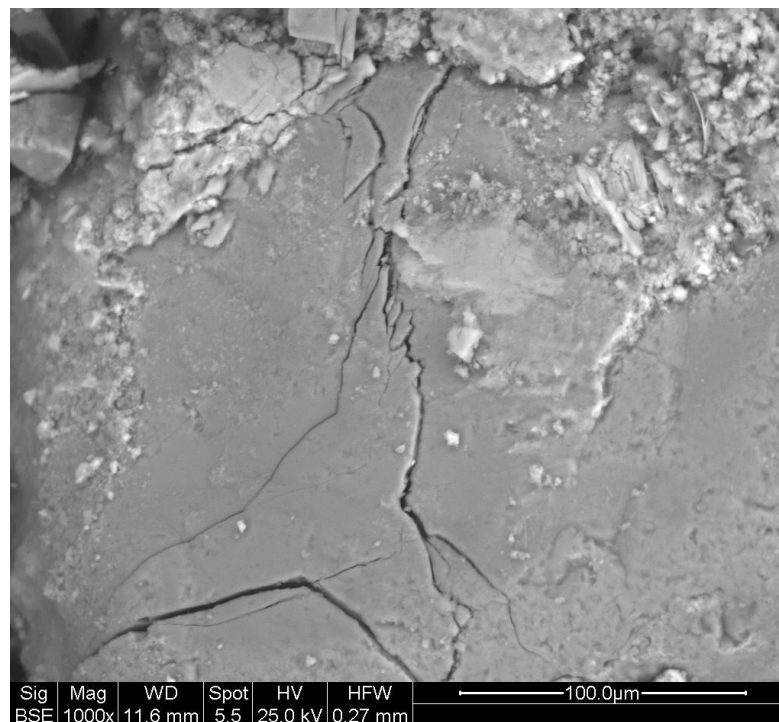


Figure 6.16 Development and coalescence of micro-structural damage during triaxial compression of cemented sand.

6.8 Summary

Triaxial drained compression tests were run on uncemented and cemented sands with different initial relative density and wide range of cement contents. The mechanism of dilatancy, its significance and dependence on density, cement content and confining pressures were investigated.

Based on experimental results carried out in the laboratory, an idealised pressure-sensitive dilatancy has been examined to describe the dilatant deformation commonly observed during the brittle failure of dense cemented sand. The dependence of dilatancy and friction angle on relative density and confining stress were investigated. The concept is summarised in the following points:

- 1) Regardless of the magnitude of the confining pressure and cement contents, there exists an initial phase of linear contraction for the cemented sand. Following an initial period of elastic contraction, the volumetric response tends to become dilatant as the material enters an inelastic stage that is characterised by the development and coalescence of micro-structural damage. Volumetric dilation becomes more pronounced with increasing cement content. This response, as expected, is suppressed by high confining pressure. The higher the confining stress, the less the degree of dilatancy occurs in the inelastic regime.
- 2) The application of confining pressure presumably causes both the propagation of micro cracks and the opening of voids within cemented sand to be suppressed, and so as the confining pressure increases, the dilatant deformation reduces.

- 3) The commencement (point of initiation of dilatancy), rate (slope of stress-dilatancy curve), and post-peak dilatancy are cement content, density and stress dependent. The volumetric dilation commences after the sample passes over the initial elastic limit also called the yield point and the rate of dilation increases immediately after bond breakage.
- 4) As the effect of dilation is significantly suppressed at high pressures; therefore, the incorporation of dilatancy factor when working at high pressures may not be of high implications.

GENERAL CEMENTED SAND BEHAVIOUR AT HIGH PRESSURES

7.1 Introduction

Many researchers have reported the cement bond breakage and particle crushing at high pressures. For instance, Lo et al. (2003) indicated the occurrence of progressive bond breakage prior to failure. However, there is not enough information about the micromechanical behaviour of cemented sand during consolidated drained and undrained shearing. The discussion in previous chapters has focussed on the experimental results, and their interpretation within the context of the individual topics of each chapter. The present chapter attempts to examine the macro and micro-mechanics of yielding, pre-failure deformation and critical state behaviour of cemented sand. Summary of the test results with corresponding parameters are shown in Table 7.1, Table 7.2, and Table 7.3.

7.2 Yielding characteristics of cemented sand

Modelling the behaviour of soil, rock, or concrete under general stress conditions requires the assumption of a yield and failure surface in principal stress space. Yielding and normalized failure conditions are the two key elements that are used in most constitutive models developed for frictional materials. The yield surface is usually convex and the state of stress inside the yield surface is elastic. When the stress state lies on the surface, the material is said to have reached its yield point and the material is said to have become plastic. Further deformation of the material causes

the stress state to remain on the yield surface, even though the surface itself may change shape and size as the plastic deformation evolves. The effect of cementation and confining pressure on the shape and size of the yield surface is quite significant at conventional pressures. In this study, the effect of cementation on the yield surface has been elaborated to the high confining pressures.

7.2.1 Location of yield point

Classically, the term yielding refers to the transition from elastic to plastic behaviour, and is associated with sharp curvature developing in $e-\ln(p')$ during isotropic compression and stress-strain curve during triaxial shear (Kuwano and Jardine 2007). At the other end of the spectrum, it can be argued that the ultimate yielding of sands under all round compression is delayed until the far later stage when particle breakage becomes dominant (Coop and Lee 1993). Wang and Leung (2008) simply determined the yield point as the starting point of the transition from a stiff to a less-stiff response.

As reported in chapter 2, cementation complicates the yield point of soil and therefore, the well-defined yield stress can be tried from the compression lines using different methods. Difficulties in determining the yield point have also been reported by other authors, for example, Kavvas *et al.* (1993) for the Corinth marl, Barksdale and Blight (1997) for residual soils, Cecconi *et al.* (1998) for soft rocks and Rotta *et al.* (2003) for silty sand. This has often been explained as a result of a gradual onset of the breakage of the cement bonds.

Table 7.1 Summary of isotropic compression tests (yield parameters).

Test	σ'_3 (MPa)	C (%)	γ_d (kN/m ³)	D_r (%)	e_0	e_c	p'_y (MPa)
IC-0C20M	20	0	17.4	90	0.493	0.383	0.4
IC-5C20M	20	5	17.6	90	0.493	0.394	0.8
IC-10C20M	20	10	17.7	90	0.493	0.444	1.9
IC-15C20M	20	15	17.9	90	0.493	0.459	4.7

Table 7.2 Summary of isotropically consolidated drained compression tests (elastic parameters).

Test	σ'_3 (MPa)	C (%)	e_0	q_v (kPa)	p'_y (kPa)	E (MPa)	ν	G (MPa)	K (MPa)
CD-0C1M	1	0	0.50	350	1099	89	0.36	33	106
CD-0C4M	4	0	0.50	2556	4470	289	0.34	108	306
CD-0C8M	8	0	0.49	3083	8349	390	0.32	147	366
CD-0C10M	10	0	0.49	3884	10509	478	0.32	181	453
CD-0C12M	12	0	0.49	4525	12519	564	0.31	215	506
CD-0C20M	20	0	0.49	5906	20881	672	0.30	259	558
CD-5C1M	1	5	0.51	1066	1418	143	0.37	52	188
CD-5C2M	2	5	0.51	1872	2467	287	0.36	105	351
CD-5C4M	4	5	0.51	3037	5084	393	0.35	145	442
CD-5C6M	6	5	0.51	3797	7019	527	0.33	197	530
CD-5C8M	8	5	0.51	4576	9372	540	0.33	204	515
CD-5C10M	10	5	0.51	5062	11022	624	0.32	236	588
CD-5C12M	12	5	0.51	5485	13142	694	0.32	263	648
CD-5C20M	20	5	0.51	6961	21308	839	0.30	322	712
CD-10C1M	1	10	0.52	2074	1470	297	0.40	106	487
CD-10C4M	4	10	0.52	4230	5916	555	0.36	203	684
CD-10C6M	6	10	0.52	4597	7871	638	0.37	233	811
CD-10C8M	8	10	0.52	5589	10091	673	0.36	248	776
CD-10C10M	10	10	0.52	6129	11656	810	0.35	301	877
CD-10C12M	12	10	0.52	6574	13791	942	0.33	354	921
CD-10C20M	20	10	0.52	8028	22530	1058	0.32	402	959
CD-15C1M	1	15	0.54	3528	1909	449	0.41	159	822
CD-15C4M	4	15	0.53	5296	6564	661	0.39	238	997
CD-15C8M	8	15	0.53	7586	11056	905	0.36	333	1062
CD-15C10M	10	15	0.54	7617		1017	0.35	376	1139
CD-15C12M	12	15	0.53	8408	14801	1123	0.34	417	1203
CD-15C20M	20	15	0.53	9586	23449	1265	0.33	475	1258

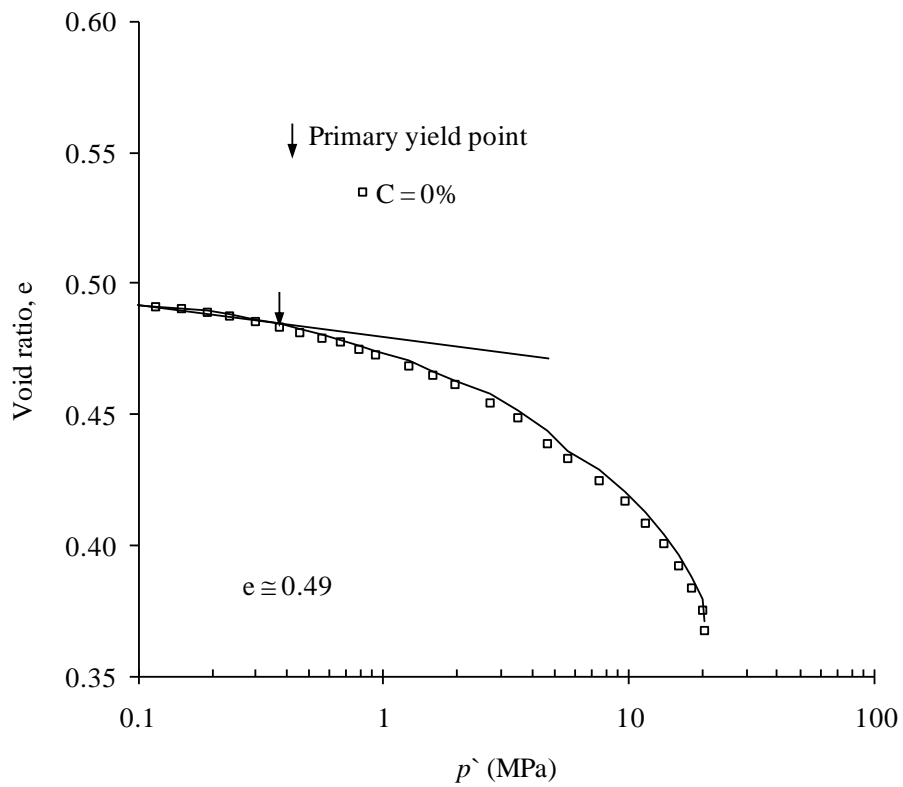


Figure 7.1 The primary yield point during isotropic compression of Portaway sand.

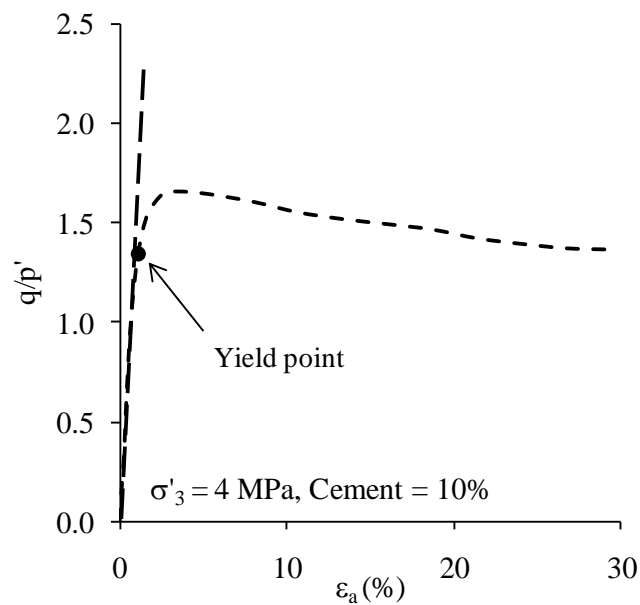


Figure 7.2 Location of the primary yield point in the stress-strain curve.

Following the Wang and Leung (2008) procedure, the primary yield is taken as the point at which breakage of the cement bonds commences and was considered to be

a state where the $e-\ln(p')$ and stress-strain curves deviates from the initial linear behaviour during isotropic compression (see Figure 7.1) and triaxial shearing (see Figure 7.2) respectively. This is also consistent with that used in other works (e.g. Cucovillo and Coop, 1997 and Rotta *et al.* 2003).

7.2.2 Yield stress during isotropic compression

The yield point during isotropic compression can be added to yield points for other stress paths to create a yield locus. The size and shape of this will depend on both the degree of cementing and the density during cementing. Below the yield locus, the behaviour is generally elastic, provided there has been no damage to the cementing. The summary of yield stress parameters during isotropic compression are given in Table 7.1. The effect of cement content on yielding during isotropic compression is shown in Figure 7.3, where it appears that the yield stress increases with increasing cement content. The cemented specimens are initially stiffer than the uncemented sand specimen, then becoming gradually softer as the isotropic stress increases.

For the relationship between cement content and corresponding isotropic yield stress ($p'y$), as shown in Figure 7.4, it appears that the $p'y$ increases exponentially with the increase in cement content. These results are consistent with that of cemented treated soft Bangkok clay (Bergado *et al.* 2006) and cement treated dredged materials (Chiu *et al.* 2009), which can be attributed to the increasing amount of cement content that consequently increases the amount of solid content per unit volume.

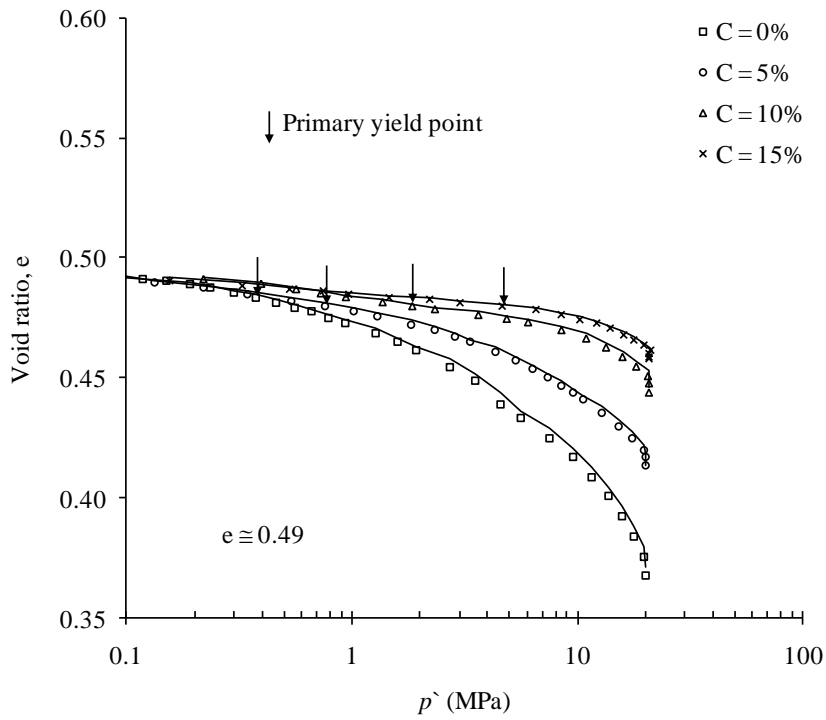


Figure 7.3 Effect of cement content on the primary yield point of cement treated Portaway sand during isotropic compression.

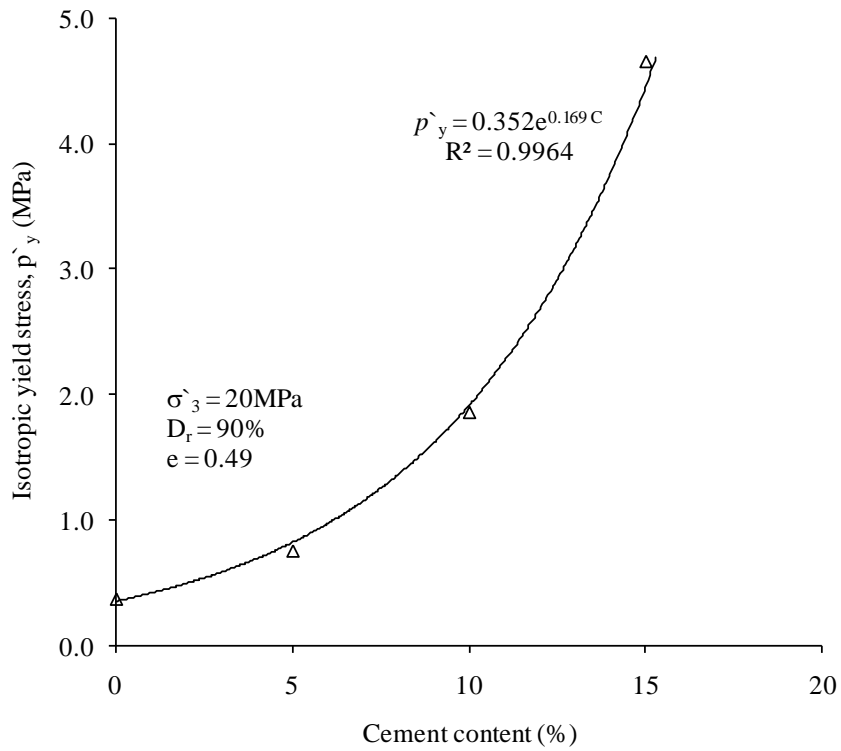


Figure 7.4 Effect of cement content on the primary yield point of cement treated Portaway sand during isotropic compression.

7.2.3 Yield stress during triaxial shearing

The stress-strain curve is plotted on normalized stress ratio versus axial strain. The yield point is located at starting point of the transition from a stiff to a less-stiff response (i.e. deviation from linearity). The yield points for cemented sand at various confining pressures are located as shown in Figure 7.5, where it can be seen that by the increase in cement content, there is increase in the normalized primary yield stress and the position of the yield point is marginally shifting towards left. On the other hand, by the increase in confining pressure there is decrease in the normalized primary yield stress. For instance the highest yield point is located around 2.25 of stress ratio at 1 MPa (Figure 7.5 (a)), and gradually decreasing to around 1.0 at 12 MPa (Figure 7.5 (d)).

The effect of cement content on the primary yield stress of Portaway sand at different effective confining pressures is shown in Figure 7.6. From the figure, it can be seen that irrespective of confining pressures there is increase in the yield stress by the increase in cement content.

The effect of confining pressures on the primary yield stress of Portaway sand at different cement contents is shown in Figure 7.7. The results show that the confining pressure has a significant effect on the yield strength q_y , during triaxial compression. The relationship between the yield stress q_y vs. effective confining pressure σ'_3 follows a curve pattern with convex shape and the yield curves expand with increasing cement. Moreover, the primary yield loci observed to be expanding with the in-

crease in the cement content as shown in Figure 7.8. Cementation appeared to have enlarged the elastic domain in the specimens.

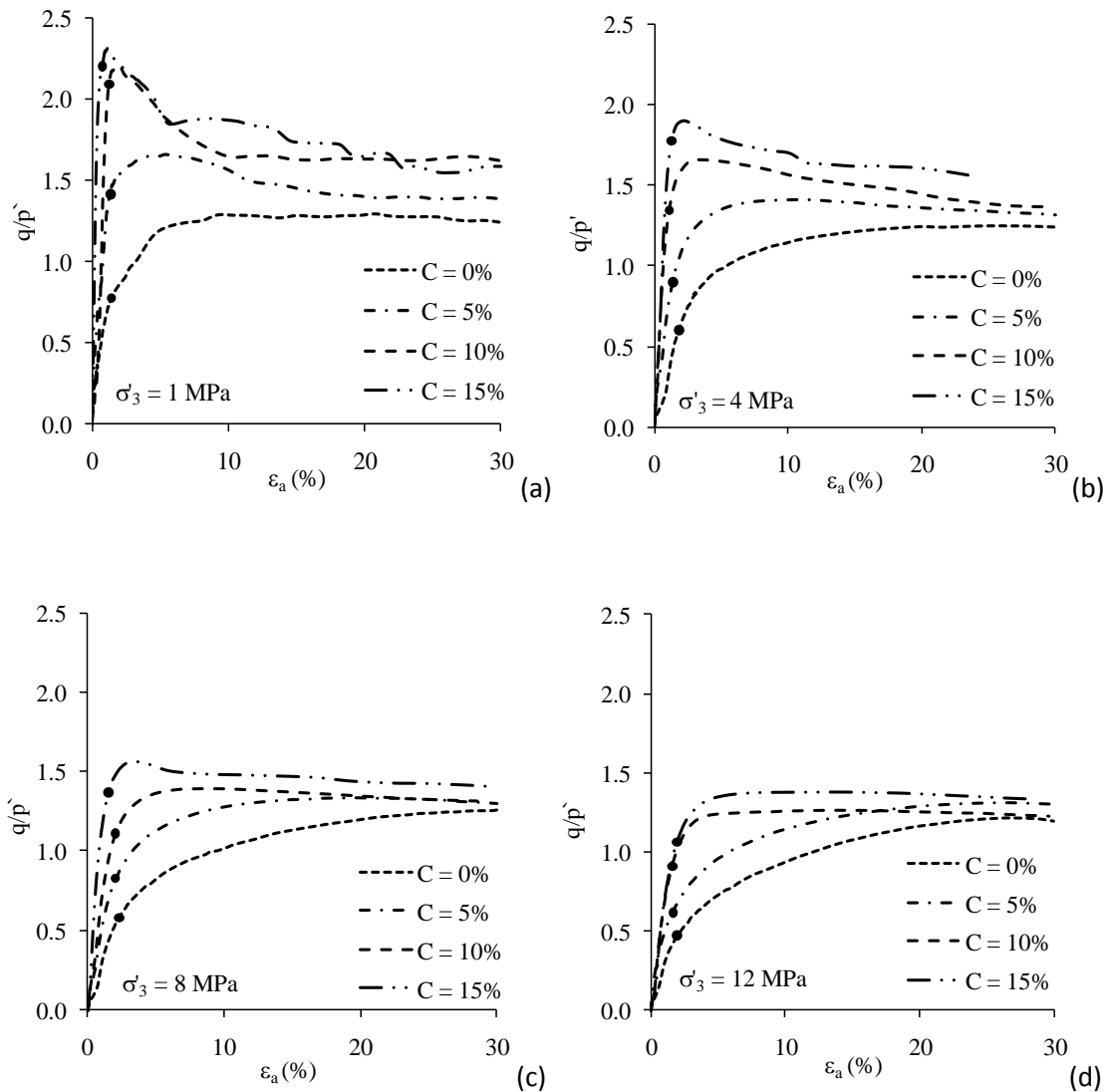


Figure 7.5 Effect of cement content and confining pressure on the location of primary yield point at the effective confining pressures of: (a) 1MPa; (b) 4MPa; (c) 8MPa; and (d) 12MPa.

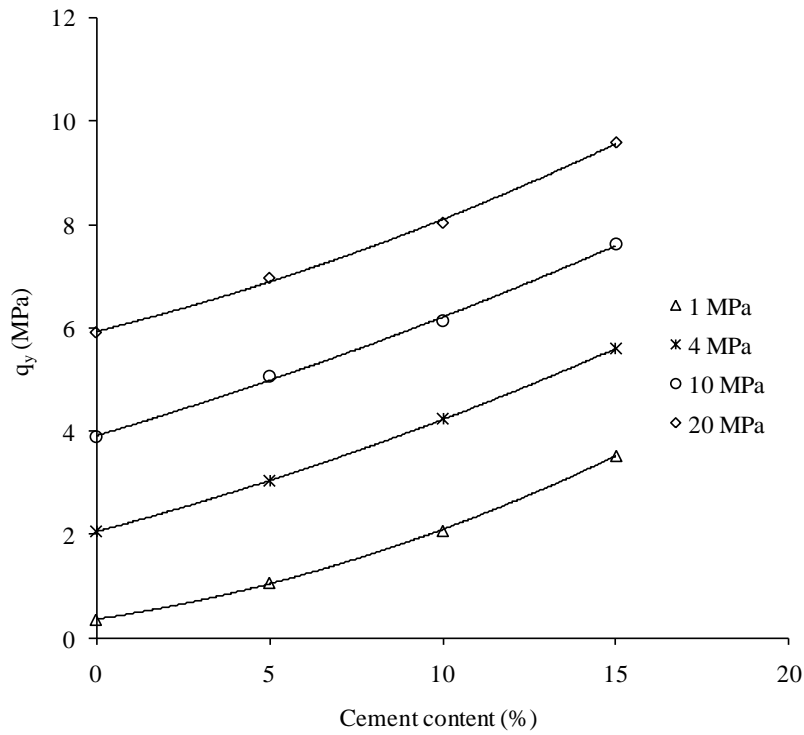


Figure 7.6 Effect of cement content on primary yield stress at different confining pressures.

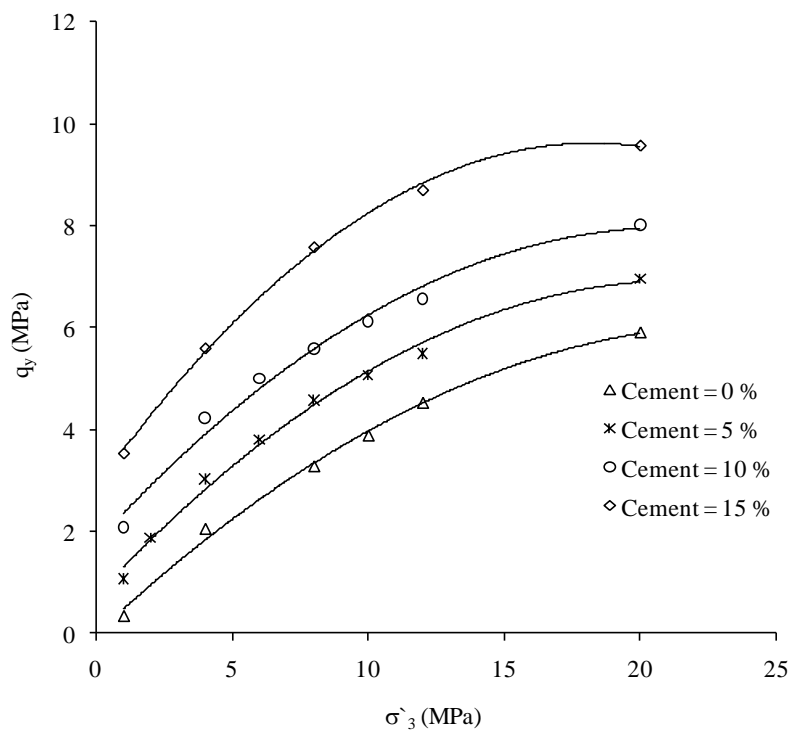


Figure 7.7 Effect of confining pressure on the primary yield stress at different cement contents.

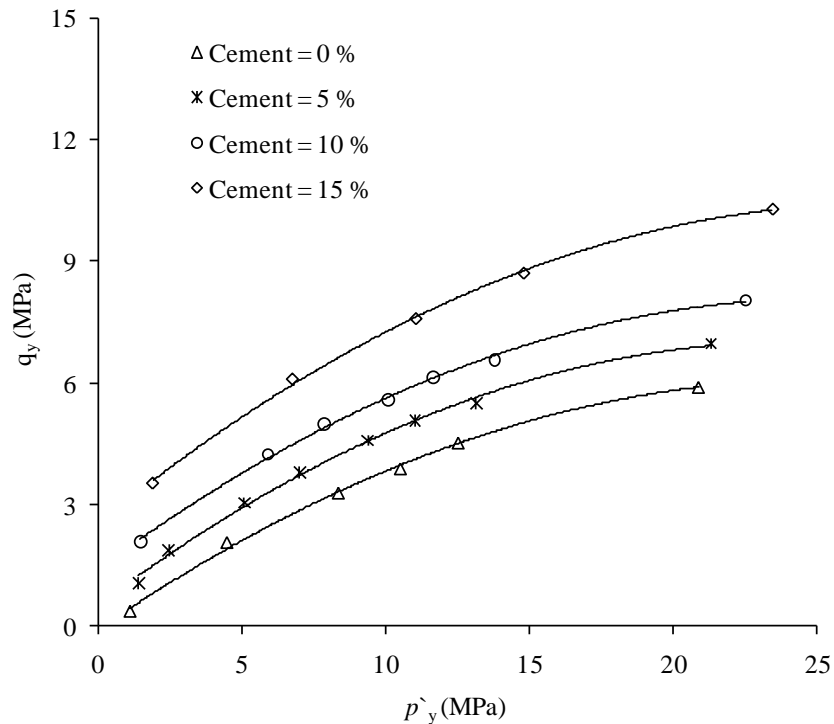


Figure 7.8 Effect of cement contents on the yield locus of Portaway sand at high pressures.

7.3 Deformation characteristics

Deformation is the phenomenon in which a material undergoes changes in dimensions in response to mechanical forces. The deformation is said to be elastic if the material returns to its original size and shape upon removal of the applied load. On the other hand, it refers to as inelastic deformation if the application of the mechanical load results in a permanent change in the dimensions of the material, i.e., it does not return to its original size and shape even if the mechanical load is no longer being applied to it. Another difference between elastic and plastic deformation is in how they change the shape and volume of a specimen. A specimen that's under elastic deformation will change more in volume than its shape, since only the separation distance between particles change, while retaining the particles' nearest neighbours. A specimen that is under plastic deformation, however, will change more in shape

than in volume, since this type of deformation does not alter the bond lengths, but results in slip processes within its microstructure.

The deformation properties of elastic materials are described most often by Young's modulus (E) and Poisson's ratio (ν). They are used commonly in a generic sense with inelastic materials. These properties are obtained most often from the results of tri-axial compression tests. The modulus is the ratio of stress to strain and is obtained from the slope of deviator stress-axial strain curves. The deformation moduli vary with confining pressure, and therefore, are described as being non-linear and stress dependent. Modulus of elasticity and shear modulus are used as deformation indicators. Moduli obtained from undrained conditions are known as undrained modulus (E_u) and that obtained from drained conditions is the drained modulus (E_d).

Two types of modulus can be defined for non-linear elastic curves, namely, tangent modulus and secant modulus. Tangent modulus is the slope of the stress-strain curve, which varies from point to point.

$$E_T = \frac{dq}{d\varepsilon_a} \quad (7.1)$$

Secant modulus is defined as the ratio of difference in deviatoric stress to the corresponding axial strain.

$$E_S = \frac{\Delta q}{\Delta\varepsilon_a} \quad (7.2)$$

Shear modulus (G) and bulk modulus (K) and constraint modulus (M) can be determined from the following equations.

$$G = \frac{E}{2(1 + \nu)} \quad (7.3)$$

$$K = \frac{E}{3(1 - 2\nu)} \quad (7.4)$$

$$M = \frac{E(1 - \nu)}{(1 + \nu)(1 - 2\nu)} \quad (7.5)$$

Poisson's ratio is defined as ratio of lateral strain ε_r to axial strain ε_a in triaxial compression tests. Poisson's ratio for soil is not constant but depends on stress and strain levels. Value of Poisson's ratio changes from 0.0-0.5. Poisson's ratio is deduced from the initial slope of the curve in the contraction domain.

$$\nu = \frac{\varepsilon_r}{\varepsilon_a} \quad (7.6)$$

7.3.1 Determination of elastic parameters

Measurement of elastic parameters is a fundamental problem in soil mechanics. Five independent elastic parameters are required to fully describe soil behaviour. The elastic/ deformation modulus of cemented sands is often not a well-known or easily measured parameter. However, it is possible to determine all of these parameters in triaxial testing conditions to a reasonable approximation. The elastic parameters of both cemented and uncemented soils were calculated using the initial portion of the stress-strain curves obtained from monotonic drained/undrained triaxial tests.

The elastic parameters, which are considered here as deformation moduli were examined for various cement contents over a wide range of confining pressures for a

laboratory, prepared cemented Portaway sand. Results of a series of tests on isotropically consolidated drained compression tests yielded values of modulus and Poisson's ratio that are consistent with published literature. The effect of cement content and confining pressure on the Poisson's ratio were investigated as shown in Figure 7.9. From the figure, it can be seen that by the increase in cement content the variation of Poisson's ratio is not significant, however, in general there is slight increase in Poisson's ratio that can be noticed by the increase in the cement content as shown in Figure 7.9(a). The effect of confining pressure on Poisson's is shown in Figure 7.9(b), where it can be seen that there is slight decrease in the Poisson's ratio of the material by the increase in the confining pressure. At large strain levels of approximately 0.8%, the value of the Poisson's ratio, for uncemented sands as well as for cemented sands, is between 0.30 and 0.40.

The elastic/deformation moduli of cemented sand are controlled by the properties and volume fraction of the matrix. Consolidated drained/undrained triaxial compression tests were carried to estimate the deformation modulus of cemented sand. Samples with different levels of cementation were created and tested at different consolidation pressures under isotropic conditions. Typical values of elastic parameters are summarized in Table 7.2. Variation of elastic moduli with different cement contents and confining pressures are shown in Figure 7.10. Examination of Figure 7.10 clearly demonstrates that increasing the cement content there is approximately linear increase in the elastic moduli, however, the effect of confining pressures reveal increase in the moduli in a convex shape envelope. These observations suggest that the level of cementation and confining pressures controls the deformation

moduli of the samples and the degradation of cementation is more likely to occur with increasing deviator stress than with increasing isotropic mean effective stress.

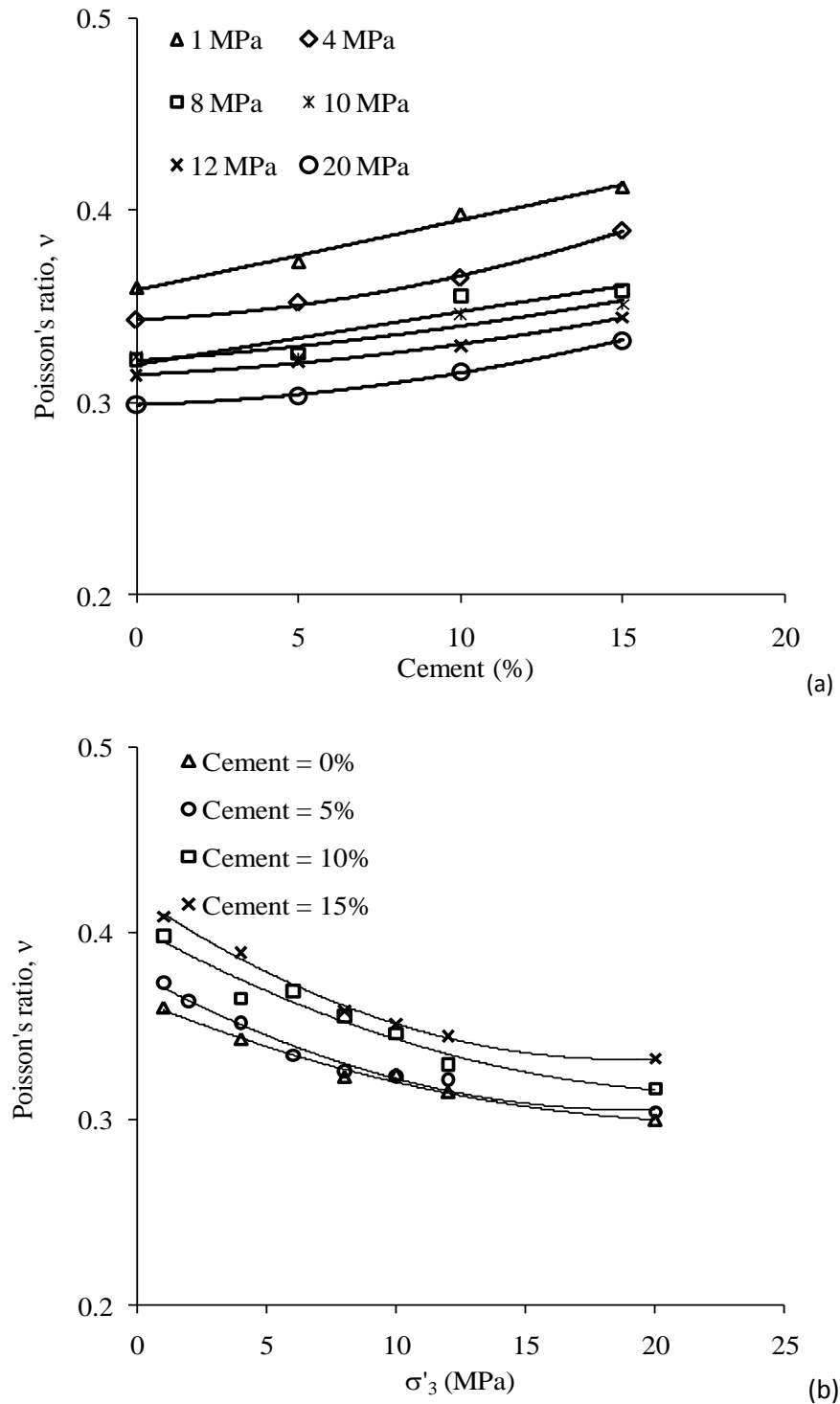
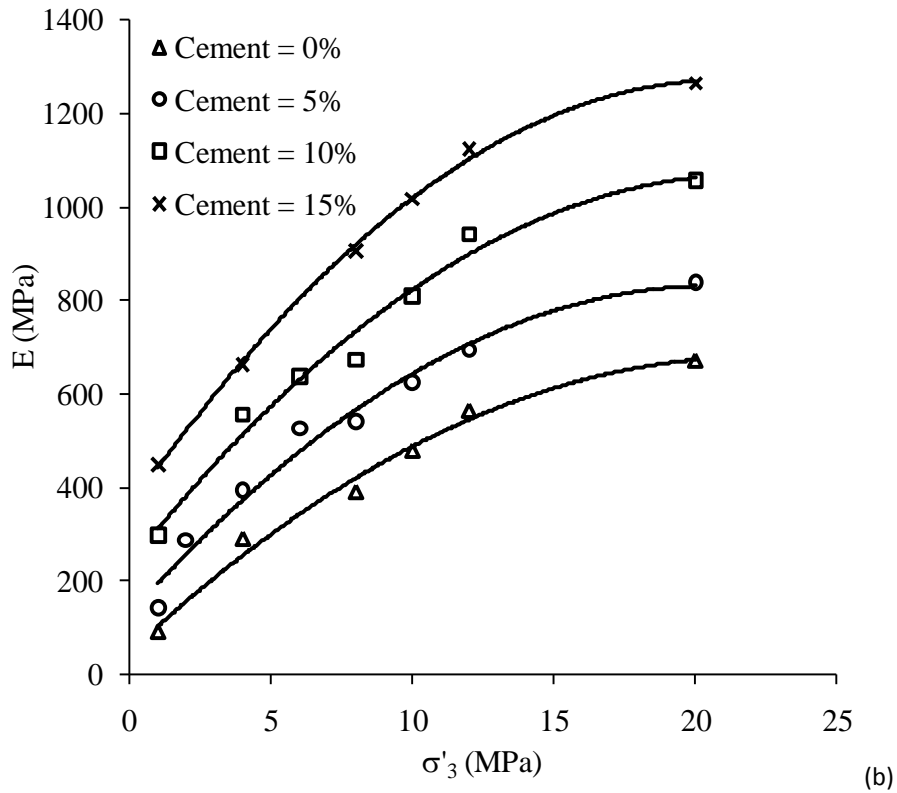
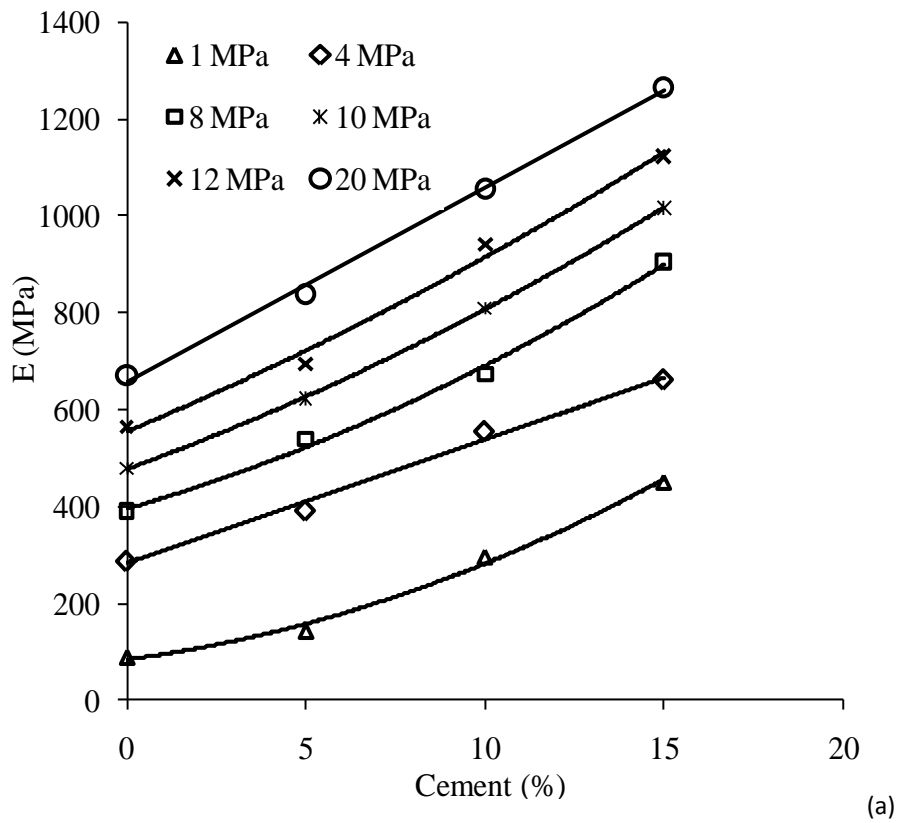
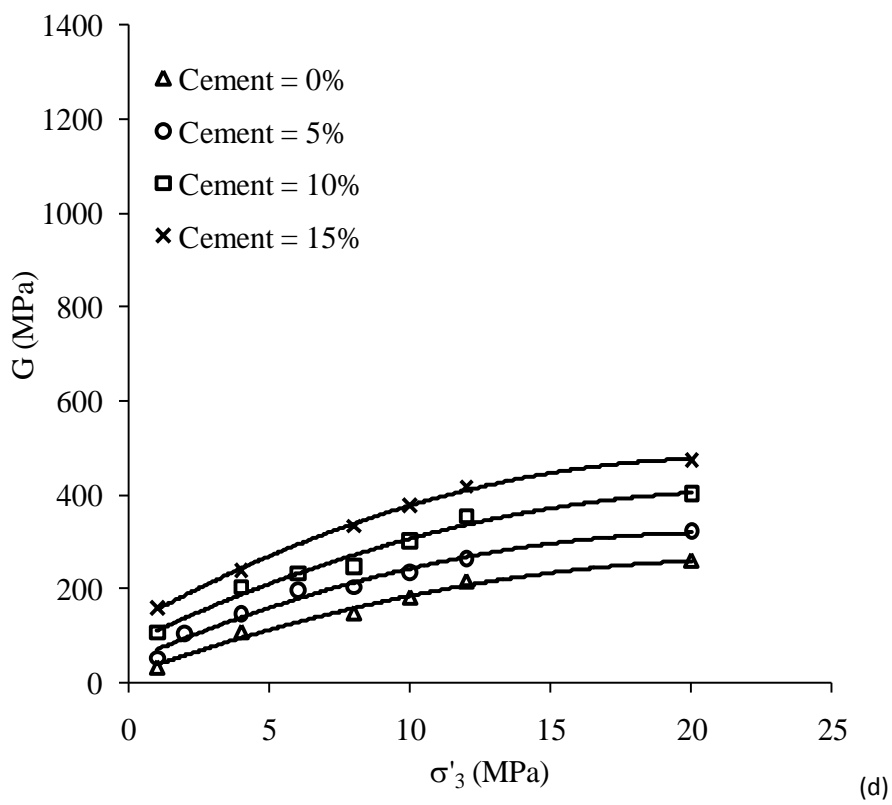
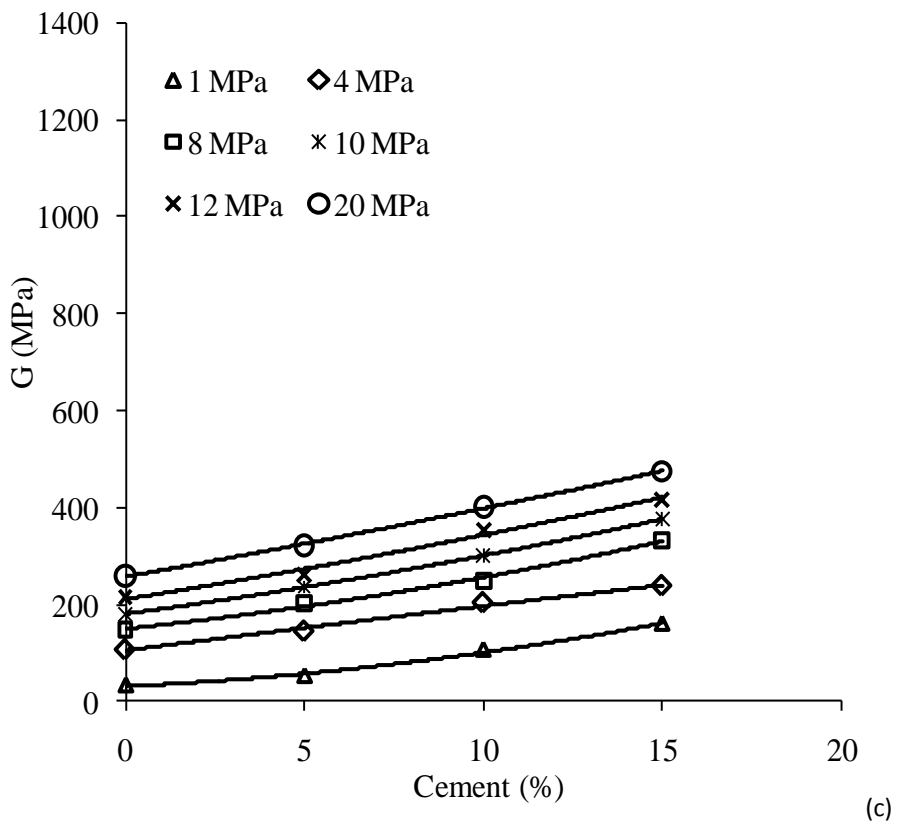


Figure 7.9 Variation of Poisson's ratio with: (a) different cement contents; (b) effective confining pressures.





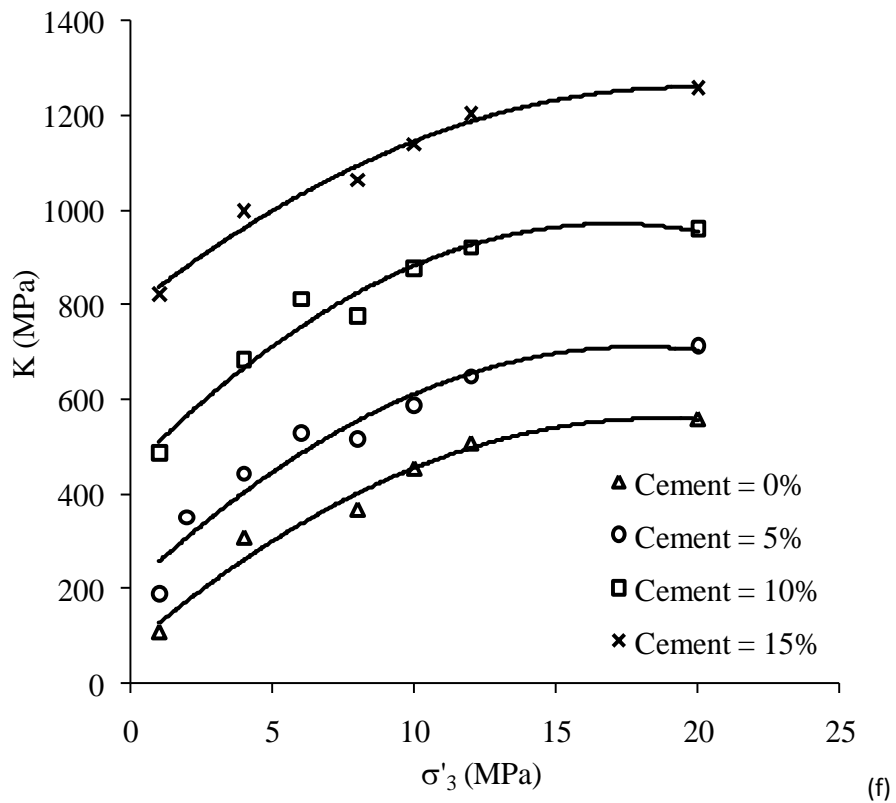
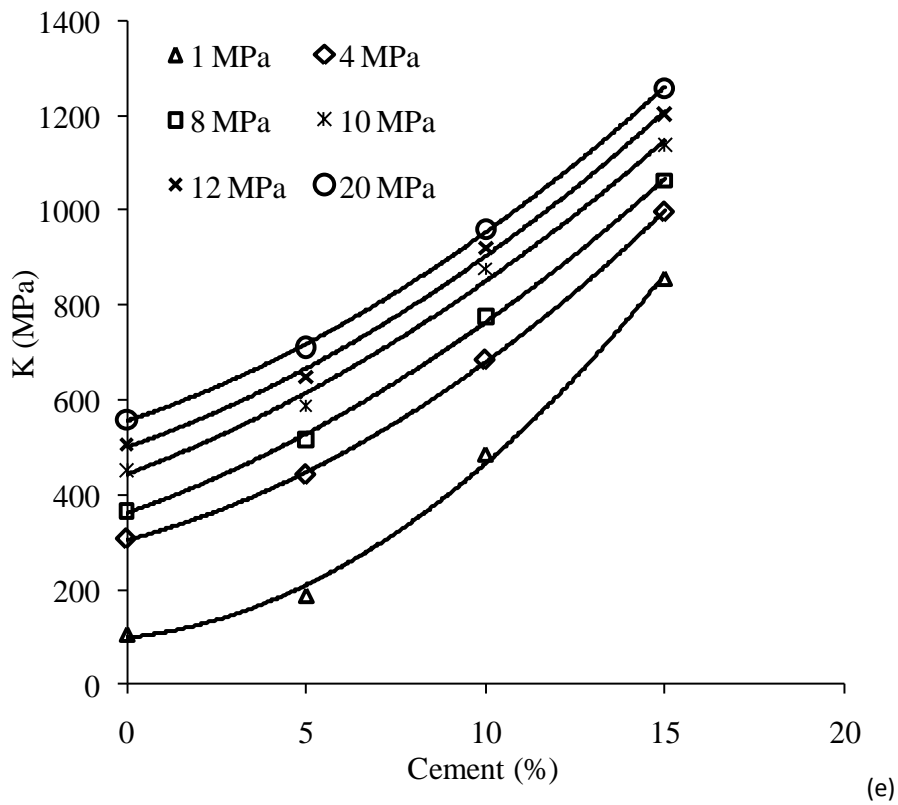


Figure 7.10 Variation of elastic moduli with different cement contents and confining pressures.

7.3.2 Deformation during drained shearing

In order to see the effect of drained shearing on particle crushing and cement bond breakage, uncemented and cemented samples were investigated after drained shearing. Figure 7.11 shows the microstructure of uncemented sand after shearing at a confining pressure of 20 MPa. It can be seen that there is significant crushing of sand particles; lumps of crushed particles and clear fractures on the sand grains are obvious.

Figure 7.12 shows the SEM photograph of cemented sand with 10% of cement content. From the figure, it can be seen that the amount of particle crushing as compared to uncemented sand is noticeably lesser. Only a few fractures on the surface of the sand grains can be seen as shown on magnified picture (Figure 7.12). Along with fractured particles, there exist intact particles as well as undamaged bonds.

For the cemented sand, the mode of failure during shear is also significant. Therefore, samples with brittle and ductile mode of failures were also investigated. The samples during shear with brittle mode and ductile mode of failure usually observed to be forming shear band and bulging respectively, as discussed in chapter 7. It is also worth noting that the increase of confining pressure changes the mode of failure of cemented sand from brittle to ductile. Therefore, samples were picked after shearing, tested at different confining pressures, one with shear band and other with barrelling effect having same cement contents and initial densities. For example, the samples with 15% cement content prepared to a dry unit weight of 17.4 MPa, show shear banding and bulging effects when tested at 1 MPa and 20 MPa of effective

confining pressure respectively. The SEM photographs of the subsections of bulging (tested at 20 MPa) and shear band (tested at 1 MPa) are shown in Figure 7.12 and Figure 7.13 respectively. From Figure 7.12 it can be seen that along with bond breakage there is particle crushing as well. On the other hand, from Figure 7.13 it is evident that during shear at 1 MPa of confining pressure, cement bonds were broken along the shear plane; however, there is no significant particle breakage.

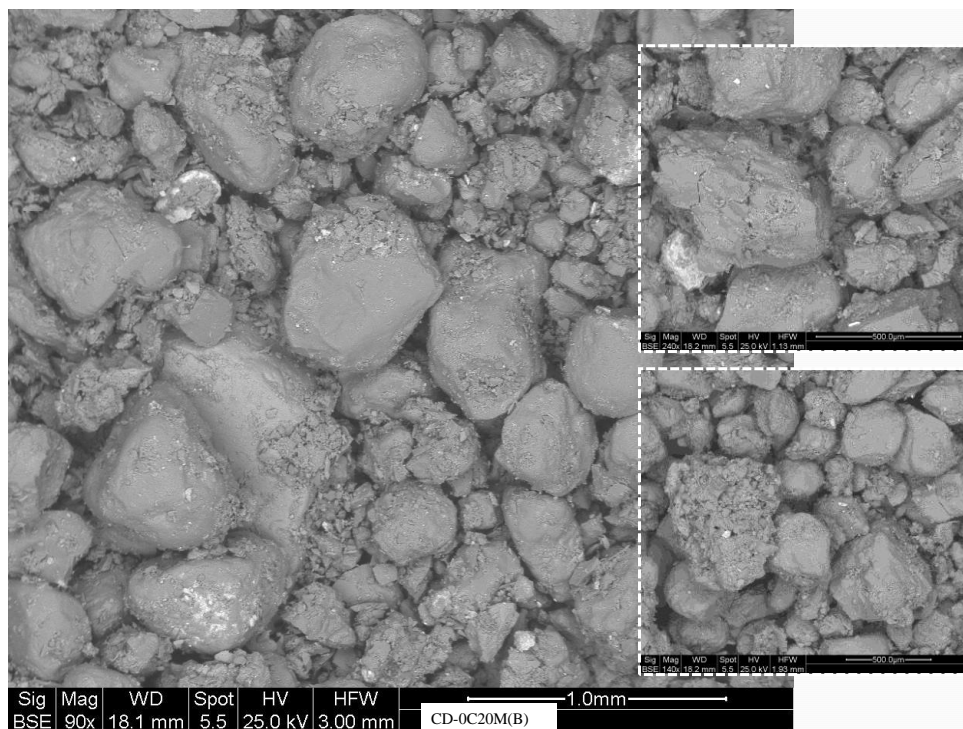


Figure 7.11 Microstructure of the uncemented Portaway sand after CD test at 20 MPa.

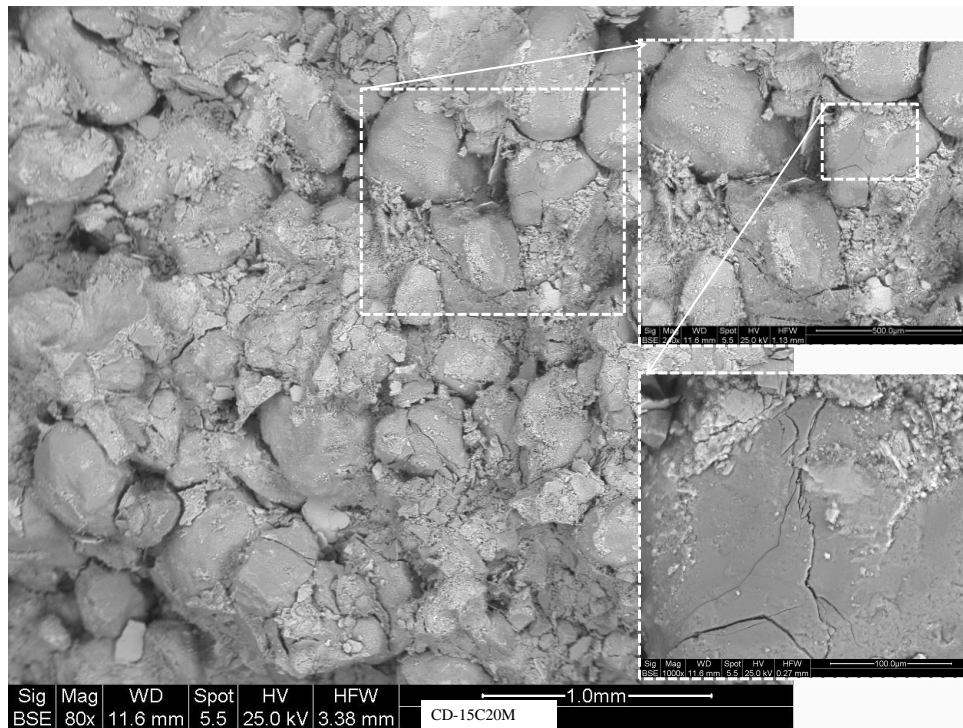


Figure 7.12 SEM photograph of bulging section of cemented sand after isotropically consolidated drained shearing at $c = 15\%$ and $\sigma'_3 = 20$ MPa.

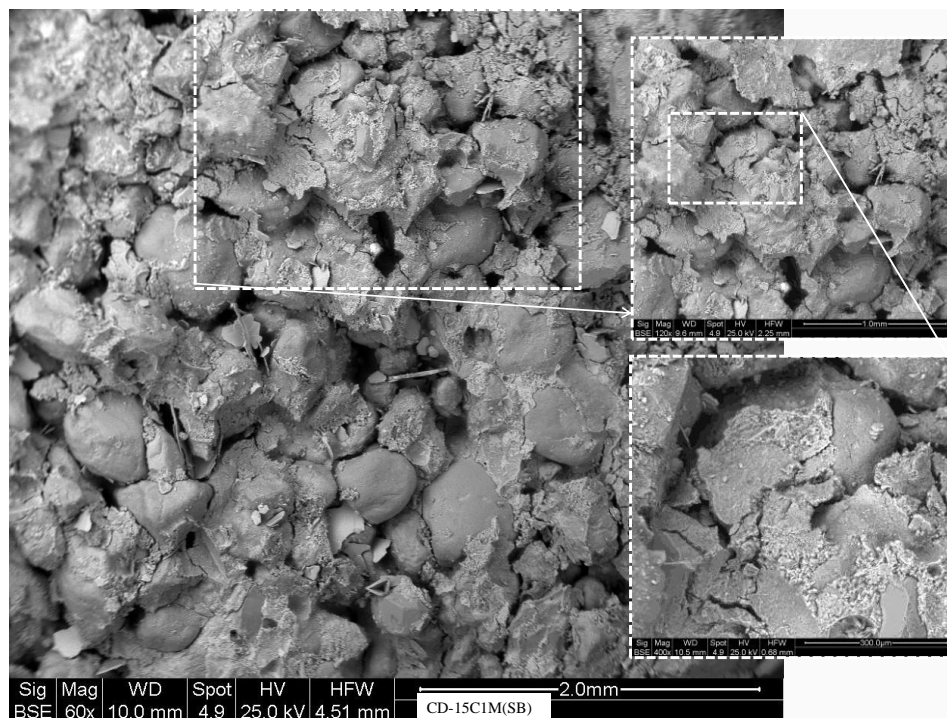


Figure 7.13 SEM photograph of shear plane section of cemented sand after isotropically consolidated drained shearing at $c = 15\%$ and $\sigma'_3 = 1$ MPa.

7.3.3 Deformation during undrained shearing

In order to see the effect of undrained shearing on particle crushing and cement bond breakage, cemented samples were investigated after isotropically consolidated undrained shearing. Figure 7.14 shows the microstructure of cemented sand with 15% cement content after undrained shearing at an effective confining pressure of 20 MPa. It can be seen that there is significant crushing of sand particles; lumps of crushed particles and clear fractures on the sand grains are obvious.

Figure 7.15 shows the SEM photograph of cemented sand with 10% of cement content after undrained shearing at an effective confining pressure of 20 MPa. From the figure, it can be seen that along the shear plane the amount of particle crushing is noticeably high. There can be seen a significant deformation of cement bonding and particles which is visible from the pictures taken at high magnification. One reason of more deformation during undrained conditions as compared to the drained conditions can be the higher confining pressures.

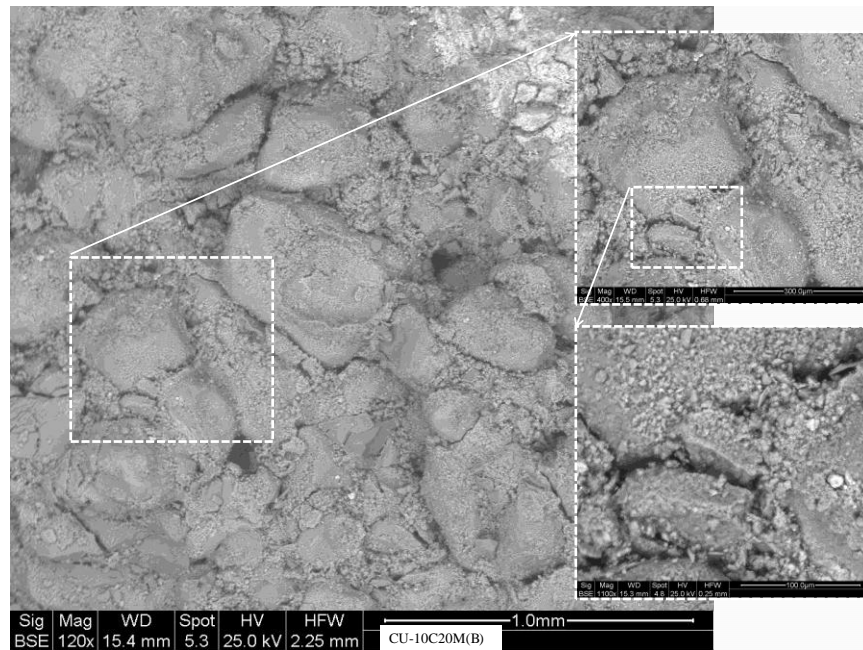


Figure 7.14 SEM photograph of bulging section of cemented sand after isotropically consolidated undrained shearing at $c=15\%$ and $\sigma'_3 = 20$ MPa.

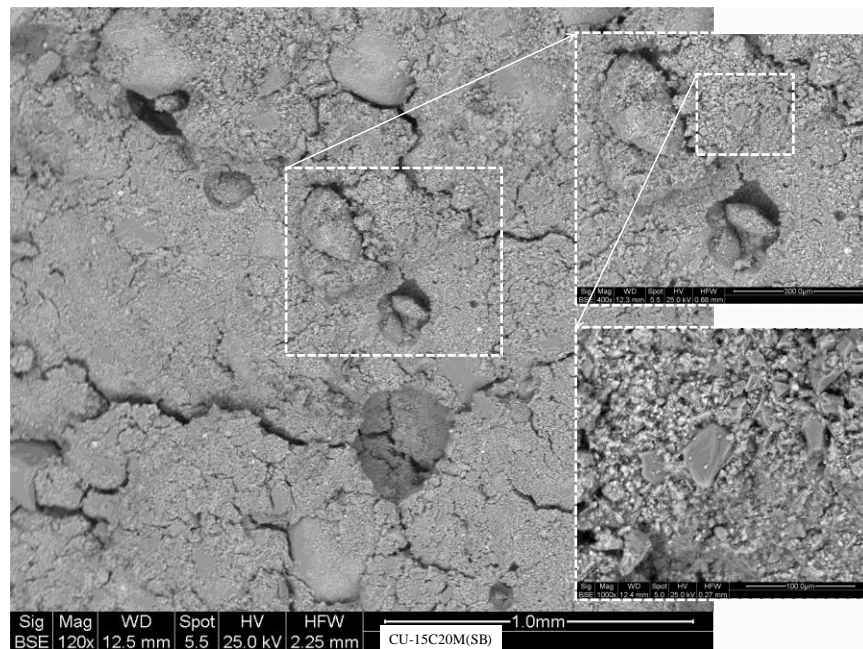


Figure 7.15 SEM photograph of shear plane section of cemented sand after isotropically consolidated undrained shearing at $c=15\%$ and $\sigma'_3 = 20$ MPa.

7.3.4 Measurement of stiffness and stiffness degradation

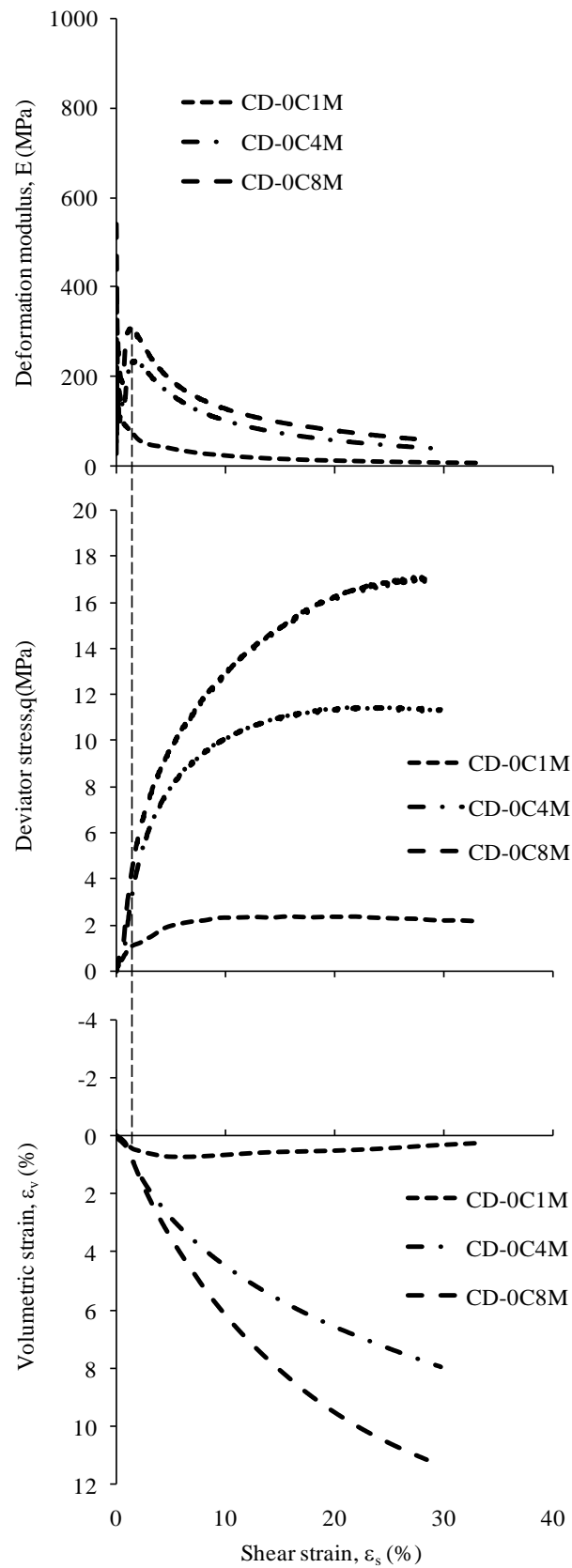
Stiffness is the resistance of an elastic body to deformation by an applied force. Accurate determination of soil stiffness is difficult to achieve in routine laboratory test-

ing. Conventionally, the determination of the axial stiffness of a triaxial sample is based on external measurements of displacement, which include a number of extraneous movements. The present method of soil strain measurement with external load measurement devices has a certain limitations particularly where the soil exhibits high stiffness at small strains but still this could give a reasonable approximation to the real values for measuring the stiffness of cemented sand at high pressures. The system resolutions with other technical specification were given in Table 3.2.

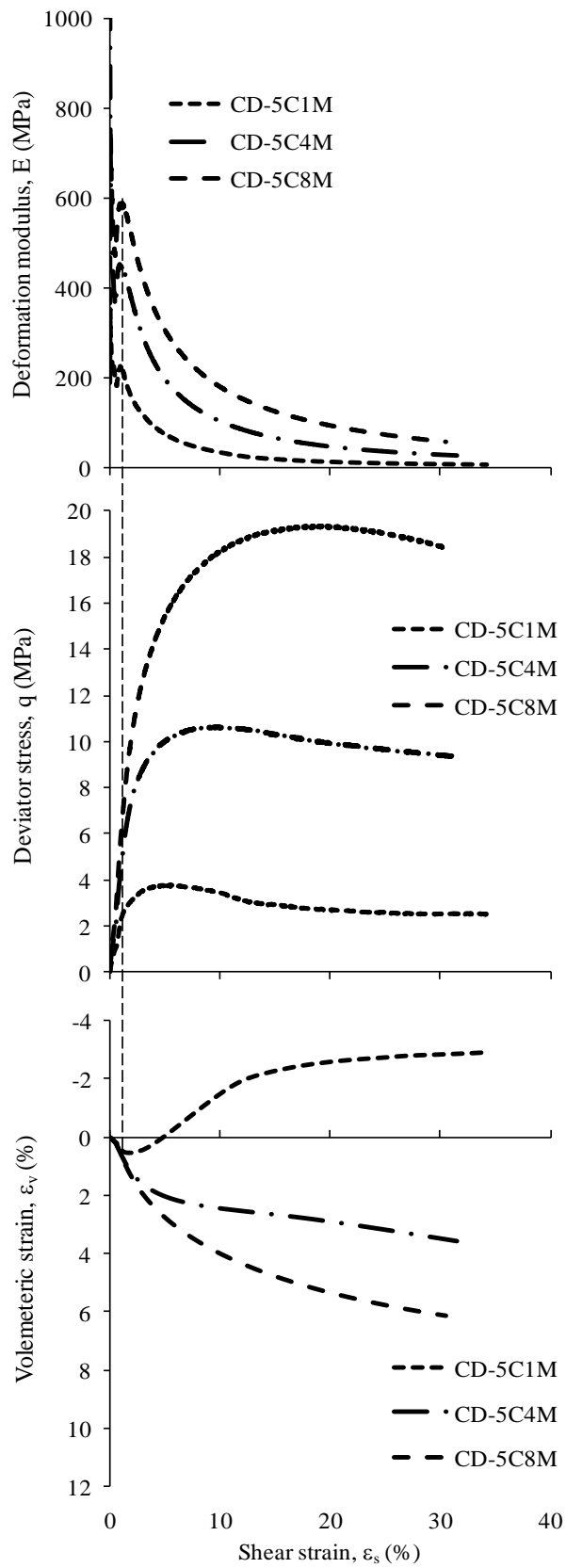
The stiffness degradation curves are shown in Figure 7.17. From the figure, it can be seen that at very small initial strain levels the effect of cement content and confining pressure is quite significant. However, after reaching to a maximum stiffness there is sudden drop in the stiffness magnitude by the increase in shear strain. At large strain levels (let say 10% of shear strain) the effect of cement content on stiffness modulus is diminishing as shown in Figure 7.17(a), however, the effect of confining pressure still persists even beyond 30% of shear strain as shown in Figure 7.17 (b).

The effect of cement content and confining pressure on stiffness degradation during undrained compression is shown in Figure 7.18. From the figure, it can be seen that, similar to the drained compressions the cement content and confining pressure effects are profound in the start of the deformation and then quickly degrading to a small and stable state. At large strain levels the effect of cement and confining pressure still persists. Moreover, comparing the effect during drained and undrained compression tests as shown in Figure 7.19, it can be seen that at large strain levels the magnitude of drained deformation modulus is relatively higher than that of

undrained deformation modulus. Although the cementation induces a considerable increase in the stiffness up to yield stress, the damage of cementation bondage near yield stress causes a significant reduction in the stiffness. Once the cementation bondage is completely broken, the stiffness of the cemented sands become similar, regardless of the degree of cementation. Therefore, it can be concluded that the deformation modulus of cemented sand depends on the cementation bondage as well as on the degree of cementation damage induced due to the stress/strain level increase. Lee *et al.* (2010) drew similar conclusions for the evaluation of deformation modulus of cemented sand using CPT and DMT.



(a)



(b)

Figure 7.16 Onset of pre-failure deformation correlated with deviatoric stress and volumetric strain curves with the cement content of: (a) 0%; and (b) 5%.

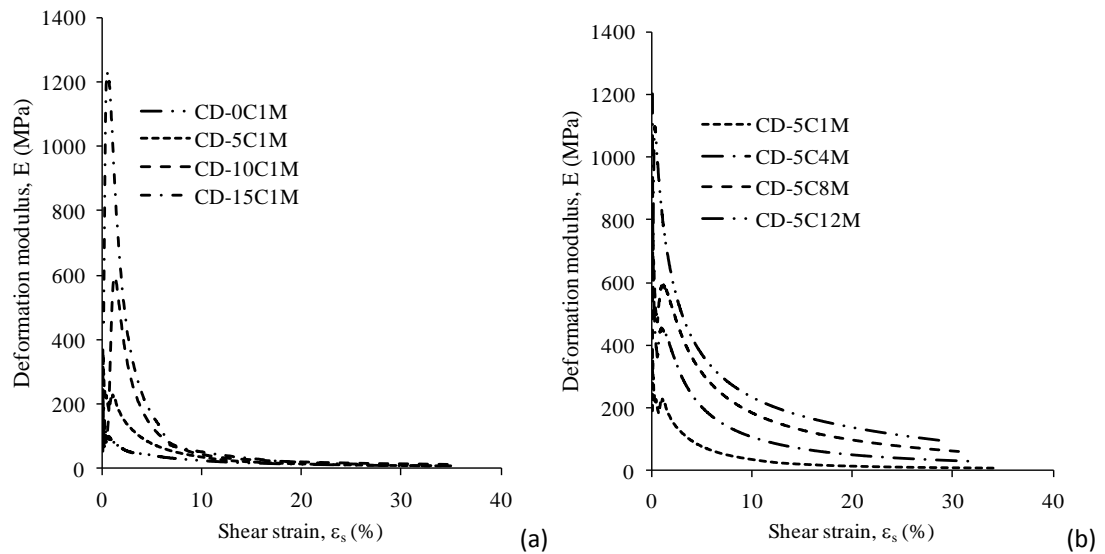


Figure 7.17 Effect of: (a) cement content; and (b) confining pressure on stiffness degradation during drained compression.

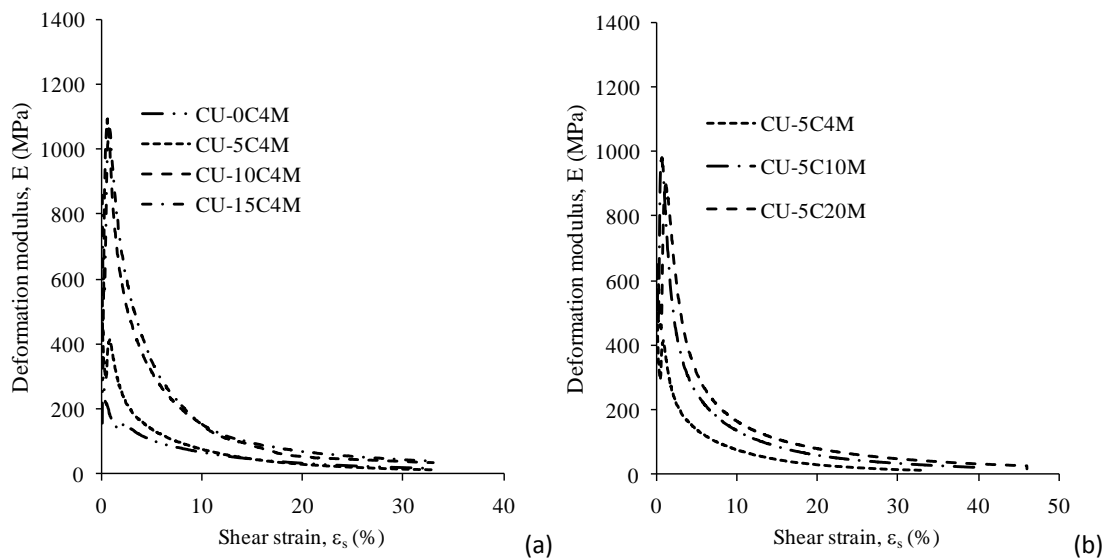


Figure 7.18 Effect of: (a) cement content; (b) confining pressure on stiffness degradation during undrained compression.

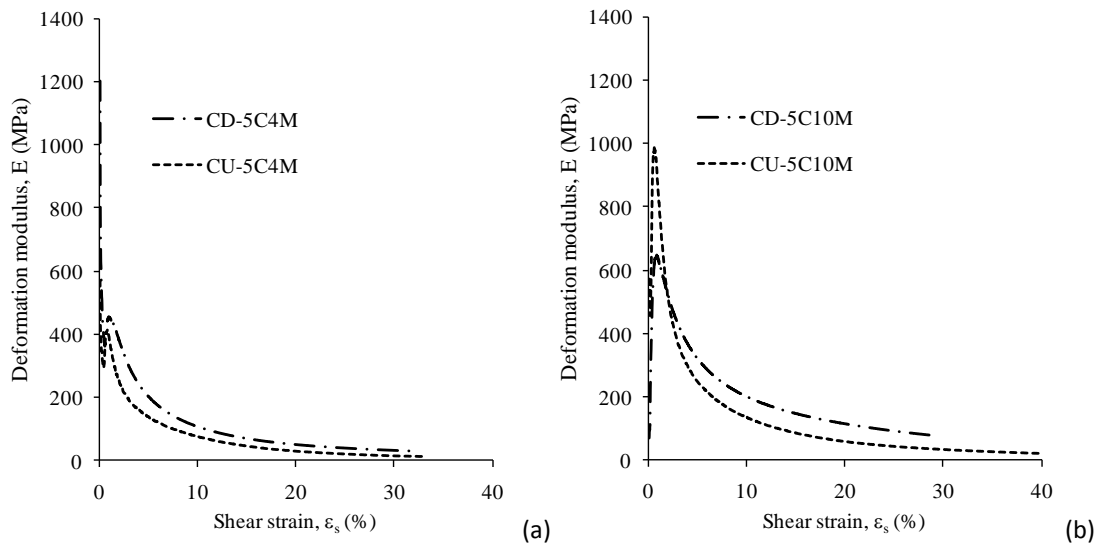


Figure 7.19 Comparison of the effect of: (a) cement content; and (b) confining pressure on stiffness degradation during undrained and drained compression.

7.4 Critical state behaviour

Critical state concepts have been used as a framework to illustrate the mechanical behaviour of the sandy soils for many decades. The critical state strength rather than peak strength is the only strength that can be relied upon in the long term. The critical state framework has been effective in the formulation of constitutive models and the quantification of the mechanical behaviour of sands.

There are quite a number of papers and case studies available in literature regarding the critical state concepts in sandy soil. The existence of a critical state wherein indefinite shear occurs is a major feature of the family of elastic-plastic models known as critical state soil mechanics (Schofield and Wroth 1968). However, it should be noted that the majority of these studies are associated to fine and uniform sands and are at conventional pressures. There is a lack of data for the uncemented or cemented sands at high pressures.

Table 7.3 Summary of isotropically consolidated drained compression tests (critical/ultimate state parameters).

Test	σ'_3 (MPa)	C (%)	e_c	e_{ult}	ϕ'_{peak} (°)	ϕ'_{ult} (°)	$\phi'_{peak} - \phi'_{ult}$ (°)	p'_{ult} (kPa)	q_{ult} (kPa)	$(q/p')_{ult}$
CD-0C0.05M	0.05	0	0.49	0.57	40.4	35.8	4.6	94	137	1.5
CD-0C0.1M	0.1	0	0.49	0.56	38.1	33.1	5.0	178	237	1.3
CD-0C0.2M	0.2	0	0.48	0.56	37.3	32.0	5.3	389	473	1.2
CD-0C0.3M	0.3	0	0.48	0.55	36.6	31.9	4.7	516	662	1.3
CD-0C0.5M	0.5	0	0.49	0.52	35.6	32.2	3.4	879	1138	1.3
CD-0C1M	1	0	0.47	0.46	32.4	30.9	1.5	1732	2144	1.2
CD-0C4M	4	0	0.44	0.33	31.9	30.5	1.4	7768	9769	1.3
CD-0C8M	8	0	0.43	0.28	31.3	30.3	1.0	13690	17188	1.3
CD-0C10M	10	0	0.43	0.26	30.6	30.0	0.6	17450	22505	1.3
CD-0C12M	12	0	0.41	0.22	30.4	29.8	0.6	19879	23718	1.2
CD-0C20M	20	0	0.39	0.21	29.4	28.1	1.3	31517	34712	1.1
CD-5C0.05M	0.05	5	0.50	0.60	58.2	41.9	16.3	145	249	1.7
CD-5C0.1M	0.1	5	0.50	0.57	52.6	37.1	15.5	202	303	1.5
CD-5C0.3M	0.3	5	0.50	0.55	44.2	34.3	9.9	555	761	1.4
CD-5C1M	1	5	0.50	0.53	40.6	33.5	7.1	1815	2519	1.4
CD-5C2M	2	5	0.49	0.50	37.2	32.9	4.3	3525	4670	1.3
CD-5C4M	4	5	0.48	0.43	34.8	32.6	2.2	7099	9332	1.3
CD-5C6M	6	5	0.47	0.39	34.1	32.0	2.1	10486	13482	1.3
CD-5C8M	8	5	0.47	0.36	33.2	31.7	1.5	14149	18409	1.3
CD-5C10M	10	5	0.46	0.33	32.6	31.2	1.4	17622	22907	1.3
CD-5C12M	12	5	0.45	0.30	32.1	31.0	1.1	21072	27305	1.3
CD-5C20M	20	5	0.43	0.26	29.7	28.5	1.2	31868	33930	1.1
CD-10C0.05M	0.05	10	0.52	0.71	71.9	46.2	25.7	143	272	1.9
CD-10C0.5M	0.5	10	0.52	0.64	59.0	40.3	18.7	1190	1963	1.6
CD-10C1M	1	10	0.51	0.57	52.4	38.5	13.9	2221	3601	1.6
CD-10C4M	4	10	0.51	0.49	40.5	33.8	6.7	7280	9932	1.4
CD-10C6M	6	10	0.51	0.45	36.0	33.1	2.9	10591	13904	1.3
CD-10C8M	8	10	0.50	0.43	34.5	32.7	1.8	14174	18643	1.3
CD-10C10M	10	10	0.49	0.39	33.6	32.4	1.2	17491	22479	1.3
CD-10C12M	12	10	0.49	0.37	33.3	32.0	1.3	21345	26015	1.2
CD-10C20M	20	10	0.47	0.36	30.5	29.1	1.4	31371	34124	1.1
CD-15C1M	1	15	0.53	0.56	56.6	39.5	17.1	2139	3393	1.6
CD-15C4M	4	15	0.52	0.44	46.2	36.2	10.0	8309	12952	1.6
CD-15C8M	8	15	0.51	0.38	38.2	34.5	3.7	14913	20844	1.4
CD-15C10M	10	15	0.51	0.37	36.5	34	2.5	17055	21227	1.2
CD-15C12M	12	15	0.51	0.34	35.2	33.2	2.0	21602	27563	1.3
CD-15C20M	20	15	0.50	0.32	31.2	30.0	1.2	31003	35003	1.1

$\gamma_d = 17.4 \text{ kN/m}^3$ for the above test data.

However, there are quite often cases of high pressures in the field of geotechnical engineering and therefore, it is worth to elaborate the critical state concept for ce-

mented sand at high pressures as well. The summary of the triaxial compression test data stating the critical/ultimate state parameters is shown in Table 7.3.

7.4.1 Problems in identifying critical state for cemented sand

The development of shear banding in sands near peak stress levels and the subsequent continued deformation within shear bands during observed softening render important issues such as critical state difficult to investigate. The determination and overall validity of critical state behaviour is of considerable importance, as it provides the basis both for failure criteria/post-failure behaviour in sand constitutive models and for stability analysis.

From Figure 7.20, it could be observed that for specimens with different cement contents prepared at constant initial dry unit weights and then prior to shearing isotropically consolidated up to required targeted effective confining pressures are showing different ultimate void ratios (e_{ult}) at the end of triaxial compression. For the effective confining pressures up to 20 MPa and axial deformation of 30%, there could not be seen the general tendency of approaching to a critical state void ratio (e_{cr}), this indicates the intricacy of achieving e_{cr} for cemented sand having variable cement contents.

Figure 7.21 shows the variation of the specific volume with mean effective stress for uncemented sand for different confining stresses. At conventional pressure level, the variation of the specific volume in uncemented dense sand in drained state confirms a contractive behaviour with continuous increase in volume at final state.

State paths (q against average effective stress, p' , and specific volume, v , against p') followed during the isotropically consolidated drained compression tests (CD) on samples of uncemented and cemented Portaway sand. These state paths enable an onset of dilation envelope, critical state envelope and a peak strength failure envelope to be determined in the $q:p'$ plane at conventional pressure as shown in Figure 7.21.

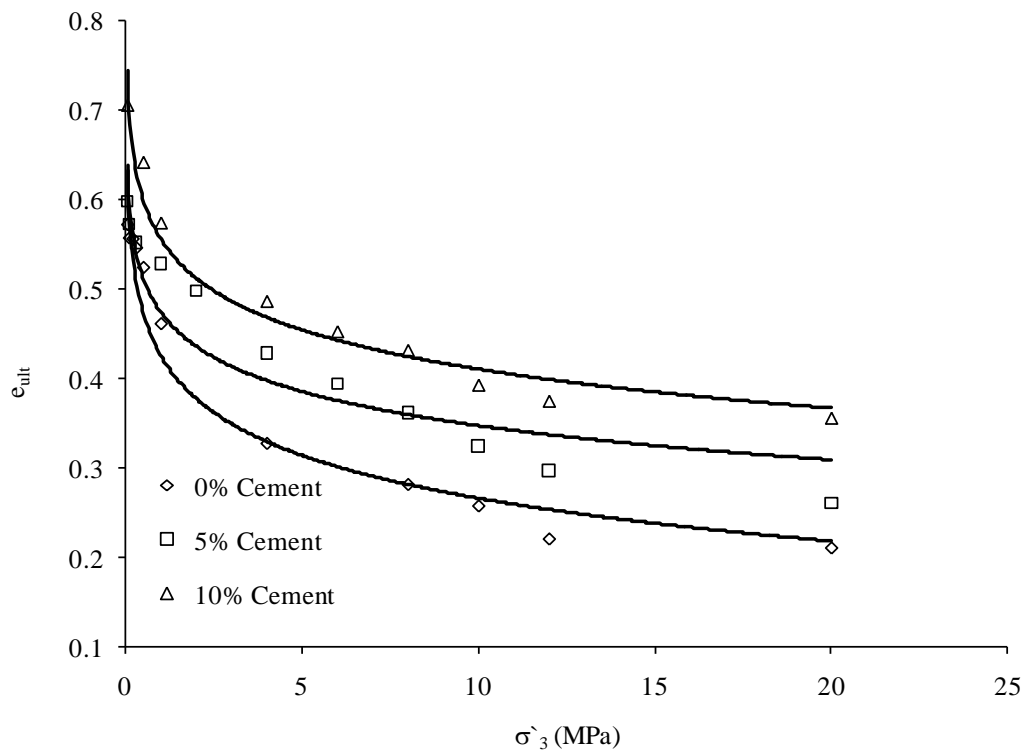


Figure 7.20 Effect of confining pressure on ultimate state/critical state void ratio during triaxial compression.

The failure, dilation and critical state/ ultimate state envelopes can clearly be distinguished and marked on $q:p'$ and $v:p'$ space in the figure. From Figure 7.21, it can be seen that by the increase in mean effective stress the extent of initial compression is extending and the extent of post peak dilation is shortening. For instance, at 50 kPa

there is continuous dilation and at 200 kPa there can be seen some sort of tendency towards critical state to achieve constant volume change during shear.

Figure 7.22 shows the variation of the specific volume with mean effective stress for uncemented and 5, 10, and 15 percent cemented sand for different confining stresses. At relatively high confining pressures, the variation of the specific volume in uncemented sand in drained state confirms a contractive behaviour with continuous reduction in volume at final state except at 1 MPa as shown in Figure 7.22(a). For the cemented sand, the specific volume decreases initially and then increases at the confining pressures of 1 MPa for 5% cement content and at 1 MPa and 4 MPa for 10% and 15% cement content, which shows a dilative behaviour in final strains for the sand. However, for confining pressures above 4 MPa it can be seen that there is contractive behaviour with continuous reduction in volume at final state.

At high confining pressures as shown in Figure 7.22, the failure envelope is curved convex upward, and the dilation is suppressed. Therefore, it is difficult to indicate dilation envelope except at confining pressures below 1 MPa. From Figure 7.22 (a) and (b), with cement contents of 0% and 5%, it can be seen that after initial compression, the dilation can only be seen for 1 MPa of confining pressure. This could be attributed to the gliding and rolling-over of granular particles and cement bond breakage resulting to volumetric expansion under the given confining pressure. However, for the rest of higher pressures (>1 MPa) after initial compression, there can be seen increase in the rate of compression. This might be due to the cement bond breakage

and tumbling of particles under higher magnitude of pressure and subsequent suppression of dilation.

On the other hand, increase in the cement content observed to have more tendency of inducing dilatancy and subsequent reduction in the compression of the material. For instance, from Figure 7.22 (c) and (d) with cement contents of 10% and 15%, there can be seen post peak dilation for 1 MPa and even at 4 MPa of mean effective stress. For the higher confining pressures of 10 and 20 MPa, the tendency of compression is slower than that for 0% and 5% of cement content. A possible projection of the critical state line (CSL) is indicated corresponding to critical state parameters as shown in Figure 7.22. However, it has been argued by many researchers in the past (which has also been discussed in the literature) that in reality it is rather ultimate state line (USL) because the volumetric change more often could not reach to a constant value.

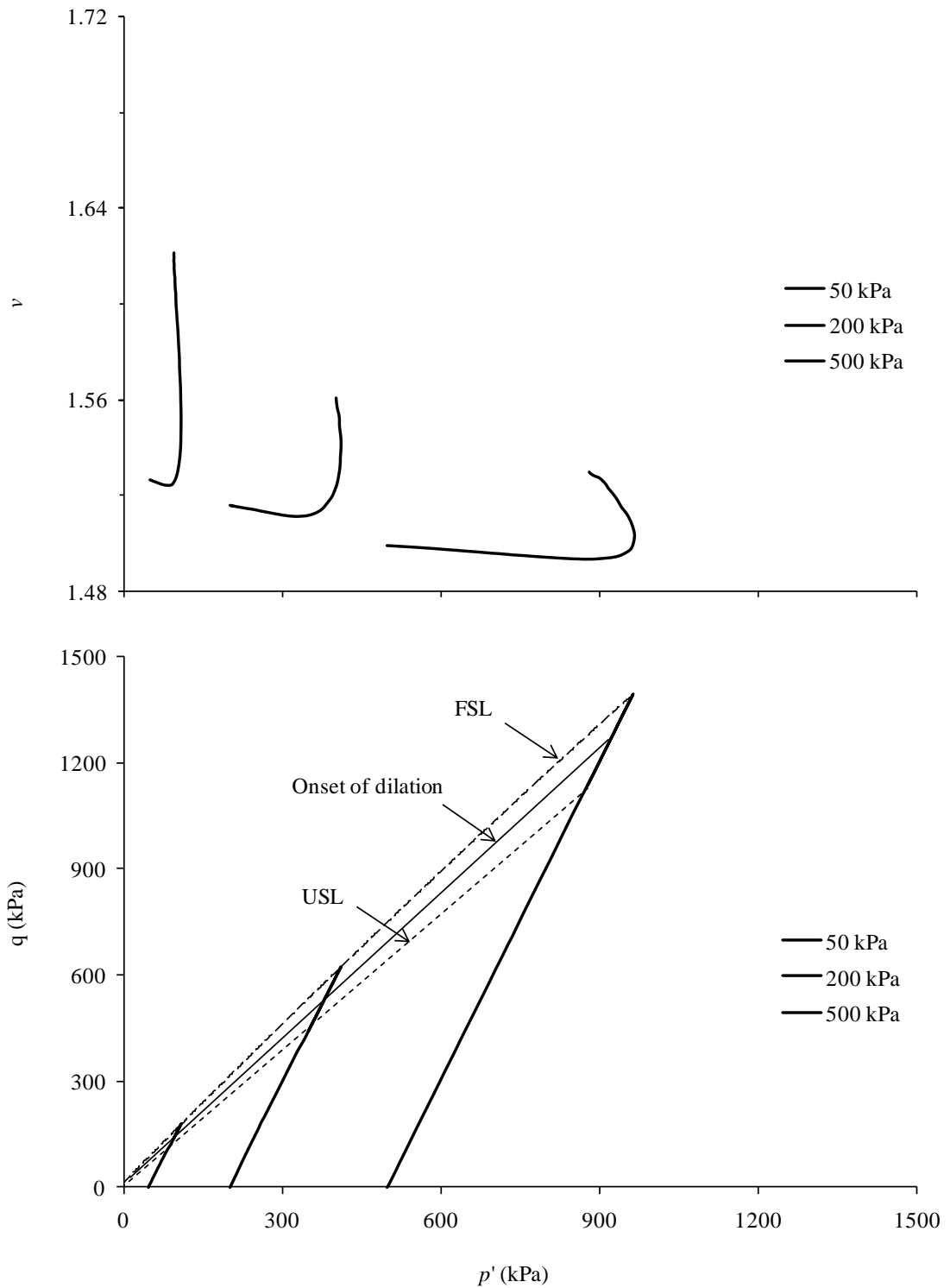


Figure 7.21 State paths and limiting stress envelopes at conventional pressure.

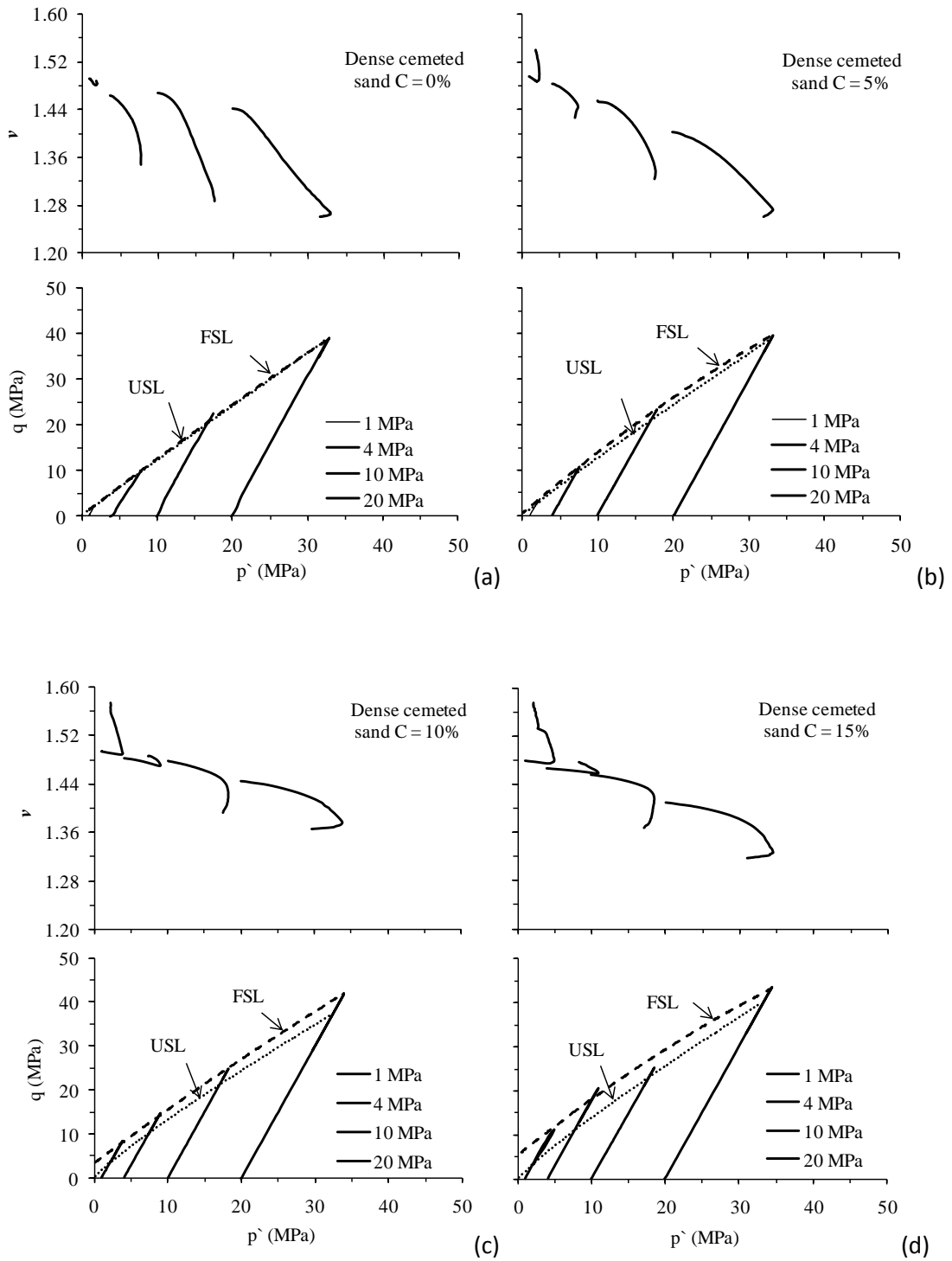


Figure 7.22 Effect of cement contents on state paths and limiting stress envelopes at high pressures with cement contents of: (a) 0%; (b) 5%; (c) 10%; and (d) 15%.

7.4.2 Critical state surface

The results of triaxial tests on uncemented and cemented sands are shown in Figure 7.23. The figure shows the stress paths for drained and undrained triaxial tests conducted on the uncemented and 5, 10, and 15 percent cemented sand with Portland cement. The peak and final states are nearly coincided for uncemented sand samples. As a result, the failure envelope and the critical state line are nearly equal for uncemented sand. However, for the cemented sand, the peak points of the stress paths are different from the final states shear stress and this difference is increasing with the increase in the cement content. This results in two different lines for failure envelope and critical state. It seems that cementation increases the distance between failure envelope and the critical state line. Also the figure shows that the final state for drained and undrained tests at high pressures are slightly scattered and are showing somewhat inconsistent trend. This may result in different critical state lines in drained and undrained conditions. However, according to Hamidi and Haeri (2005) at conventional pressures for gravely sand the final state for drained tests are somewhat higher than that for undrained one. However, ignoring this case, in the present study, a unique line is used to define the critical state of the soil.

It seems that critical state can be determined in $v: \ln(p')$ coordinates for the two groups. Using the results of the tests, the projection of the critical state surface on $q:p'$ and $v:\ln(p')$ planes were derived. The projection of the critical state surface on $q-p'$ and $v:\ln(p')$ planes can be shown with the following equations that results in two straight lines as follow:

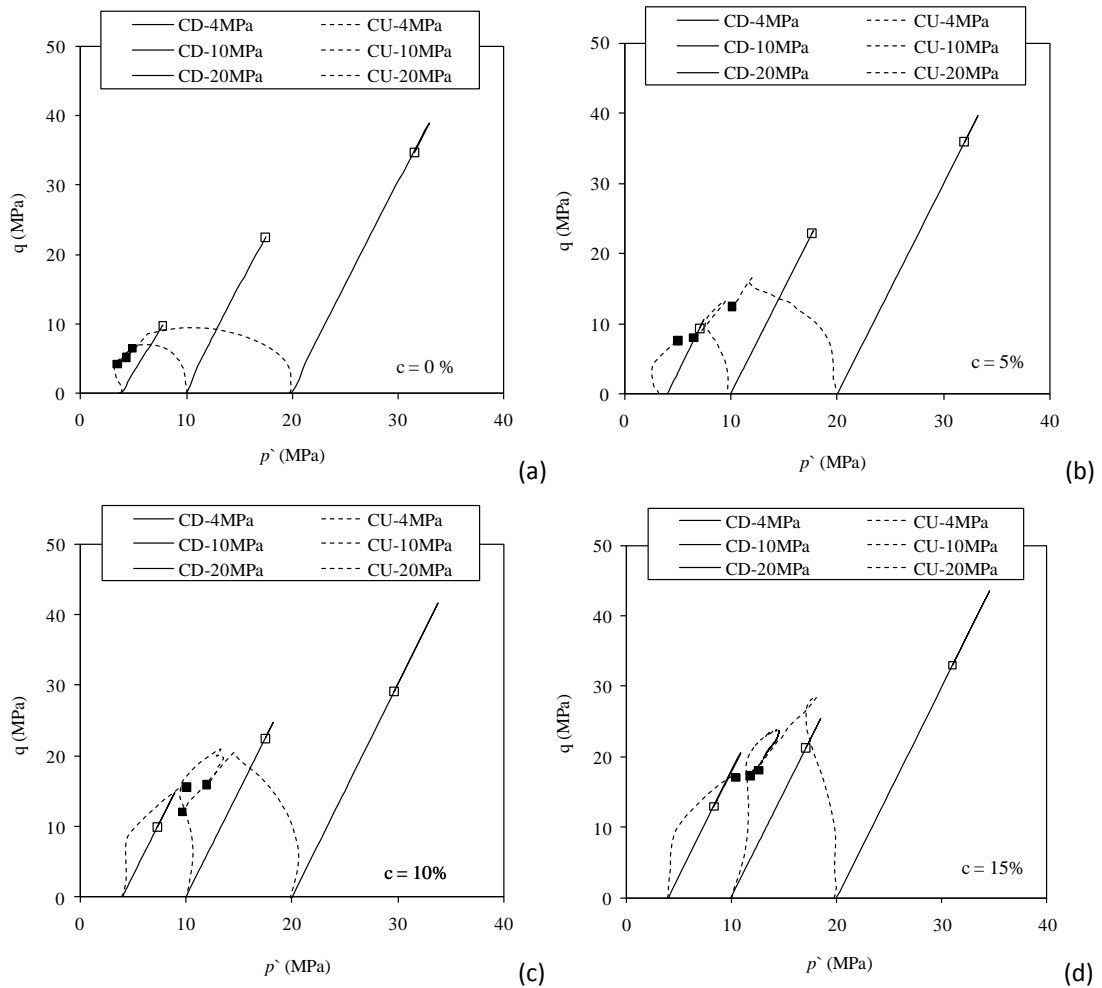


Figure 7.23 The stress paths for uncemented and cemented sand with cement content of: (a) 0%; (b) 5%; (c) 10%; and (d) 15%.

$$q = Mp \tag{7.7}$$

$$v = \tau - \lambda \ln(p) \tag{7.8}$$

τ is a constant indicating the value of v at the mean effective stress of 1 kPa. This is dependent on the intrinsic characteristics of the soil. The triaxial tests continued until the strain level of above 30%. However, the majority of samples experienced the strain level of about 30 percent. Haeri and Hamidi (2005) showed that the actual

critical state in which the mechanical parameters of gravely sand remain constant occurs in strain level of 20 percent or more. As a result there is some approximation in determining the critical state parameters from these tests. However, in the present study, the results of tests in which the final axial strain are about 30 percent or more are considered in critical state calculations.

The critical state of cemented and uncemented soil in $q-p'$ space is shown in Figure 7.24. As indicated in this figure, a unique line can be assigned to the points associated with the uncemented sand with a very low scatter, which is slightly curved instead of being straight line for a wide range of confining pressures. While there is upper critical state curve associated with the cemented sands. It might be reasonable to define a critical state zone for cemented sand. The critical state zone is shown in Figure 7.25. As these data points show, the critical state line of the cemented soil may be upper or coincident with the uncemented sand at conventional pressure; however, for high confining pressure levels it can be seen that the critical state data points for cemented sand are slightly upper than uncemented one. In this regard, Coop and Atkinson (1993) showed that the critical state line of cemented soil is lower than that of uncemented soil. In addition, Cuccovillo and Coop (1999) indicated that the critical state lines for reconstituted and intact samples are almost coincided. The difference between these researches can be attributed to the different soil fabric, soil structure, cement type and the amount of confining pressures.

The projection of the critical state on $v:\ln(p')$ space is shown in Figure 7.26. Only the tests with the final axial strains of about 30% or more are considered in this Figure.

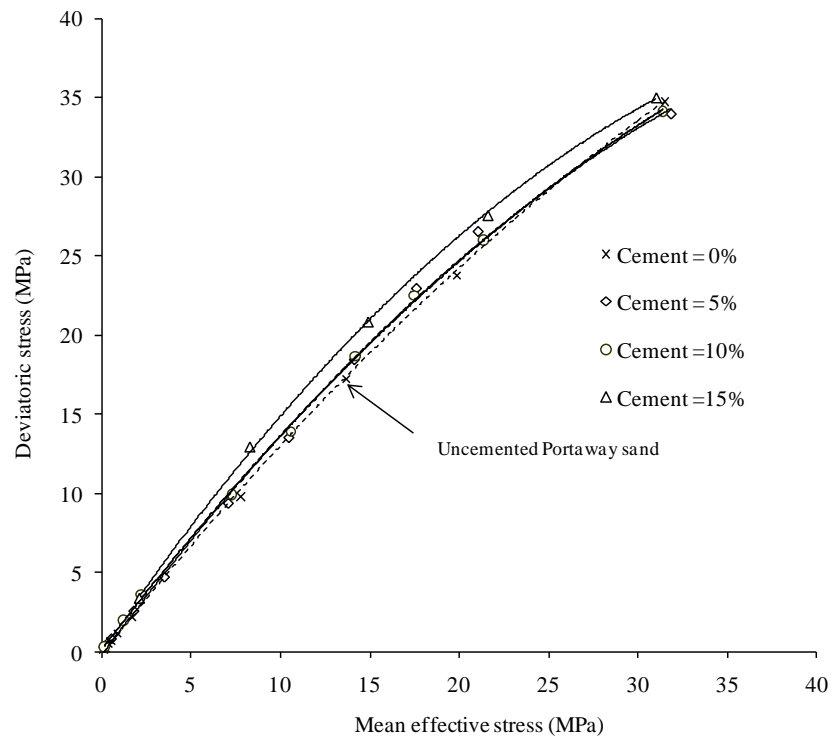


Figure 7.24 Critical state lines in q - p' space.

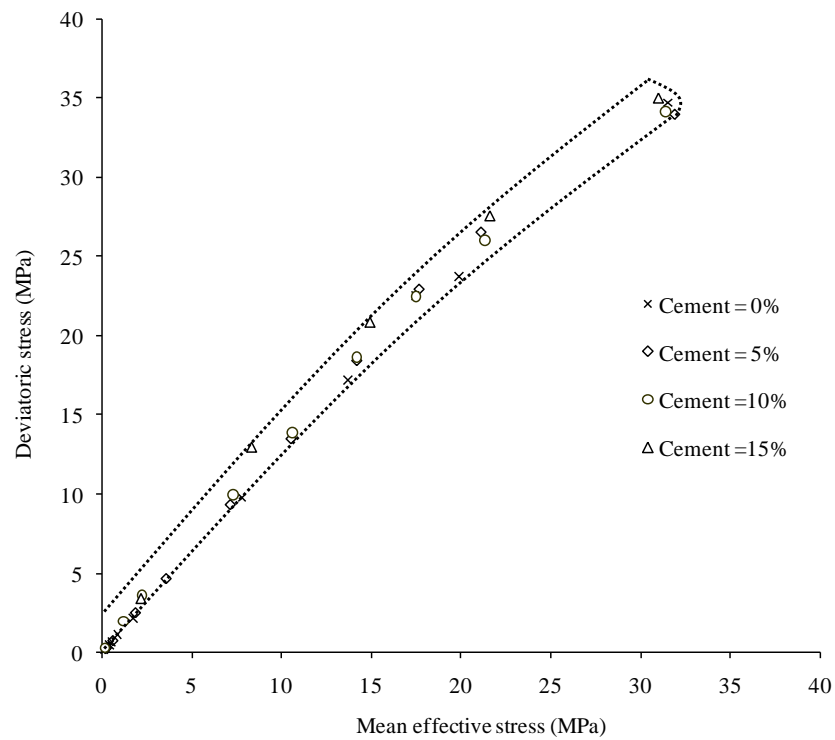


Figure 7.25 Critical state zone in q - p' space.

This figure shows more scatter in data for uncemented soil compared to that of $q:p'$ space shown in Figure 7.25. This may be attributed to the effect of soil fabric and structure and also to the method of void ratio calculation after consolidation. The scatter in data is more profound for cemented soil as it was observed in $q:p'$ space as well for that in uncemented soil. However, all the data are located at the right side of the critical state line of uncemented soil. By using a linear regression for both uncemented and cemented sands, two parallel lines could be drawn. It can be concluded that the critical state lines of uncemented and cemented Portaway sands are nearly parallel in $v:\ln(p')$ coordinates, the cemented one being at higher specific volumes.

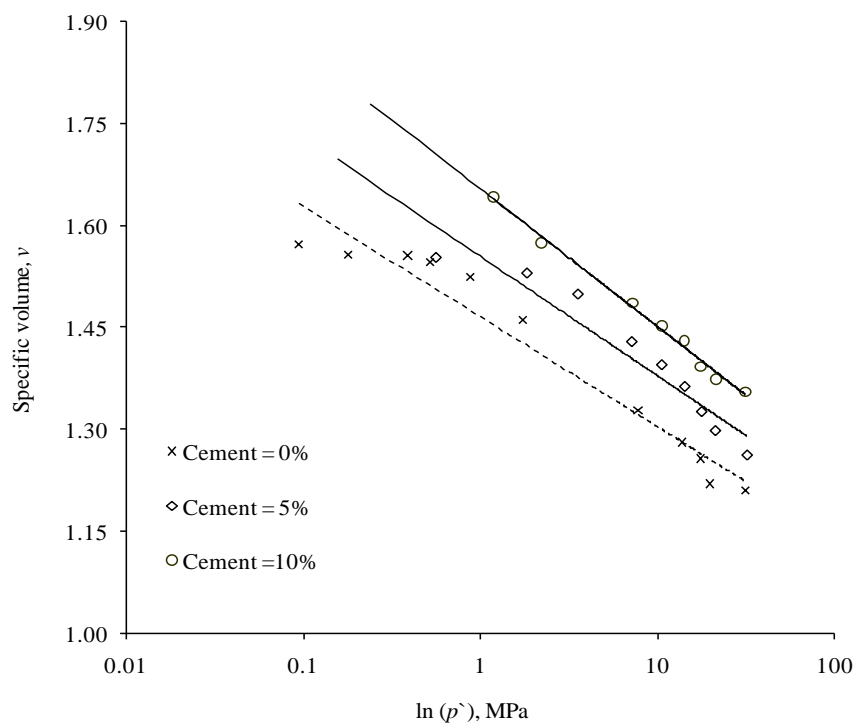


Figure 7.26 Critical state lines for cemented and uncemented soils in $v:\ln(p')$ space the curvatures were ignored.

7.5 Summary

The effect of cement contents and confining pressures were investigated on the yielding characteristics, pre-failure deformation, and critical state behaviour through laboratory testing. The brief summary of the experimental results is described as follows:

- 1) It appears that the yield stress increases with increasing cement content. This result is consistent with that of cemented treated soft Bangkok clay (Bergado *et al.* 2006) and cement treated dredged materials (Chiu *et al.* 2009), which can be attributed to the increasing amount of cementitious products being formed and the amount of solid content per unit volume is increased consequently. The yield stress was observed to increasing with increasing cement content and confining pressures.
- 2) The elastic parameters, which are considered here as deformation moduli were examined for various cement contents over a wide range of confining pressures for a laboratory, prepared cemented Portaway sand. Results of a series of tests on isotropically consolidated drained compression tests yielded values of modulus and Poisson's ratio that are consistent with published literature. It is observed that by the increase in cement content the variation of Poisson's ratio is not significant; however, in general there is slight increase in Poisson's ratio that can be noticed by the increase in the cement content. On the other hand, there is slight decrease in the Poisson's ratio of the material by the increase in the confining pressure. At large strain levels of approximately 0.8%, the value of

the Poisson's ratio, for uncemented sands as well as for cemented sands, is between 0.30 and 0.40.

- 3) Typical values of elastic parameters are summarized in Table 7.2. Variation of elastic moduli with different cement contents and confining pressures were investigated. The experimental results clearly demonstrates that there is approximately linear increase in the elastic moduli by increasing the cement content, however, the effect of confining pressures reveal increase in the moduli in a convex shape envelope. These observations suggest that the level of cementation and confining pressures controls the deformation moduli of the samples and the degradation of cementation is more likely to occur with increasing deviator stress than with increasing isotropic mean effective stress.
- 4) The critical state concepts were used to investigate the mechanical behaviour of cemented Portaway sand. The data associated with the critical state condition of cemented soil in $q:p'$ space has some scatter. As a result, it might be better to define a range for the critical state. The defined range shows that the critical state line of a particular cemented soil may be upper, or the same as that of uncemented soil. In $v:\ln(p')$ space the data of uncemented soil has more scatter. As a result, a critical zone is defined in this space for uncemented and cemented soils.
- 5) The rate of dilation is higher for denser samples, i.e. those initially at a lower voids ratio. The samples dilate until they reach the same critical void ratio, irrespective of their initial density, at which they can continue to shear with no further changes of density according to the concept of critical voids ratio. The criti-

cal voids ratio is, however, not unique, since it reduces slightly with increasing normal stress and increases with increasing cement content.

CONCLUSIONS AND RECOMMENDATIONS

8.1 Introduction

Considering the geotechnical challenges in the foundations of the offshore pile constructions, foundations on oil-bearing strata, and deep pile foundations laid on loose to densely cemented strata, the current study was intended. In order to capture the mechanical behaviour of naturally cemented sand at high pressures, a comprehensive experimental investigation has been carried out on artificially cemented sand. For this purpose, a new computer controlled high-pressure triaxial apparatus designed with the collaboration from GDS was introduced for the first time. This system is capable to apply confining pressure up to 64 MPa, axial loads up to 100 kN and can accommodate the samples with sizes, ranging from 50 mm×100 mm to 70 mm ×140 mm. The vertical load applied on the specimens can be stress controlled or vertical strain controlled.

In order to capture the actual materials behaviour, artificially cemented sand specimens were prepared with varying degree of cement content and initial relative densities. Unconfined compression, isotropic loading-unloading, isotropically drained, undrained triaxial shear, and SEM analysis were carried out to study the effects of cement content and confining pressure on the mechanical behaviour of sand at high pressures. This study also presents an extension of the cemented soil behaviour by incorporating the wider range of cementation and high confining pressures.

This chapter summarizes first the technical difficulties with specimen preparation and high-pressure triaxial testing, and then the experimental findings followed by potential applications and recommendations for further research.

8.2 Summary of experimental results

From the literature review, it is apparent that there have not been many studies of cemented sand behaviour at high pressures. There appears to be some disagreement regarding specimen preparation procedures, shape of failure envelope, critical state framework validity, frictional angle, cement-sand bond breakage, particle crushing, and effect of cement contents at high pressures. A comprehensive understanding of the nature of shearing resistance and compression behaviour of cemented sand is essential to adequate design of foundations. Research in these areas was largely performed at low stress levels. The maximum confining pressure was reported to be 0.1-5.0 MPa (Huang and Airey 1998). However, the maximum pressure at the tip of a pile foundation may reach around 350 MPa (Yamamuro and Lade 1996). In particular, the foundations of offshore constructions resting on naturally cemented sand.

Focussing on aforementioned matters, the major results and findings of comprehensive laboratory testing carried out on cemented and uncemented Portaway sand at high pressures are summarized as follows:

8.2.1 Difficulties in high-pressure triaxial testing

1. It was observed that the cemented specimens prepared in the split mould were sticking with the walls of the mould, which ultimately were resulting to hamper

the safe extrusion of the specimen. This was suitably avoided by providing a transparency sheet inside the mould when preparing a cemented specimen.

2. Membrane puncture at high pressures were observed in abundance, which was ultimately resulting to the test failure. This was overcome by providing membrane strips at the contact point of top and bottom edges of specimen with porous stone and top cap/ bottom pedestal. Moreover, additional membranes were provided to avoid punctures and subsequent failures.
3. Undercompaction method using wet soil to prepare the samples to a required density by compacting into a specified number of layers was found to be leaving stratification into the sample. This was observed when the cemented specimens were exhumed after isotropic compression at high pressures (details are given in Chapter 3).
4. Data obtained from the new high-pressure triaxial apparatus demonstrates that the testing system can be used for an accurate measurement of stress-strain behaviour and failure characteristics of soils under wide range of confining pressures (up to 64 MPa). The high-pressure cell has a unique balanced ram assembly that ensures zero uplift force and zero volume/pressure change inside the cell when the specimen is loaded at high cell pressure.

8.2.2 Isotropic compression

1. During isotropic compression of uncemented sand at high pressures, a dip was noticed in the loading branch of compression curve. This dip was previously attributed to the particle crushing by Yamamuro and Lade (1996). However, no

further confirmations were reported in the past to relate this dip with particle crushing. During this study, it was further confirmed with the help of SEM analysis of the exhumed specimens after compression. The SEM micrographs were showing particle crushing for the specimens which had dip in the compression curve and there were seen no significant particle crushing for the specimens which had shown no dip in the compression curve during isotropic compression.

2. Double dipping in the compression curves, first dip around 5 MPa and second around 10 MPa of mean effective stress was observed in the loose cemented sand. These dips could be attributed to the bulk of cement bond degradation and the bulk of particle crushing respectively. The SEM micrographs for loose cemented specimens exhumed after compression were also showing cement bond breakage and particle crushing.
3. At high confining pressures, the effect of initial void ratio for both cemented and uncemented sands appeared to diminishing and convergence were seen in the compression curves.
4. The effect of cement contents was examined during isotropic compression at high pressures at constant initial void ratio as well as constant initial dry unit weight. From the compression curves, it could be seen that the effect of cement contents is progressively becoming more significant by the gradual increase in the confining pressure. For instance, the specimens with constant initial void ratio of 0.493 and cement contents of 0, 5, 10, and 15% were showing the final void ratio of 0.383, 0.394, 0.444, and 0.459 respectively at the end of isotropic compression at 20 MPa of effective confining pressure. Similar trends were no-

ticed for initial dry unit weight as well. The reason could be the decrease in contraction due to the increase in the cement content.

8.2.3 Failure characteristics

1. It was observed that both cement content and confining pressure affect stress-strain and failure behaviours of cemented sand. For instance, increase in cement content and confining pressure generally increased the triaxial deviatoric stress at failure. An increase in cement content increases the peak deviatoric stress but reduces the axial strain to the peak and the amount of contraction during shearing (i.e. increases the amount of dilation). On the other hand, an increase in confining pressure increases the peak deviatoric stress, the axial strain to the peak and the amount of contraction during shearing. Therefore, the stress-strain behaviour becomes increasingly ductile with increasing confining pressure. The experimental data also showed that the influence of cement content is greater at low confining stresses and it reduces with increasing confining stress where the effect of the confining pressure becomes dominant.
2. The effective stress ratio and the friction angle of cemented sand increase with increasing cement content but reduce with increasing confining pressure. It was observed that the failure parameters of uncemented dense sand determined at the high confining pressure coincide with the critical state parameters determined for loose specimens at low pressures. Furthermore, failure states of cemented specimens at high pressures approached asymptotically to the critical state of uncemented sand.

3. The experimental results suggest that there is significant effect of cement content and confining pressure on the mode of failure of cemented specimens. For instance, the cement content has tendency to induce brittleness and the confining pressure has tendency of inducing ductility into the specimens during shear failure. This was observed from the stress-strain curves and the exhumed specimens after shearing.
4. The behaviour of the cemented soil is found to be more brittle in drained conditions as compared to the undrained conditions.
5. From SEM micrographs it was observed that in case of the formation of shear bands the maximum deformation of cement bonding and particle crushing were observed along the shear plane.
6. In the literature, there is no general agreement regarding the effects of cement content on the peak friction angle (ϕ'). Whereas some researchers reported increase of the friction angle due to cement content, others reported a parallel movement of the failure envelope (i.e. no change in ϕ') caused by increase of cement content. In present study, the friction angle for cemented sand at low confining pressures (<500 kPa) was observed significantly high reaching around 70° degree. However, by the gradual increase in the confining pressures there were seen decrease in the friction angle and had tendency towards a more stable value. For example, up to 20 MPa of effective confining pressure the approximate angle of friction for various cement contents were approaching to 30° degree.

7. The experimental results indicated that strength enhancement, volumetric dilation, and the shear banding associated failure mode observed in Portland cement sand; these features become more pronounced with increasing cement content.
8. Cement content affects the effective stress paths. Increase in cement contents shifts the effective stress paths upward, increase the peak deviatoric stress, and reduce the excess pore water pressure developed during consolidated undrained compression tests.

8.2.4 Stress-dilatancy

1. The stress-dilatancy relationships of cemented sand are affected by cement content and confining pressure. The presence of cement content introduces the component of cohesion into the stress-dilatancy relationship and increases bonding between particles at a given stress. As a result, the stress-ratios at the peak and ultimate states increase with increasing cement content. An increase in confining pressure prevents dilatancy at a given stress. This is consistent with experimental data reported by Schnaid *et al.* (2001) and the computed behaviour reported by Yu *et al.* (2007) at low confining pressures.
2. Test results indicate that besides the relative density, the dilation angles of granular soils are also very sensitive to cement contents and confining pressures. For instance, the dilatancy properties of sand are augmented by the increase in the cement content and gradually suppresses by the progressive increase in the confining pressure.

8.2.5 Yielding characteristics

1. The effect of cementation and confining pressure on the shape and size of the yield surface is quite significant at conventional pressures. In this study, the effect of cementation on the yield surface has been elaborated to the high confining pressures. Following the Wang and Leung (2008) procedure, the yield points for cemented sand at various confining pressures were located at starting point of the transition from a stiff to a less-stiff response. It was observed that by the increase in cement content, there is increase in the normalized primary yield stress and the position of the yield point is marginally shifting towards left. On the other hand, by the increase in confining pressure there is decrease in the normalized primary yield stress.
2. For the relationship between cement content and corresponding isotropic yield stress (p'_y), it appears that the p'_y increases exponentially with the increase in cement content. These results are consistent with that of cemented treated soft Bangkok clay (Bergado *et al.* 2006) and cement treated dredged materials (Chiu *et al.* 2009), which can be attributed to the increasing amount of cement content and the amount of solid content per unit volume is increased consequently.

8.2.6 Strength and deformation

1. The cement content and the confining pressure exert significant influence on the strength and stiffness characteristics of the material. Basically cement content increases shear strength, stiffness, and confers brittle characteristics on the specimen. Moreover, increasing confining pressure confers on the cemented

sand an increase in shear strength, and ultimate strength. In addition, larger confining pressures cause a tendency for the cemented sand to have a ductile behaviour.

2. The SEM analysis carried out in this study also shows that the isotropic consolidation of cemented specimens to high pressures does not cause any significant damage to the specimen fabrics. Most crushing of sand particles and breakage of cement bonds were observed during shearing.
3. SEM micrographs revealed that the stress level and the cement content affect the particle breakage. The amount of particles crushing during consolidated drained and undrained shear at high pressures increases with increasing confining pressure and reduces with increasing cement content.

8.2.7 Critical state behaviour

1. The critical state concepts were used to investigate the mechanical behaviour of cemented Portaway sand. The data associated with the critical state condition of cemented soil in $q:p'$ space has some scatter. As a result, it might be better to define a range for the critical state. The defined range shows that the critical state line of a particular cemented soil may be upper, or the same as that of uncemented soil. In $v:\ln(p')$ space the data of uncemented soil has more scatter. As a result, a critical zone is defined in this space for uncemented and cemented soils.
2. For the effective confining pressures up to 20 MPa and axial deformation of 30%, there could not be seen the general tendency of approaching to a critical state void ratio (e_{cr}) during triaxial compression, which indicates the intricacy of

achieving e_{cr} for cemented sand having variable cement contents. Corresponding to critical state parameters a possible projection of the critical state line (CSL) was indicated. However, it has been argued by many researchers in the past (which has also been discussed in the literature) that in reality it is rather ultimate state line (USL) because the volumetric change could not reach to a constant value.

8.3 Potential applications

In practical problems such as high earth-rock dams and deep foundations in civil engineering or deep oil drilling and open pit mining, the soil is subjected to pressures considerably higher than those commonly encountered in soil mechanics practice are. Moreover, the research on cemented soils has become increasingly important with the search for new offshore oil fields throughout the world such as the North Sea, the Gulf of Mexico, offshore West Africa, in areas where the deeper soil profile is dominated by weakly cemented sands and sandstones. Different cement contents, varying densities, and wide range of confining pressures under unconfined compression, isotropic compression, drained shearing and undrained shearing; altogether, unveils certain hidden aspects of the cemented materials.

From the laboratory investigations and subsequent test data, it is possible to extract fundamental material parameters, such as cohesion (c), frictional angle (ϕ), dilatancy angle (ψ), void ratio (e), deformation modulus (E), Poisson's ratio (ν) etc. These parameters can be used in understanding the true material's behaviour and in computer models to predict how the material will behave in a larger-scale engineering

applications. The materials real behaviour can be useful for any numerical modelling and designing the geotechnical structures.

8.4 Recommendations

1. By the addition of cement it is also, obvious that same amount of fine is being added into the sand. Therefore, the effect of cement content compared with uncemented sand having equal amount of fine added will eliminate the fine content effect and the comparison would only give the effect of cementation.
2. During natural process of cementation, the process undergoes under the effect of confining pressure. Therefore, it would also be worth investigating the mechanical behaviour of cemented sand specimens prepared under stress at high pressures.
3. It would be significant to measure the stiffness of the sand particles and cement bond at various percentages of cement content by introducing different small-strain measuring devices to the high-pressure triaxial system. This will lead to evaluation of the initial maximum stiffness and stiffness degradation curves for different cement contents and densities at high pressures, which can provide guidelines for calculating ground movement.
4. Identification of critical axial strain/shear strain that would cause the maximum damage to the cement bonding and particle crushing during triaxial compression is an important parameter for investigation and understanding the behaviour of cemented materials.

5. From the experimental investigations, it is evident that the increase in cement content results to a significant decrease in the amount of particle crushing. Therefore, it would be important to measure quantitatively the percentage decrease in the particle crushing due to the percentage increase for content. This could be done by measuring the amount of crushed particles or by numerical simulations.
6. From the SEM analysis and compression curves, it is obvious that there is particle crushing during isotropic compression and shearing. The particle crushing ultimately, changes the gradation of the base material, and subsequently resulting to change the permeability and dissipation of excess pore water pressure of the material. Therefore, it would be interesting to correlate the cement content and confining pressure effects on the permeability of the material.
7. During laboratory investigations and from the review of the literature, it is confirmed that by the increase in the cement content the materials behaviour gets more inclined towards brittleness. In case of the addition of cement as a reinforcing agent, the effect of fibre reinforcement on the mechanical behaviour of cemented sand at high pressures would be a new dynamic feature for improving the reinforcing techniques.
8. On the bases of SEM analysis of the specimens obtained after consolidation and shearing, it is evident that further investigations are essential to fully understand the way in which the micro-fabric changes in response to the stress and strain imposed on the cemented soil at high confining pressures. This could be carried out through the microscopic study of the specimens with different cement con-

tents, tested at various confining pressures-and at different stages of axial deformation.

9. Modelling of naturally microstructured sands is very important to geomechanics with the aim to efficiently capture the effect of cementation between particles (bonds). The relative stiffness of bonds and sand particles could give a reasonable understanding of the deformation phenomena, which would be significant for finding the effect of cementation on particle crushing and the location of primary yielding of the materials. Because it is believed that, the gross yielding (the yielding defined in terms of strains) on macroscopic scale may be associated with bond breakage on microscopic scale.

REFERENCES

- Abdulla, A. A. and Kioussis, P. D. (1997). Behaviour of cemented sands .1. Testing, *International Journal for Numerical and Analytical methods in Geomechanics*, **21**(8), 533-547.
- Airey, D. W. (1993). Triaxial testing of naturally cemented carbonate soil, *Journal of Geotechnical Engineering-ASCE*, **119**(9), 1379-1398.
- Airey, D. W., and Fahey, M. (1991). Cyclic response of calcareous soil from the northwest shelf of Australia, *Geomechanics*, **41**(1), 101-122.
- Alsaleh, M. I., Alshibli, K. A. and Voyiadjis, G. Z. (2006). Influence of micromaterial heterogeneity on strain localization in granular materials, *International Journal of Geomechanics*, **6**(4), 248-259.
- Amini, F. and Sama, K. M. (1999). Behaviour of stratified sand-silt-gravel composites under seismic liquefaction conditions, *Soil Dynamics and Earthquake Engineering*, **18**(6), 445-455.
- Arroyo, M., Castellanza, R. and Nova, R. (2005). Compaction bands and oedometric testing in cemented soils, *Soils and Foundations*, **45**(2), 181-194.
- Arthur, J. F. R., Dustan, T., Al-Ani, Q. A. J. and Assadi, A. (1977). Plastic deformation and failure in granular media, *Geotechnique*, **27**, 53-74.
- Asghari, E., Toll, D. G. and Haeri, S. M. (2003). Triaxial behaviour of a cemented gravely sand, Tehran alluvium, *Geotechnical and Geological Engineering*, **21**(1), 1-28.
- Barksdale, R. D. and Blight, G. E. (1997). Compressibility and settlement of residual soils. In mechanics of residual soils, (G. E. Blight Ed.) 95-154. Rotterdam: A. A. Balkema.
- Been, K., and Jefferies, M. (2004). Stress-dilatancy in very loose sand, *Canadian Geotechnical Journal*, **41**, 972-989.
- Bergado, D. T., Taechakumthorn, C., Lorenzo, G. A. and Abuel-Naga, H. M. (2006). Stress-deformation behaviour under anisotropic drained triaxial consolidation of cement-treated soft Bangkok clay, *Soils and Foundations*, **46**(5), 629-637.
- Bolton, M. D. (1986). The strength and dilatancy of sands, *Geotechnique*, **20**(1), 65-78.
- Bopp, P. A. and Lade, P. V. (2005). Relative density effects on undrained sand behaviour at high pressures, *Soils and Foundations*, **45**(1), 15-26.
- Boukpeti, N. and Drescher, A. (2000). Triaxial behaviour of refined Superior sand model, *Computers and Geotechnics*, **26**(1), 65-81.

- Bowles, J. E. (1997). *Foundation Analysis and Design*, 5th ed., McGraw-Hill.
- Bradshaw, A. S. and Baxter, C. D. P. (2007). Sample preparation of silts for liquefaction testing, *Geotechnical Testing Journal*, **30**(4), 324-332.
- Brown, S. F., Juspi, S., and Yu, H. S. (2008). Experimental observations and theoretical predictions of shakedown in soils under wheel loading, *In Advances in Transportation Geotechnics*,
- Butterfield, R. and Baligh, F. (1996). A new evaluation of loading cycles in an oedometer, *Geotechnique*, **46**(3), 547-553.
- Castellanza, R. and Nova, R. (2004). Oedometric tests on artificially weathered carbonatic soft rocks, *Journal of Geotechnical and Geoenvironmental Engineering*, **130**(7), 728-739.
- Castro, G. (1969). Liquefaction of sands, Harvard Soil Mechanics Series 87, Harvard University, Cambridge, Massachusetts.
- Cecconi, M., Viggiani, G. and Rampello, S. (1998). An experimental investigation of the mechanical behaviour of a pyroclastic soft rock. Proc. 2nd Int. Symp. on Geotech. Engng of Hard Soils-Soft Rocks, Naples **1**, 473-482
- Chen, J. W., Lin, C. Y. and Lee, W. (2003). Dilative behaviour of granular materials, *International Journal of Offshore and Polar Engineering*, **13**(4), 301-307.
- Chakraborty, T. and Salgado, R. (2010). Dilatancy and Shear Strength of Sand at Low Confining Pressures, *Journal of Geotechnical and Geoenvironmental Engineering*, **136**(3), 527-532.
- Cheng, Y. P., Nakata, Y. and Bolton, M. D. (2003). Discrete element simulation of crushable soil, *Geotechnique*, **53**(7), 633-641.
- Chiu, C. F., Zhu, W. and Zhang, C. L. (2009). Yielding and shear behaviour of cement-treated dredged materials, *Engineering Geology*, **103**(1-2), 1-12.
- Clough, G. W., Sitar, N., Bachus, R. C. and Rad, N. S. (1981). Cemented sands under static loading, *Journal of the Geotechnical Engineering Division-ASCE*, **107**(6), 799-817.
- Clough, G. W., Iwabuchi, J., Rad, N. S. and Kuppusamy, T. (1989). Influence of Cementation on Liquefaction of Sands, *Journal of Geotechnical Engineering-ASCE*, **115**(8), 1102-1117.
- Consoli, N. C., da Fonseca, A. V., Cruz, R. C. and Heineck, K. S. (2009). Fundamental Parameters for the Stiffness and Strength Control of Artificially Cemented

- Sand, *Journal of Geotechnical and Geoenvironmental Engineering*, **135**(9), 1347-1353.
- Consoli, N. C., Casagrande, M. D. T. and Coop, M. R. (2005). Effect of fibre reinforcement on the isotropic compression behaviour of a sand, *Journal of Geotechnical and Geoenvironmental Engineering*, **131**(11), 1434-1436.
- Consoli, N. C., Foppa, D., Festugato, L. and Heineck, K. S. (2007a). Key parameters for strength control of artificially cemented soils, *Journal of Geotechnical and Geoenvironmental Engineering*, **133**(2), 197-205.
- Consoli, N. C., Prietto, P. D. M. and Ulbrich, L. A. (1998). Influence of fibre and cement addition on behaviour of sandy soil, *Journal of Geotechnical and Geoenvironmental Engineering*, **124**(12), 1211-1214.
- Consoli, N. C., Rotta, G. V., Foppa, D. and Fahey, M. (2007b). Mathematical model for isotropic compression behaviour of cemented soil cured under stress, *Geomechanics and Geoengineering*, **2**(4), 269-280.
- Consoli, N. C., Rotta, G. V. and Prietto, P. D. M. (2000). Influence of curing under stress on the triaxial response of cemented soils, *Geotechnique*, **50**(1), 99-105.
- Coop, M. R. and Atkinson, J. H. (1993). The mechanics of cemented carbonate sands, *Geotechnique*, **43**(1), 53-67.
- Coop, M. R. and Lee, I. K. (1993). The behaviour of granular soils at elevated stresses, translated by London: Thomas Telford, 186-198.
- Coop, M. R. and Willson, S. M. (2003). Behaviour of hydrocarbon reservoir sands and sandstones, *Journal of Geotechnical and Geoenvironmental Engineering*, **129**(11), 1010-1019.
- Chung, S. G., Prasad, K. N., Nagaraj, T. S., Chung, J. G. and Jo, K. Y. (2004). Assessment of compressibility behavior of naturally cemented soft clays, *Marine Georesources & Geotechnology*, **22**(1-2), 1-20.
- Chakraborty, T. and Salgado, R. (2010). Dilatancy and Shear Strength of Sand at Low Confining Pressures, *Journal of Geotechnical and Geoenvironmental Engineering*, **136**(3), 527-532.
- Cresswell, A. W. and Barton, M. E. (2003). Direct shear tests on an uncemented, and a very slightly cemented, locked sand, *Quarterly Journal of Engineering Geology and Hydrogeology*, **36**, 119-132.
- Cuccovillo, T. and Coop, M. (1999). On the mechanics of structured sands, *Geotechnique*, **49**(6), 741-760.

- Cuccovillo, T. and Coop, M. R. (1997). The measurement of local axial strains in triaxial tests using LVDTs, *Geotechnique*, **47**(1), 167-171.
- Cuccovillo, T. and Coop, M. R. (1999). On the mechanics of structured sands, *Geotechnique*, **49**(6), 741-760.
- Dano, C., Hicher, P. Y. and Tailliez, S. (2004). Engineering properties of grouted sands, *Journal of Geotechnical and Geoenvironmental Engineering*, **130**(3), 328-338.
- DeJong, J. T., Fritzsche, M. B. and Nusslein, K. (2006). Microbially induced cement content to control sand response to undrained shear, *Journal of Geotechnical and Geoenvironmental Engineering*, **132**(11), 1381-1392.
- Desrues, J. and Viggiani, G. (2004). Strain localization in sand: an overview of the experimental results obtained in Grenoble using stereophotogrammetry, *International Journal for Numerical and Analytical Methods in Geomechanics*, **28**(4), 279-321.
- Donaghe, R. T., Chaney, R. C. and Silver, M. L. (1988) *Advanced triaxial testing of soil and rock*, ASTM special technical publication.
- Dos Santos, A. P. S., Consoli, N. C., Heineck, K. S. and Coop, M. P. (2009). High-pressure isotropic compression tests on fibre-reinforced cemented sand, *Journal of Geotechnical and Geoenvironmental Engineering*, In press.
- dos Santos, A. P. S., Consoli, N. C., Heineck, K. S. and Coop, M. R. (2010). High-Pressure Isotropic Compression Tests on Fiber-Reinforced Cemented Sand, *Journal of Geotechnical and Geoenvironmental Engineering*, **136**(6), 885-890.
- Ferreira, P. and Bica, A. (2006). Problems in identifying the effects of structure and critical state in a soil with a transitional behaviour, *Geotechnique*, **56**(7), 445-454.
- Frost, J. D. and Park, J. Y. (2003). A critical assessment of the moist tamping technique, *Geotechnical Testing Journal*, **26**(1) 57-70.
- Futai, M. M., Almeida, M. S. S. and Lacerda, W. A. (2004). *Journal of Geotechnical and Geoenvironmental Engineering*, **130**(11), 1169- 1179.
- Kavvas, M. J., Anagnostopoulos, A. G. and Kalteziotis, N. (1993). A framework for the mechanical behaviour of cemented Corinthmarl. Proc. 1st Int. Symp. on Geotech. Engng of Hard Soils–Soft Rocks, 1, Athens, 577–583.
- Kuo, C. Y. and Frost, J. D. (1996). Uniformity evaluation of cohesionless specimens using digital image analysis, *Journal of Geotechnical Engineering-ASCE*, **122**, 390-396.

- Kuwano, R. and Jardine, R. J. (2007). A triaxial investigation of kinematic yielding in sand. *Geotechnique*, **57**, 563-579.
- Gilbert, P. A. and Marcuson, W. F. (1988). Density variation in specimens subjected to cyclic and monotonic loads. *Journal of Geotechnical Engineering*, **114**(1), 1-20.
- Grine, K. and Glendinning, S. (2007). Creation of an artificial carbonate sand, *Geotechnical and Geological Engineering*, **25**(4), 441-448.
- Goto, S., Tatsuka, F., Shibuya, S., Kim, Y. S. and Sato, T. (1991). A simple gauge for local small strain measurements in the laboratory, *Soils and Foundations*, **31**(1), 169-180.
- Haeri, S. M., Hamidi, A., Hosseini, S. M., Asghari, E. and Toll, D. G. (2006). Effect of cement type on the mechanical behaviour of a gravely sand, *Geotechnical and Geological Engineering*, **24**(2), 335-360.
- Hamidi, A. and Haeri, S. M. (2008). Stiffness and Deformation Characteristics of a Cemented Gravely Sand, *International Journal of Civil Engineering*, **6**(3), 159-173.
- Horpibulsuk, S., Miura, N. and Bergado, D. T. (2004). Undrained shear behaviour of cement admixed clay at high water content, *Journal of Geotechnical and Geoenvironmental Engineering*, **130**(10), 1096-1105.
- Houlsby, G. T. (1986). A general failure criterion for frictional and cohesive materials, *Soils and foundations*, **26**(2), 97-101.
- Huang, A., Hsu, S. and Kuhn, H. (1994). A multiple purpose soil testing apparatus, *Geotechnical Testing Journal*, **17**(2), 227-232.
- Huang, J. T. and Airey, D. W. (1993). Effects of cement and density on artificially cemented sand, *Geotechnical Engineering of hard soils and soft rocks*, **1**, 553-560.
- Huang, J. T. and Airey, D. W. (1998). Properties of artificially cemented carbonate sand, *Journal of Geotechnical and Geoenvironmental Engineering*, **124**(6), 492-499.
- Huang, W. X., Sun, D. and Sloan, S. W. (2007). Analysis of the failure mode and softening behaviour of sands in true triaxial tests, *International Journal of Solids and Structures*, **44**(5), 1423-1437.
- Hyodo, M., Hyde, A. F. L., Aramaki, N. and Nakata, Y. (2002). Undrained monotonic and cyclic shear behaviour of sand under low and high confining stresses, *Soils and Foundations*, **42**(3), 63-76.

- Ishihara, K. (1993). Liquefaction and Flow Failure during Earthquakes. The 33rd Rankine lecture. *Geotechnique*, 43(3), 351-415.
- Ismael, N. F. (2000). Influence of artificial cement content on the properties of Kuwaiti sands, *Kuwait Journal of Science & Engineering*, 27(1), 59-76.
- Ismael, N. F. (2001). Axial load tests on bored piles and pile groups in cemented sands, *Journal of Geotechnical and Geoenvironmental Engineering*, 127(9), 766-773.
- Ismail, M. A., Joer, H. A. and Randolph, M. F. (2000). Sample preparation technique for artificially cemented soils, *Geotechnical Testing Journal*, 23(2), 171-177.
- Ismail, M. A., Joer, H. A., Sim, W. H. and Randolph, M. F. (2002). Effect of cement type on shear behaviour of cemented calcareous soil, *Journal of Geotechnical and Geoenvironmental Engineering*, 128(6), 520-529.
- Jardine, R. J., Symes, M. J. and Burland, J. B. (1984). The measurement of soil stiffness in the triaxial apparatus, *Geotechnique*, 34(3), 323-340.
- Jardine, R. J., Potts, D. M., Fourie, A. B. and Burland, J. B. (1986). Studies of the Influence of Nonlinear Stress-Strain Characteristics in Soil Structure Interaction, *Geotechnique*, 36(3), 377-396.
- Jefferies, M. and Been, K. (2000). Implications for critical state theory from isotropic compression of sand, *Geotechnique*, 50(4), 419-429.
- Jiang, M. J., Yu, H. S. and Leroueil, S. (2007). A simple and efficient approach to capturing bonding effect in naturally microstructured sands by discrete element method, *International Journal for Numerical Methods in Engineering*, 69(6), 1158-1193.
- Karner, S. L., Chester, F. M., Kronenberg, A. K. and Chester, J. S. (2003). Subcritical compaction and yielding of granular quartz sand, *Tectonophysics*, 357– 381. Available online at sciencedirect.com
- Kim, Y. S., Tatsuoka, F. and Ochi, K. (1994). Deformation Characteristics at Small Strains of Sedimentary Soft Rocks by Triaxial Compression Tests, *Geotechnique*, 44(3), 461-478.
- Klein, E., Baud, P., Reuschle, T. and Wong, T. F. (2001). Mechanical behaviour and failure mode of Bentheim sandstone under triaxial compression, *Physics and chemistry of the earth part A-solid earth and geodesy*, 26(1-2), 21-25.
- Kuo, C. Y. and Frost, J. D. (1996). Uniformity evaluation of cohesionless specimens using digital image analysis, *Journal of Geotechnical Engineering-ASCE*, 122, 390-396.

- Kwag, J. M., Ochiai, H. Yasufuku, N. (1999). Yielding stress characteristics of carbonate sand in relation to individual particle fragmentation strength, *Engineering for Calcareous Sediments, Al-Shafei (ed.) Balkema, Rotterdam*.
- Ladd, R. S. (1974). Specimen preparation and liquefaction of sand, *Journal of Geotechnical Engineering-ASCE*, **100**(10), 1180-1184.
- Ladd, R. S. (1977). Specimen preparation and cyclic stability of sands, *Journal of Geotechnical Engineering-ASCE*, **103**(6), 535-547.
- Ladd, R. S. (1978). Preparing test specimens using undercompaction, *Geotechnical Testing Journal*, **1**(1), 16-23.
- Lade, P. V., Yamamuro, J. A. and Bopp, P. (1996). Significance of particle crushing in granular materials, *Journal of Geotechnical Engineering-ASCE*, **122**(4), 309-316.
- Lade, P. V. (1992). Static instability and liquefaction of loose fine sandy slopes, *Journal of Geotechnical Engineering-ASCE*, **118**(1), 51-71.
- Lade, P. V. and Yamamuro, J. A. (1996). Undrained sand behaviour in axisymmetric tests at high pressures, *Journal of Geotechnical Engineering-ASCE*, **122**(2), 120-129.
- Lade, P. V. and Overton, D. D. (1989). Cementation effects in frictional materials, *Journal of Geotechnical Engineering-ASCE*, **115**, 1373-1387.
- Lee, K. L. and Farhoomand, I. (1967). Compressibility and crushing of granular soils in anisotropic triaxial compression, *Canadian Geotechnical Journal*, **4**(1), 68-86.
- Lee, K. L. and Seed, H. B. (1967). Drained strength characteristics of sands, *Journal of Soil Mechanics and Foundation-ASCE*, **93**(6), 117-141.
- Lee, M. J., Hong, S. J., Choi, Y. M. and Lee, W. (2010). Evaluation of deformation modulus of cemented sand using CPT and DMT, *Engineering Geology*, **115**(1-2), 28-35.
- Leeson, J. and Campbell, D. (1983). The variation of soil critical state parameters with water-content and its relevance to the compaction of two agricultural soils, *Journal of Soil Science*, **34**(1), 33-44.
- Leroueil, S. and Vaughan, P. (1990). The general and congruent effects of structure in natural soils and weak rocks, *Geotechnique*, **40**(3), 467-488.
- Lo, S. C. R., Lade, P. V. and Wardani, S. P. R. (2003). An experimental study of the mechanics of two weakly cemented soils, *Geotechnical Testing Journal*, **26**(3), 328-341.
- Maccarini, M. (1987). Laboratory investigations on artificial soil. PhD thesis, University of London.

- Marri, A., Wanatowski, D. and Yu, H.-S. (2010). Drained behaviour of cemented sand at high pressures, in The 17th Southeast Asian Geotechnical Conference, Taiwan, **1**, 29-32.
- McClelland, B. (1988) *Calcareous Sediments: An Engineering Enigma*, translated by Perth, Australia: 777-784.
- McClelland, B. (1988). Calcareous sediments: and engineering enigma, Engineering for calcareous sediments, Balkema, Rotterdam: R. J. Jewell and M. S. Khorshid Eds.
- McDowell, G. and Bolton, M. (1998). On the micromechanics of crushable aggregates, *Geotechnique*, **48**(5), 667-679.
- Mitchell, J. and Soga, K. (2005) *Fundamentals of Soil Behaviour*, 3rd ed., JohnWiley & Sons.
- Moller, P. C. F., Mewis, J. and Bonn, D. (2006). Yield stress and thixotropy: on the difficulty of measuring yield stresses in practice, *Soft Matter*, **2**(4), 274-283.
- Molenaar, N. and Venmans, A. A. M. (1993). Calcium-carbonate cementation of sand - a method for producing artificially cemented samples for geotechnical testing and a comparison with natural cementation processes, *Engineering Geology*, 103-122.
- Mulilis, J. P., Seed, H. B., Chan, C. K., Mitchell, J. K., Arulanandan, K. (1977). Effects of sample preparation on sand liquefaction, *Journal of Geotechnical Engineering-ASCE*, **103**(2), 91-109.
- Miura, S. and Toki, S. (1982). A sample preparation method and its effect on static and cyclic deformation-strength properties of sand, *Soils and Foundations*, **22**(1), 61-77.
- Naeini, S. A. and Baziar, M. H. (2004). Effect of fines content on steady-state strength of mixed and layered samples of a sand, *Soil Dynamics and Earthquake Engineering*, **24**, 181-187.
- Nygaard, R., Gutierrez, M., Bratli, R. K. and Hoeg, K. (2006). Brittle-ductile transition, shear failure and leakage in shales and mudrocks, *Marine and Petroleum Geology*, **23**(2), 201-212.
- Oda, M. (1972). The mechanism of fabric changes during compressional deformation of sand, *Soils and foundations*, **12**(2), 1-18.
- Pestana, J. M. and Whittle, A. J. (1995). Predicted Effects of Confining Stress and Density on Shear Behaviour of Sand, 4th Int. Conference on Computational Plasticity, Barcelona, **2**, 2319-2330.

- Poulos, S. J., Castro, G. and W, F. J. (1985). Liquefaction evaluation procedure, *Journal of Geotechnical Engineering-ASCE*, 772-792.
- Reddy, K. R. and Saxena, S. K. (1992). Constitutive modeling of cemented sand, *Mechanics of Materials*, **14**(2), 155-178.
- Reynolds, O. (1885). On the dilatancy of media composed of rigid particles in contact, with experimental illustrations, *Phil. Mag., Series 5*, **20**, 469–481.
- Rosa, F. D., Consoli, N. C. and Baudet, B. A. (2008). An experimental investigation of the behaviour of artificially cemented soil cured under stress, *Geotechnique*, **58**(8), 675-679.
- Roscoe, K. H. (1970). Influence of strains in soil mechanics, *Geotechnique*, **20**(2).
- Roscoe, K. H., Schofield, A. N. and Wroth, C. P. (1958). On the yielding of soils, *Geotechnique*, **8**, 22-53.
- Rotta, G. V., Consoli, N. C., Prietto, P. D. M., Coop, M. R. and Graham, J. (2003). Isotropic yielding in an artificially cemented soil cured under stress, *Geotechnique*, **53**(5), 493-501.
- Rowe, P. W. and Barden, L. (1964). Importance of free ends in triaxial, *Journal of Soil Mechanics and Foundations*, **90**(1), 1-28.
- Russell, A. R. and Khalili, N. (2004). A bounding surface plasticity model for sands exhibiting particle crushing, *Canadian Geotechnical Journal*, **41**(6), 1179-1192.
- Schnaid, F., Prietto, P. D. M. and Consoli, N. C. (2001). Characterization of cemented sand in triaxial compression, *Journal of Geotechnical and Geoenvironmental Engineering*, **127**(10), 857-868.
- Schofield, A. N. and Wroth, C. P. (1968). *Critical State Soil Mechanics* McGraw Hill, Maidenhead.
- Sebastian, L. G., Luis, E. V. and Luis, F. V. (2006). Visualization of crushing evolution in granular materials under compression using DEM, *International Journal of Geomechanics*, **6**(3), 195-200.
- Semple, R. M. (1988). Mechanical properties of calcareous soils, State of the art report on engineering properties of carbonate soils. Proc Int Conf Calcareous Sediments, **2**. Perth, Australia, 807–836
- Sharma, S. S. and Fahey, M. (2003). Degradation of stiffness of cemented calcareous soil in cyclic triaxial tests, *Journal of Geotechnical and Geoenvironmental Engineering*, **129**(7), 619-629.
- Saxena, S. K., Reddy, K. R. and Avramidis, A. S. (1988). Static behaviour of artificially cemented sand, *Indian Geotechnical Journal*, **18**, 111 141

- Suzuki, K. and Yamada, T. (2006). Double strain softening and diagonally crossing Shear bands of sand in drained triaxial tests, *International Journal of Geomechanics*, **6**(6), 440-446.
- Tai, T. (1970) Strength and deformation characteristics of cohesionless materials at high pressures, unpublished thesis (PhD Dissertation), Duke University.
- Tatsuoka, F., Kohata, Y., Kim, Y. S., Ochi, K. and Shi, D. M. (1993). Measuring Small Strain Stiffness of Soft Rocks, *Geotechnical Engineering of Hard Soils - Soft Rocks*, **1**, 809-816.
- Tatsuoka, F., Sato, T., Park, C. S., Kim, Y. S., Mukabi, J. N. and Kohata, Y. (1994). 'Measurements of Elastic Properties of Geomaterials in Laboratory Compression Tests, *Geotechnical Testing Journal*, **17**(1), 80-94.
- Taylor (1948). *Fundamentals of Soil Mechanics*, Wiley, New York.
- Vaid, Y. P. and Negussey, D. (1988). Preparation of reconstituted sand specimens, In advanced triaxial testing of soil and rock, ASTM Special Technical Publication 977, Philadelphia. 405–417.
- Vardoulakis, I. and Sulem, J. (1995). *Bifurcation analysis in Geomechanics*, Chapman & Hall.
- Vaughan, P. R. (1985) *Mechanical and hydraulic properties of In-situ residual soils*, translated by Brasilia: 231–263.
- Vesic A. S. and Clough G. W. (1968). Behaviour of granular materials under high stresses, *Journal of Soil Mechanics & Foundation Division-ASCE* **94**(SM3):661-688
- Voyiadjis, G. Z., Thiagarajan, G. and Petrakis, E. (1995). Constitutive modelling for granular media using an anisotropic distortional yield model, *Acta Mechanica*, 151-171.
- Wan, R. and Guo, P. (2001). Effect of microstructure on undrained behaviour of sands, *Geotechnical Testing Journal*, **38**(1), 16-28.
- Wang, J. (2005). *The stress-strain and strength characteristics of Portaway sand*, unpublished thesis The University of Nottingham.
- Wang, Y. H. and Leung, S. C. (2008). A particulate-scale investigation of cemented sand behaviour, *Canadian Geotechnical Journal*, **45**(1), 29-44.
- Wanatowski, D. and Chu, J. (2008). Effect of specimen preparation method on the stress-strain behaviour of sand in plane-strain compression tests, *Geotechnical Testing Journal*, **31**(4), 308-320.

- Wissa, A. E. Z., McGillivray, R. T. and Paniagua, J. G. (1971). The effects of mixing conditions, method of compaction, and curing conditions on the effective stress-strength behaviour of a stabilized soil, Research Report No. R71-34, Soils Publication No. 287, Department of Civil Engineering, Massachusetts Institute of Technology, Cambridge, MA.
- Wood, D. M. 1990. Soil Behaviour and Critical State Soil Mechanics. Cambridge, England: Cambridge University Press.
- Yamamuro, J., Bopp, P. and Lade, P. (1996). One-dimensional compression of sands at high pressures, *Journal of Geotechnical Engineering-ASCE*, **122**(2), 147-154.
- Yamamuro, J. and Wood, F. (2004). Effect of depositional method on the undrained behaviour and microstructure of sand with silt, *Soil Dynamics and Earthquake Engineering*, **24**(9-10), 751-760.
- Yamamuro, J. A. and Lade, P. V. (1996). Drained sand behaviour in axisymmetric tests at high pressures, *Journal of Geotechnical Engineering-ASCE*, **122**(2), 109-119.
- Yoshimine, M. and Ishihara, K. (1998). Flow potential of sand during liquefaction, *Soils and Foundations*, **38**(3), 179-188.
- Yoshimine, M., Robertson, P. K. and Wride, C. E. (1999). Undrained shear strength of clean sands to trigger flow liquefaction, *Canadian Geotechnical Journal*, **36**(5), 891-906.
- Yoshimine, M. Koike, R. (2005). Liquefaction of clean sand with stratified structure due to segregation of particle size, *Soils and Foundations*, **45**(4), 89-98.
- Yu, H. S., Tan, S. M. and Schnaid, F. (2007). A critical state framework for modelling bonded geomaterials, *Geomechanics and Geoengineering: An International Journal*, **2**(1), 61-74.
- Yu, H. S. (1998). CASM: A unified state parameter model for clay and sand, *International Journal for Numerical and Analytical Methods in Geomechanics*, **22**(8), 621-653.
- Yu, H. S. and Khong, C. D. (2003). Bounding surface formulation of a unified critical state model for clay and sand, *Deformation Characteristics of Geomaterials*, 1111-1118.
- Yu, H. S., Khong, C. D., Wang, J. and Zhang, G. (2005). Experimental evaluation and extension of a simple critical state model for sand, *Granular Matter*, **7**(4), 213-225.
- Youwai, S. and Bergado, D. T. (2003). Strength and deformation characteristics of shredded rubber tire-sand mixtures, *Canadian Geotechnical Journal*, **40**(2), 254-264.